INFORMATION TO USERS

This manuscript has been reproduced from the microfilm master. UMI films the text directly from the original or copy submitted. Thus, some thesis and dissertation copies are in typewriter face, while others may be from any type of computer printer.

The quality of this reproduction is dependent upon the quality of the copy submitted. Broken or indistinct print, colored or poor quality illustrations and photographs, print bleedthrough, substandard margins, and improper alignment can adversely affect reproduction.

In the unlikely event that the author did not send UMI a complete manuscript and there are missing pages, these will be noted. Also, if unauthorized copyright material had to be removed, a note will indicate the deletion.

Oversize materials (e.g., maps, drawings, charts) are reproduced by sectioning the original, beginning at the upper left-hand corner and continuing from left to right in equal sections with small overlaps.

ProQuest Information and Learning
300 North Zeeb Road, Ann Arbor, MI 48106-1346 USA
800-521-0600

WAKE FLOW WITH VARYING SEPARATION POINTS

BY

TAOFEEK FOLUSO AYINDE

A Dissertation Presented to the

DEANSHIP OF GRADUATE STUDIES

KING FAHD UNIVERSITY OF PETROLEUM & MINERALS

DHAHRAN, SAUDI ARABIA

In Partial Fulfillment of the
Requirements for the Degree of

DOCTOR OF PHILOSOPHY

In

MECHANICAL ENGINEERING

NOVEMBER, 2002

KING FAHD UNIVERSITY OF PETROLEUM AND MINERALS

DHAHRAN, SAUDI ARABIA

COLLEGE OF GRADUATE STUDIES

This dissertation, written by

TAOFEEK FOLUSO AYINDE

under the direction of his Dissertation advisors, and approved by his Dissertation committee, has been presented to and accepted by the Dean of the College of Graduate Studies, in partial fulfillment of the requirements for the degree of

DOCTOR OF PHILOSOPHY IN MECHANICAL ENGINEERING

Dissertation Committee

Dissertation Advisor (Dr. Muhammed O. Budair)

Dissertation Co-Advisor (Dr. M.A. Zaqir Hasan)

Member (Dr. Hassan M. Badr)

Dr. Faleh A. Al-Sulaimon
Department Chairman

Member (Dr. Bekir S. Yilbas)

Dr. Osama A. Jannadi
Dean, College of Graduate Studies

Member (Dr. Mohamed A. El-Gebeily)

Date: 9-3-2003

This work is dedicated to my mother, who passed away while I was pursuing my academic program. May Allah grant her eternal bliss.

ACKNOWLEDGEMENT

Acknowledgement is due to the King Fahd University of Petroleum and Minerals for providing financial support and the facilities required for this research. I am grateful for the cooperation received from the Mechanical Engineering department.

I wish to express my heart-felt appreciation to my dissertation advisor, Dr. M.O. Budair, for his interest, encouragement, advise and constructive criticism of the work. His support, in spite of his overwhelming busy schedule as the university's Vice Rector, has contributed a great deal in the successful completion of this work. I am greatly indebted to my dissertation co-advisor, Dr. M.A.Z. Hasan, who introduced me into experimental fluid mechanics and provided valuable intellectual inputs into the subject of this research. Even though he left the university before this work was completed, he remained engaged till the end.

My sincere appreciation goes to other members of my dissertation committee, Dr. H.M. Badr, Dr. B.S. Yilbas and Dr. M.A. El-Gebeily, for their cooperation, advise and support. I have benefited immensely from their constructive criticism of the work.

The assistance rendered by Mr. Abdul-Aziz Al-Abdul Lateef and Mr. Mosood Khan of the machine shop of Mechanical Engineering department, in machining the plates used for the study, is greatly appreciated.

I duly appreciate the support given to me by my wife, Adeola, throughout the duration of this work. My sincere appreciation goes to my father, brothers, sisters and numerous friends for their moral support.

The greatest gratitude is due to the almighty Allah for granting me good health and knowledge to accomplish the goal of this endeavor.

TABLE OF CONTENTS

LIST OF TABLES

LIST OF FIGURES

ملخص الرسالة

الإسم : توفيق فولوسو أيـــندى
العنوان : الأثر الخلفي للسريان مع نقاط إنفصال متغيرة
المجال الرئيسي : الهندسة الميكانيكية .
التاريخ : نوفمبر ٢٠٠٢

تمت دراسة الأثر الخلفي لسريان الموائع خلف أربعة ألواح مستوية عملياً وعددياً. أحد هذه الألواح وهو اللوح الأول كان ذا شكل مستطيل بينما صممت الألواح الأخرى بحيث يكون لها حافة خلفية في الإتجاه المستعرض كي ينتج عنه سرياناً ثلاثي الأبعاد ، ولقد تمت الدراسة العملية بإستخدام قياسات السلك الساخن (hot-wire) وتصوير سريان الدخان. وقد تم حساب هذه القياسات عند سرعات سريان حر مقدارها 7.5 و 10 م/ث بينما تم إجراء تصوير السريان الدخاني عند سرعة سريان حر مقدارها 2م/ ث ، ولقد بينت النتائج العملية أن معدل نمو الأثر الخلفي للسريان في وسط الإتجاه العرضي لأحد الألواح وهو اللوح رقم 4 كان مختلفاً إختلافاً ملحوظاً عن الألواح الأخرى. ويذكر أن حالة الثبات الخاصة باللوح رقم 1 قد وجدت بقيمة $Wo = 0.996$ و $\Delta o = 0.501$. أما اللوحين 2 و 3 فقد أعطيا نتائج في حدود 2 % من نتائج اللوح الأول ، أما اللوح الرابع فقد كانت قيمه $Wo = 1.099$ و$\Delta o = 0.458$ ، و تناقص معدل النمو كان نابعاً من إحداثيات الحافة الخلفية. ولقد تم إكتشاف أن التغير العرضي في الحافة الخلفية ينتج عنه تغير عرضي في حالات الثبات ممثلة في قيم Wo و Δo. دراسات صور السريان أوضحت أن تأثير شكل الحافة الخلفية يستمر إلى الآثار الخلفية البعيدة للسريان. كما أوضح التحليل الطيفي أن الآثار الخلفية المتولدة تحت تأثير قوى خارجية ومعدلات النمو المتزايدة والناتجة من هذه القوى كانت متوافقة مع النتائج التي حصل عليها بواسطة الآخرين. أما الحسابات العددية فقد تم إجراؤها لثلاثة ألواح بإستخدام برنامج كمبيوتر تم تطويره لهذا الغرض. وقد تم حل معادلات بقاء كمية الحركة الثلاثية(Navier-Stokes) للسريان مع إستخدام نموذج $k - \epsilon$ للسريان المضطرب وذلك للحصول على وصف عددي للسريان ، ولقد كانت نتائج الحسابات العددية ذات توافق شكلي مع نتائج القياسات العملية ، وبالرغم من ذلك لم نحصل على توافق كمي وذلك نتيجة تأثير القوى الخارجية والتي لم يمكن تضمينها في النموذج الرياضي.

DISSERTATION ABSTRACT

NAME OF STUDENT : TAOFEEK FOLUSO AYINDE

TITLE OF STUDY : Wake Flow with Varying Separation Points

MAJOR FIELD : Mechanical Engineering

DATE OF DEGREE : November, 2002

The wakes formed behind four different flat plates have been investigated experimentally and numerically. One of the plates (called plate 1) had rectangular shape while the rest were made to have varying trailing edge in the spanwise direction in order to introduce three-dimensionality into the flow. The experimental investigations were carried out through hot-wire measurements and smoke flow visualization. The experimental measurements were conducted at freestream speeds of $7.5\,m/s$ *and* $10\,m/s$ *while flow visualization was done at freestream speed of about* $2\,m/s$*. Experimental results showed that the wake growth rate at the mid-span position for one of the plates (called plate 4) was significantly different from the others. The self-preservation state for plate 1 was found to be* $W_o = 0.996$ *and* $\Delta_o = 0.501$*. Plates 2 and 3 gave values that are within 2% of the values for plate 1. However, plate 4 gave* $W_o = 1.099$ *and* $\Delta_o = 0.458$*, the reduced growth rate having its origin from the trailing edge configuration. It was discovered that spanwise variation of trailing edge results in spanwise variation of the self-preservation states (represented by* W_o *and* Δ_o*). The flow visualization studies showed that the influence of the shape of the trailing edges persisted to the far wake. Spectrum analysis revealed that the wakes generated in our experimental facility were under the influence of some external forcing. The increased growth rates, which result from the forcing, are consistent with the results obtained by previous authors. Numerical computations were performed for three of the plates using a computer program developed for that purpose. The three-dimensional Navier-Stokes equations were solved employing the* $k-\varepsilon$ *turbulence model to obtain the flow field. The computational results were in qualitative agreements with the experimental results. However, quantitative agreements could not be obtained because the influence of external forcing could not be incorporated into the numerical computation.*

CHAPTER 1

INTRODUCTION

1.1 Background

When a fluid stream passes over a body, it is retarded by it. The region of decelerated fluid flow behind a body is called the wake. A turbulent wake belongs to the class of free turbulent flows. The characteristic features of these flows are [1]:

i) They are bounded on at least one side by ambient flow of nearly the same density, which is not turbulent and is usually in irrotational motion.

ii) At any moment, the fluid in turbulent, vortical motion is divided from the fluid in irrotational motion by a fairly well-defined intermittency surface.

iii) Within the intermittency surface, the turbulence is roughly homogeneous in scale and turbulent intensity, unlike flows confined by rigid boundaries that restrict the lateral extent of eddy motions.

iv) They nearly always spread into the surrounding fluid and they are necessarily inhomogeneous in the stream direction as well as in a transverse direction.

Wake flow is a subject of interest in nature. Aquatic animals often have to cope with conditions where visibility is drastically reduced. For such animals, water movements generated by prey and predators, as well as abiotic sources such as tides and currents, provide important sensory information. For example, experiments with seal (a sea animal) have shown that the animal locates its prey (i.e. fish) by using its whiskers to detect the hydrodynamic signature left in the wake of the swimming fish [2]. This is possible because the whiskers of a swimming seal vibrate with characteristic frequencies and a hydrodynamic trail intersected by the seal will cause a modulation of this characteristic vibration that might be sensed by the seal [3].

The engineering application of wake flow is immense. Its properties, and especially the associated entrainment and mixing processes, influence directly phenomena such as heating and cooling, chemical reaction development, aerodynamic performance, dispersion of atmospheric pollutants, etc [4]. This has led to tremendous amount of research work on its various manifestations. The fluctuating pressure on a bluff body surface is due to the velocity fluctuations in the incident stream and to various instabilities in the wake region, such as vortex shedding, recirculation and intermittent reattachments [5]. Therefore, the study of flow around circular, rectangular, square and other bodies is of immense value in the construction of high-rise towers and other buildings. One factor that seriously limits the capacity of many airports today is the phenomenon of wake vortices, which are the counter-rotating vortices created at the wing tips and at the edges of the flaps of aircrafts. These vortices may exert a serious danger on following aircrafts [6]. The main hazard

associated with wake vortex encounter occurs when the following aircraft happens to fly along the axis of rotation of a trailing wake vortex behind the leading aircraft. If this occurs, the vortex can effect a potentially hazardous rolling moment on the following aircraft, especially if it is in a low-airspeed, low-altitude state, as is usual for aircraft approaching touch down [7]. Aircraft wake vortex hazard has been a subject of continuing research, with attention focused on preventing the formation of strong and concentrated vortices as well as disintegrating the already formed trailing vortices [8]. Attempts have also been made to develop sensors that could adequately detect and predict wake vortex dangers and expeditiously notify air traffic controllers so that the spacing between subsequent aircraft arrivals can be adjusted accordingly [9]. One of the important technological issues in modern warfare is the detection of fighter aircrafts. There exist now stealth aircrafts that can dodge most detection radar systems. However, it has been recognized that if systems are developed that can detect the aerodynamic wakes of stealth aircraft at long range it could jeopardize the existing stealth fleet [10]. For such systems to accurately predict the location of an enemy aircraft, information about the decay rate of far wake must be available.

Due to the various manifestations of the wake phenomenon, some of which are briefly mentioned above, studies of wake that will lead to its better understanding in various applications are desirable. Over the years, many researchers have undertaken a lot of studies on wake and these have enriched our knowledge of the phenomenon. However, our understanding of the evolution of wake is still very limited. Townsend [1] observed that the wake of a cylinder, when it is sufficiently far downstream from

the generator, evolves into a self-preserving state for which the flow can be described by a single velocity scale and a single length scale. Similar observations have been made on the wake of flat plates, twin plates, airfoils and screens of various solidities [11 – 15]. The view often expressed is that, in the self-preserving state, all wakes lose memory of their origins, until recently when Wygnanski et al. [15] demonstrated that the self-preserving state is indeed dependent on the size and shape of the wake generator. This is the motivation for the present work.

1.2 Objective

Up till now, investigations of self-similarity in wake flow have been confined to two-dimensional bodies only. In view of the results from Wygnaski et al. [15] on the dependence of the self-preservation state on the nature of the generator, the objective of this research is to investigate the effect of spanwise variation of separation points on the self-preserving state of wakes. The investigation, which is both experimental and numerical, is on the wakes generated behind four flat plates whose details will be discussed in chapter 3. The term "separation points", as used here, refers to the trailing edge of the plates. The experimental investigation involves hot-wire measurements as well as flow visualization in the wakes of the four plates. The computational investigation entails the numerical solution of the three-dimensional

Navier-Stokes equations, together with an appropriate turbulence model, over the spatial domain considered in the experiments.

To achieve the objective, instantaneous velocity measurements will be made in the wakes of the plates and numerical computation will be performed to obtain the velocity and stress fields in the wake. The self-preservation state of the wake of each plate will be established from the results. The flow visualization experiment will be used to examine the flow structures in order to gain qualitative insight into the flow phenomenon.

CHAPTER 2

LITERATURE REVIEW

It is well known that practically all wake flows in engineering applications are turbulent. This is expected since, according to Rayleigh's theorem, velocity profiles that possess a point of inflexion are unstable [16]. In the past, many investigators have observed the formation of vortices in the wake of two-dimensional bodies, including a thin flat plate [17]. The formation and breakdown of these vortices have been subjects of intense investigations since these studies can contribute to our understanding of laminar-turbulent transition and lead to ways to actively control the features of the flow. Many investigators [17-21] have considered the stability and transition of free shear flows. Michalke [18] used stability analysis to study the effects of temporally growing disturbances on a free shear layer. After obtaining the eigenvalues and eigenvectors from the solution of the Rayleigh equation, he computed the vorticity distribution for the most amplified disturbance. The arrangement of vorticity obtained corresponds to two parallel vortex rows which are displaced relative to one another. Using the same method as in [18] and for the same flow problem, Michalke [19] obtained the pathlines for particles initially placed along straight lines. The lines show

a tendency to roll up with a simultaneous concentration of particles. Michalke [20] performed the same analysis as in [18] and [19] for the case of spatially growing disturbances and found that many essential features of the instability properties of shear layers which were known from experiment were predicted better than that based on temporally growing disturbances. The results showed that a disturbed free boundary layer rolls up into discrete vortices for large Reynolds number. Sato and Kuriki [17] used experimental measurements and stability analysis to study the process of transition in the wakes of flat plates. Through the study, they classified the transition region into three sub-regions as follows:

i) The linear region: In this region the two-dimensional sinusoidal velocity fluctuations are amplified exponentially downstream. Fluctuations may be described by the linearized theory. The region is modeled as a single row of vortices traveling in the longitudinal direction. The adjacent vortices rotate in opposite directions.

ii) The non-linear region: In this region the growth rate deviates from being exponential due to non-linear effects and higher harmonics are found in the wave- form. The two-dimensionality of the fluctuations is still maintained because $\overline{w^2}$ is small compared with $\overline{u^2}$ and $\overline{v^2}$. As a result of the disturbance of the single row of vortices of the linear region, a double row of vortices develops in this region.

iii) The three-dimensional region in which the distortion of the two-dimensional waves takes place and the regularities in the fluctuations gradually diminish until the fully turbulent wake is formed.

Mattingly and Criminale [21] considered the instability of the wake to natural disturbances in both time and space. From the comparisons with experimental results, it was discovered that stability analysis considered from the spatial viewpoint gave superior predictions to temporal stability analysis. In contrast to the vortex model of Sato and Kuriki [17], they argued that the vortex street development begins in the very near wake and that it is a result of the superposition of the disturbance vorticity upon that of the mean flow. This gives rise to vorticity concentrations located off the wake center plane.

Attempts have been made by some investigators to develop analytical solutions to the momentum equations in the wake of a thin flat plate. Through series expansion of the boundary layer equations for a steady two-dimensional motion, Goldstein [22] obtained solution for the laminar wake of an infinitely thin flat plate. Messiter [23] observed that Goldstein's solution results in singularity in the vertical velocity component at the trailing edge and was able to develop a theory that removed this singularity. Using an inner and outer layer coordinate expansion technique, Alber [24] developed analytical solution for the turbulent near-wake of a flat plate. Comparison with the experimental data of Chevray and Kovasznay [25] showed that the analytical

solution is valid only up to a downstream distance equivalent to about ten boundary-layer thicknesses from the trailing edge.

The far wake generated in the absence of a pressure gradient appears to be more amenable to mathematical analysis due to the simplicity offered by the vanishing velocity defect and the cross stream velocity being almost zero. This has been observed in experiments and has led to the theory of self-preservation in turbulent wakes (Townsend [1], Wygnanski et al. [15]). In this theory it is postulated that, sufficiently far downstream from the wake generator, an asymptotic self-preserving state is achieved for which the flow can be described by a single velocity scale w_o and a single length scale L_o. These scales have been found to be the center-line velocity defect and the half-width of the wake respectively [26]. The nomenclature of the self-preservation theory for wakes is shown in figure 2.1. In effect, the self-preservation theory implies that the transverse distributions of mean velocity and Reynolds stress must be independent of the streamwise coordinate x when normalized by these scales. Physically, this means that the profiles of the velocity at different x locations collapse onto a single curve. The same holds for the stresses. Mathematically, the theory can be expressed as follows [15]:

$$U = U_\infty - w_o f(\eta) \qquad (2.1)$$

$$\overline{u}^2 = w_0^{\,2} g_{11}(\eta) \qquad (2.2)$$

$$\overline{uv} = w_o^{\,2} g_{12}(\eta) \tag{2.3}$$

$$\overline{v}^2 = w_o^{\,2} g_{22}(\eta) \tag{2.4}$$

$$\overline{w}^2 = w_o^{\,2} g_{33}(\eta), \tag{2.5}$$

where $\eta = y / L_o$. By substituting the self-preserving distributions into the momentum equation and making use of the momentum integral constraint together with an eddy viscosity assumption, the conditions under which self-preserving flow is possible can be obtained [26 and 15]. This leads to the following forms for the mean velocity function and the velocity and length scales:

$$f(\eta) = \exp\{-\eta^2 \ln 2\} \tag{2.6}$$

$$\left(\frac{U_\infty}{w_o}\right)^2 = A\bar{x} \tag{2.7}$$

$$\left(\frac{L_o}{\theta}\right)^2 = B\bar{x}, \tag{2.8}$$

where A and B are constants, $\bar{x} = (x - x_0)/2\theta$, x_0 is the location of the virtual origin (see figure 2.1) and θ is the momentum thickness, which is given by:

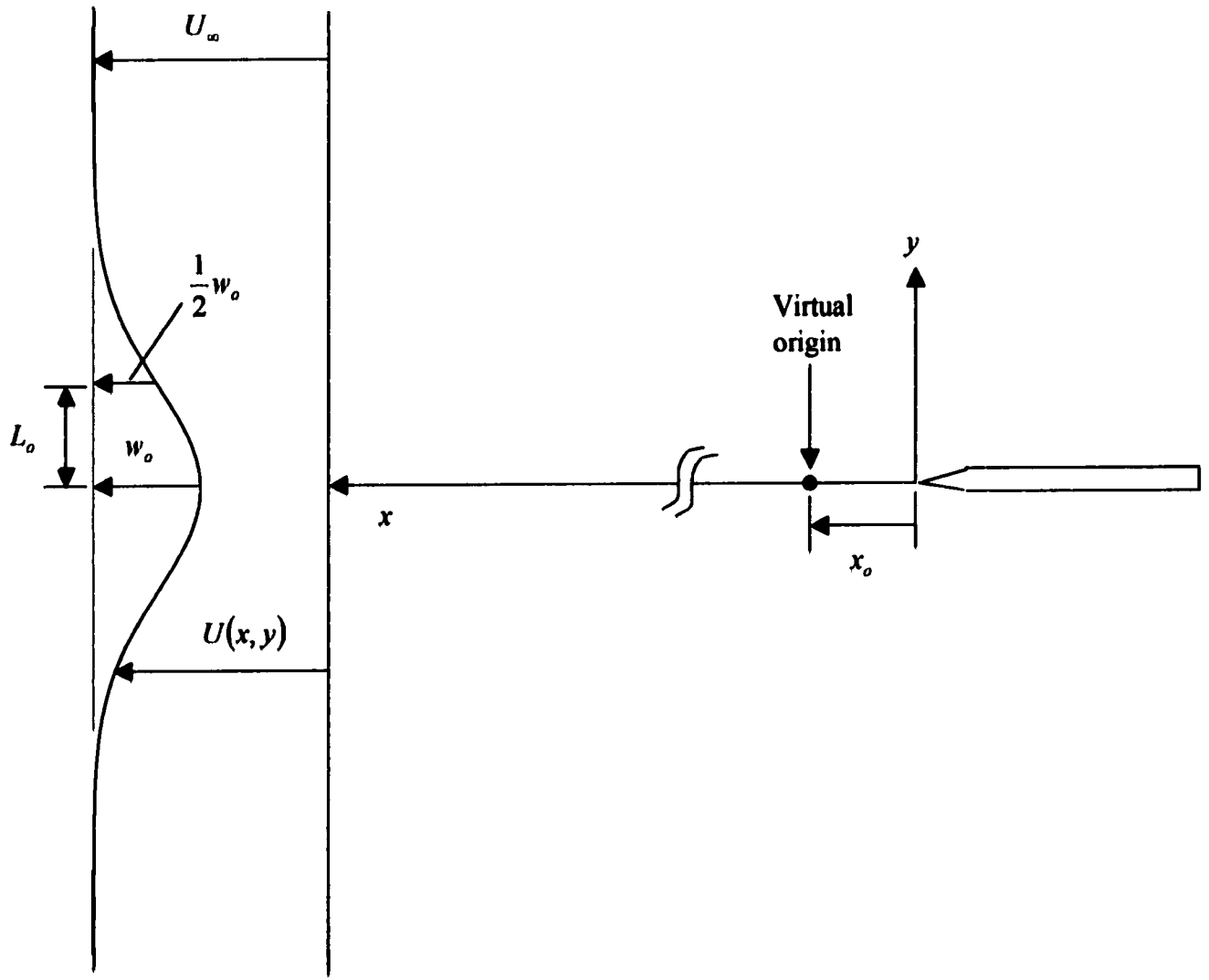

Figure 2.1. Nomenclature of the Self-Preservation Theory

$$\theta = \int_{-\infty}^{\infty} \frac{U}{U_\infty}\left(1-\frac{U}{U_\infty}\right)dy \qquad (2.9)$$

Details of the derivations of equations (2.6) – (2.8) are given in appendix A.

Some researchers have examined self-preservation by computing the following parameters:

$$W = \frac{w_o}{U_\infty}\left(\frac{x}{\theta}\right)^{1/2} \qquad (2.10)$$

$$\Delta = L_o(x\theta)^{-1/2} \qquad (2.11)$$

If W_o and Δ_o are defined by equations *(2.10)* and *(2.11)*, where x is replaced by $x-x_o$, then $A = 2/W_o^2$ and $B = 2\Delta_o^2$.

There is no explicit dividing line (in terms of downstream distance from the wake generator) that separates the far wake from the near wake as this may vary, depending on the generator and the operating conditions. Ramaprian et al. [12] noted that the development of wake into the asymptotic state takes place in three stages described by the level of mixing between the two boundary layers at the trailing edge. The asymptotic state is reached when the mixing is completed. It has been observed that the maximum velocity defect in the far wake is of the order not more than 5 % of

the freestream velocity (Wygnanski et al. [15]). Experimental investigation of far wake has received much less attention compared with the near wake. Wygnanski et al. [15] attributed this is to the difficulty of obtaining reliable data on $w_o(x)$ and $L_o(x)$ [15]. With such a small velocity defect, the results are very sensitive to any minor calibration changes due to drift.

Even though experimental investigations with various generators have unanimously confirmed the self-preservation of far wake, there has not been agreement on the universality or otherwise of the self-preserving state. If a universal self-preserving state exists, it means that the constants A and B of equations *(2.7)* and *(2.8)* (or parameters W and Δ of equations *(2.10)* and *(2.11)*) will be the same for all wake generators irrespective of shape or size. This implies that the wake completely loses memory of its origin. For the wake of a cylinder, Townsend [27] indicated that at sufficiently high Reynolds number, L_o/d and w_o/U_∞ are universal functions of x/d only, where d is the diameter of the cylinder. Sreenivasan [13] took measurements in the wakes of circular and square cylinders, flat plates and a twin-plate in order to study the approach of the different generators to their self-preserving states. By extrapolating linearly to zero defect, he concluded that all the wakes seemed to approach the asymptotic values $W^* = 1.63 \pm 0.02$ and $\Delta^* = 0.3 \pm 0.005$. However, his results (figure 1 of [13]) show that there are substantial differences in the wakes and only the wake of the twin-plate seemed to approach the value of W^* quoted. Sreenivasan and Narasimha [14] repeated the same experiment and analysis for the twin-plate and confirmed the asymptotic values stated above. It will be incorrect to

take these values as applicable to any plane wake since there is no evidence that it is so. In order to investigate the universality of the self-preserving state, Wygnanski et al. [15] studied the wakes of circular cylinders, flat plate, airfoil and screens of various solidities. They obtained different values of W_o and Δ_o for the different generators, which shows that the velocity and length scales do not exhibit universal behavior and do depend on the inflow conditions. They noted that the nature of the flow in the vicinity of the generator, including any vortices shed, could provide a plausible explanation for the apparent dependence of the small-deficit wake on the shape of the generator. By introducing external forcing (through a small trailing-edge flap externally driven by acoustic excitation) into the wake of the flat plate they obtained different values of W_o and Δ_o depending on the frequency and amplitude of the forcing. Using the linear inviscid stability analysis, they obtained results that predicted quite well the amplification and the transverse distributions of amplitudes and phases of externally imposed sinuous waves in the wake of a flat plate.

It was argued by Townsend [1] that, almost without exception, self-preserving flows must be either axisymmetric or homogenous in one transverse direction. This is because the spreading rate in, say the z direction, depends on the magnitude of Reynolds stress $-\overline{u'w'}$ which appears as a response to distortion of turbulence by the mean velocity gradients. If gradients of U in the z direction are larger than those in the y direction, the distortion leads to larger values of $\overline{u'w'}$ than $\overline{u'v'}$, and so the flow tends to spread more rapidly in the direction for which its width is least. To preserve constant ratios of flow widths in different directions, it is necessary either that the

distributions are axisymmetric or that the width in one direction is effectively infinite. Obviously, the condition of infinite extent in one direction cannot be met in any wind tunnel experiment. Therefore, the contribution of the three-dimensionality introduced into the flow field as a result of the finite width of the wind tunnel needs to be assessed. There has recently been an upsurge in activity concerning the development of three-dimensionality in the wakes of nominally two-dimensional bodies. Prasad and Williamson [28] demonstrated how oblique or parallel shedding could be generated over long spanlengths in the wake of a cylinder simply by manipulating the end plates on each side of the cylinder. Their results showed that the Strouhal number $S(=frD/U_\infty$, where fr is the vortex shedding frequency and D is the cylinder diameter) dropped as the inclination of one of the end plates was increased. This three-dimensional effect has practical significance in reducing the unsteady fluid forces on a body. In order to unveil the three-dimensional nature of the large-scale organized motions in a turbulent plane wake, Hayakawa and Hussain [29] used several combinations of x-wire rakes to measure the vorticity distributions in the spanwise and transverse planes in the intermediate region of the wake of a cylinder. They detected that the typical spanwise extent of two-dimensionality of the primary vortices is quite small and is comparable with the local half-width of the wake. They suggested that the spatial behavior of organized structures in the far wake should bear qualitative resemblance to that of the intermediate wake.

Numerical prediction of the far wake flows has been as challenging as its experimental investigation. Patel and Scheuerer [30] employed the $k-\varepsilon$ model to

perform calculation of two-dimensional near and far wakes. While the prediction was good in the near wake ($x/\theta < 350$), the performance of the model in the far wake was found to be poor. The poor performance was attributed to intermittency in the outer region of the wake. Since the $k-\varepsilon$ model (or any of its variants) was constructed essentially for fully turbulent flows it is most unlikely to succeed in the highly intermittent far wake. They attempted to remedy the situation by incorporating an intermittency function to the eddy viscosity formula. The corrections yielded only a marginal improvement in the far wake while the near wake prediction was found to become poorer. The $k-\varepsilon$ model has been reported not to perform well in other unconfined flows like mixing layers and jets [31] unless ad hoc adjustments are made to the model constants. Robinson et al. [32] and Robinson and Hassan [33] proposed a new two-equation model, the $k-\xi$ model, which replaces the dissipation equation with the variance of vorticity or enstrophy equation. They showed that the model performs well in unconfined flow. However, the model lacks the simplicity of the $k-\varepsilon$ model and it is not surprising that it has not received wide acceptance in the computational fluid dynamics community.

In order to adequately account for intermittency in free-shear flows, Cho and Chung [34] proposed a $k-\varepsilon-\gamma$ model based on the Reynolds-averaged quantities. The computational results showed considerable improvements for plane jets, round jets, far wake and plane mixing layer. The same model has been used by Dewan and Arakeri [35] to improve prediction in turbulent boundary layers. Surprisingly, the model has been found to perform better than the standard $k-\varepsilon$ model in predicting

the Reynolds shear stress in the inlet region of confined flows (Wang and Derksen [36]). In spite of the success of the $k-\varepsilon-\gamma$ model in predicting the self-preservation of the mean velocity and shear stress in the far wake it cannot account for the different growth rates observed for different generators as reported by Wygnaski et al. [15]. Indeed Moser et al. [37] concluded that no standard turbulence model would be capable of predicting the wake flow since all those models are insensitive to the features of the initial or inlet conditions that control the state of the wake.

It will be noted that all investigations of far wake reported so far have addressed only two-dimensional wakes. In spite of ample evidence that there is considerable three-dimensionality in the far wake, no work has been reported on the assessment of its effect on the spreading rate of far wake. Most wake generators in real life situation have three-dimensional bodies. It is therefore important to extend our knowledge of the subject to this practical situation, hence the choice of the wake generators for this study.

CHAPTER 3

EXPERIMENTAL SET-UP AND TECHNIQUES

3.1 The Wind Tunnel

The experiments were conducted in the subsonic wind tunnel of the mechanical engineering department. A schematic diagram of the wind tunnel is shown in figure 3.1. It is an open-circuit type driven by a centrifugal blower, which is powered by a variable-speed motor. The motor/blower section is supported on vibration dampers and connected to the diffuser through flexible coupling to minimize the effect of vibration on the flowing air. The diffuser section is followed by a plenum chamber, which contains five screens and a honeycomb. This is followed by a contraction section with a contraction ratio of about 6.5. The test section smoothly joins the contraction section and maintains its uniform rectangular cross-section up to the exhaust section. The test section is 3m long, 1.1m wide and 0.8m high. It is made of three equal subsections, each provided with a glass window on each of its two sides and a removable roof. One of the roofs has a slot drilled on it to enable the insertion of the probe holder into the test section. The probe holder is carried by the traverse mechanism, which sits on a moveable carriage. The carriage stands astride the

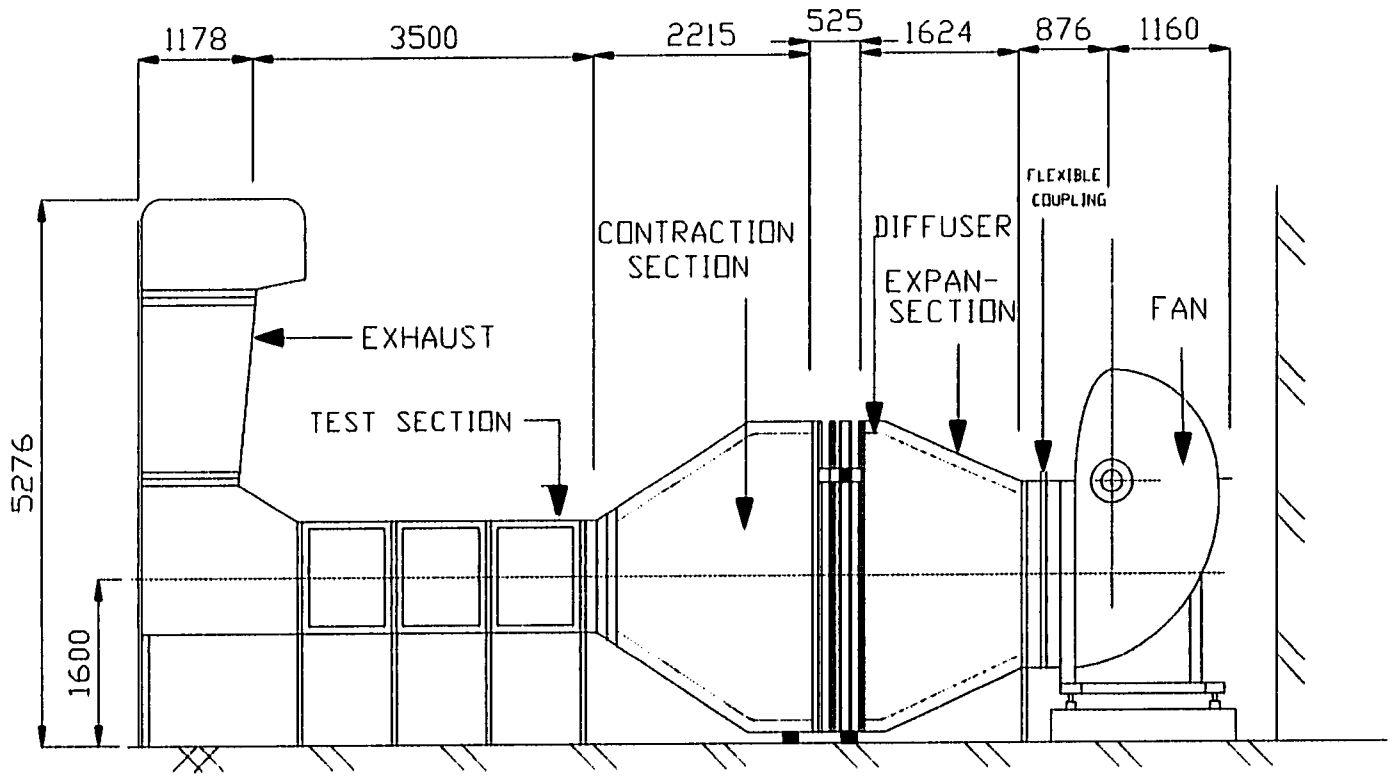

Figure 3.1. Schematic of the subsonic wind tunnel. All dimensions are in mm.

test section on four castors. The traverse mechanism is driven by two "slo-syn" stepping motors each operated via a traverse controller. The traverse controllers ensure movement of the probe holder in the x- and y-directions to a resolution of 0.0254 *mm*. The free-stream turbulence intensity in the test section was less than 0.5%.

3.2 The Wake Generators

Four flat plates were used as wake generators. The plates are shown in figure 3.2. They were made from 6*mm*-thick aluminum sheets. The machining was done in the mechanical engineering department workshop. Each plate is 1.07*m* wide, thus spanning the width of the tunnel test section except for the space occupied by the two bars holding the plate in place. The lengths are such that all the plates are of equal surface area. The leading edges were rounded to a 2:3 elliptical shape in order to ensure that the bodies are streamlined and avoid having separated flow on the plates. The last 127*mm* of each plate was machined down symmetrically on both faces so that the thickness was tapered linearly down to 1*mm* at the trailing edge. This is to minimize the possibility of flow reversal at the plate trailing edge. The plates' surfaces were polished and sprayed with black paints. The first subsection of the test section was used for mounting of plates. For each run of the experiments, a plate was placed at the middle (with respect to the height) of the tunnel and held in place inside the slots in the aluminum bars bolted to the tunnel walls. The slots were large enough to permit

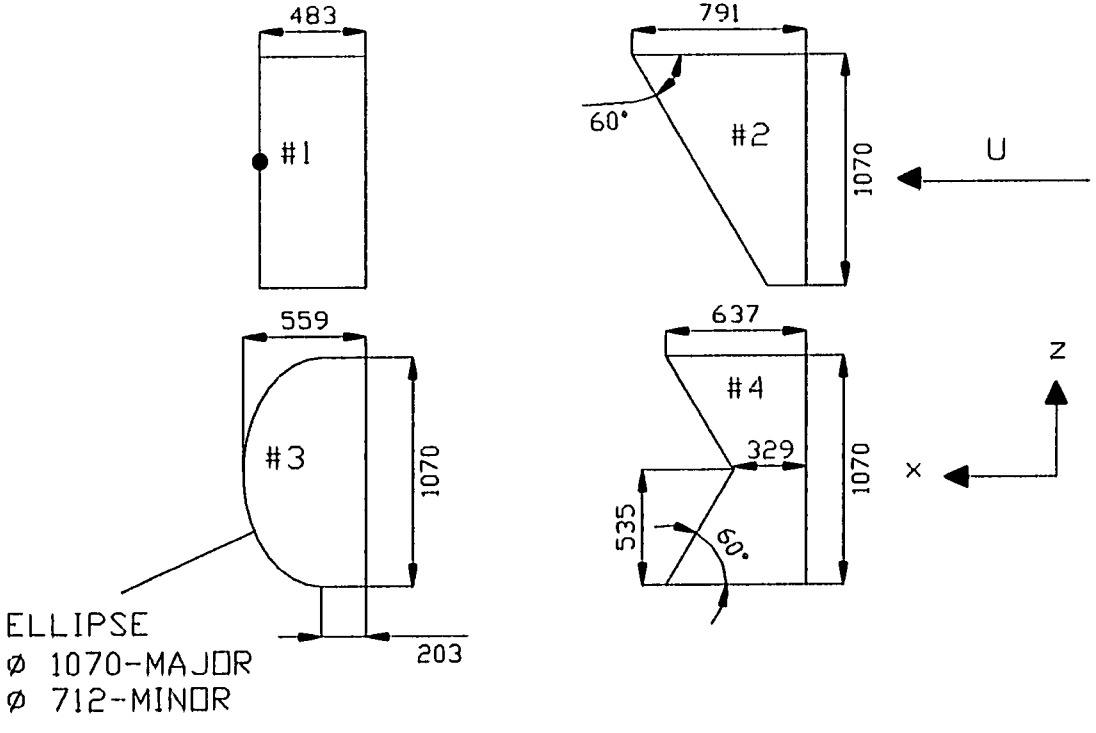

Figure 3.2. The Flat plates used for the experiments. All dimensions are in mm.
Note: The origin of the coordinate system is at the mid-span position on the trailing edge, as shown with a dot for plate 1.

adjustment of the plate level. To ensure that identical boundary layer developed on both sides of the plate the horizontal level of the plate was first checked with a spirit level and then boundary-layer measurements were made on both sides of the trailing edge. The process was repeated until satisfactory results were obtained.

3.3 Measuring Equipment and Measurement Techniques

Measurements were performed with DISA P11 and P15 single-wire, DISA P61 cross-wire and TSI 1210-T1.5 single-wire probes. The probes were connected, via $5m$ length coaxial cables, to a four-channel TSI IFA100 constant-temperature anemometer. The probes were mounted through a thin elliptical shaped holder, placing the probes upstream of any region of flow interference by the holder. The anemometer signals were sampled at 20 KHz through the analog-to-digital converter system consisting of the TSI IFA 200 (digitizer), a 486 computer and the MODEL 6260/6225 'Direct Memory Access' (DMA) interface board installed into one of the slots of the computer's motherboard. The sampling task was performed with the TSI MODEL DAP thermal anemometry software package. Processing of the data was done offline with some self-developed FORTRAN programs. A TEKTRONIX TYPE 3A3/3B3 oscilloscope was connected to the anemometer to aid in the frequency-response tuning during calibration as well as to monitor signal quality and check if probe was broken. Two DISA TYPE 55D31 digital voltmeters and a DISA TYPE 55D35 rms meter were

also connected to the anemometer for inspection of signals during flat plate (wake generator) leveling. A flowchart of the data acquisition process is shown in figure 3.3.

Calibration was performed by placing the hot wires in the free-stream, well outside the wake, along with a Pitot tube inserted through the roof of the test section. The Pitot tube was connected to a Dwyer type inclined-tube manometer with red gauge oil of specific gravity of 0.826. The manometer reading has a resolution of 0.01inches of water. In the far wake, the velocity defect is less than 5%. Operating at a free-stream velocity of 10m/s, the manometer resolution translates to an error of less than 1% for calibration in the speed range of 9.5-10 *m/s*. This was considered adequate for the calibration. The anemometer was operated with an overheat ratio of 1.8. This high overheat ratio was selected in order to minimize the temperature sensitivity of the wires. A 3rd order polynomial $U = P_3(E)$, where the independent variable E is the anemometer voltage, was fit for each hotwire. This form of calibration was preferred to others like the use of King's law or employing a linearizer because of the need to compensate for the inevitable temperature change during the process of taking a complete wake profile at a certain x-location. A sample of the calibration curves obtained is shown in figure 3.4. For cross-wires, both calibration and actual measurements were performed by aligning the probe axis parallel to the mean flow direction. The effective velocity was obtained by using

$$U_{eff} = U(\cos^2\varphi + k^2\sin^2\varphi)^2, \qquad (3.1)$$

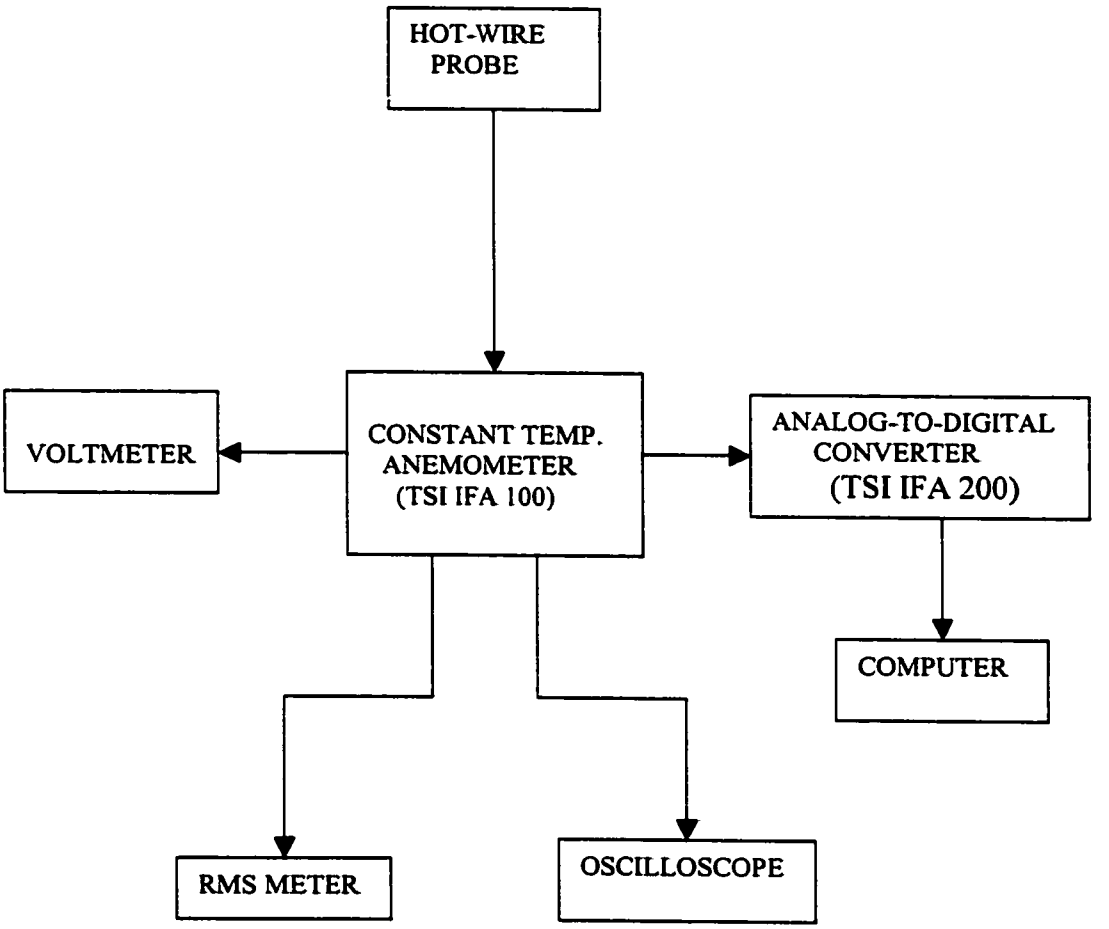

Figure 3.3 Block Diagram for Data Acquisition

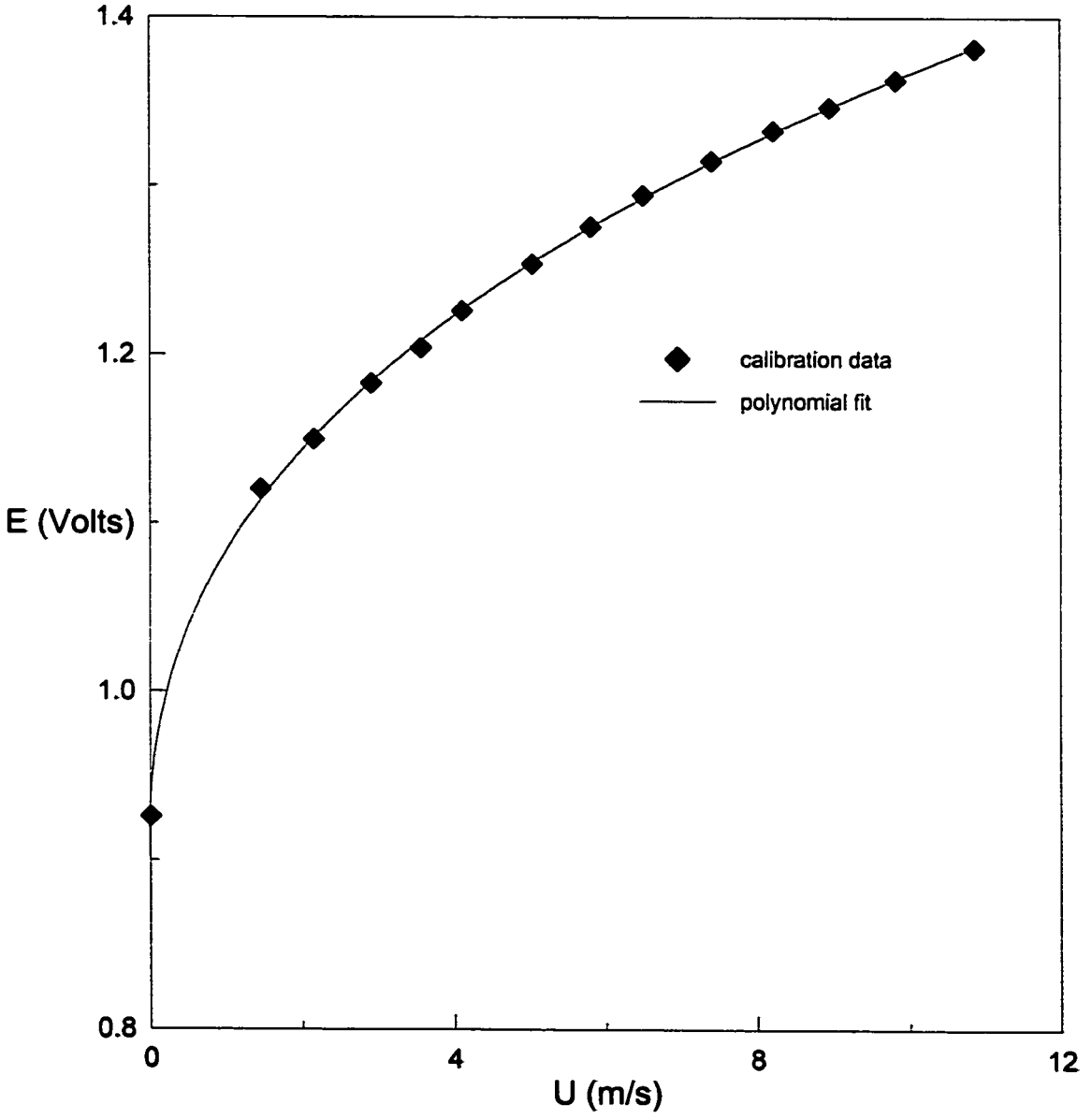

Figure 3.4 A sample calibration curve

where $k = 0.2$ [38]. Details of the calibration and data processing procedure with the use of equation (3.1) above are given in Appendix B.

Due to the fact that the differences to be resolved in the far wake were very small, (with centerline velocity defect of 5% or less) the measurement was very sensitive to fluid temperature changes of as small as $0.25^0 C$. Therefore, measurements were taken at about the same temperature at which calibration was done. Fluid temperature was monitored with a thermometer inserted into the tunnel test section through the wall. For each streamwise location where the wake profile was to be obtained, the fluid temperature at the first and last measuring stations were recorded (to the nearest $0.25^0 C$). The fluid temperatures at the instances of taking measurements at the other stations were obtained by interpolation between those two temperatures, assuming a linear variation of temperature with time during the measurements. This results in the following equation:

$$T_j = T_1 + \left(\frac{j-1}{N-1}\right)(T_N - T_1) \qquad (3.2)$$

where, T_1 and T_N are the temperatures at the first and last points respectively and T_j is the temperature at a particular point j. During data processing, the anemometer output voltage E_m was compensated for temperature changes using the formula:

$$E = E_m \sqrt{\frac{T_s - T_j}{T_s - T_c}} \qquad (3.3)$$

where T_s, T_c, and T_j are the sensor operating temperature, calibration temperature and the temperature of the fluid during actual measurement, respectively [39].

During data acquisition, the analog-to-digital converter system generated compressed raw data files with extension name .r*, where * represents the experiment number. A utility program, "Daprdata.exe", which is part of the TSI MODEL DAP thermal anemometry software package, was used to convert the data into readable text format and written into another file with extension .p*. The format of the output was a column of channel number followed by a column of raw voltages for each channel in sequence. The set of data files of the measurements taken at a certain x location was then processed with a FORTRAN program to obtain the wake properties at that location. The program is presented in Appendix C.

3.4 Measurement Details

Measurements were carried out at free-stream velocities of 7.5 and 10m/s. At the mid-span position ($z = 0$), the measurements taken were the velocity profiles for the boundary layer on both sides of the trailing edge and in the wake from just outside the trailing edge to the downstream positions where asymptotic growth rates were well established. The boundary-layer measurements were taken with single wires while

measurements in the wake were obtained mainly with cross-wires. In order to detect the presence of three-dimensionality in the wake, the cross-wire was rotated by 90° and the U-W profiles were taken at some locations. Measurements were taken at $z/d = \pm 20$ for a number of locations in order to check two-dimensionality of the flow. Here, d is the thickness of the plate (i.e. 6 *mm*). A schematic of the experimental set-up is shown in figure 3.5.

The most challenging aspect of the experiments was temperature control. Even though the room housing the wind tunnel was air-conditioned there was usually a steady rise of the room temperature, though minimal, while the tunnel was running. This is unacceptable for far wake measurements in which the velocity defect is less than *5%* and it accounts for the rejection of most of the data collected during the earlier parts of the experiments. To minimize the problem, therefore, all measurements were taken at night when the air-conditioning system could be more efficient. In addition, equations *(3.2)* and *(3.3)* were used to account for the small temperature rise (usually within $0.5°C$) that might occur during measurements. Generally, 23-25 data points were taken to define the mean velocity and Reynolds stress profiles. A minimum of 40 seconds (covering 800,000 data samples) was spent in data acquisition at each measurement location.

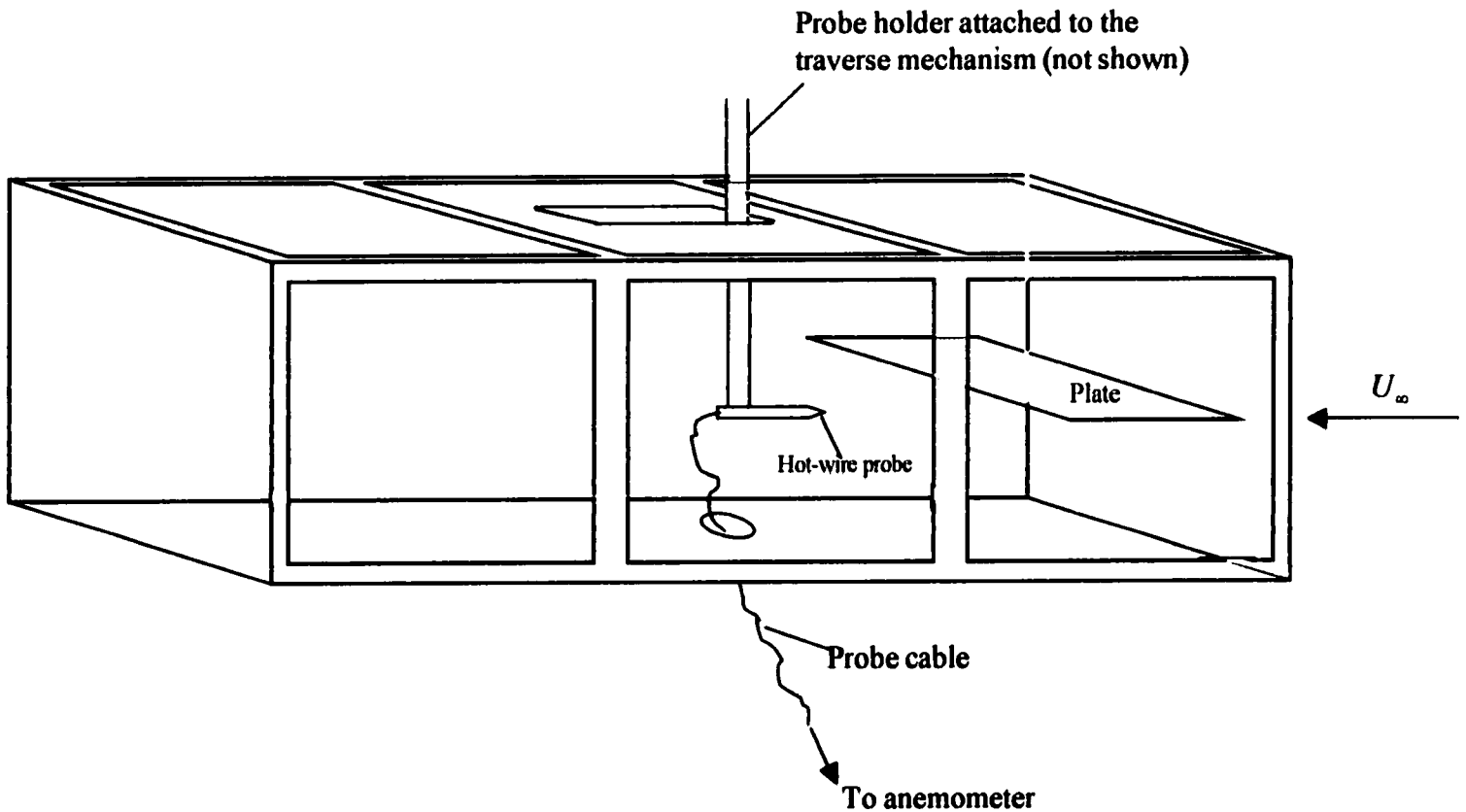

Figure 3.5 Schematic of the Experimental Arrangement

3.5 Uncertainty Analysis

An essential part of any experimentation is the assessment of the degree of goodness or uncertainty analysis of the results. The uncertainty in the results of an experiment depends, to a large extent, on the experimental apparatus used and the experimental method employed. It has been recognized that, no matter how carefully the measurement was performed or how much money was spent on the sensor and associated installation, a measured variable will contain errors [40]. The true value of a quantity rarely is known. Therefore, the errors that cause a measured variable to differ from the true value must be estimated.

In this work, uncertainty analysis of the experimental results has been performed. The detailed uncertainty analysis procedure is presented in Appendix D. The uncertainties in the velocities for a sample calibration data are presented in Table D1. The associated uncertainties in the polynomial coefficients are shown in Table D2. The uncertainties in the experimental results are included in the tables where the results are presented, the details of which will be given in Chapter 4.

3.6 Flow Visualization

Flow visualization has emerged as one of many available tools in experimental fluid mechanics. It differs from other experimental methods in that it renders certain properties of a flow field directly accessible to visual inspection, thereby yielding qualitative insights.

In order to enhance our understanding of the present problem, i.e. the wakes behind flat plates with different trailing edge configurations, a flow visualization experiment was performed on each of four plates. It was intended to obtain the flow pattern in the x-y and x-z planes. The mounting of the plates in the wind tunnel was the same as was done during hot-wire measurements. The roof of the second subsection of the tunnel test section was removed and replaced with a $2mm$-thick polythene sheet in order to facilitate photographing of the x-z plane. In order to maintain high contrast between the smoke and the background, the floor and the sidewalls of the tunnel test section were covered with black cardboard papers.

After a careful review of various visualization methods [41] and taking into consideration the facilities available in our laboratory, the smoke-wire technique was selected for this study. In this technique, smoke is generated by evaporating oil from an electrically heated wire inside the wind tunnel. Coating of the wire with oil is done manually by wiping the wire with a fine, small brush. After the wire is coated with oil, small beads form, and at each of the beads a smoke filament originates when the wire

is heated. The heating of the wire is synchronized with the illumination system and the camera.

In order to choose appropriate oil, some factors must be taken into consideration. These factors are [42]:

i) the oil must be nontoxic.

ii) the smoke particles must be small enough to follow closely the flow pattern being studied.

iii) The smoke particles must possess the necessary light-scattering qualities so that it can be readily photographed.

iv) The smoke should not adversely affect either the wind tunnel or the model being studied.

v) The oil must have low vaporization temperature.

vi) The oil must have low flammability.

A commercial "visilube oil" manufactured by VSM Technologies of the United Kingdom was found to meet all the above conditions and was therefore used in the experiment. To observe the flow, a $0.2mm$ copper wire was placed about $50mm$ upstream of the leading edge of the plate and oriented vertically or horizontally. The vertical orientation was used to observe the flow structure in the x-y plane while the horizontal position was used for the x-z plane. A schematic diagram of the arrangement of facilities for flow visualization is shown in figure 3.6. The ends of the wire were connected to the terminals of a variable-voltage D.C. power source. The

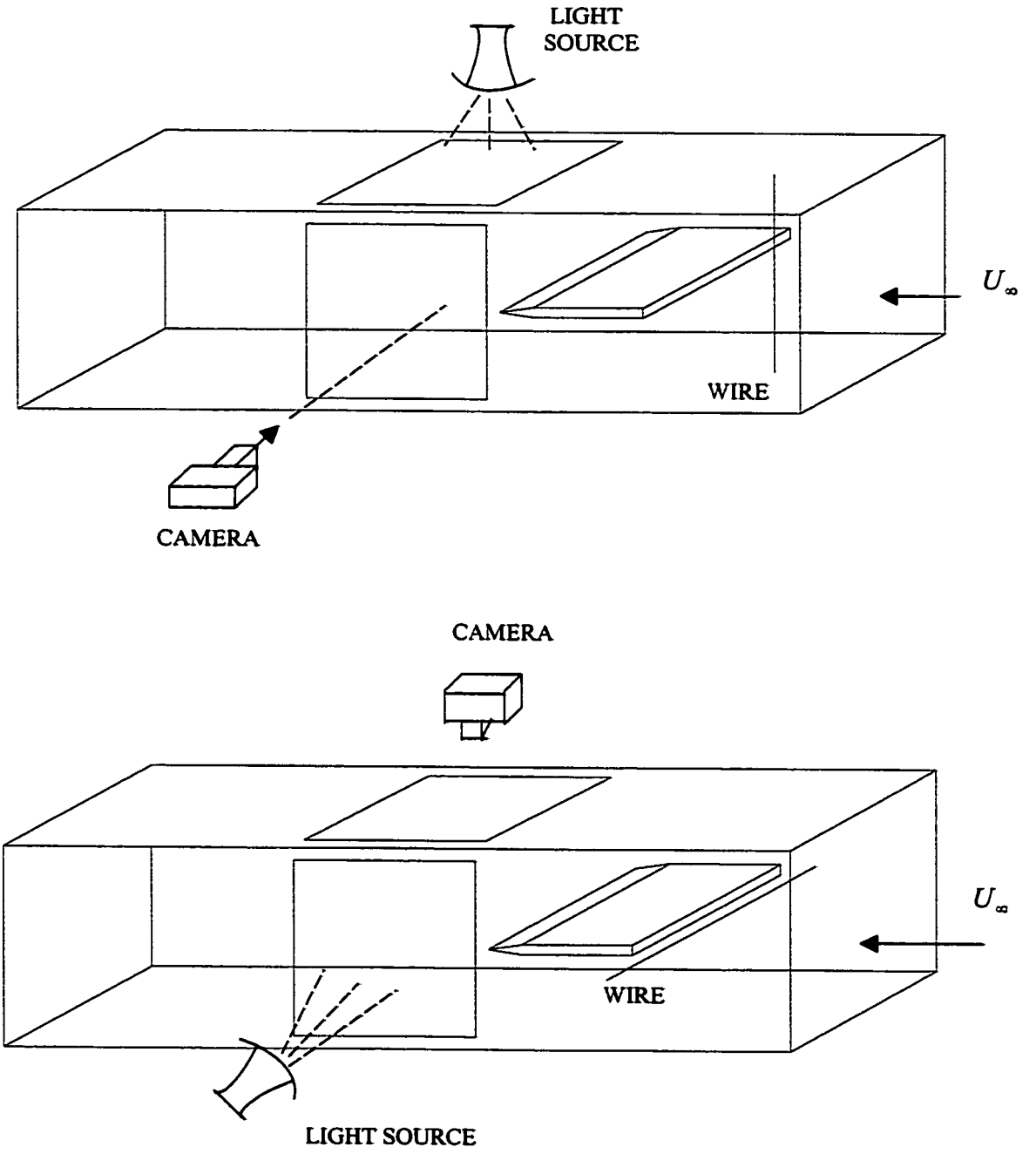

Figure 3.6 Locations of flow visualization facilities in the wind tunnel.
(a) vertical wire position (b) horizontal wire position.

voltage range applied during the experiment was 7-10 volts. Ordinarily, the wire sags and expands when it is heated and this is undesirable. Two measures were taken to overcome this. First, the wire was pre-stressed mechanically by pulling it gradually from both ends until it reached the yield point and broke into two. One of those two pieces was then used for the experiment. The second measure was to attach springs on both ends of the wire and maintain it under tension so that the spring would pick up the slack when the wire was heated. Illumination of the smoke was provided with OSRAM studio lamp using a 1000W bulb. A Sony digital camera (DIGITAL MAVICA MVC-FD88) was used for photographing the smoke. This permitted immediate viewing of results and repetition of the process whenever necessary. The wind tunnel was operated at a free-stream speed of about 2 *m/s*. This corresponds to a Reynolds number based on wire diameter of 26, which is within the range ($\mathrm{Re}_{dia} \leq 40$) of suitability of the smoke-wire technique [42]. It also corresponds to $\mathrm{Re}_{\theta} = 165$ for plates 1 and 2, $\mathrm{Re}_{\theta} = 177$ for plate 3 and $\mathrm{Re}_{\theta} = 136$ for plate 4. θ is the momentum thickness at the plate's trailing edge. This momentum thickness was not measured but calculated from the Blasius profile [16].

CHAPTER 4

EXPERIMENTAL RESULTS AND DISCUSSIONS

4.1 The Initial Boundary Layer

Since wake evolves from the interaction of two separate boundary layers formed on each side of the wake generator, the conditions of the two boundary layers are bound to affect the wake development. It is therefore important to document the boundary layers at the separation point for each plate. In this study, the development of identical boundary layers on each side of the plate was used as a criterion for ensuring that the plate under investigation was parallel to the freestream. Figures 4.1 - 4.4 show profiles of the mean velocity U and the root-mean-square (r.m.s.) values of the longitudinal velocity fluctuation u_{rms} at the trailing edges of the four plates for a freestream velocity of $10m/s$. In all cases, the mean velocity profiles collapse on the Blasius profile (shown as dotted lines in the figures). This shows that the boundary layer at the trailing edge is laminar for all the cases. The peak value of u_{rms} for plate 3 (see figure 4.3b) was found to be substantially higher than the values for the other plates. The machining of the plate surfaces was done manually. The increased peak

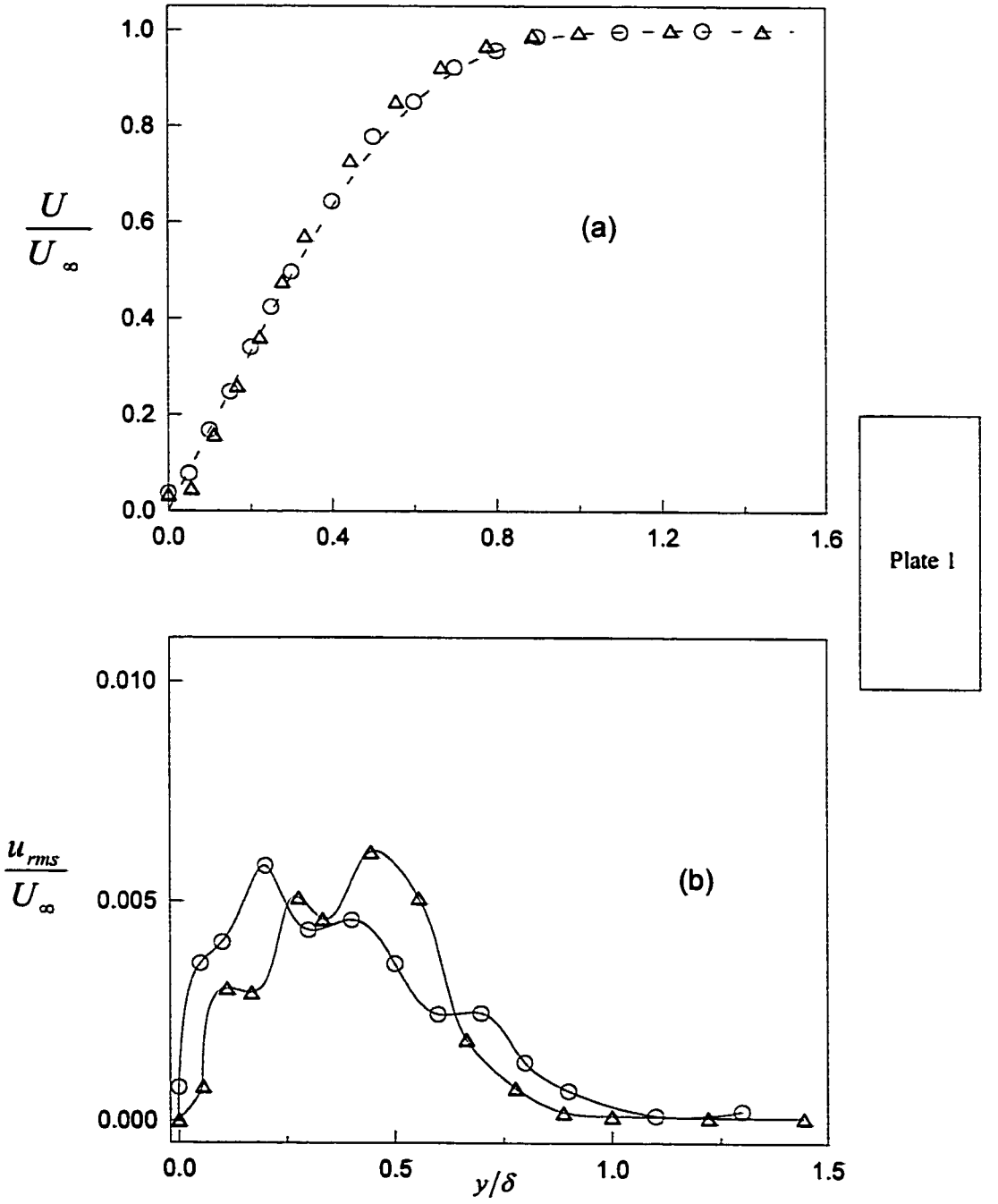

Figure 4.1. Boundary layer profile at the trailing edge of plate 1 for $U_\infty = 10 m/s$. (a) normalized mean velocity; (b) normalized longitudinal fluctuation intensity.
Δ upper surface; O lower surface; ------ Blasius profile.

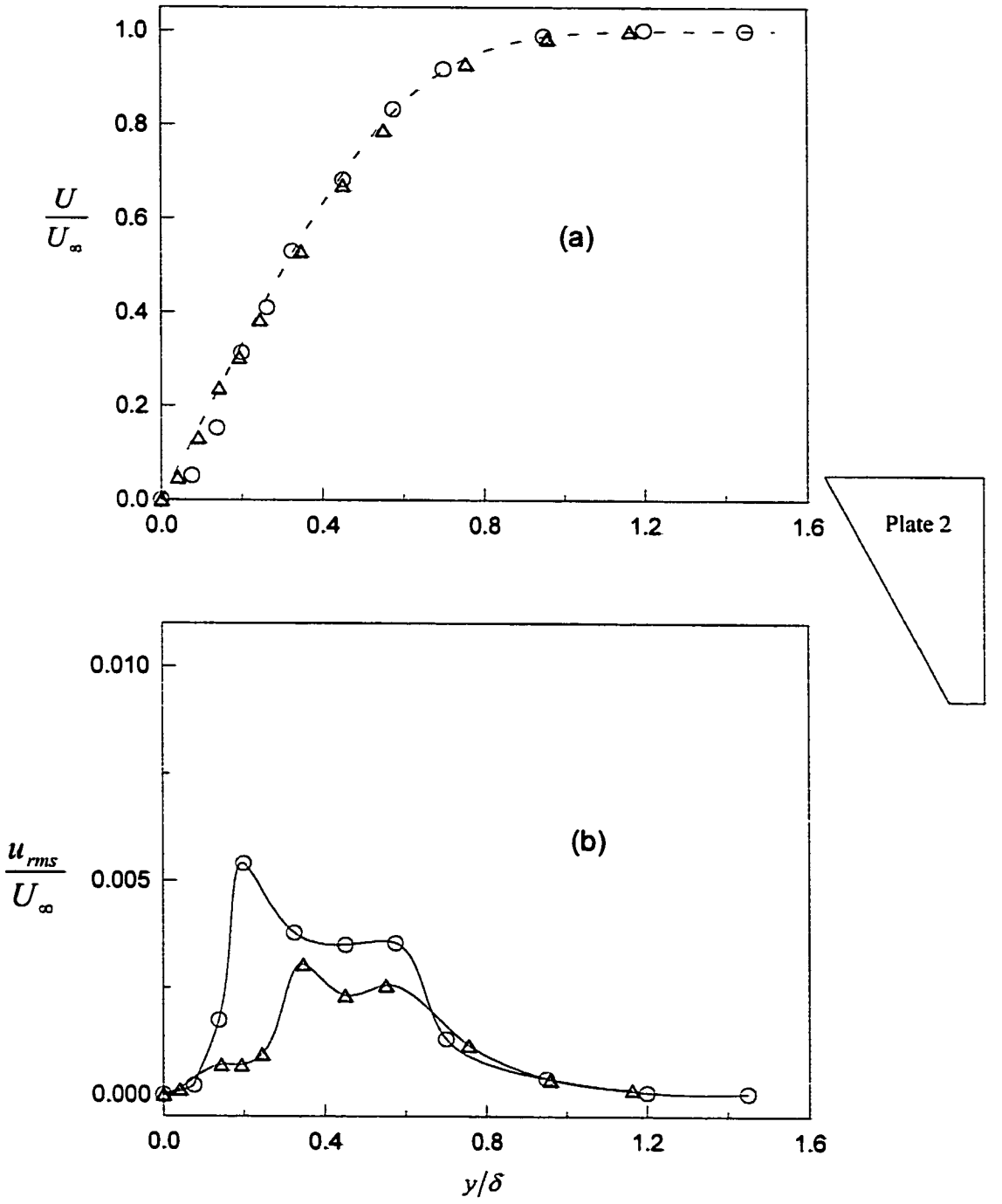

Figure 4.2. Boundary layer profile at the trailing edge of plate 2 for $U_\infty = 10 m/s$. (a) normalized mean velocity; (b) normalized longitudinal fluctuation intensity.
Δ upper surface; O lower surface; ------ Blasius profile.

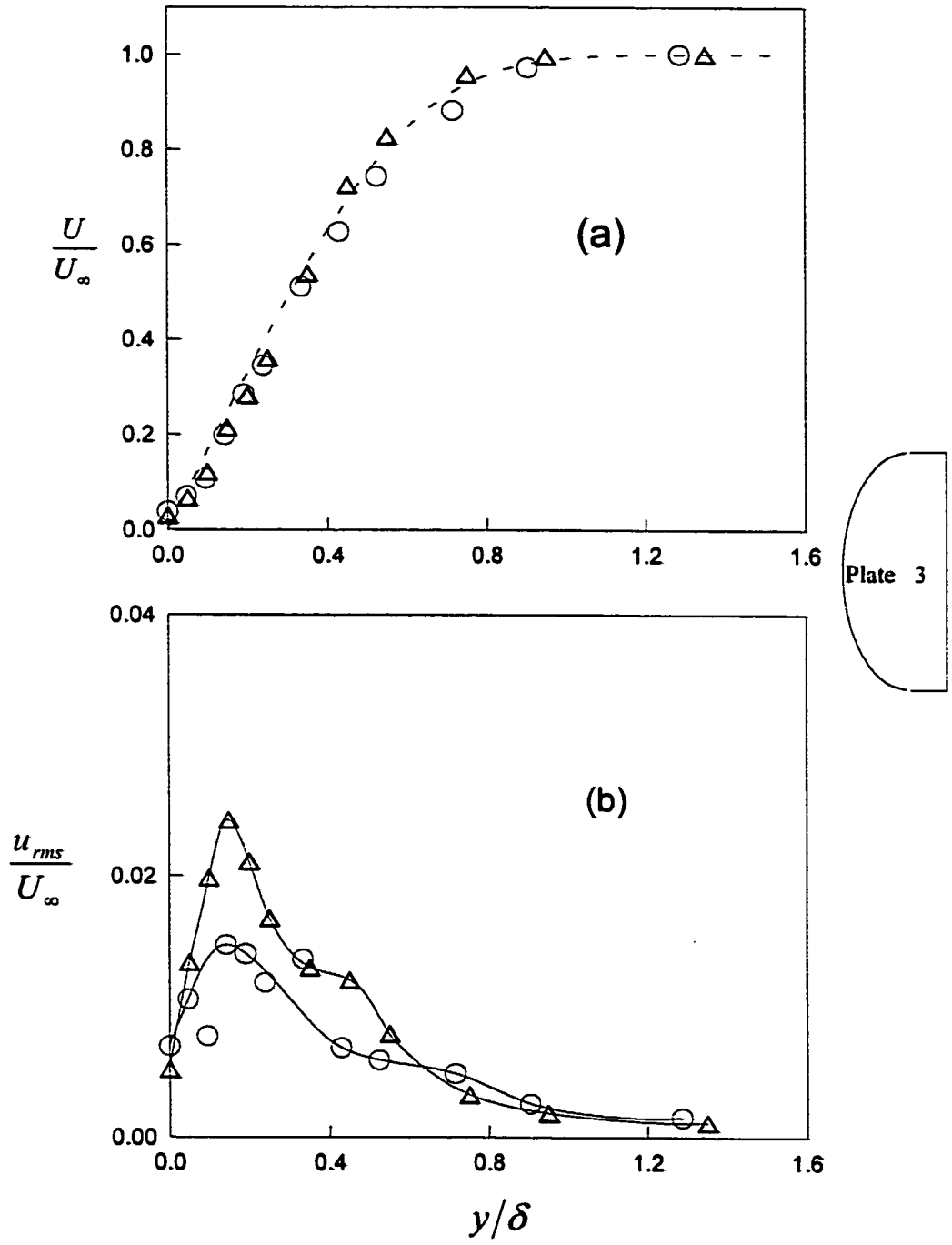

Figure 4.3. Boundary layer profile at the trailing edge of plate 3 for $U_\infty = 10 m/s$. (a) normalized mean velocity; (b) normalized longitudinal fluctuation intensity.
Δ upper surface; O lower surface; ------ Blasius profile.

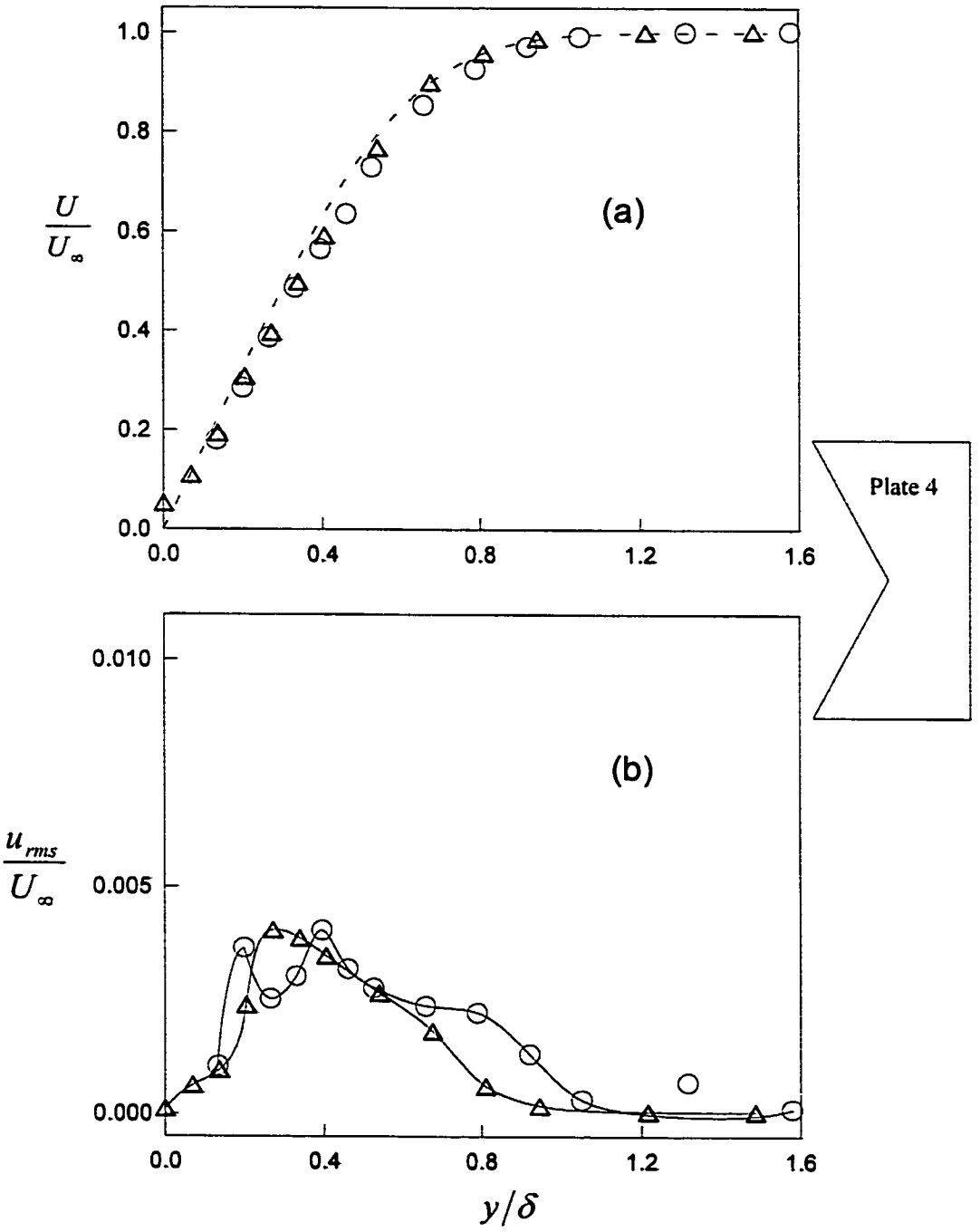

Figure 4.4. Boundary layer profile at the trailing edge of plate 4 for $U_\infty = 10 m/s$. (a) normalized mean velocity; (b) normalized longitudinal fluctuation intensity.
Δ upper surface; O lower surface; ------ Blasius profile.

value of u_{rms} for plate 3 could be due to some defects on the surfaces of the plate. Though these defects could not be detected visually, they could cause some perturbations in the flow. However, the perturbations were not strong enough to trip the boundary layer and effect transition to turbulence. The boundary layer properties for plates 1, 2 and 4 are almost identical in every respect. A summary of the boundary layer parameters corresponding to the data of figures 4.1 – 4.4 is shown in Table 4.1. The values quoted represent the averages for the two sides of the plates. Measurements of the boundary layer at $U_\infty = 7.5\,m/s$ were not taken since it has been confirmed that the boundary layer is laminar at $U_\infty = 10\,m/s$ for all the plates.

The boundary layer data were taken at the mid-span position $(z = 0)$. All wake results to be presented are for this section except for the two-dimensionality checks in which measurements were made at $z/d = -20, 0, and +20$, where d is the plate thickness (6 *mm*).

4.2 The Near Wake

The near wake is the region immediately following the trailing edge. Measurements were taken for plates 1, 2 and 4 in this region. The mean velocity distribution in the near wake of plate 1 is presented in figure 4.5. It shows that the wake experiences a rapid growth, with the flow attaining a centerline velocity of about

Table 4.1 The Parameters for the Boundary layer at the trailing edge at $U_\infty = 10 m/s$

	Plate 1	Plate 2	Plate 3	Plate 4
δ (*mm*)	1.58	1.60	1.83	1.39
θ (*mm*)	0.59	0.59	0.68	0.52
H	2.68	2.74	2.69	2.67

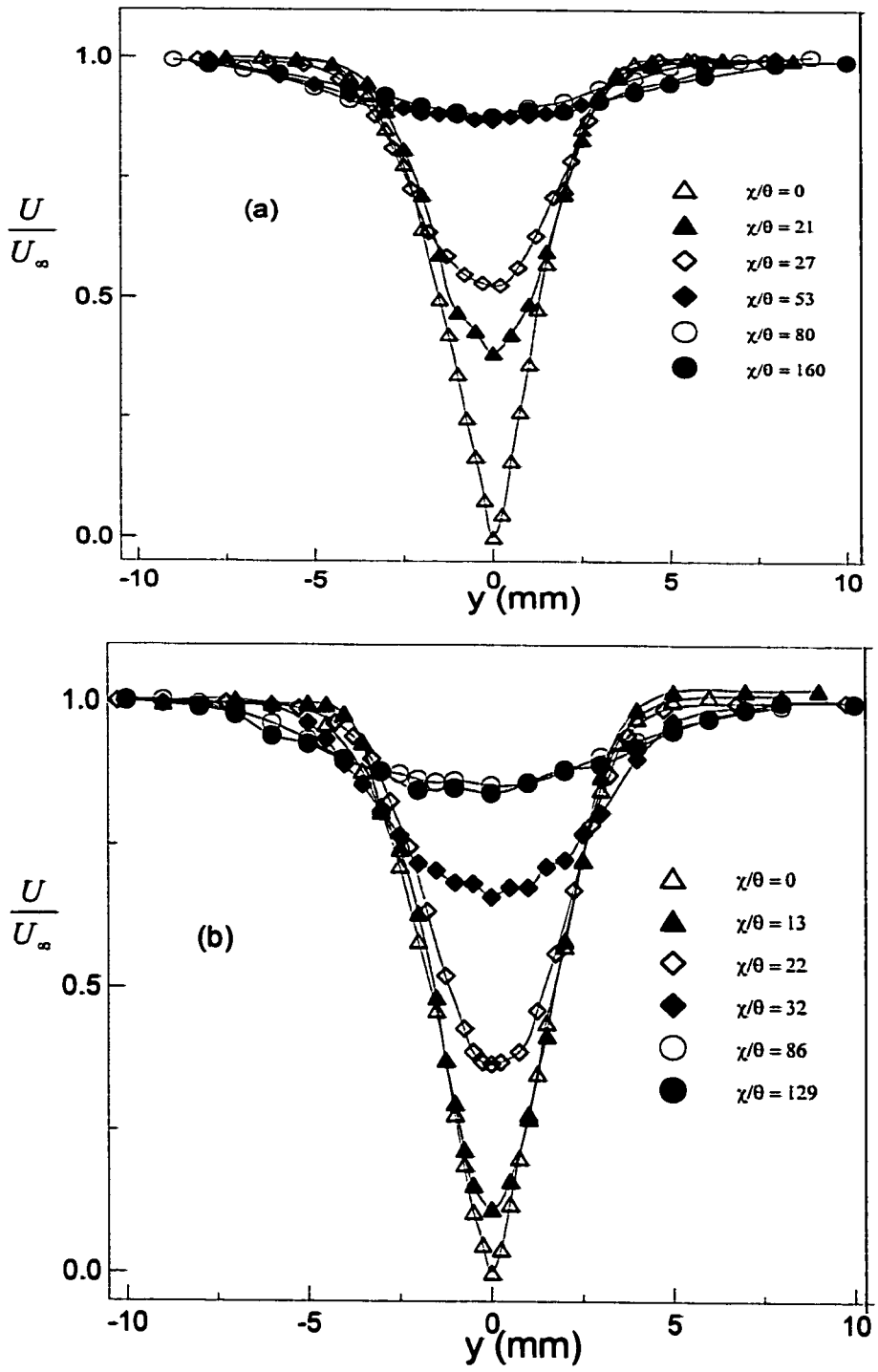

Figure 4.5. Distribution of the mean velocity in the near wake of plate 1. (a) $U_\infty = 10 m/s$, (b) $U_\infty = 7.5 m/s$.

87% of its freestream value within a streamwise distance of 100 momentum thicknesses from the trailing edge. Also in this region, there is a rapid increase of the peak r.m.s. values of the streamwise and normal components of the velocity fluctuations as well as the Reynolds shear stress. This is followed by a rapid fall of their peak values, as shown in figures 4.6 – 4.8. Sato and Kuriki [17] reported a similar trend for u_{rms}. In addition, it is observed that the fall of the peak value of $\overline{u^2}$ is accompanied by the gradual merging of the two peaks in the profile to a single peak. The two peaks observed near the trailing edge are a result of the two separate boundary layers that merged to form the wake. The transformation of the two peaks to a single peak can be attributed to the merger of the two shear layers. Distributions similar to those of plate 1 were also obtained for plates 2 and 4 and their data are presented in figures 4.9 – 4.16.

The question may be asked of whether one can compare the growth rates in the near wake for the three plates. However, such comparison may be misleading here in view of the extremely rapid growths. The location of the probe in the downstream direction was done manually using a common measuring rule. Therefore, the error in measurement of the distance from the trailing edge was up to 0.5mm. The wake experiences a rapid growth in the near wake and the change within a distance of 0.5 mm is big enough to cast doubt on any comparison of the three plates in this region. The far wake, on the other hand, does not suffer from this problem, as the downstream evolution of the wake is very slow.

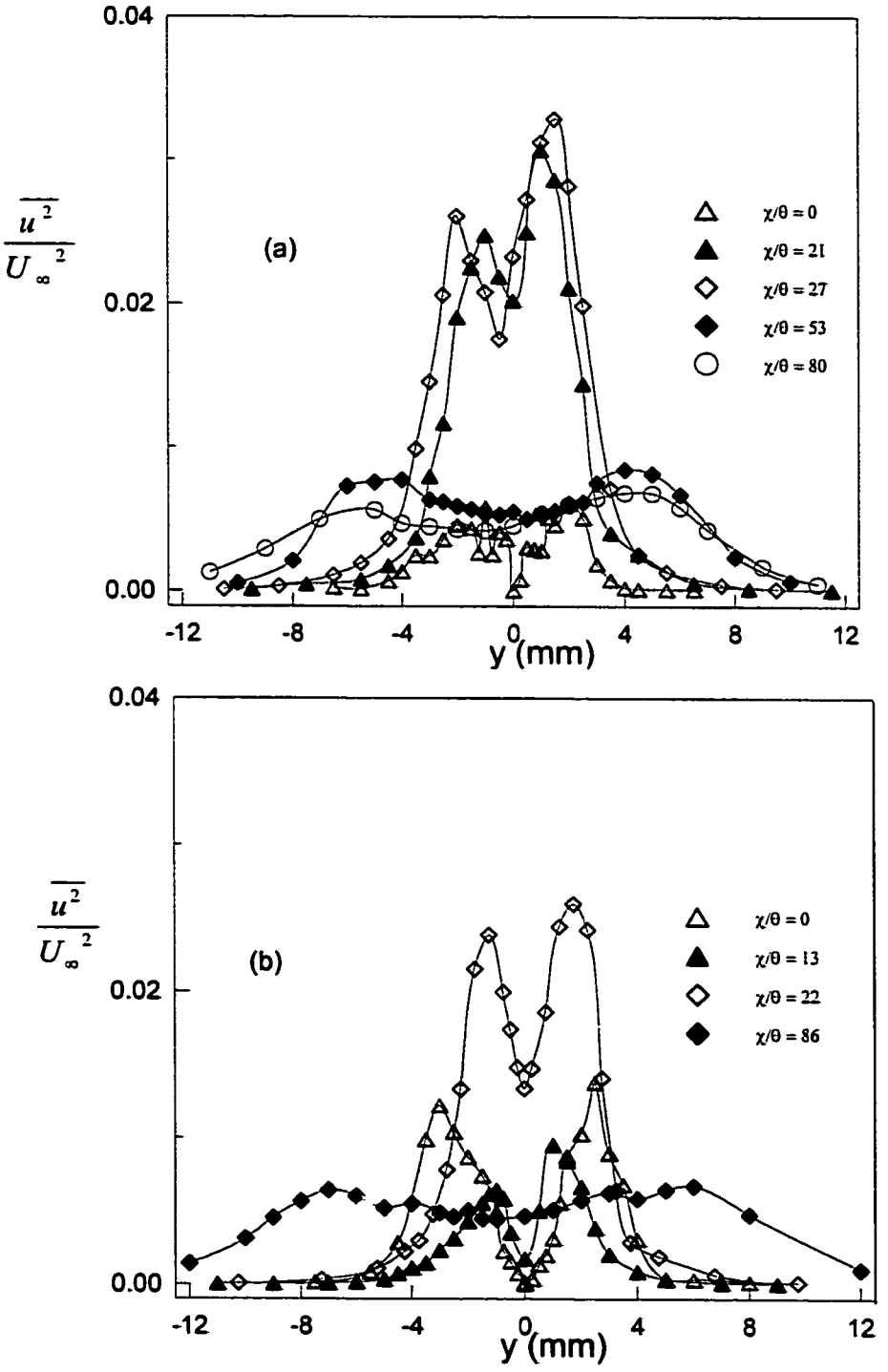

Plate 1

Figure 4.6. Distribution of the streamwise component of velocity fluctuations in the near wake of plate 1.
(a) $U_\infty = 10 m/s$, (b) $U_\infty = 7.5 m/s$.

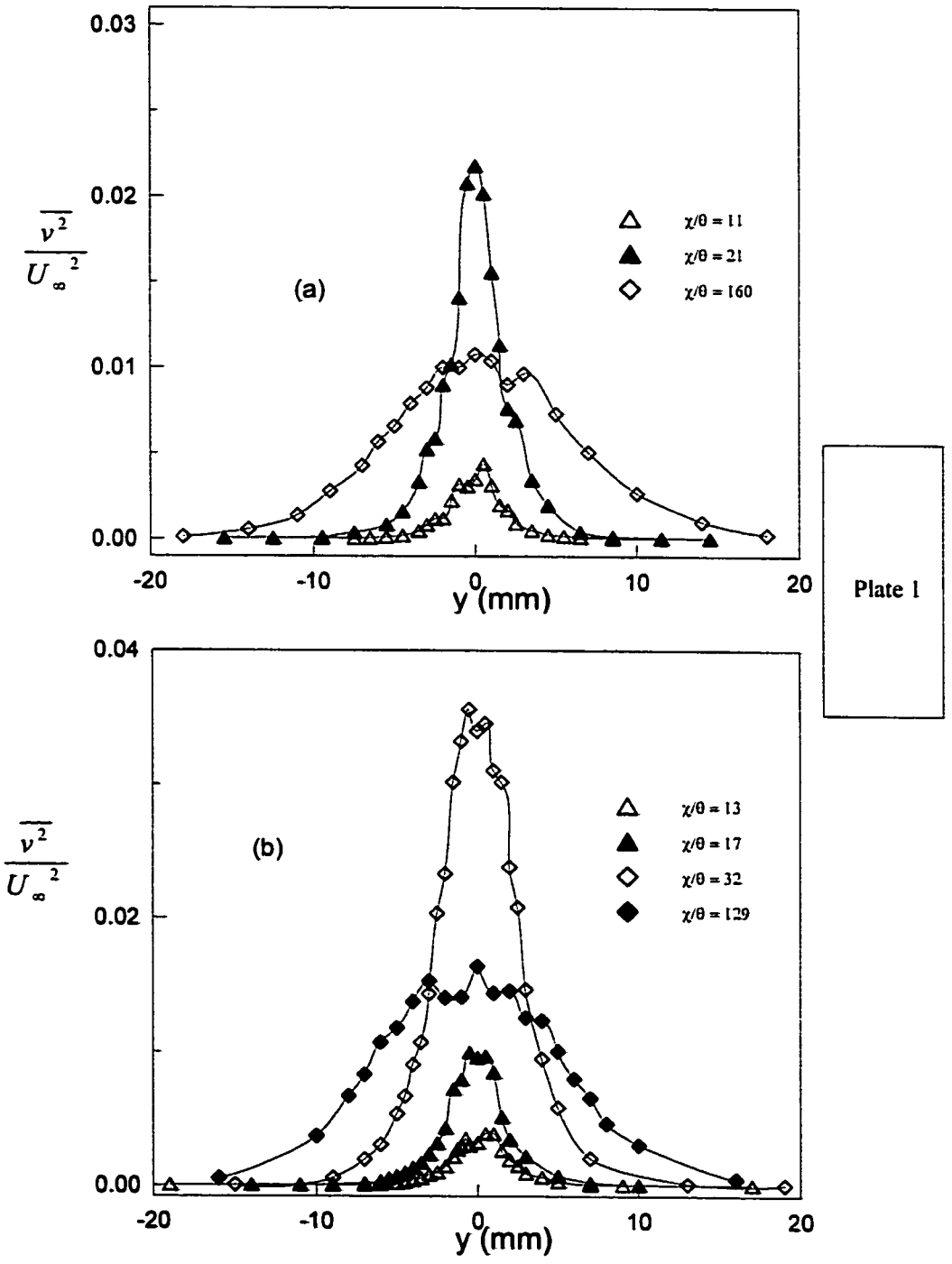

Figure 4.7. Distribution of the normal component of velocity fluctuations in the near wake of plate 1.
(a) $U_\infty = 10 m/s$, (b) $U_\infty = 7.5 m/s$.

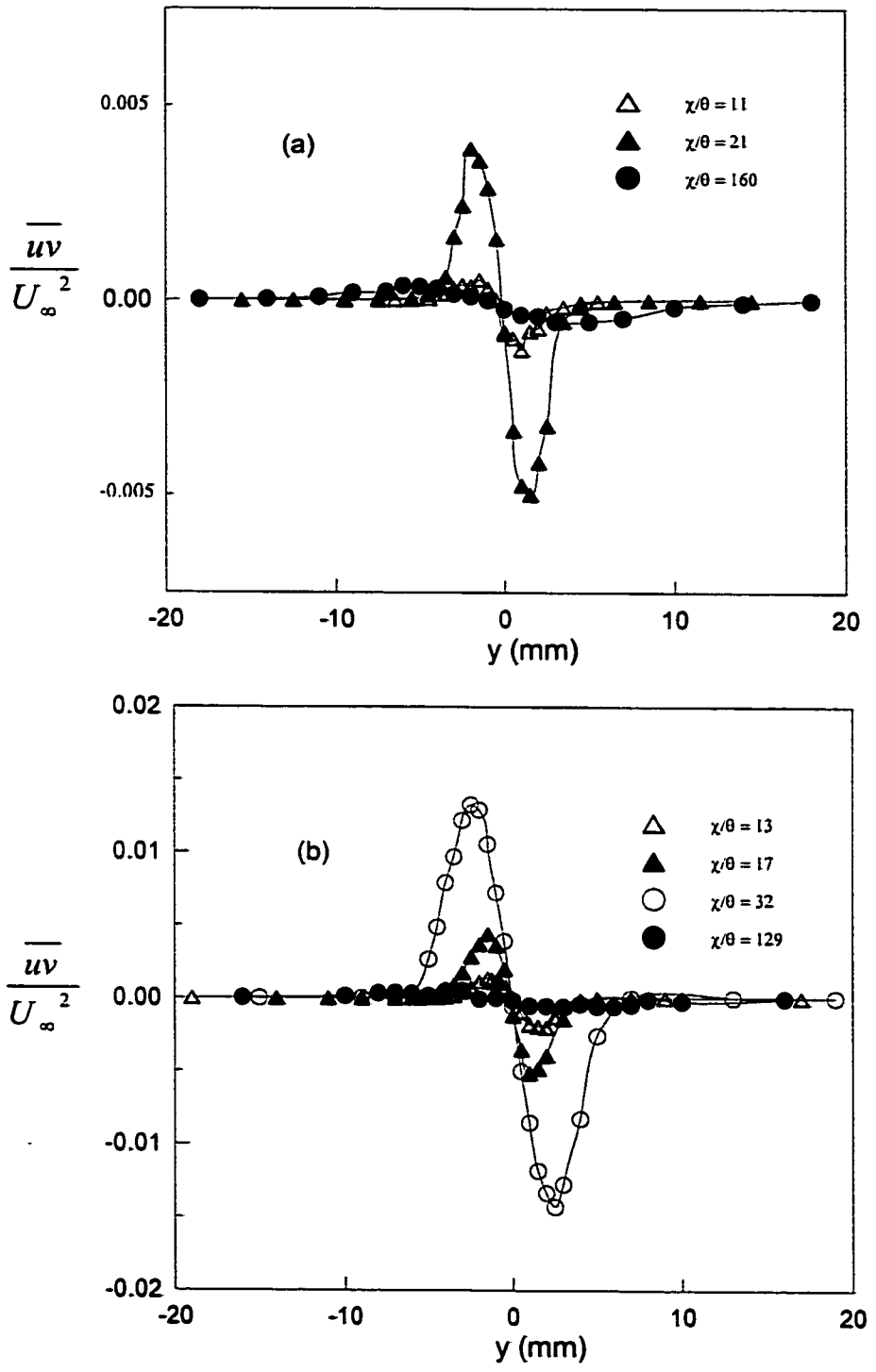

Figure 4.8. Distribution of the Reynolds shear stress in the near wake of plate 1. (a) $U_\infty = 10 m/s$, (b) $U_\infty = 7.5 m/s$.

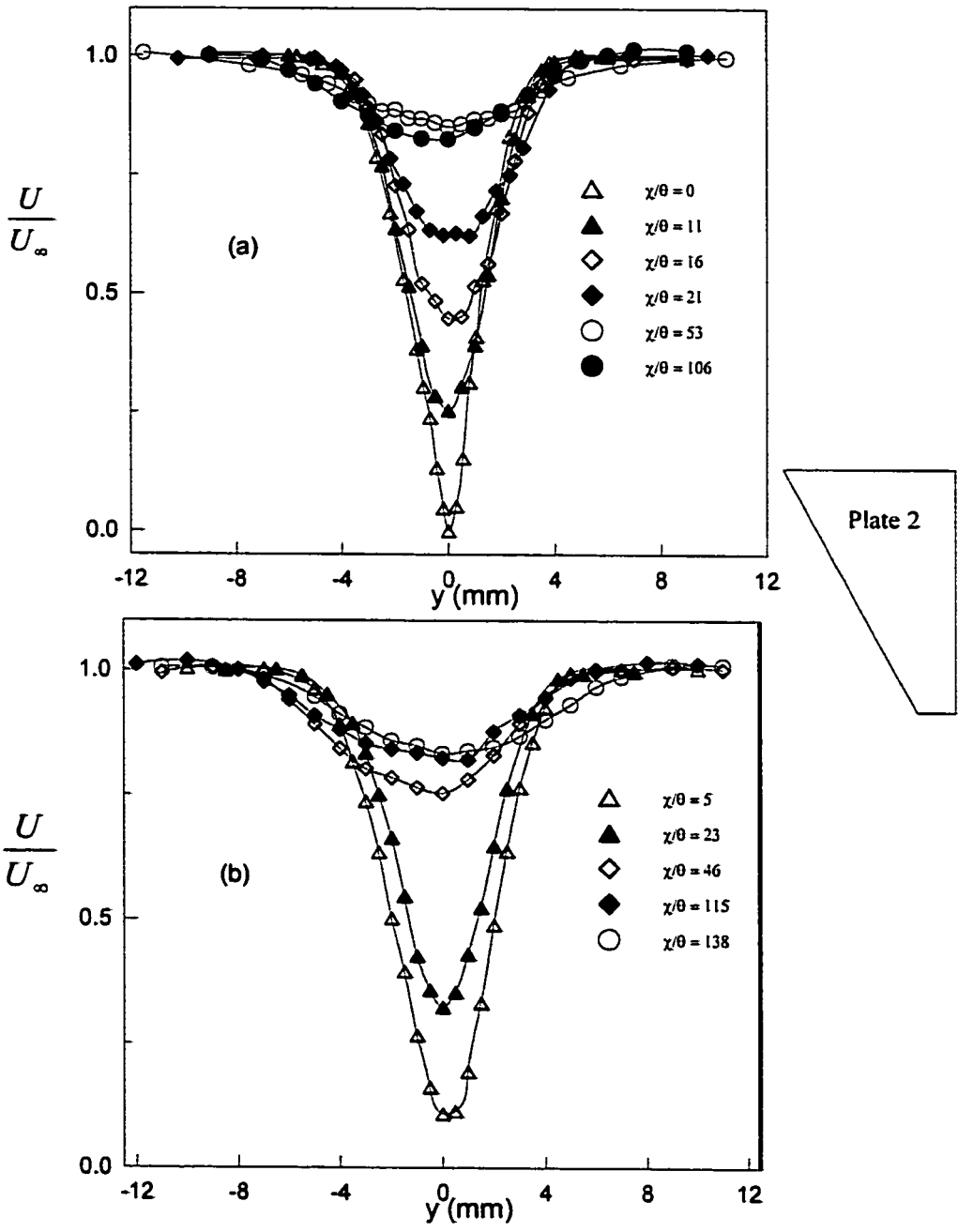

Figure 4.9. Distribution of the mean velocity in the near wake of plate 2. (a) $U_\infty = 10 m/s$, (b) $U_\infty = 7.5 m/s$.

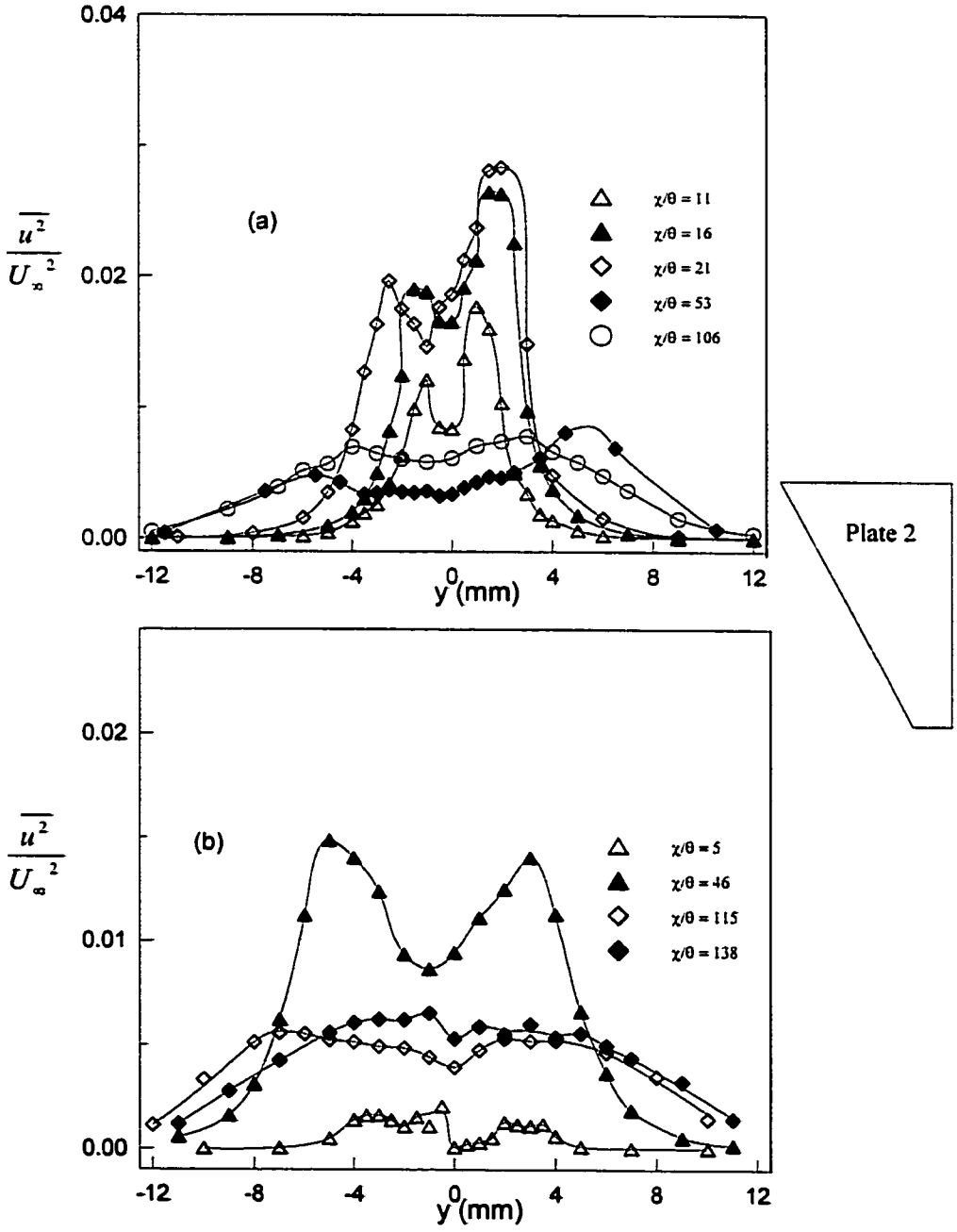

Figure 4.10. Distribution of the streamwise component of velocity fluctuations in the near wake of plate 2.
(a) $U_\infty = 10 m/s$, (b) $U_\infty = 7.5 m/s$.

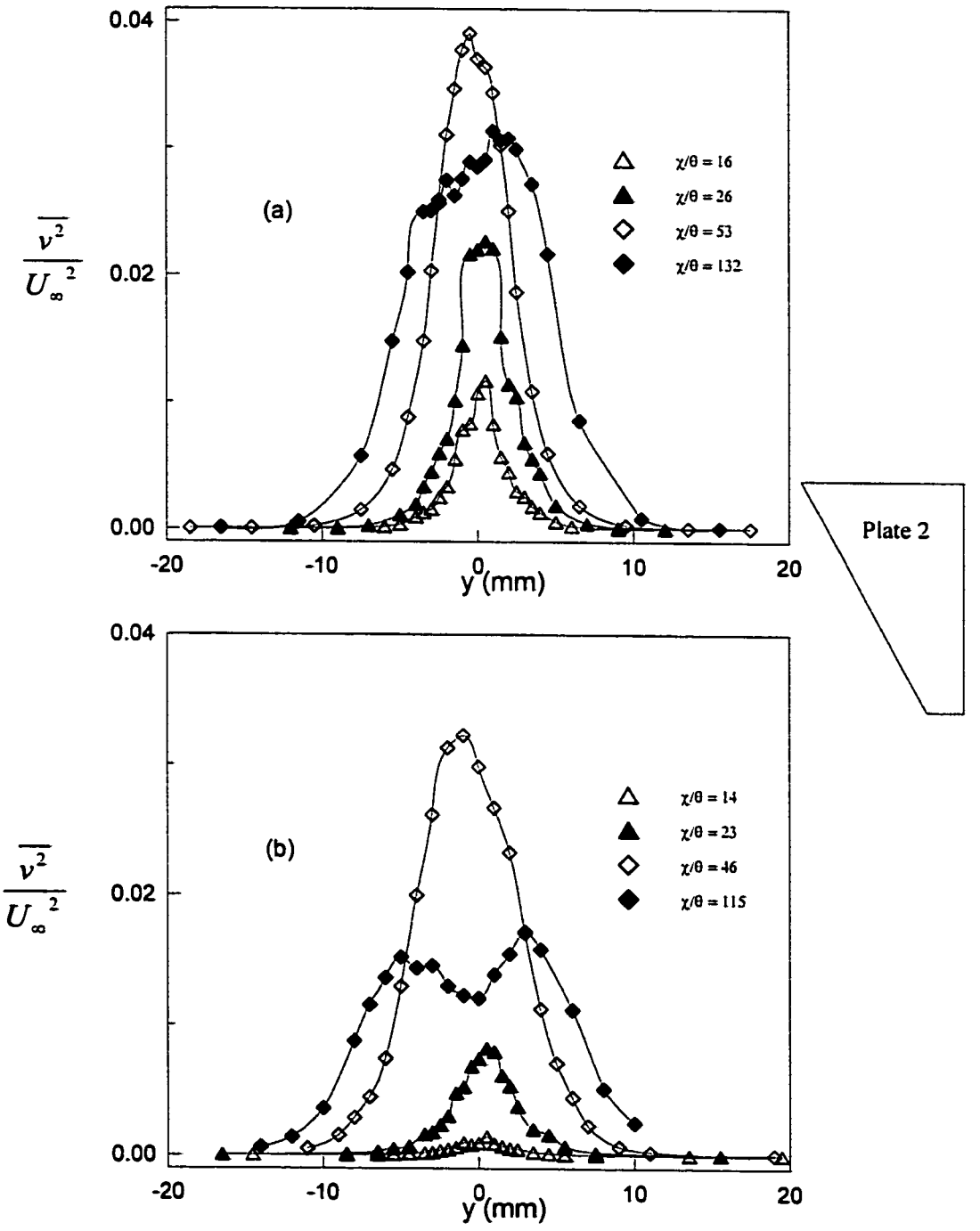

Figure 4.11. Distribution of the normal component of velocity fluctuations in the near wake of plate 2.
(a) $U_\infty = 10 m/s$, (b) $U_\infty = 7.5 m/s$.

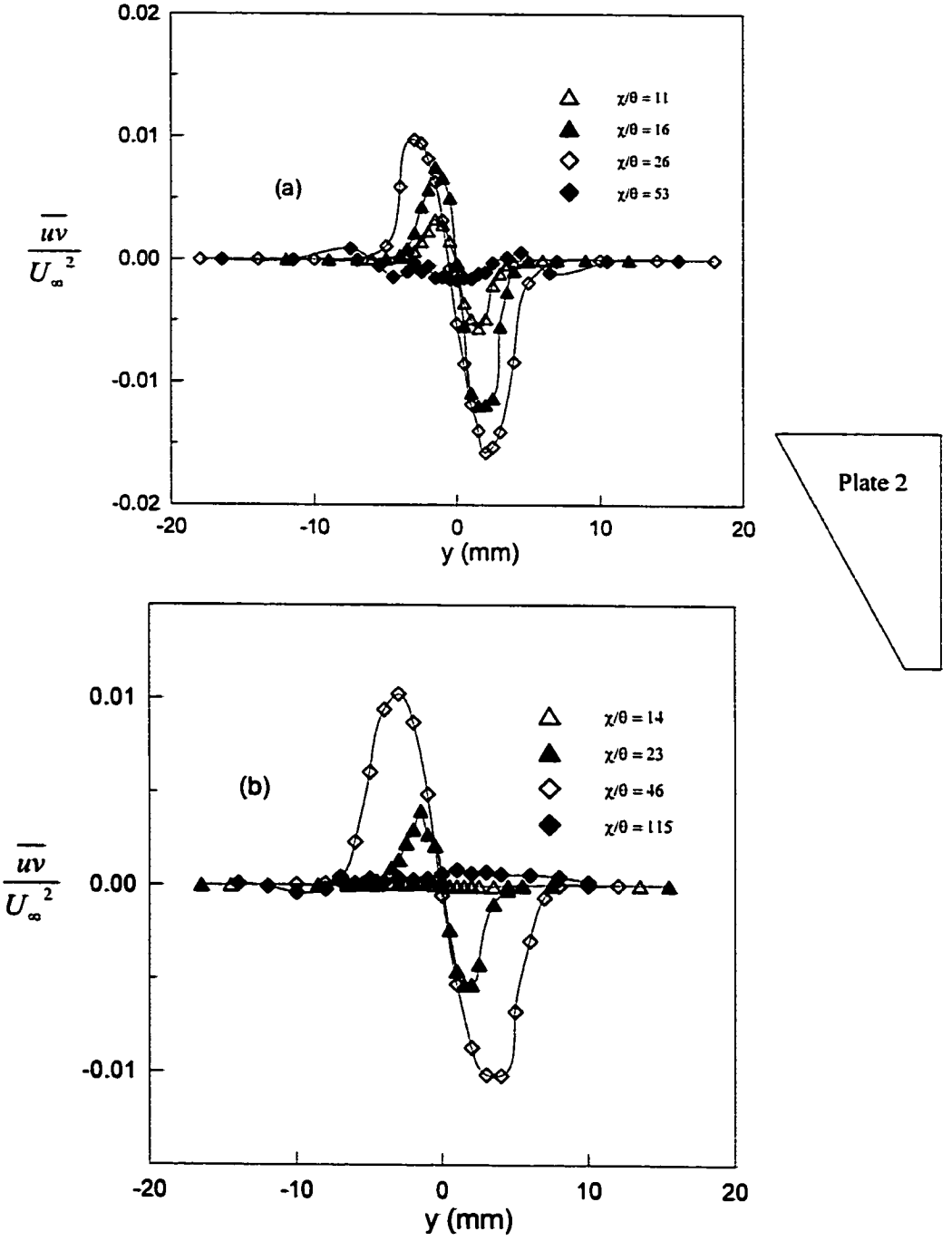

Figure 4.12. Distribution of the Reynolds shear stress in the near wake of plate 2. (a) $U_\infty = 10 m/s$, (b) $U_\infty = 7.5 m/s$.

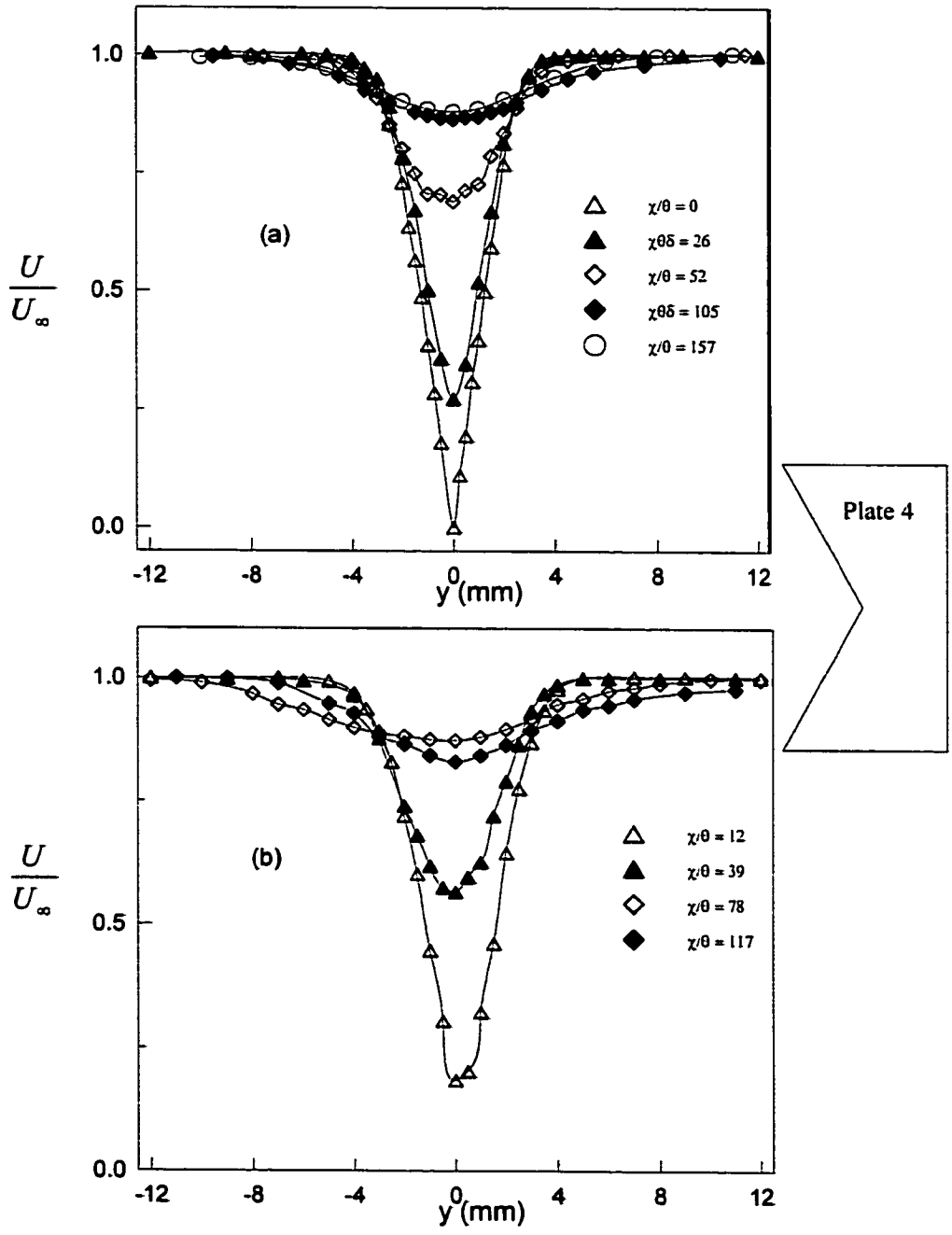

Figure 4.13. Distribution of the mean velocity in the near wake of plate 4. (a) $U_\infty = 10 m/s$, (b) $U_\infty = 7.5 m/s$.

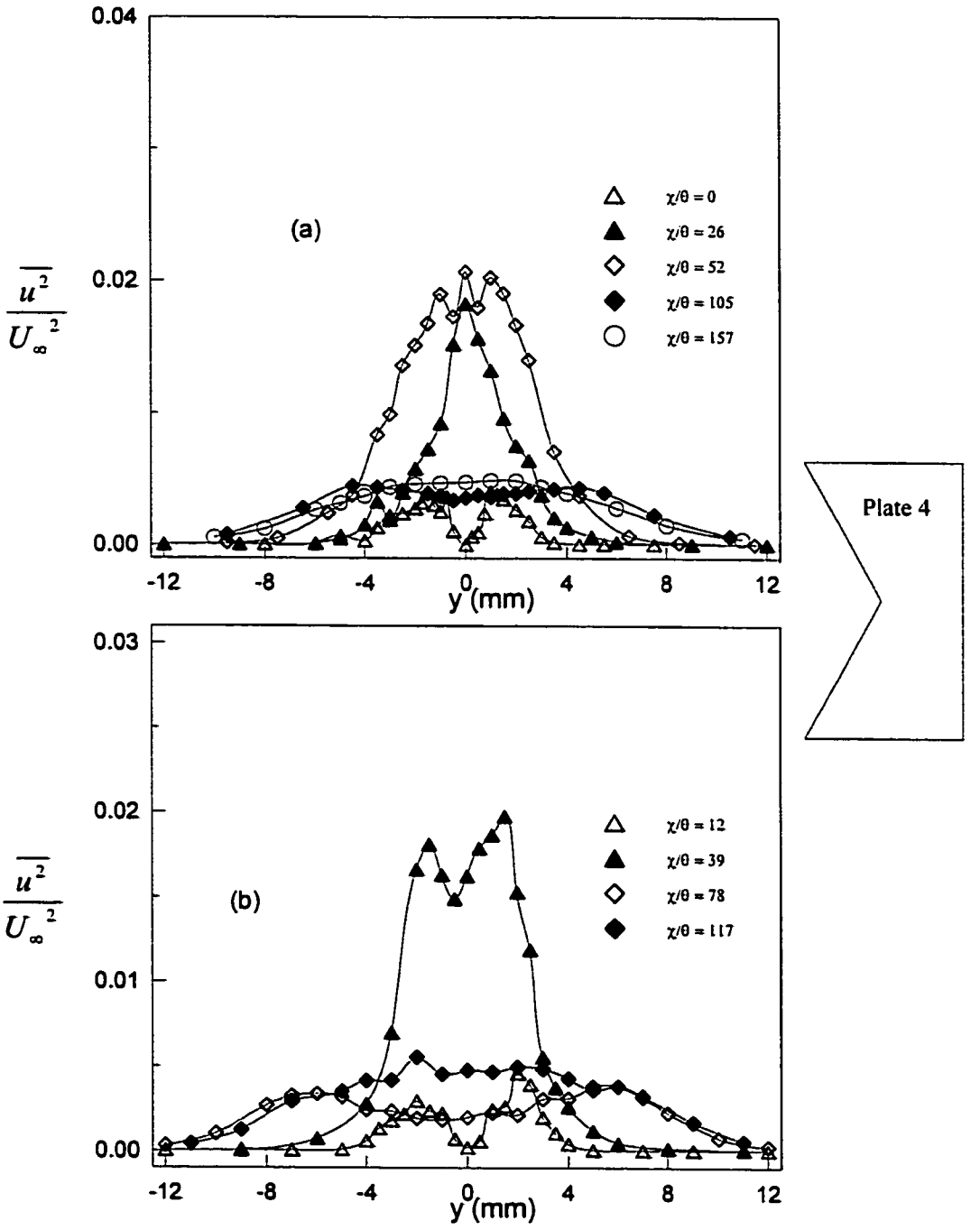

Figure 4.14. Distribution of the streamwise component of velocity fluctuations in the near wake of plate 4.
(a) $U_\infty = 10 m/s$, (b) $U_\infty = 7.5 m/s$.

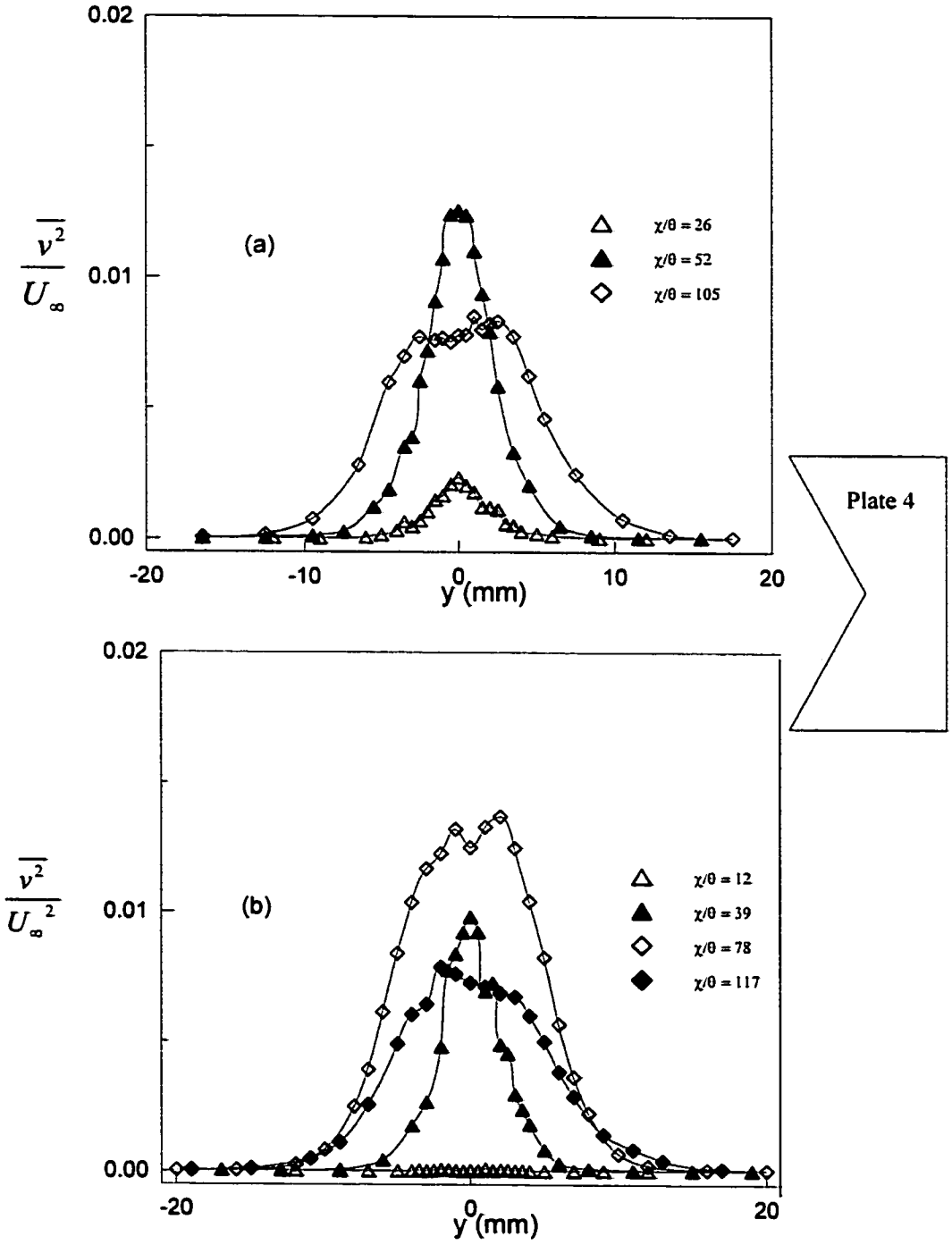

Figure 4.15. Distribution of the normal component of velocity fluctuations in the near wake of plate 4.
(a) $U_\infty = 10 m/s$, (b) $U_\infty = 7.5 m/s$.

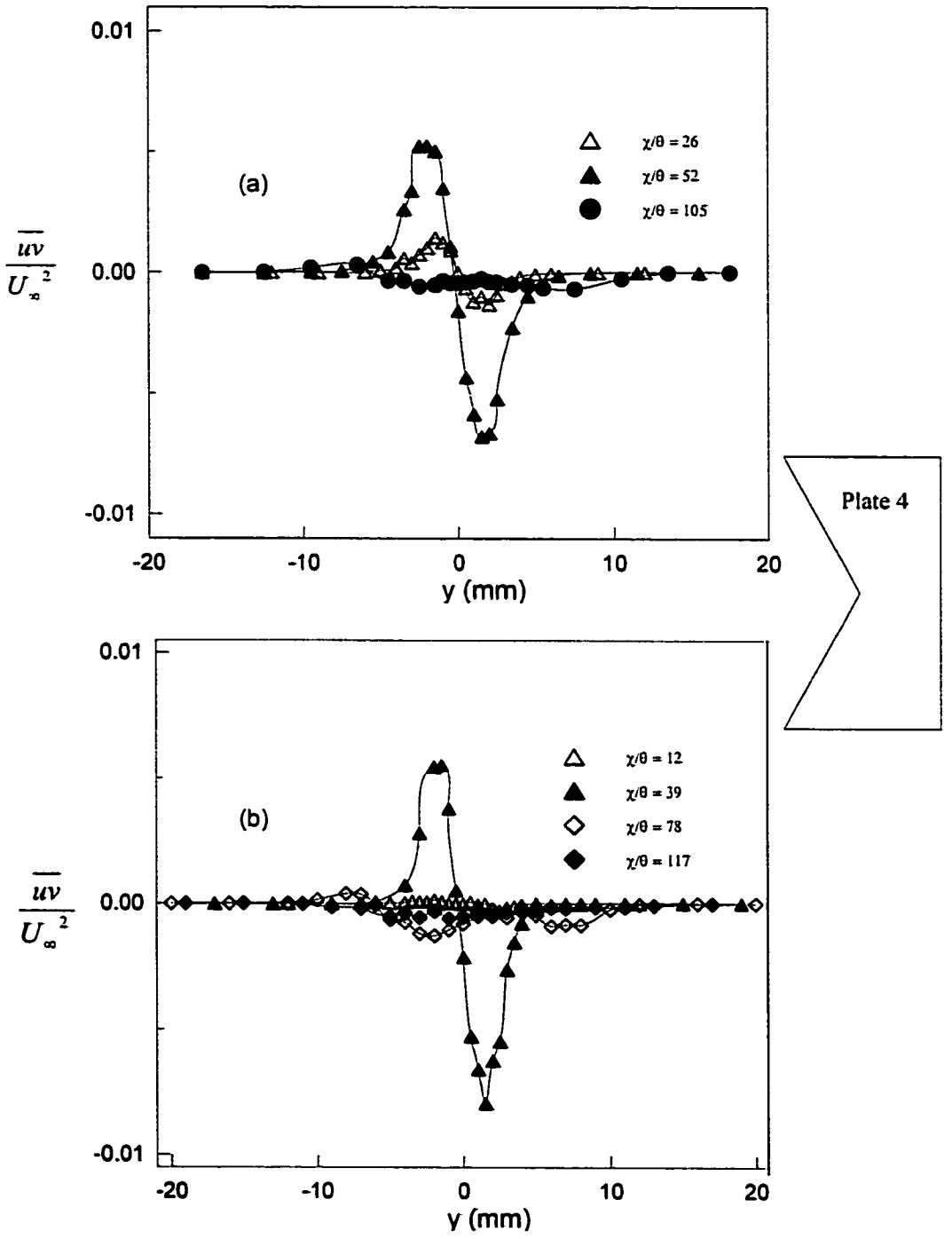

Figure 4.16. Distribution of the Reynolds shear stress in the near wake of plate 4. (a) $U_\infty = 10\,m/s$, (b) $U_\infty = 7.5\,m/s$.

4.3 The Far Wake

Measurements were taken in the far wakes of the four plates up to a downstream distance of about 1000 momentum thicknesses for each case. The range of distance covered was dictated by the attainment of self-similarity of the wakes. The results are presented in similarity coordinates according to equations *(2.1)* to *(2.11)* of chapter 2.

The streamwise developments of the important integral parameters in the wakes of the four plates are shown in figures 4.17-4.20. These parameters are the displacement thickness δ $(= \int_{-\infty}^{\infty} [1 - U/U_{\infty}] dy)$, the momentum thickness (defined in equation 2.9) and the shape factor H $(= \delta/\theta)$. From figure 4.17 it is observed that the momentum thickness remains essentially constant (within $\pm 5\%$) along the wake of plate 1, except in the region very close to the trailing edge where there is a jump. The jump near the trailing edge is the effect of the finite thickness of the trailing edge, and hence possible local flow separation. The displacement thickness is observed to have a gradual reduction of its value until it attains about the same value as the momentum thickness. This gives the shape factor a value of unity in the far wake. Chevray and Kovasznay [25] and Ramaprian et al [12] obtained similar trends in the distribution of the three integral parameters. In the case of plate 2 (figure 4.18) the momentum thickness shows significant variation in value up to a downstream distance of about

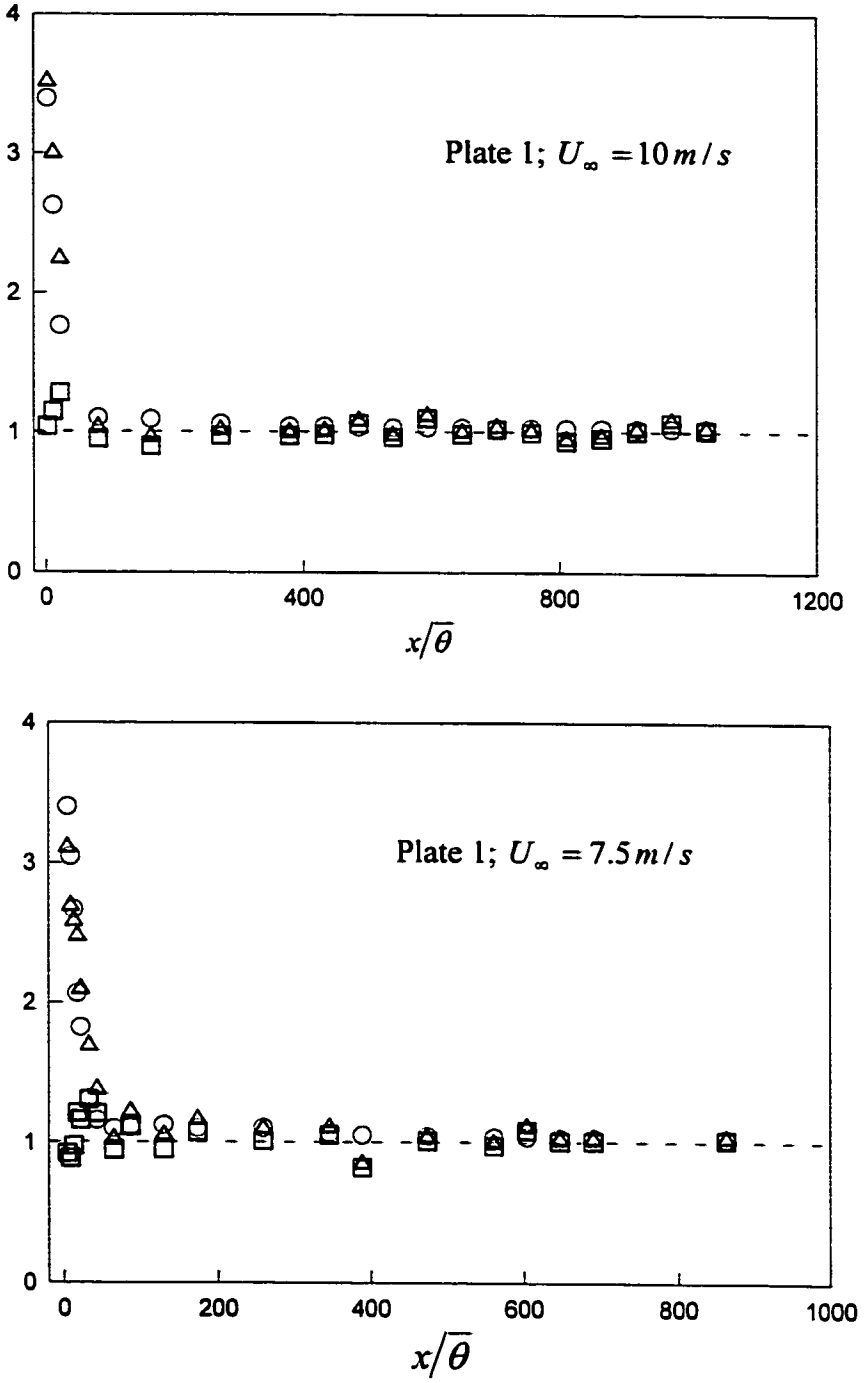

Plate 1

Figure 4.17. Integral parameters along the wake. Δ for $\delta/\overline{\theta}$, displacement thickness normalized by $\overline{\theta}$; □ for $\theta/\overline{\theta}$, momentum thickness normalized by $\overline{\theta}$; O for $H = \delta/\theta$, shape factor. $\overline{\theta}$ is the average momentum thickness in the self-preserving region.

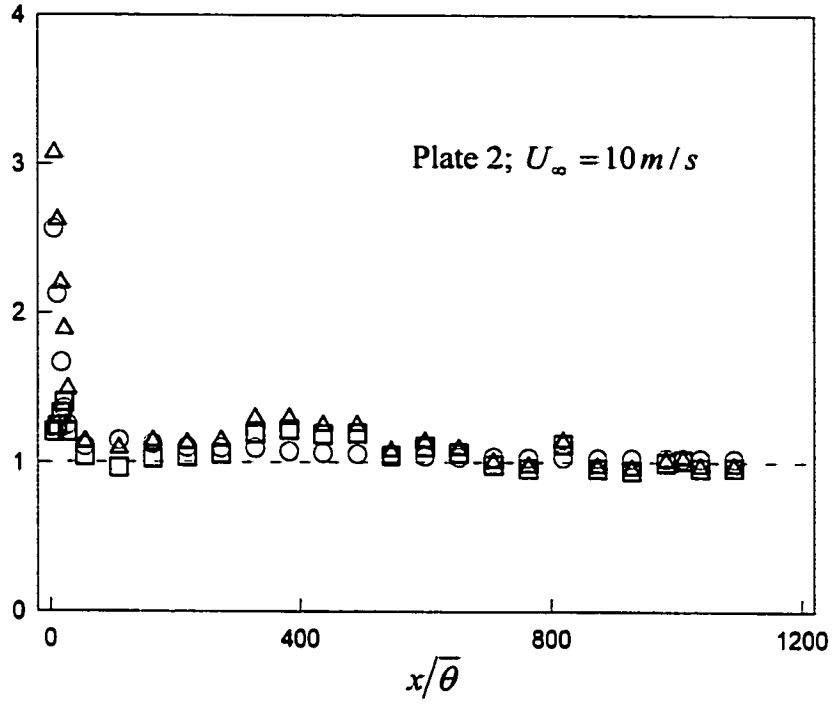

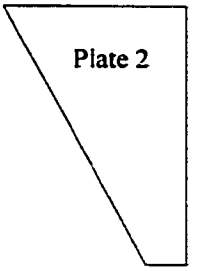

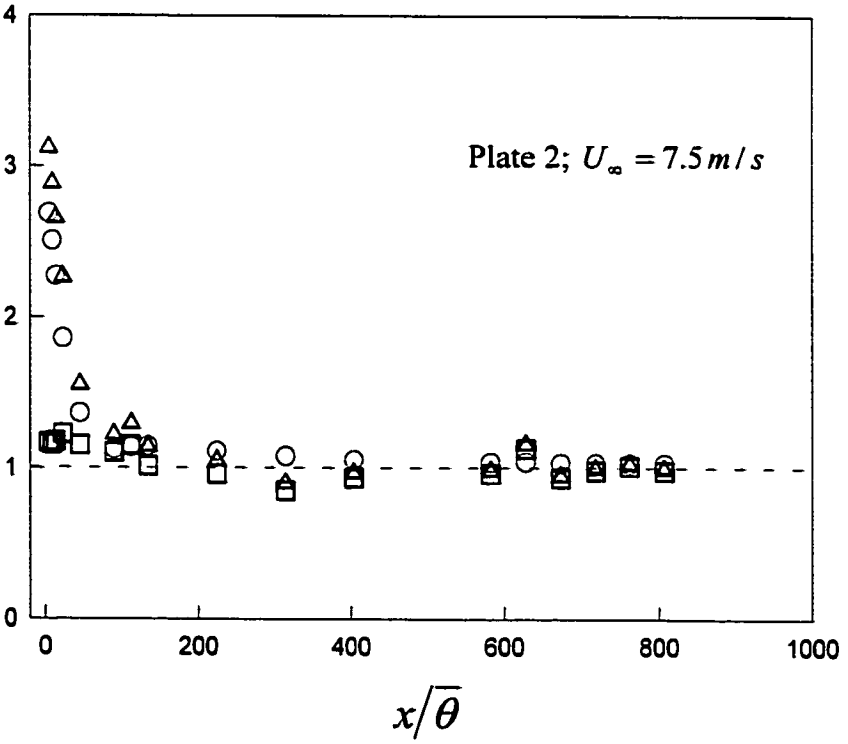

Figure 4.18. For caption and symbols see figure 4.17.

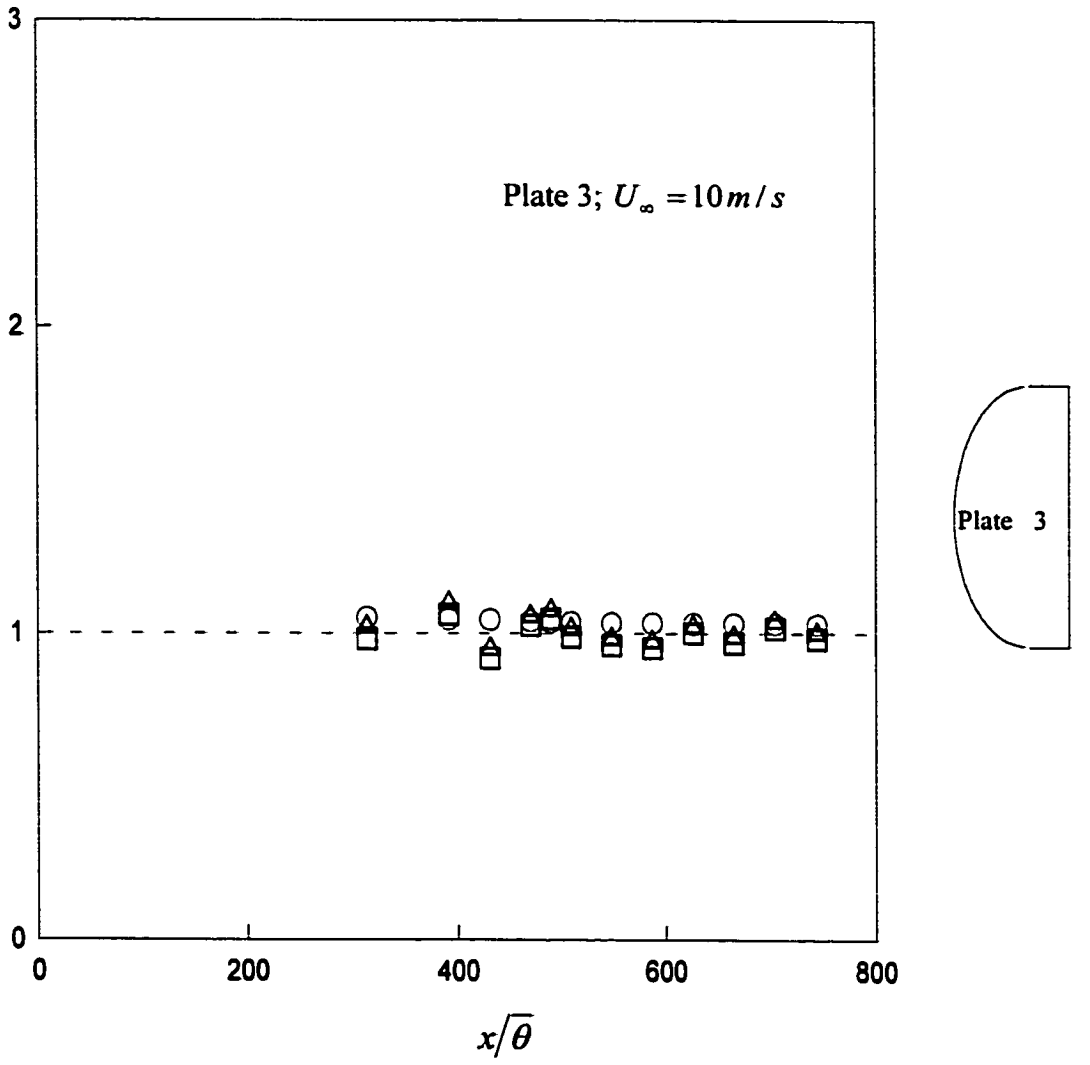

Figure 4.19. For caption and symbols see figure 4.17.

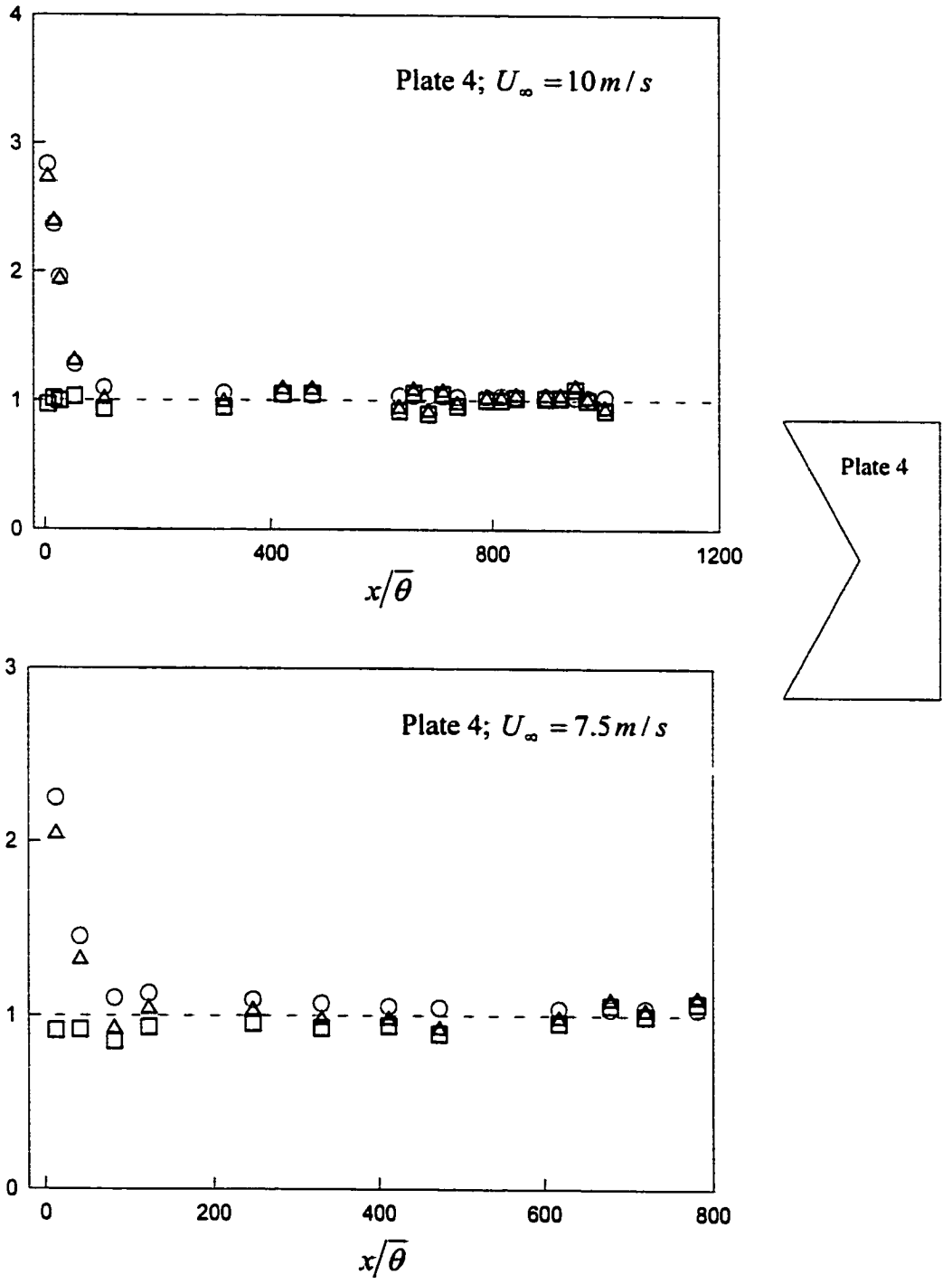

Figure 4.20. For caption and symbols see figure 4.17.

400 momentum thicknesses. This is because the variation of the trailing edge in the spanwise direction creates a three-dimensional velocity field in the immediate vicinity of the trailing edge. The influence of the plate reduces with distance downstream until the flow finally attains a constant momentum thickness. For plate 3, measurements were made only in the far wake and at $U_\infty = 10 m/s$ only. The momentum thickness (figure 4.19) remains essentially constant in the region where measurements were made. This is expected, as there is no significant variation of the trailing edge around the mid-span position of the plate. The trends in the integral parameters for plates 1 and 3 are therefore expected to be similar. The wake of plate 4 appears to attain constant momentum thickness (figure 4.20) faster than that of plate 2 even though plate 4 too has varying trailing edge around its mid-span.

The displacement thickness and momentum thickness in figures 4.17-4.20 are normalized by $\overline{\theta}$, where $\overline{\theta}$ is the average over the values of the momentum thickness at the different locations in the far wake where measurements were made. These are the values used to normalize all distances and lengths in the results presented. These values of $\overline{\theta}$ are presented in Table 4.2 together with other parameters to be discussed. The profiles of the far wake mean velocity defect, expressed in similarity coordinates, are shown in figures 4.21 – 4.24. The solid lines in the figures represent the theoretical asymptotic profile given by equation (2.6). The measured profiles agree quite well with the asymptotic profile, indicating the self-preservation in the mean

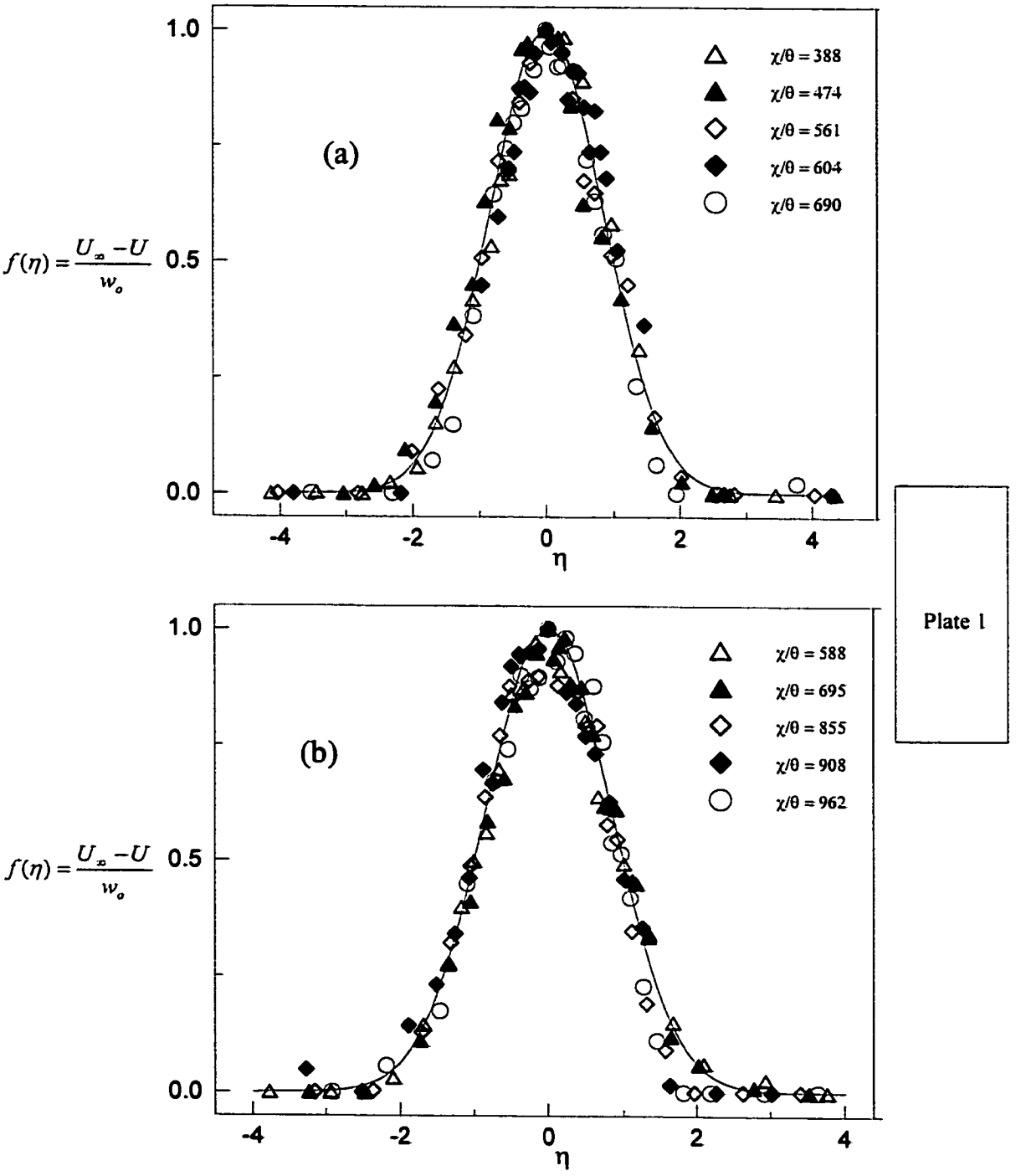

Figure 4.21. Distribution of normalized mean velocity defect in the wake of plate 1 at (a) $U_\infty = 7.5 m/s$ (b) $U_\infty = 10 m/s$.

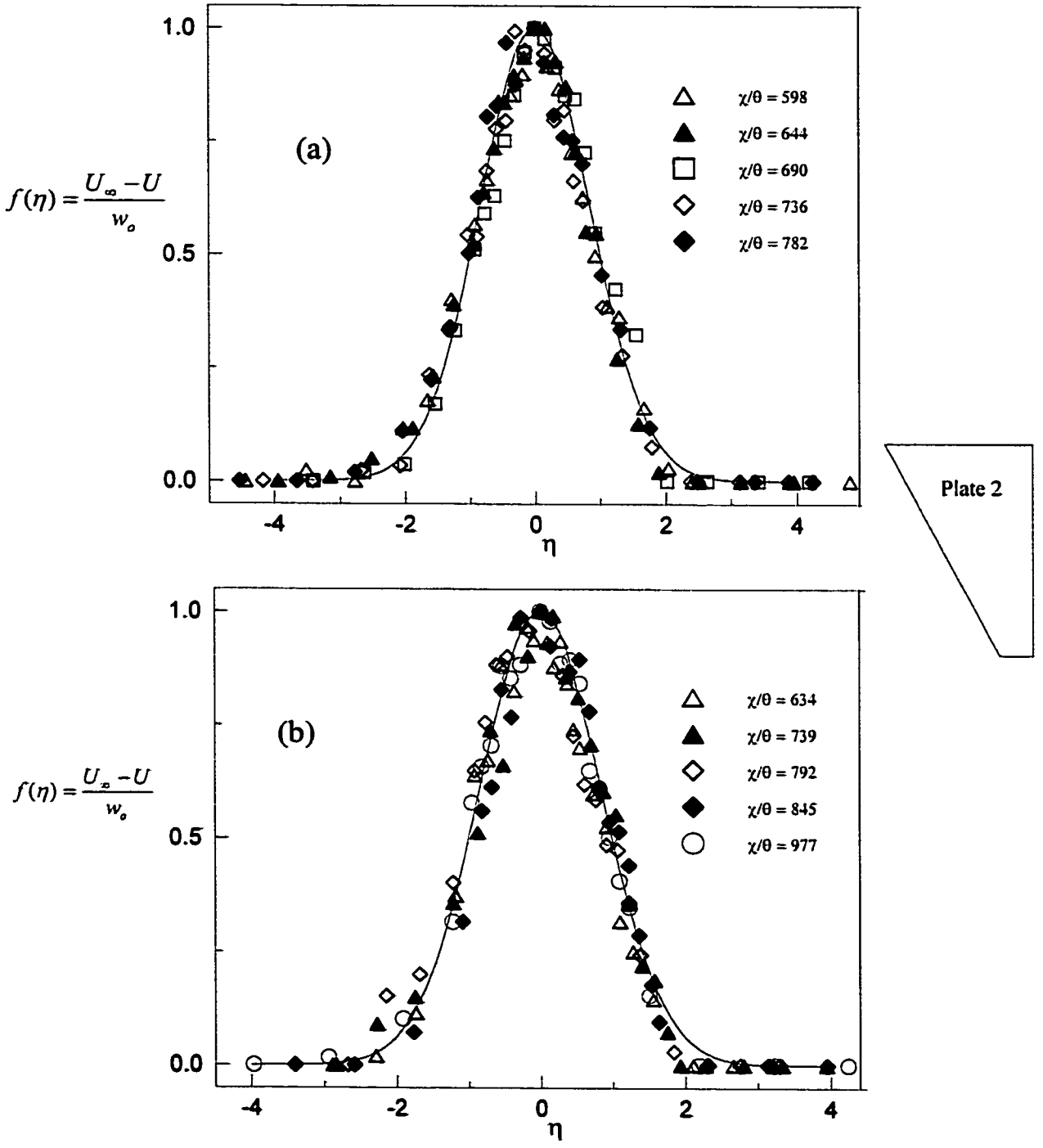

Figure 4.22. Distribution of normalized mean velocity defect in the wake of plate 2 at (a) $U_\infty = 7.5 m/s$ (b) $U_\infty = 10 m/s$.

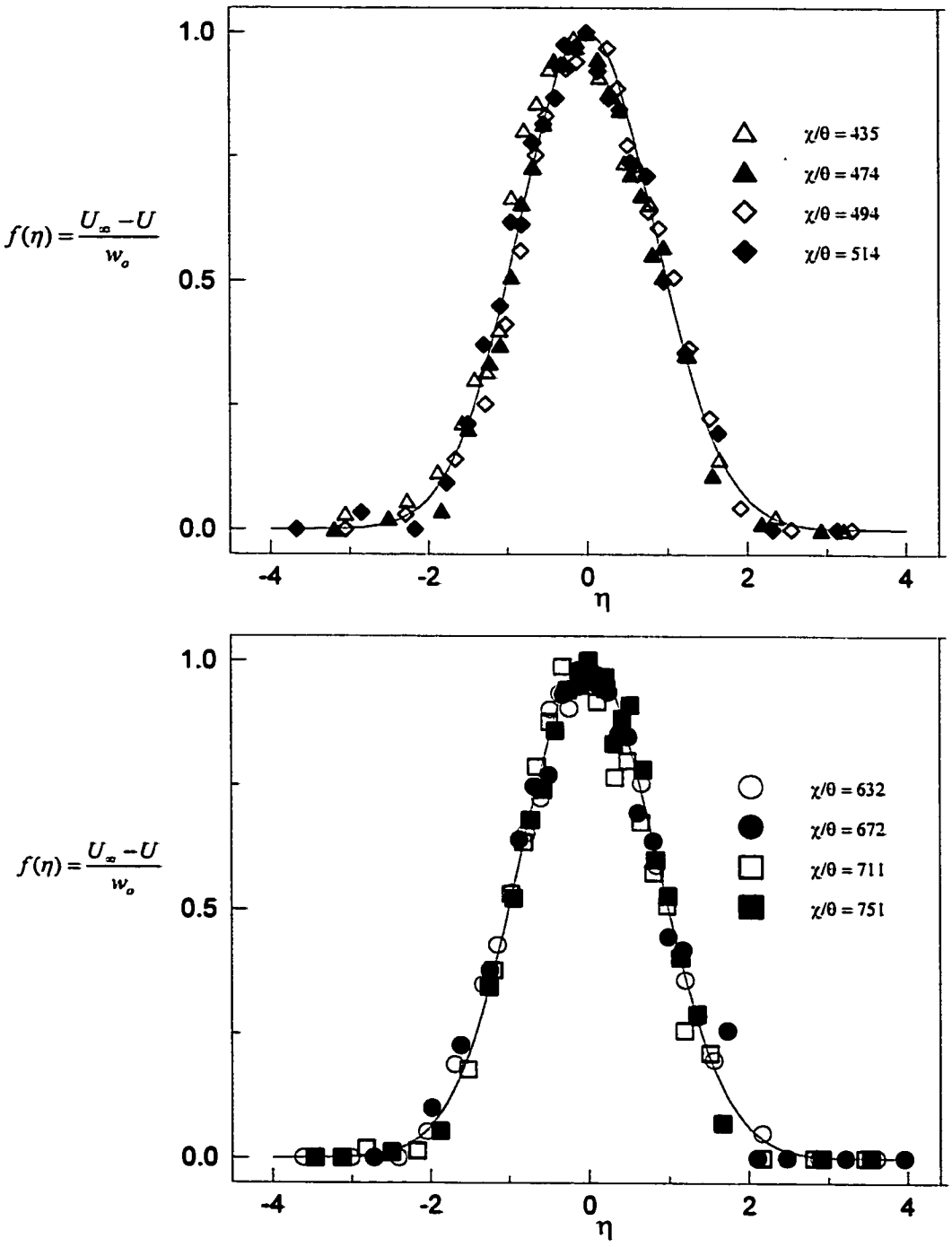

Figure 4.23. Distribution of normalized mean velocity defect in the wake of plate 3 at $U_\infty = 10\,m/s$.

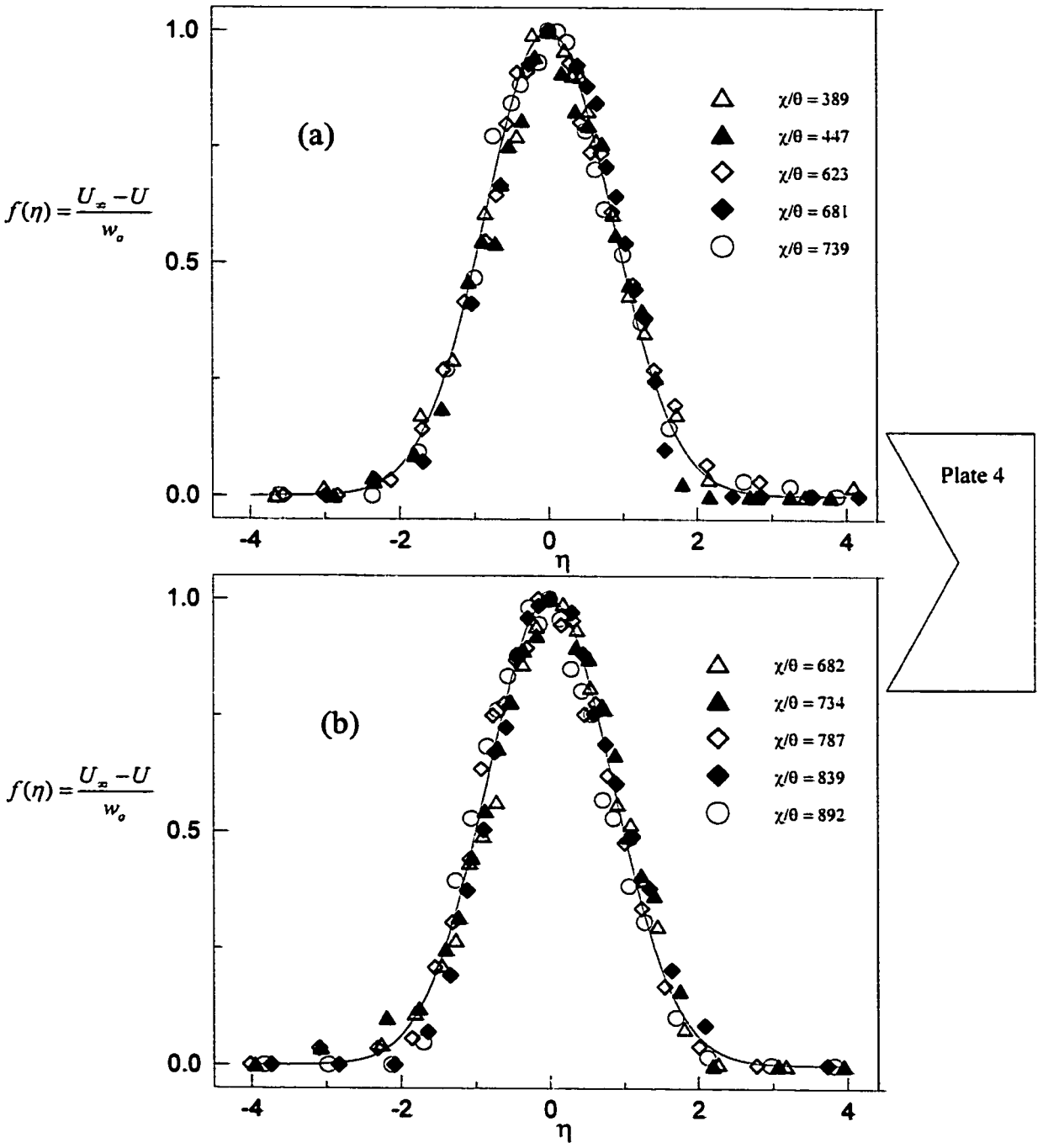

Figure 4.24. Distribution of normalized mean velocity defect in the wake of plate 4 at (a) $U_\infty = 7.5 m/s$ (b) $U_\infty = 10 m/s$.

velocity for all the four cases. The measured distribution of the longitudinal normal stress is shown in figures 4.25 – 4.28. While there is a good collapse of the data in the outer wake there is scatter around the wake center and this obscures the true shape of the normal stress in the inner region. However, it appears that the profiles have a single broad peak at the wake center. Similar profiles presented by Wygnanski et al. [15] for airfoil and screens show double peaks in the profiles. It was shown earlier that merging of the two peaks into one took place in the near-wake. Since Wygnanski et al. [15] did not present near-wake data, no definitive statement can be made on the differences in the far-wake $\overline{u^2}$ profile between the present result and theirs. It should be noted that other investigators of far-wake ([11] – [14]) did not present any $\overline{u^2}$ result. The distributions of the transverse normal stress (figures 4.29 – 4.32) collapse fairly well onto a single curve for each plate. In each case, the peak value of $\overline{v^2}$ is approximately half of the peak value of $\overline{u^2}$. The shear stress profiles (figures 4.33 – 4.36) show a very good collapse on a single curve for each plate. The peak values range from 0.07 for plate 4 to 0.12 for plate 1. Wygnanski et al [15] reported a peak value of 0.05 for airfoil wake. The higher peak value of $\overline{uv}$ obtained is the first sign that the growth rate in the present experiment will be higher than that obtained by Wygnanski et al. [15]. This is because the spreading rate depends on the magnitude of $-\overline{uv}$ which appears as a response to distortion of the turbulence by the mean velocity gradients [1].

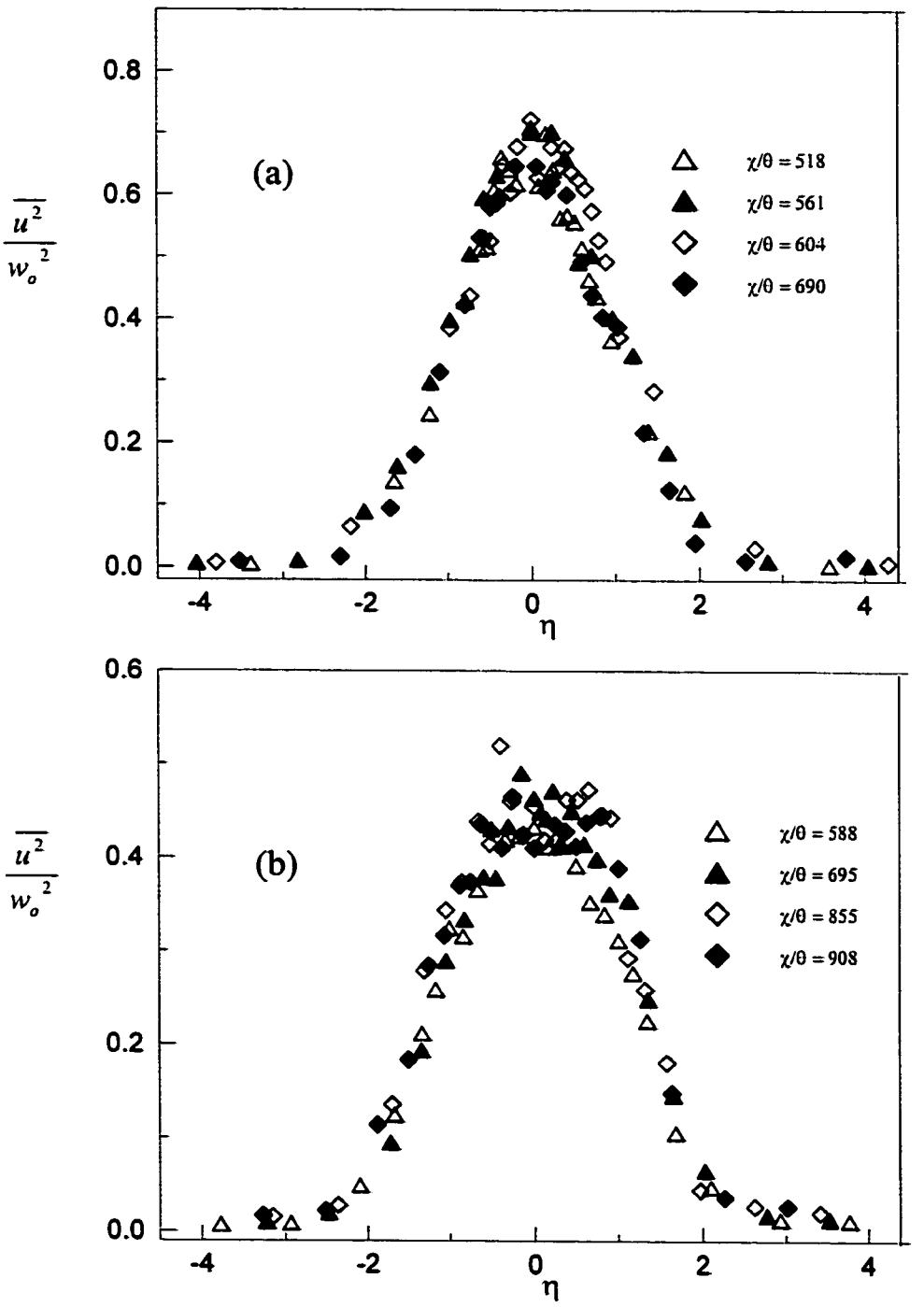

Plate 1

Figure 4.25. Measured distribution of longitudinal normal stress in the wake of plate 1 at (a) $U_\infty = 7.5 m/s$ (b) $U_\infty = 10 m/s$.

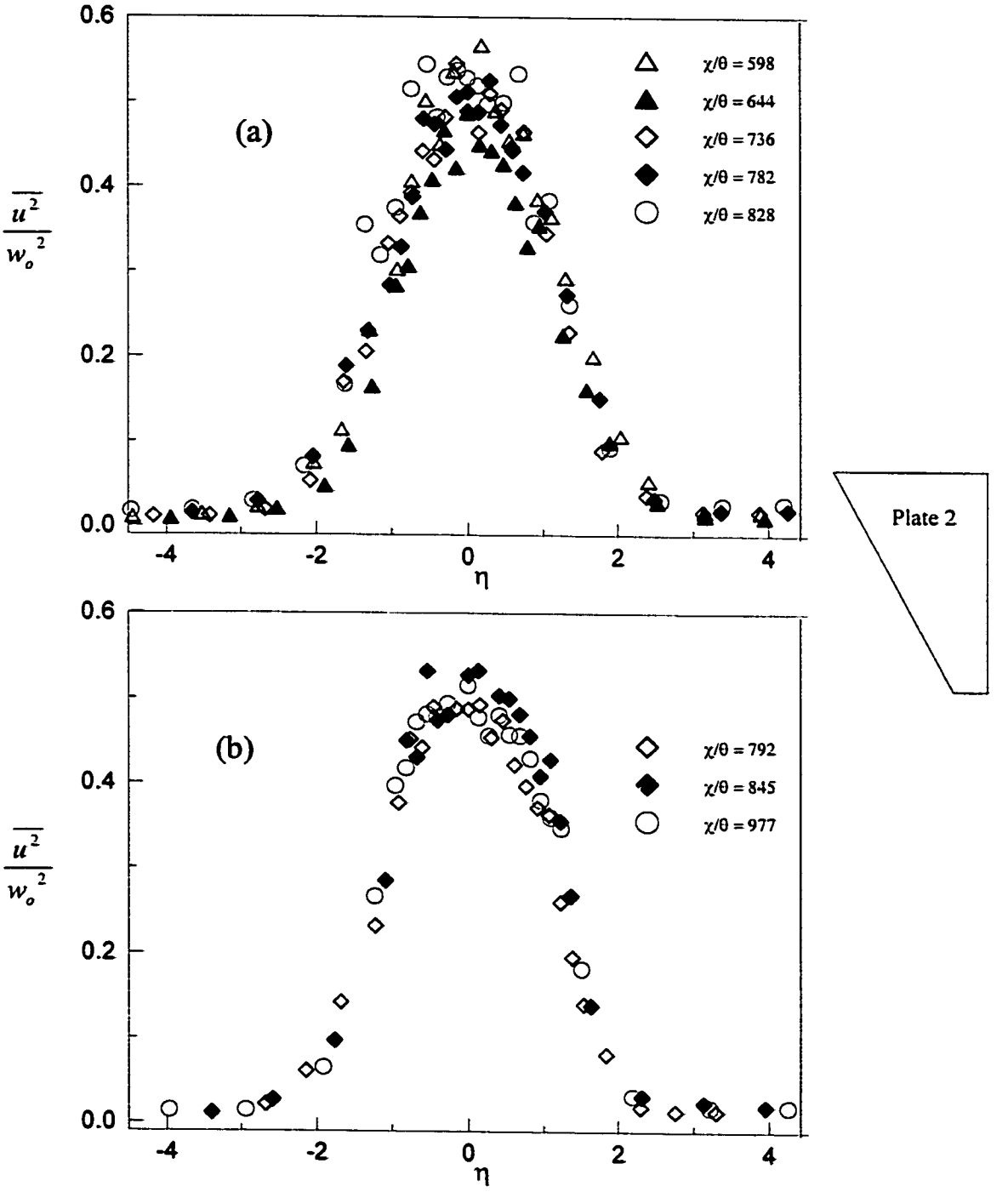

Figure 4.26. Measured distribution of longitudinal normal stress in the wake of plate 2 at (a) $U_\infty = 7.5 m/s$ (b) $U_\infty = 10 m/s$.

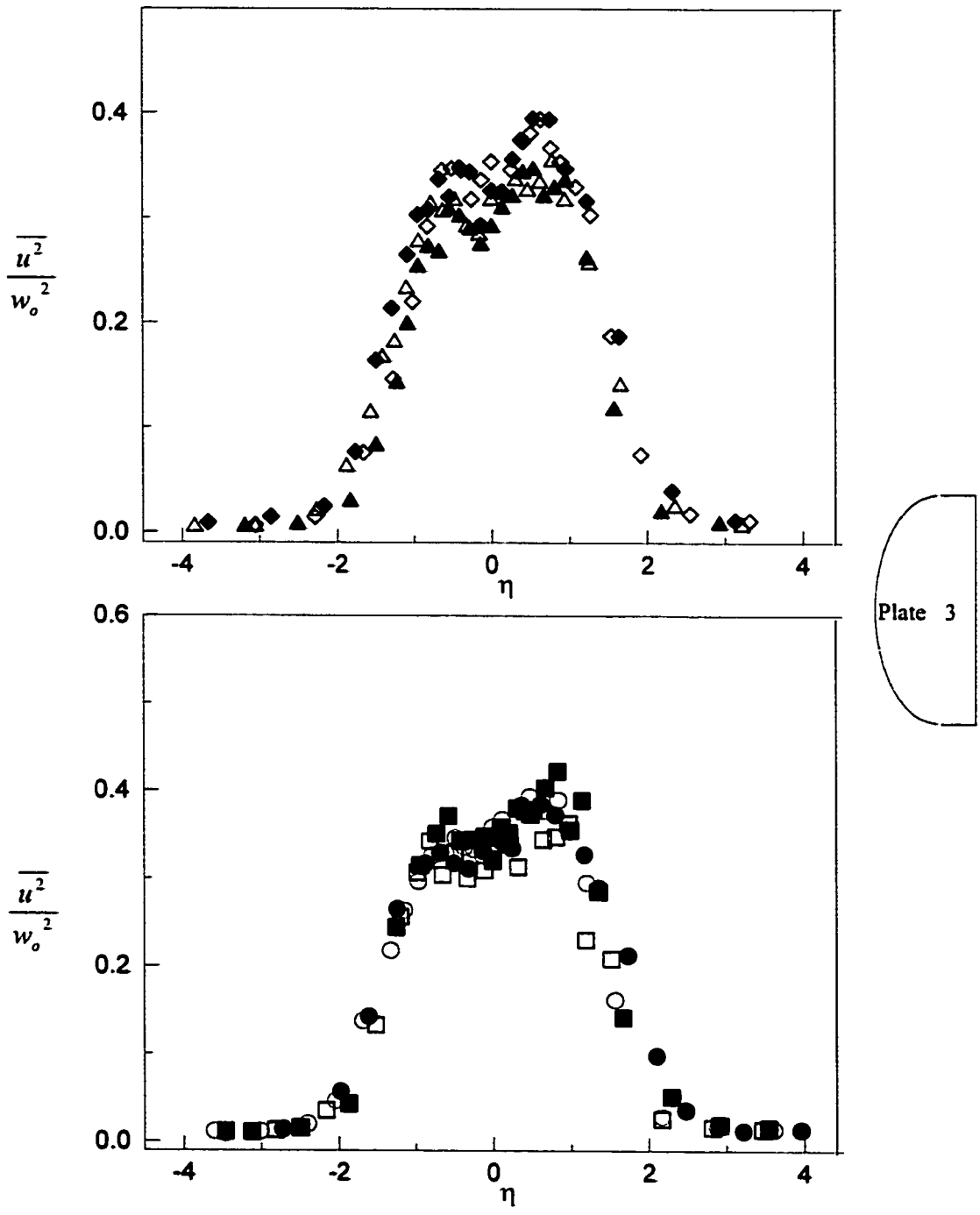

Figure 4.27. Measured distribution of longitudinal normal stress in the wake of plate 3 at $U_\infty = 10\,m/s$. For symbols see figure 4.29.

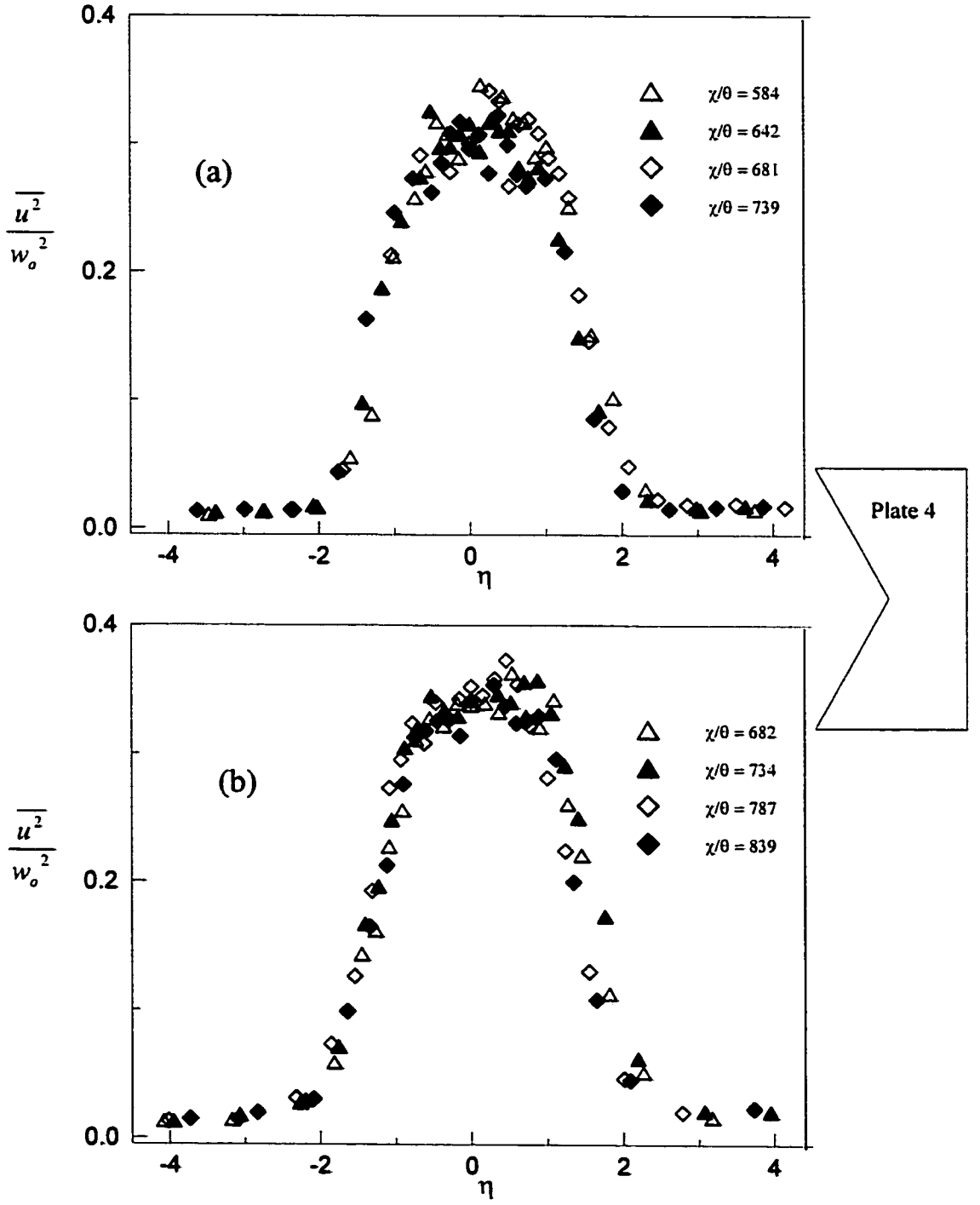

Figure 4.28. Measured distribution of longitudinal normal stress in the wake of plate 4 at (a) $U_\infty = 7.5 m/s$ (b) $U_\infty = 10 m/s$.

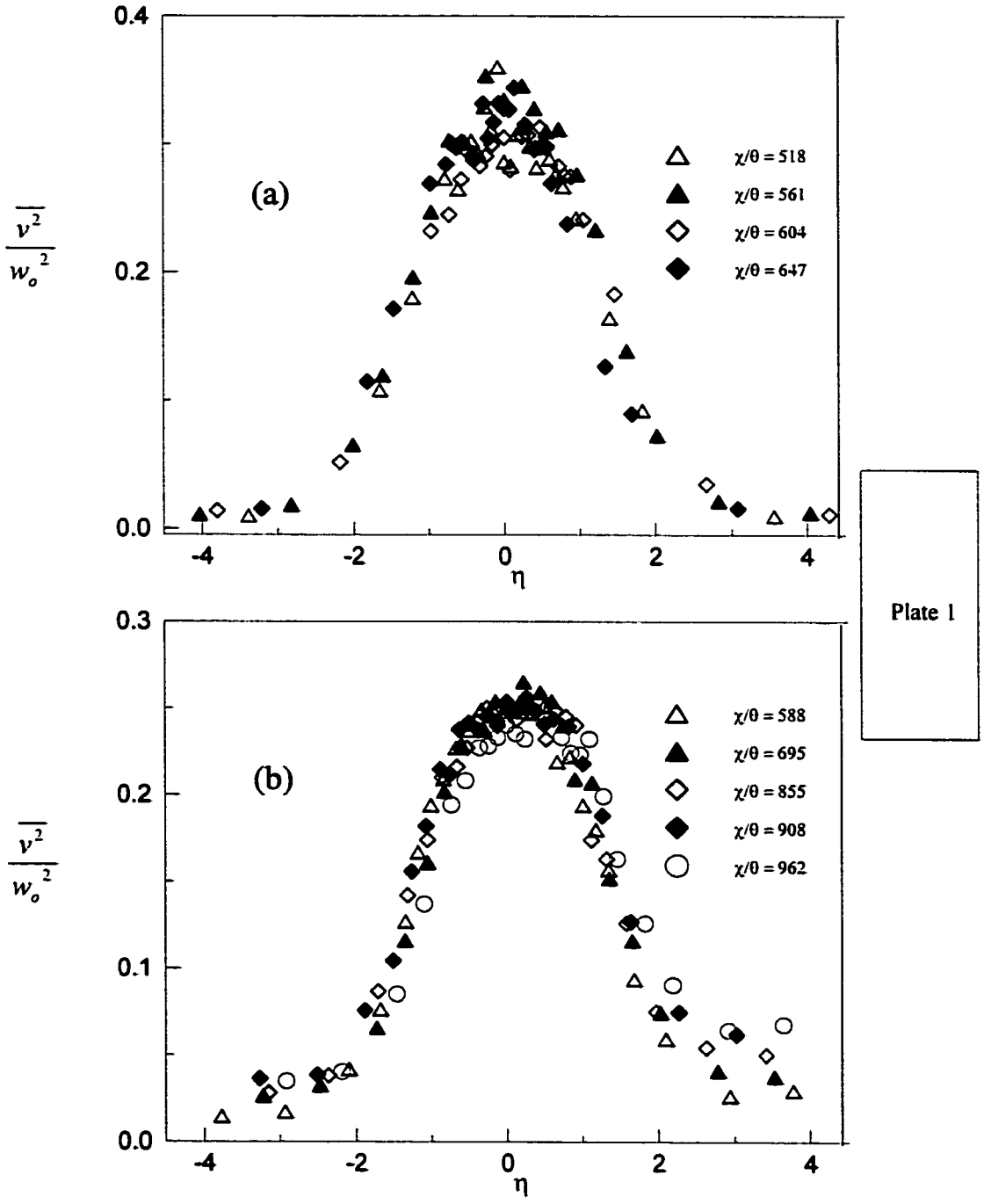

Figure 4.29. Measured distribution of transverse normal stress in the wake of plate 1 at (a) $U_\infty = 7.5 m/s$ (b) $U_\infty = 10 m/s$.

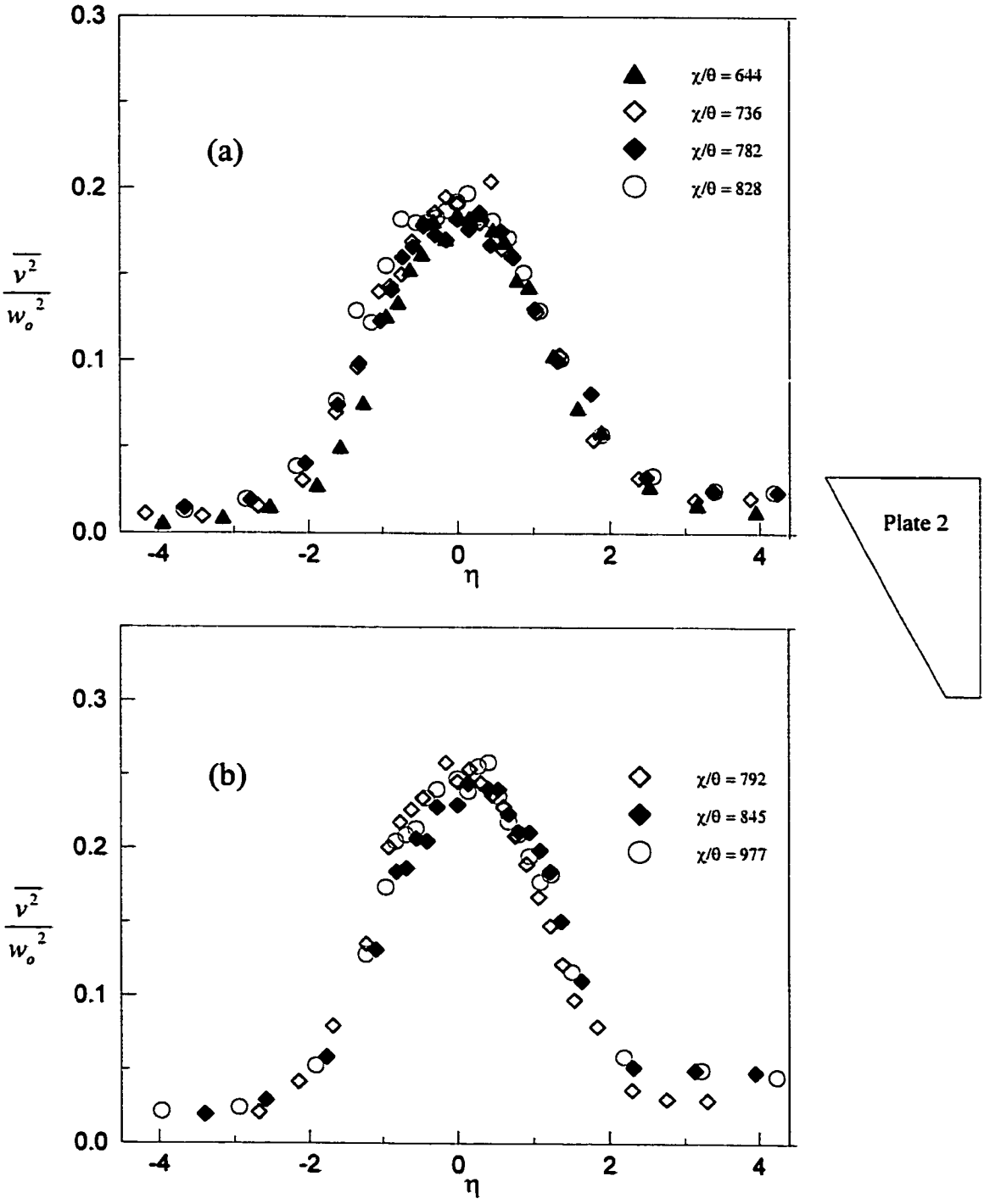

Figure 4.30. Measured distribution of transverse normal stress in the wake of plate 2 at (a) $U_\infty = 7.5 m/s$ (b) $U_\infty = 10 m/s$.

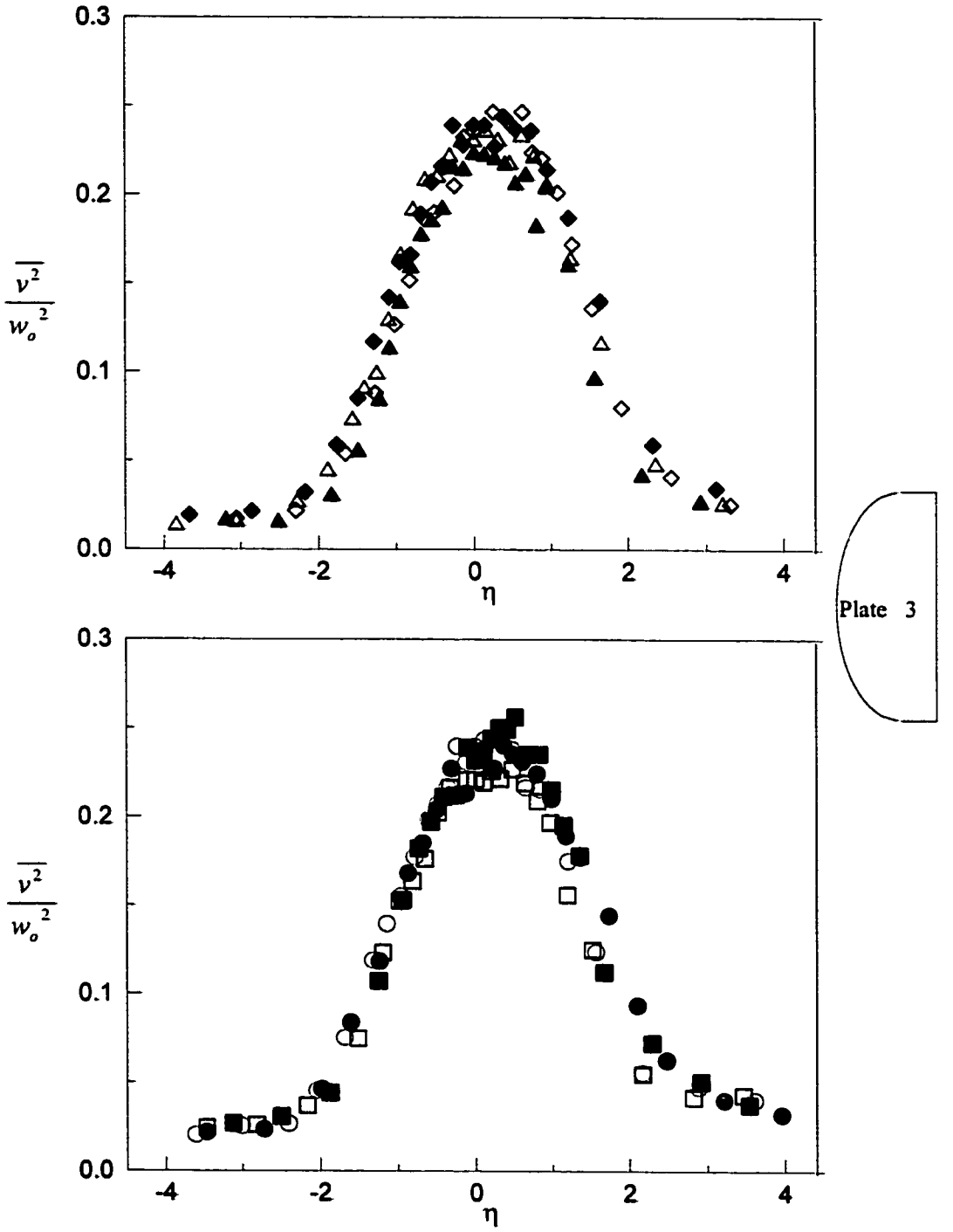

Figure 4.31. Measured distribution of transverse normal stress in the wake of plate 3 $U_\infty = 10\,m/s$. For symbols see figure 4.29.

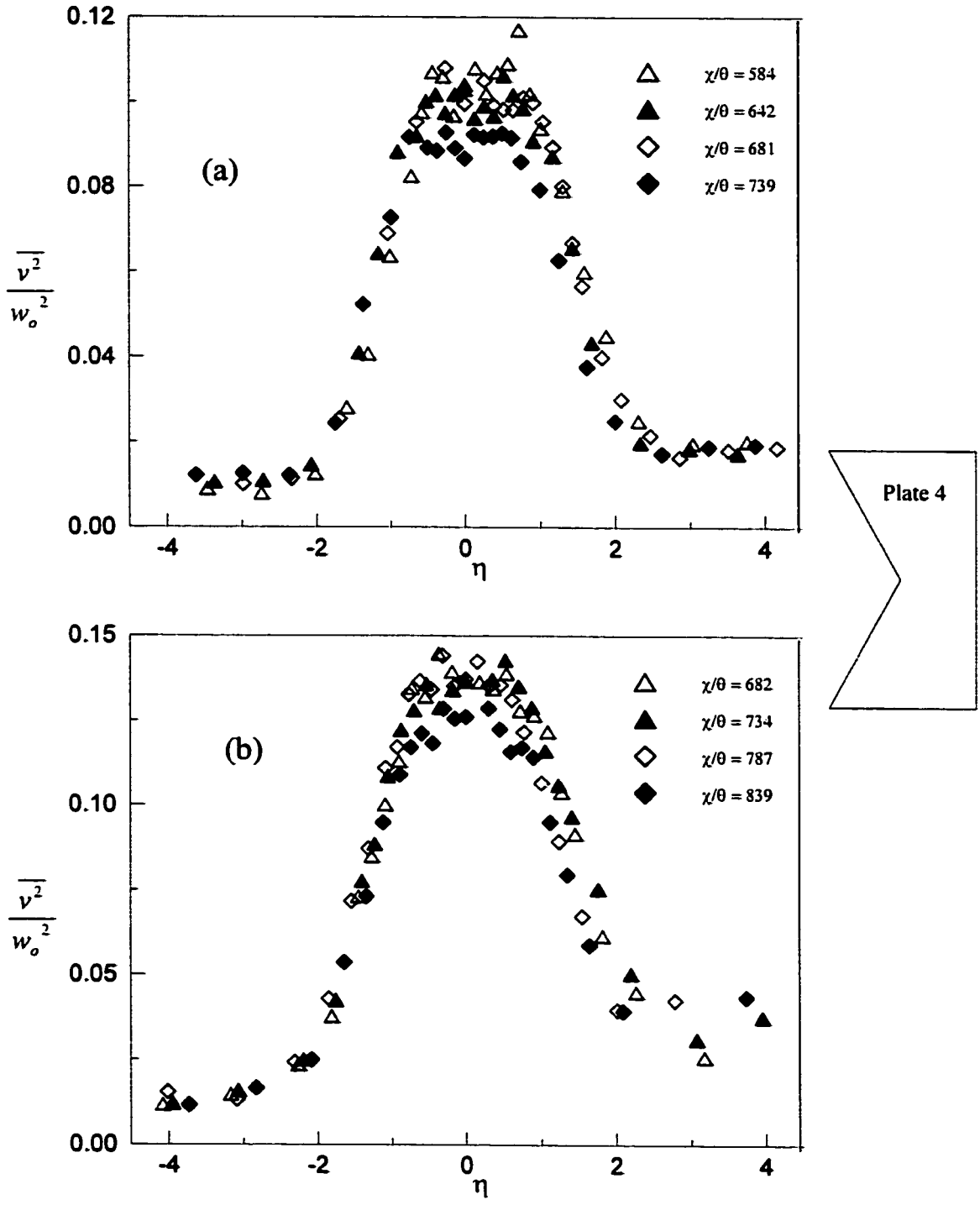

Figure 4.32. Measured distribution of transverse normal stress in the wake of plate 4 at (a) $U_\infty = 7.5 m/s$ (b) $U_\infty = 10 m/s$.

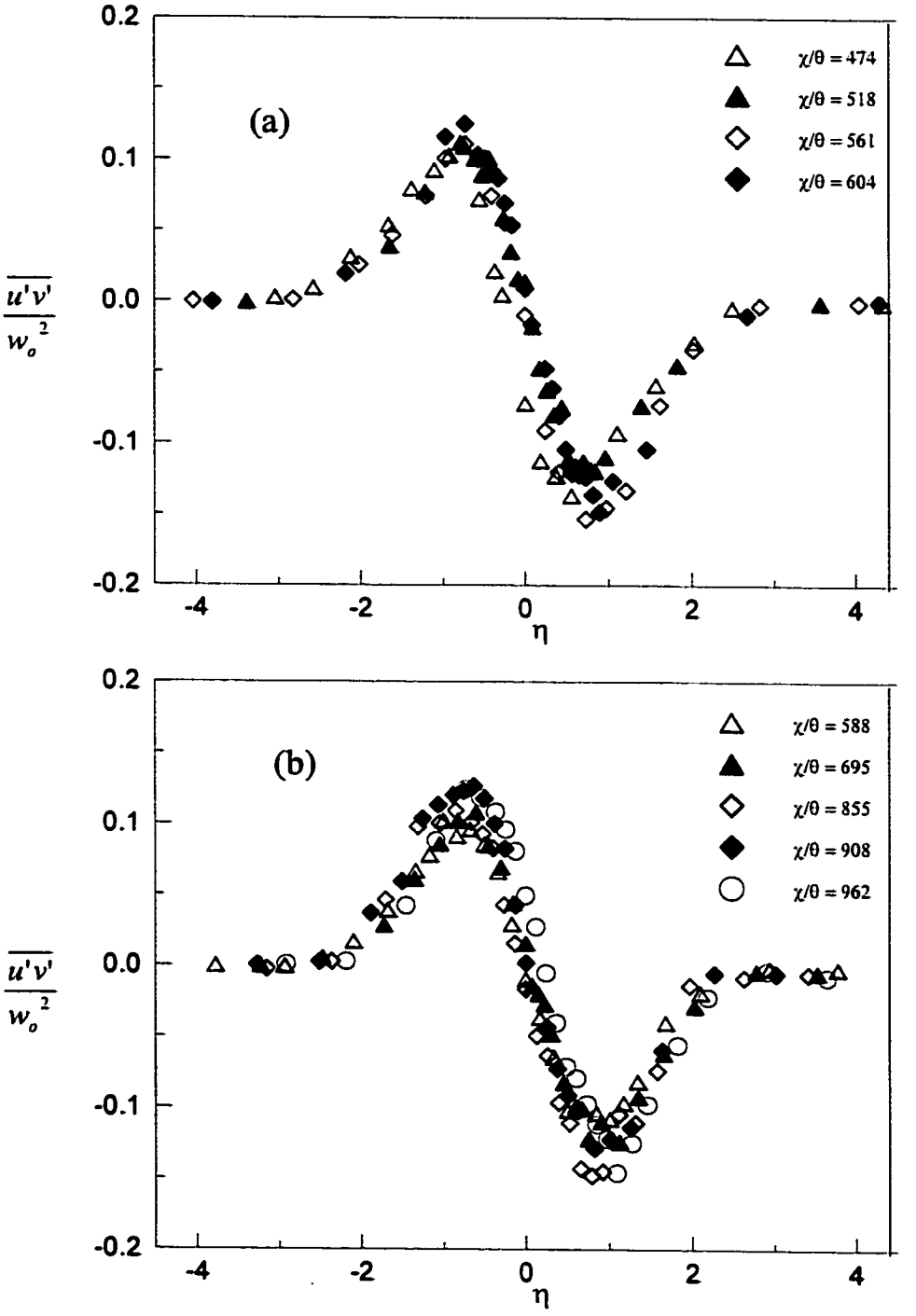

Plate 1

Figure 4.33. Measured distribution of Reynolds shear stress in the wake of plate 1 at (a) $U_\infty = 7.5 m/s$ (b) $U_\infty = 10 m/s$.

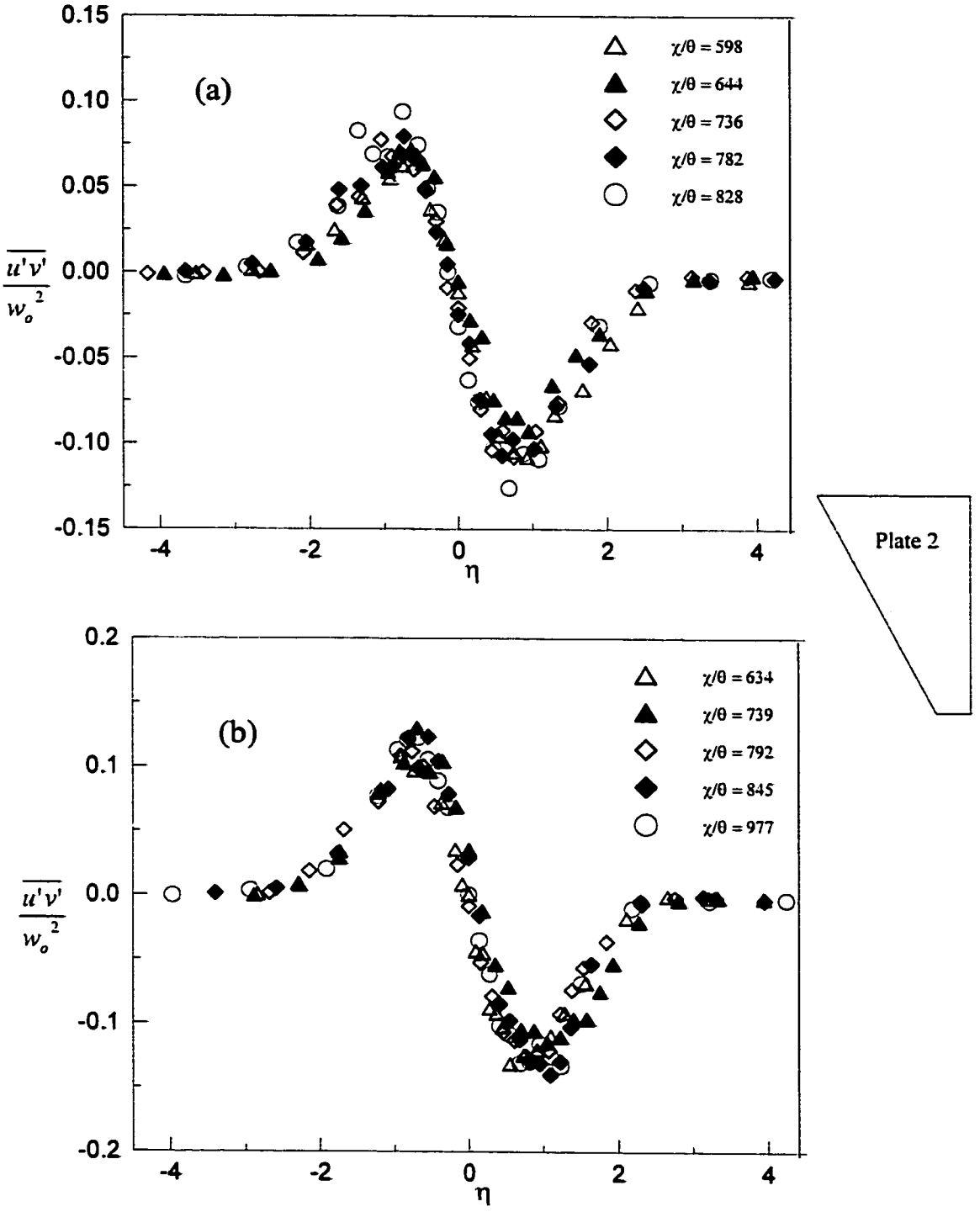

Figure 4.34. Measured distribution of Reynolds shear stress in the wake of plate 2 at (a) $U_\infty = 7.5 m/s$ (b) $U_\infty = 10 m/s$.

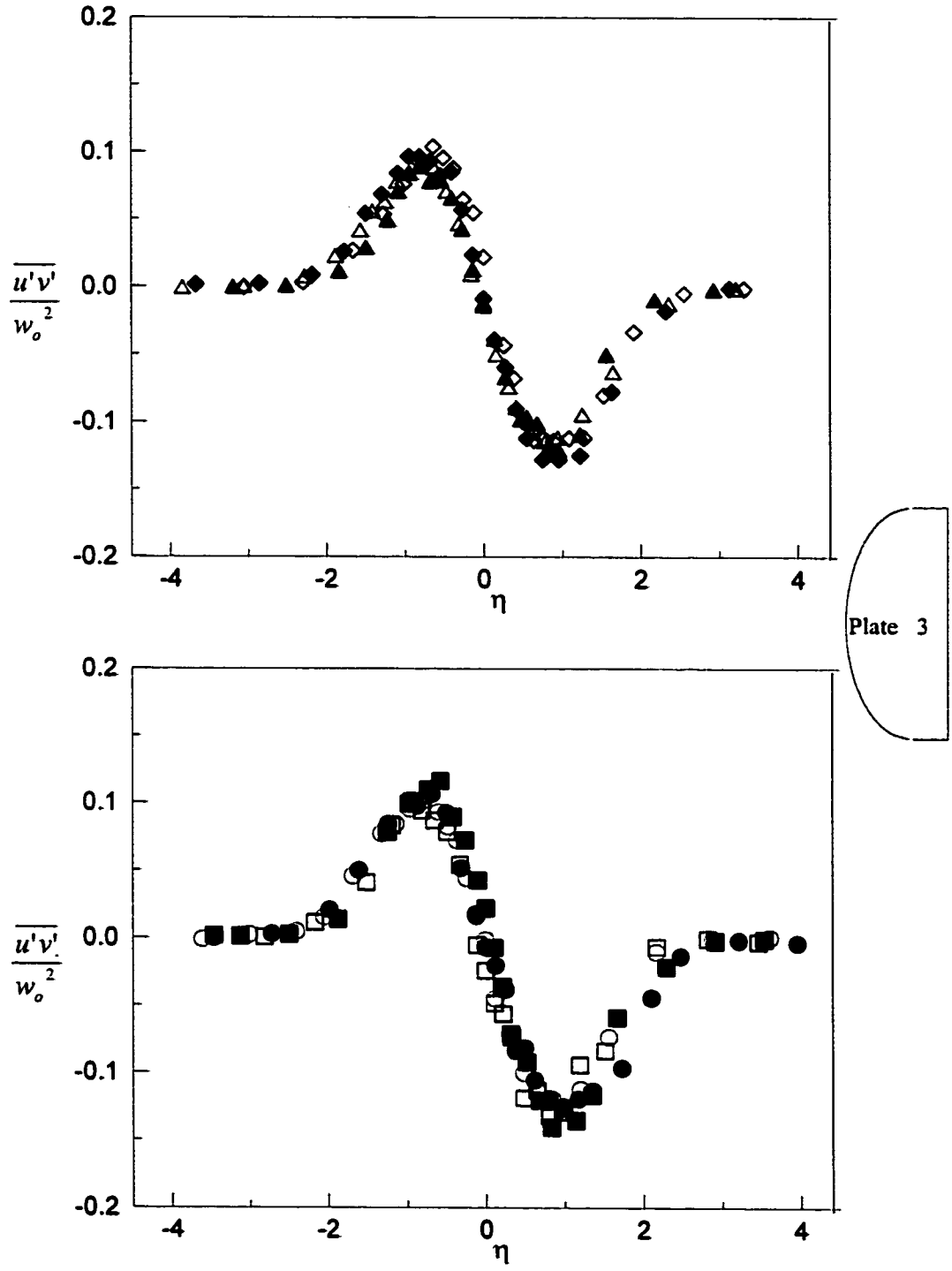

Figure 4.35. Measured distribution of Reynolds shear stress in the wake of plate 3 at $U_\infty = 10 m/s$. For symbols see figure 4.29.

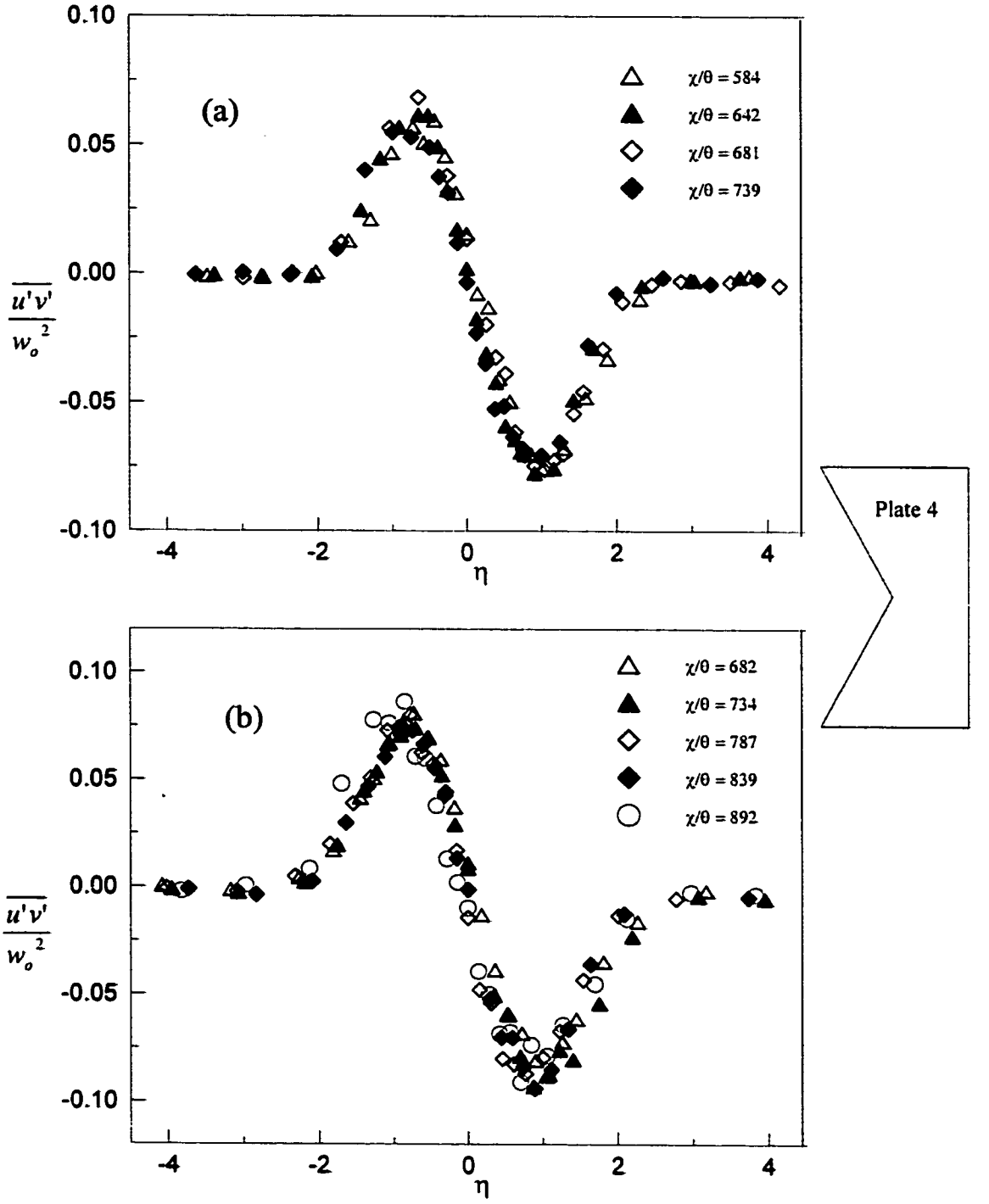

Figure 4.36. Measured distribution of Reynolds shear stress in the wake of plate 4 at (a) $U_\infty = 7.5 m/s$ (b) $U_\infty = 10 m/s$.

The streamwise development of the normalized velocity and length scales are shown in figures 4.37 – 4. 43. They all show very good agreements with equations (7) and (8). This is a clear demonstration that self-preserving condition has been reached in each case. By employing the least squares method [43] to the set of data plotted in figures 4.37 – 4.43, lines of best fit were obtained. The virtual origin and constants A and B of equations (2.7) and (2.8) were then calculated from these lines. These and other relevant wake parameters are presented in Table 4.2. The errors in the calculated values of the parameters, obtained using the uncertainty analysis procedure presented in Appendix D, are included in the table. The plots for all the plates are presented together in figure 4.44 in which x is now replaced with $x-x_0$, where x_0 is the virtual origin determined for each plate and speed. The solid lines in the figure are the lines of best fit determined for each case. It will be noted from Table 4.2 that the growth rates (i.e. constants A and B) are independent of the freestream velocity. This is demonstrated by the results for plates 1, 2 and 4 in which measurements were taken at two speeds and is consistent with the results from Wygnanski et al. [15]. It is also noted that the growth rates for plates 1, 2 and 3 are very close. This is easily observed from figure 4.44 in which the data for those three plates almost collapse on a single straight line. The growth rate for plate 4, on the other hand, is significantly different from the rest. The uncertainty analysis results show that the difference cannot be attributed to experimental error. There are very little data available on wake growth rates. Sreenivasan and Narasimha [14] suggested a universal equilibrium of $W_o = 1.63$

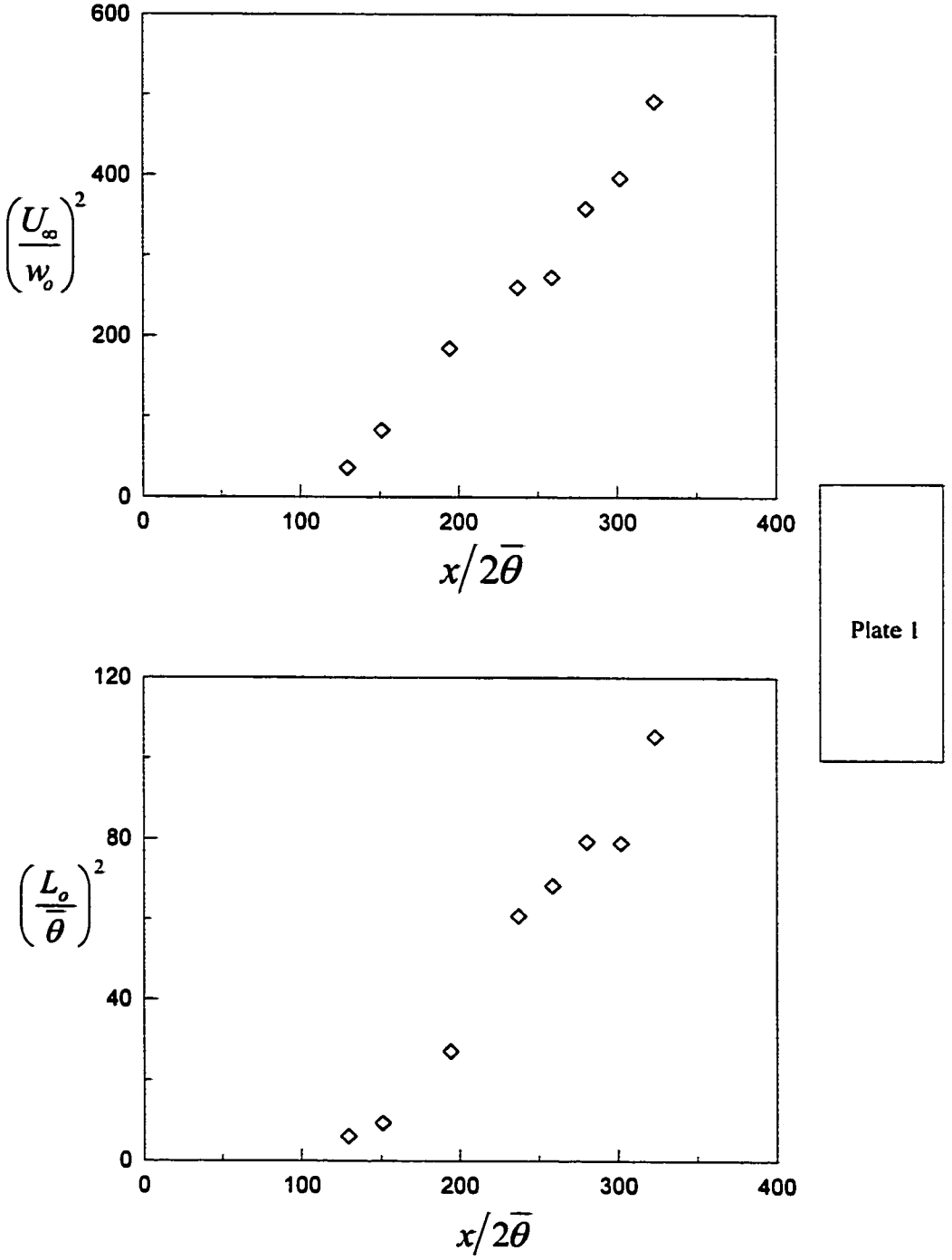

Figure 4.37. The variation of the center line velocity defect and the half-wake width along the wake. Plate 1; $U_\infty = 7.5 m/s$.

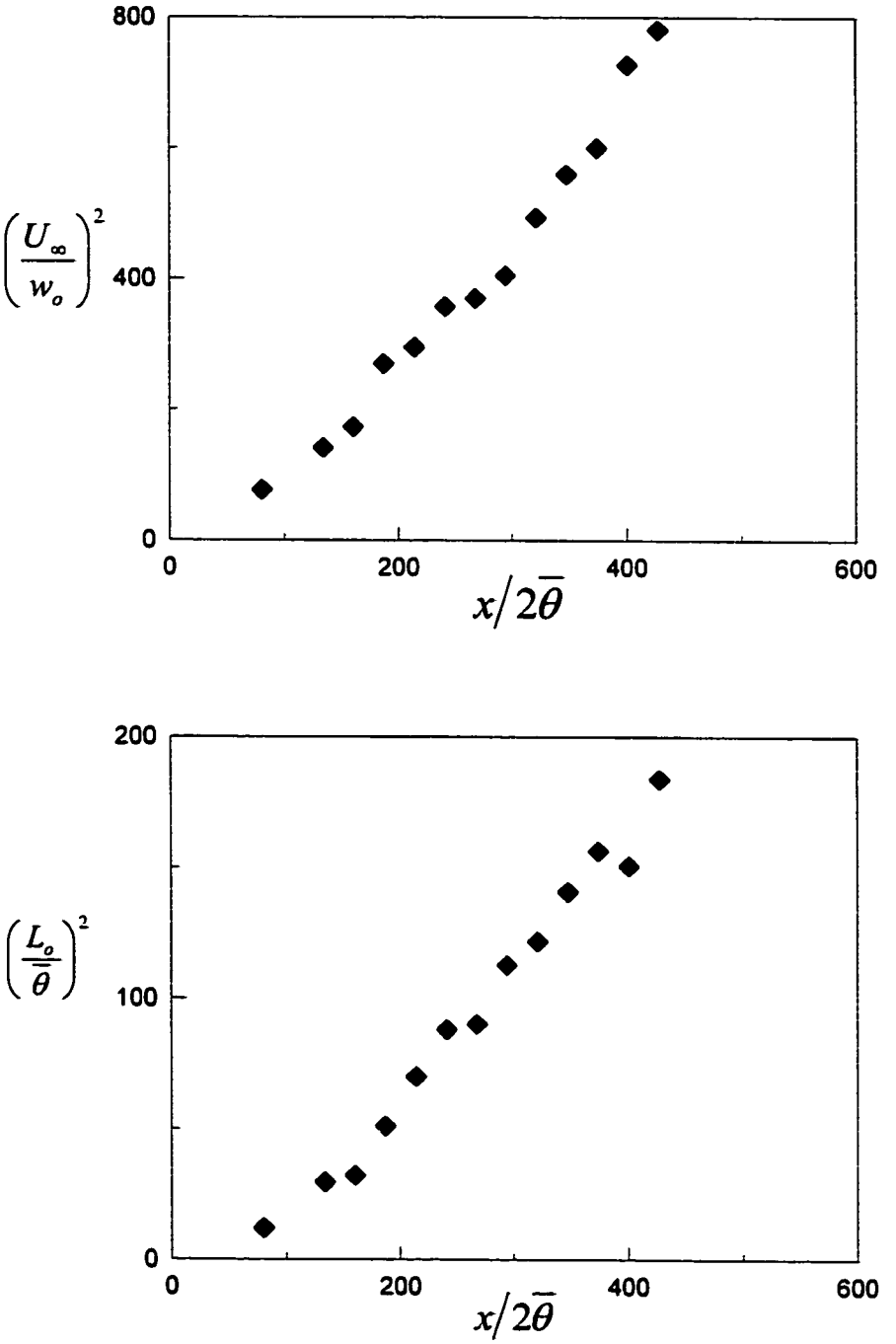

Figure 4.38. The variation of the center line velocity defect and the half-wake width along the wake. Plate 1; $U_\infty = 10m/s$.

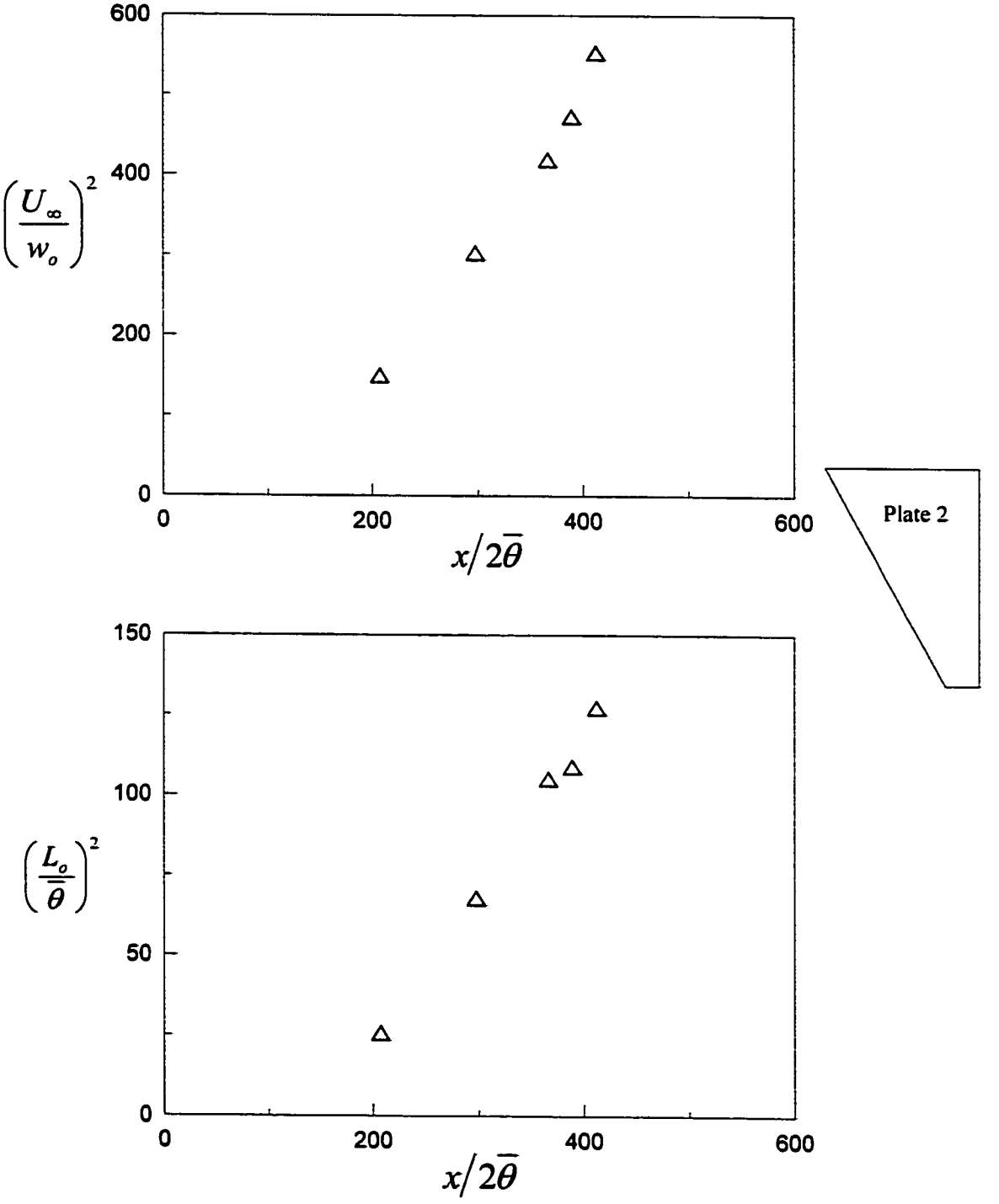

Figure 4.39. The variation of the center line velocity defect and the half-wake width along the wake. Plate 2; $U_\infty = 7.5m/s$.

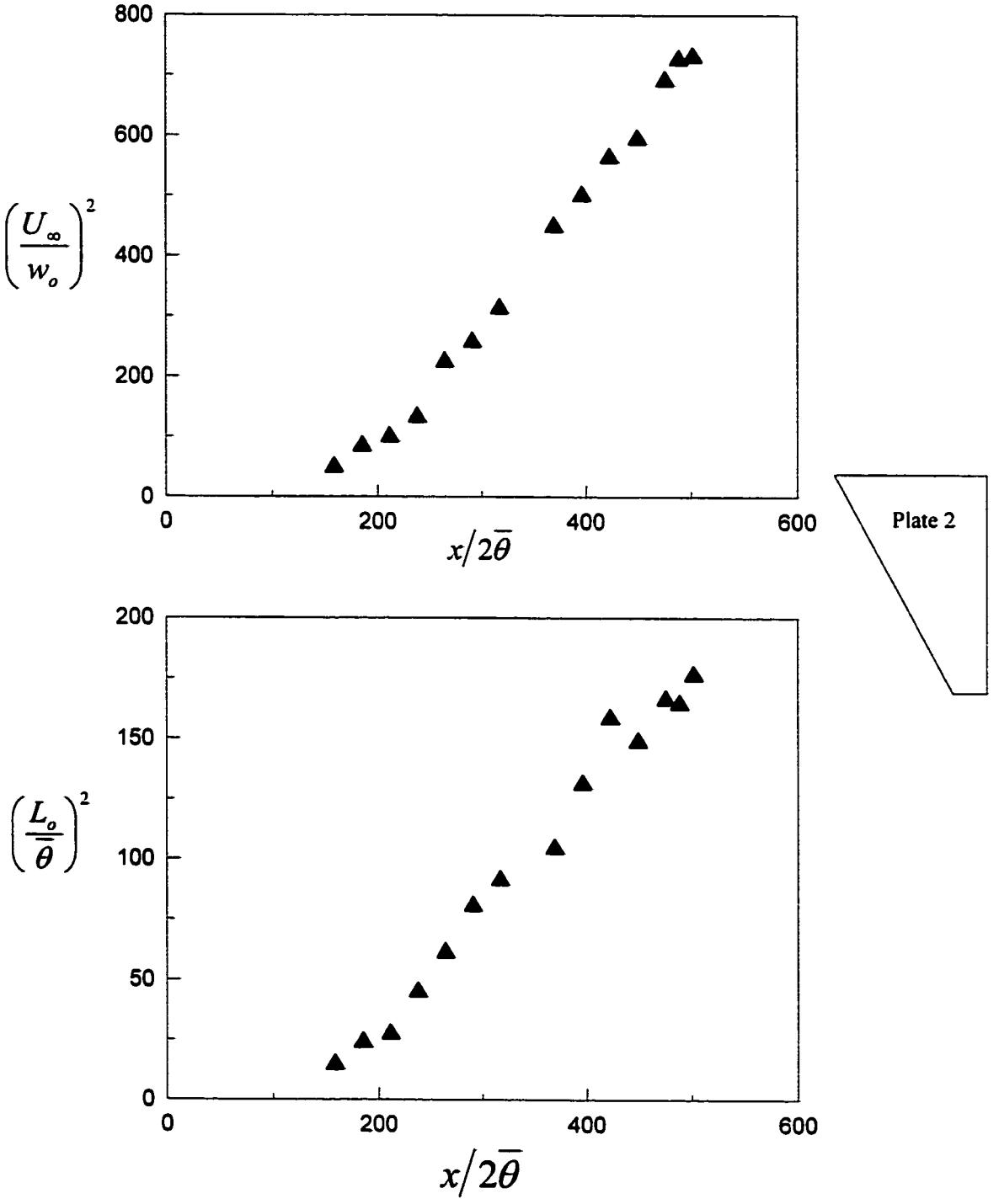

Figure 4.40. The variation of the center line velocity defect and the half-wake width along the wake. Plate 2; $U_\infty = 10 m/s$.

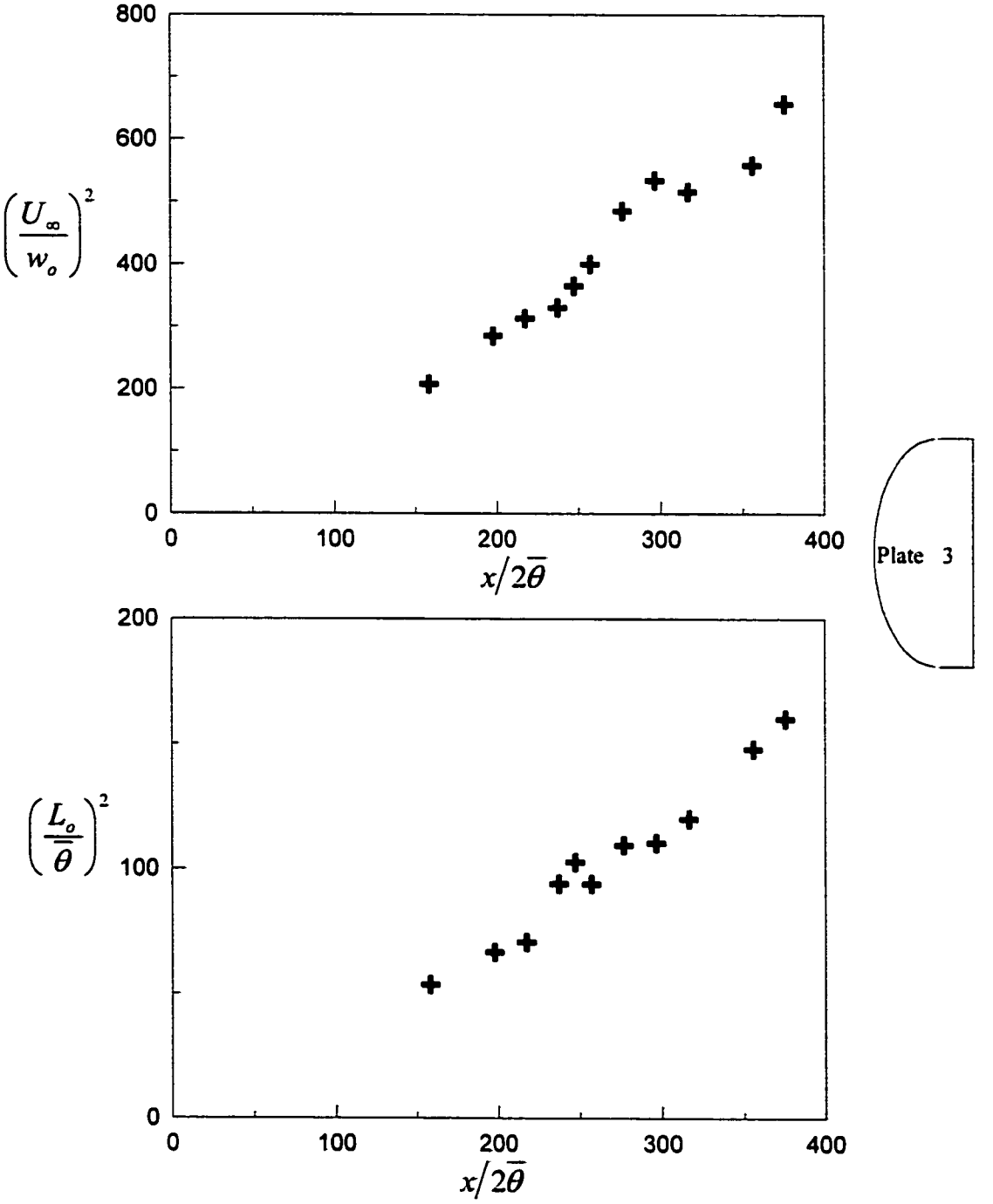

Figure 4.41. The variation of the center line velocity defect and the half-wake width along the wake. Plate 3; $U_\infty = 10 m/s$.

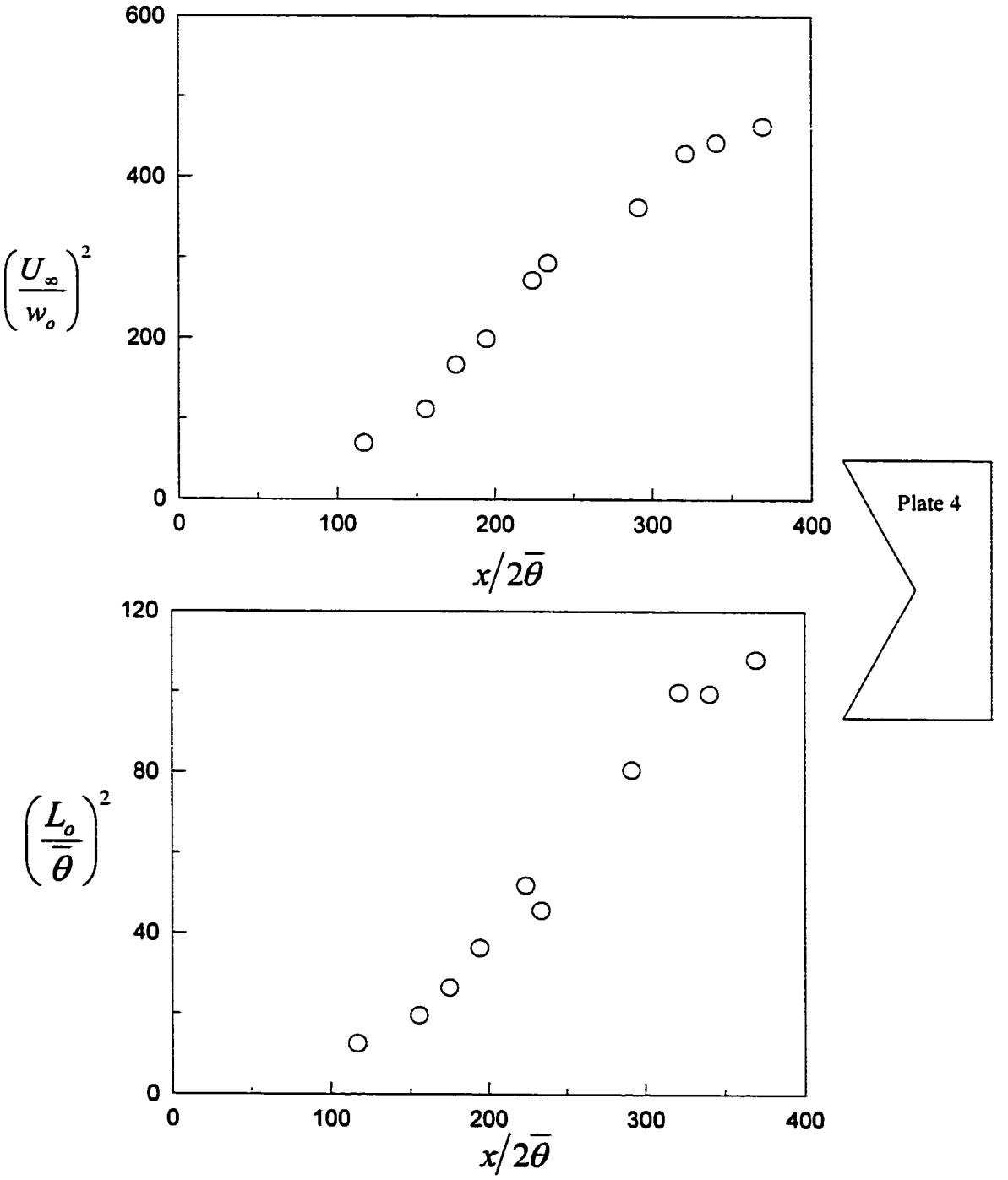

Figure 4.42. The variation of the center line velocity defect and the half-wake width along the wake. Plate 4; $U_\infty = 7.5 m/s$.

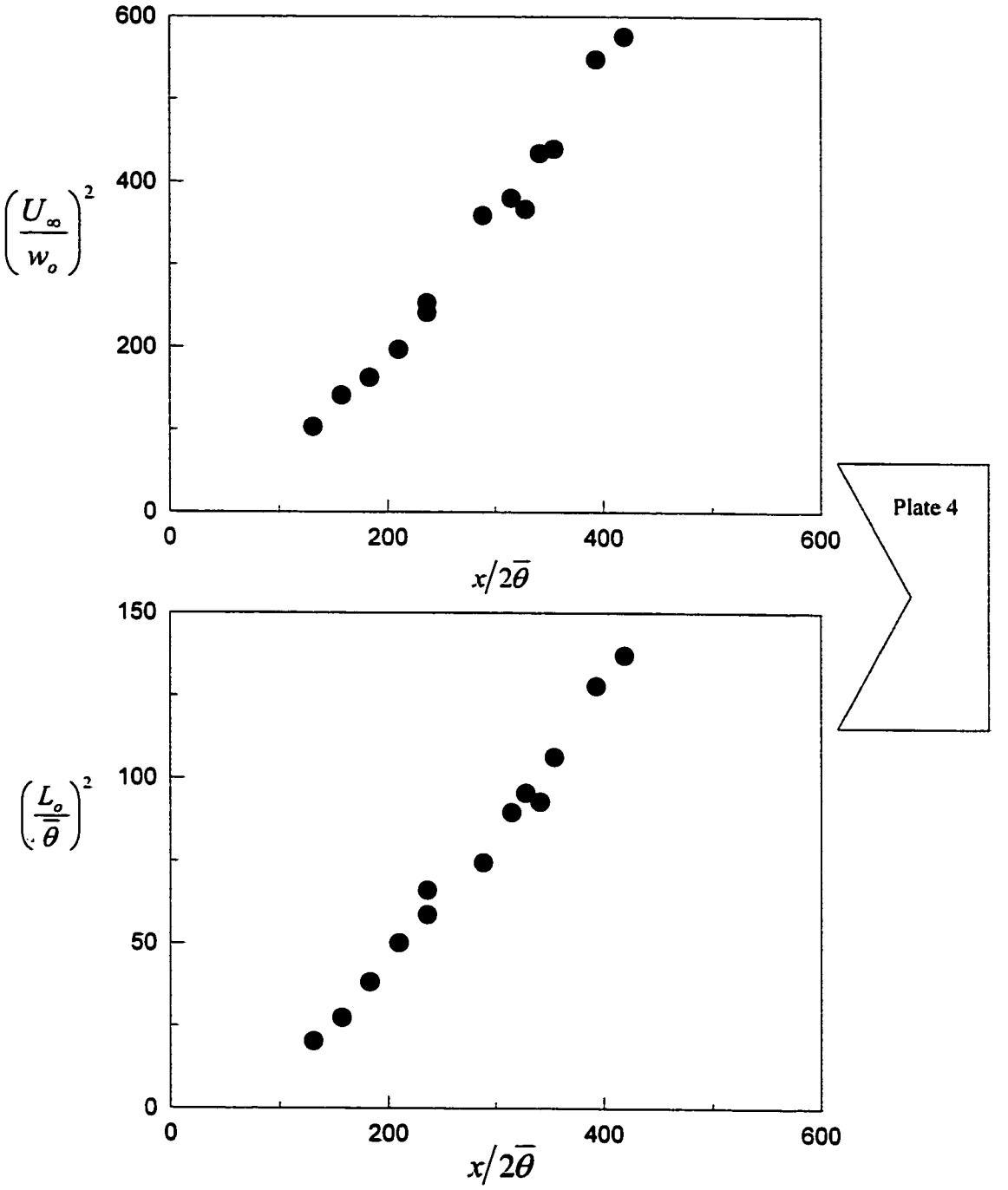

Figure 4.43. The variation of the center line velocity defect and the half-wake width along the wake. Plate 4; $U_\infty = 10 m/s$.

Table 4.2: Flow Properties in the Self-Similar Region of the Wakes

	U_∞ (m/s)	θ (mm)	$\frac{x_o}{2\theta}$	A	B	W_o	Δ_o	$W_o\Delta_o$
Plate 1	7.5	1.39 ± 0.25	121	2.181	0.506	0.958 ± 0.007	0.503 ± 0.002	0.482
Plate 1	10	1.12 ± 0.13	70	2.017	0.502	0.996 ± 0.002	0.501 ± 0.001	0.499
Plate 2	7.5	1.34 ± 0.25	160	2.082	0.501	0.980 ± 0.021	0.500 ± 0.008	0.490
Plate 2	10	1.15 ± 0.17	148	2.110	0.490	0.974 ± 0.002	0.495 ± 0.001	0.482
Plate 3	10	1.52 ± 0.16	58	2.030	0.486	0.992 ± 0.008	0.493 ± 0.004	0.489
Plate 4	7.5	1.54 ± 0.41	85	1.655	0.403	1.099 ± 0.019	0.449 ± 0.006	0.493
Plate 4	10	1.15 ± 0.15	89	1.656	0.420	1.099 ± 0.003	0.458 ± 0.001	0.504

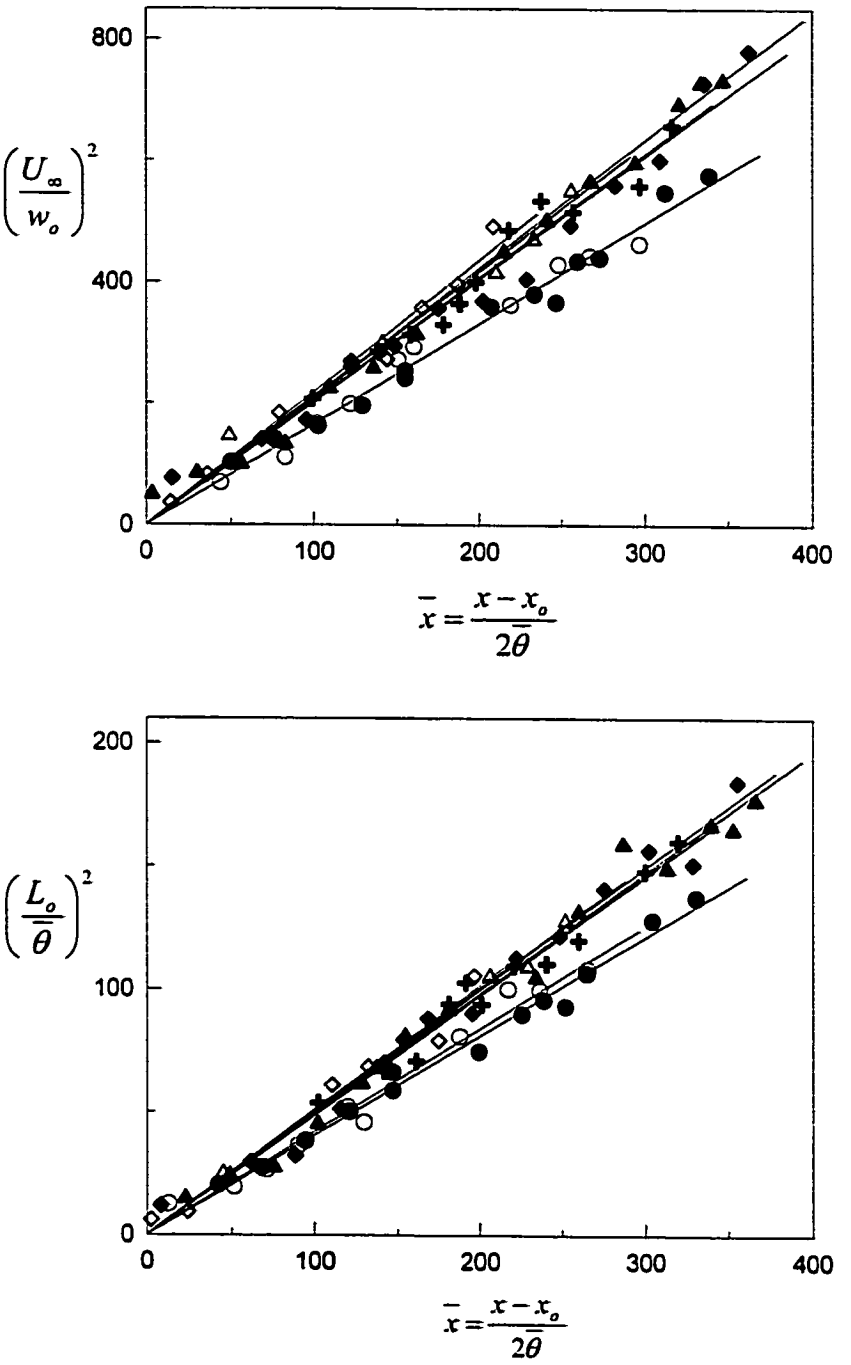

Figure 4.44 The variation of the centerline velocity defect and the half-wake width with $\bar{x}$ for the four plates. Symbols are the same as for figures 4.37 – 4.43.

and $\Delta_o = 0.300$ for all wakes. However, it could be seen from their work that only the wake behind a twin plate approached the values quoted. It is therefore not suitable for comparison with the flat plates used in the present experiments. The only credible results to use for comparison are those of Wygnaski et al. [15]. In their work, they took measurements in the wake of a flat plate, with and without external forcing. Forcing was introduced through a small trailing-edge flap externally driven by acoustic excitation. A summary of the results obtained by them for flat plates, with and without forcing, is presented with the results for plate 1 of the present experiments in Table 4.3. The table shows that the results obtained in the present experiments are significantly different from those obtained by Wygnanski et al. [15]. The low value of W_o suggests that the wake in the present experiments decays faster than theirs. It was reported in [15] that Symes and Fink [44] investigated the effect of free-stream turbulence on the development of wakes and showed that the relative scale of the external turbulence was an important parameter affecting the development of the wake. Wygnanski et al. [15] then suggested that the wakes generated in a particular facility may be unique to that facility only as each experimental facility has its own characteristic freestream disturbances. It was in an attempt to test the validity of that suggestion that they applied periodic forcing on the wake of their flat plate. Their results are included in Table 4.3. The results show that the effect of the external disturbance is to increase the wake growth rate (by reducing W_o and increasing Δ_o). Increasing either the frequency or the amplitude of the disturbance showed the same

Table 4.3: Present and Previous [15] Results for Plate 1

	U_∞ (m/s)	θ (mm)	$\frac{x_o}{2\theta}$	W_o	Δ_o	$W_o\Delta_o$	
No forcing	7.45	2.36	5	1.71	0.297	0.508	*Wygnanski et al.*[15]
flap freq = 50*Hz* *AMP* = 0.2*V*	7.45	2.36	48	1.48	0.344	0.509	
flap freq = 50*Hz* *AMP* = 0.3*V*	7.45	2.46	61	1.32	0.382	0.504	
flap freq = 20*Hz* *AMP* = 0.5*V*	7.45	2.40	48	1.57	0.323	0.507	
	7.5	1.39	121	0.958	0.503	0.482	Pr*esent*
	10	1.12	70	0.996	0.501	0.499	

trend. It is therefore possible that the wakes generated in the present experiments were under the influence of some external disturbance.

4.4 Spectrum Analysis

To investigate the possibility that the flow was under the influence of some external forcing, a spectrum analysis of the stored data was carried out digitally. Digital signal processing offers the opportunity of off-line analysis of results and of transforming a signal into a form which is in some sense more desirable (Oppenheim and Schafer [45]). The processing was done through the signal processing toolbox of MATLAB. The program was first applied to a combination of sine waves sampled at 10Khz. It faithfully displayed the exact frequencies of the sine waves.

The spectral of the streamwise component of the velocity fluctuations were computed at some x locations in the wakes of the four plates. The computations were performed for the outer boundary of the wakes, i.e. about $\eta = 3$, where the fluctuations induced by the passage of the large turbulent structures in the wakes could be captured. The spectra of the u component for different x-axis locations are presented for the four plates in figures 4.45 – 4.48. The frequency is plotted on a logarithmic scale on the horizontal axis while the vertical axis is expressed as

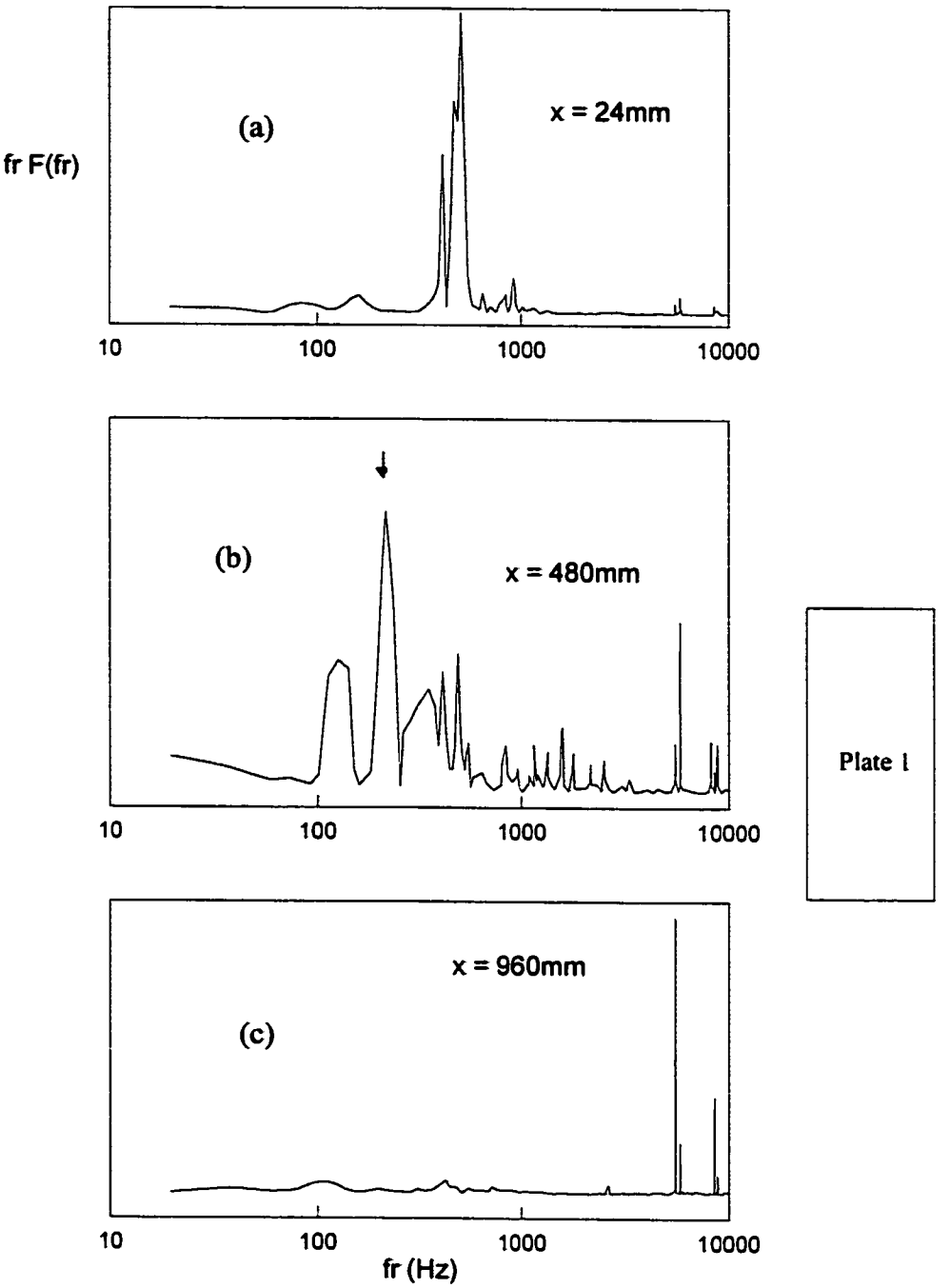

Figure 4.45 Spectra of u fluctuations on the wake outer boundary for plate 1.

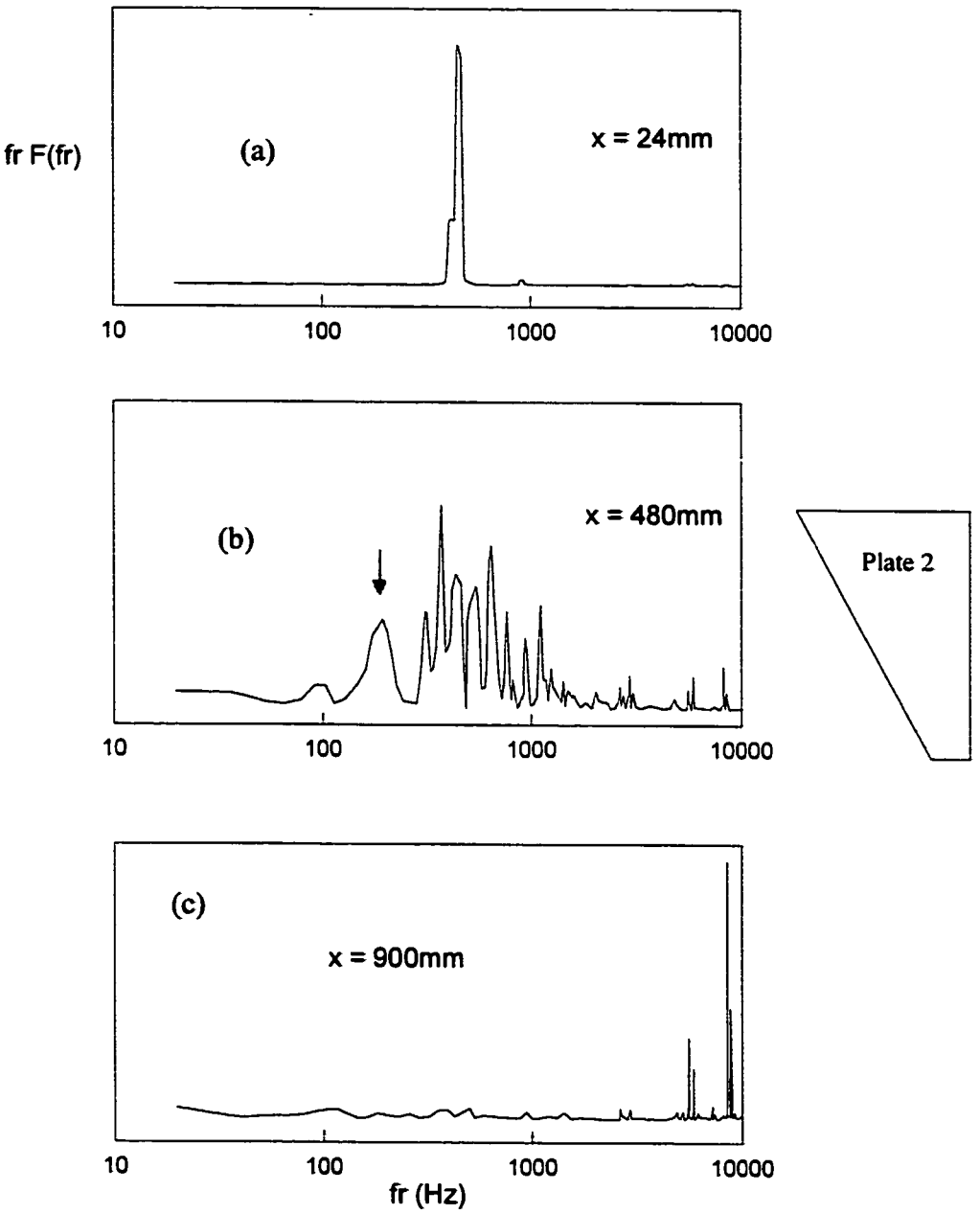

Figure 4.46 Spectra of u fluctuations on the wake outer boundary for plate 2.

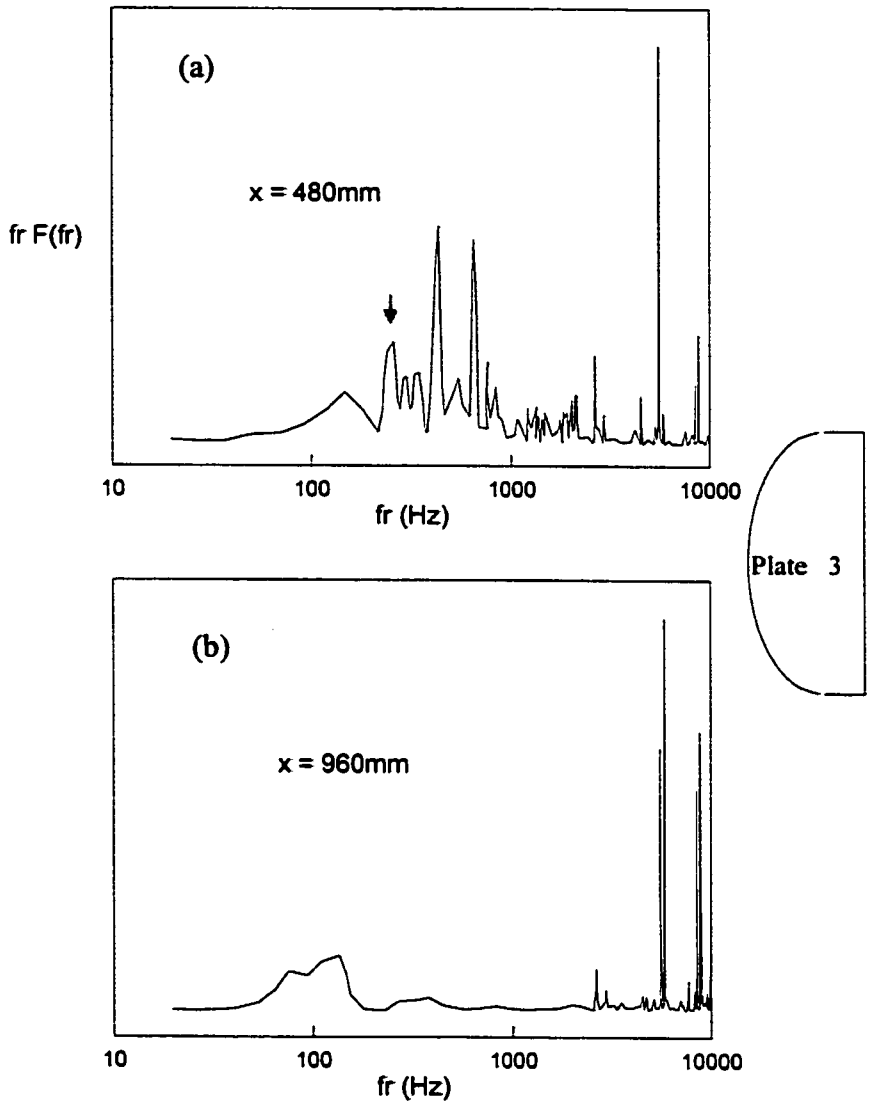

Figure 4.47 Spectra of u fluctuations on the wake outer boundary for plate 3.

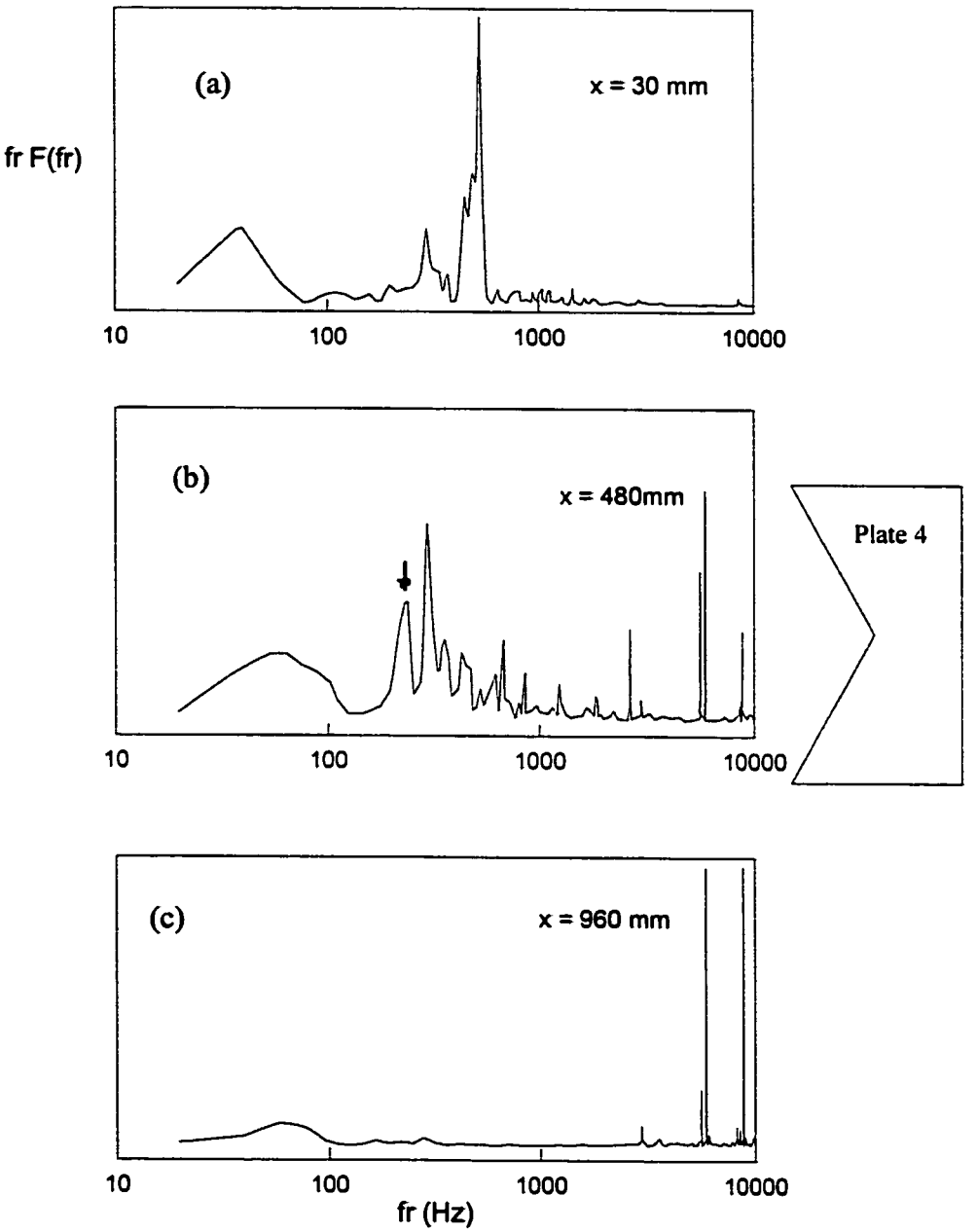

Figure 4.48 Spectra of u fluctuations on the wake outer boundary for plate 4.

$fr(F(fr))$. This is done in order to represent the relative contribution to the streamwise component of intensity at a given frequency *fr*, i.e. $\overline{u^2} \propto \int F(fr)dfr = \int frF(fr)d(\log fr)$. Wygnanski et al. [15] also used this form. In addition, it was this form of representation that clearly picked out the frequencies and relative amplitudes of the assortment of sine waves used in testing the program. For plate 1, the spectra peak is at about 508 Hz at $x = 24\ mm$ (figure 4.45(a)). At $x = 480$ *mm*, the subharmonic frequency ($\frac{1}{2}fr$) peak is at 214 Hz. This corresponds to a Strouhal number of $St_\theta = 0.0127$, where θ is the momentum thickness of the boundary layer at the trailing edge of the plate (given in Table 4.1). It has been pointed out by many authors [46-49] that the natural instability frequency of a free shear layer is at $St_{\theta_n} \cong 0.012$. This means that, in the absence of any excitation, a free shear layer rolls up at a frequency corresponding to $St_{\theta_n} \cong 0.012$. Therefore, the spectra peak at 214 Hz indicates the natural instability frequency of the wake. It is noted that a small peak with apparently no energy content shows up around *fr* = 6000Hz in figure 4.45(a). This is indicative of external forcing. The external forcing amplifies rapidly as can be seen in figure 4.45(b,c). The exact spectra behavior described above for plate 1is observed for the wakes of the other three plates. These are shown in figures 4.46-4.48. In the figures the spectra peaks indicated by arrow are the harmonic or subharmonic frequency corresponding to the natural instability frequency. The Strouhal numbers obtained for those frequencies are 0.0115 for plate 2, 0.0173 for

plate 3 and 0.0122 for plate 4. All, except plate 3, correspond to the natural instability frequency already confirmed for plane shear layer [46]. The reason why the number for plate 3 is not close to 0.012 is not entirely clear. However, it is noted that the longitudinal velocity fluctuation at the trailing edge of plate 3 has a peak r.m.s. value of about 4 times higher than those of the other plates (see figures 4.1-4.4).

The level of perturbation observed in the present experiment is far higher than the excitation applied by Wygnaski et al. [15] in their experiment. It is therefore expected that the growth rate in the present case will be much higher than those reported by them. In an experiment on the flow over a backward-facing step, Hasan [47] observed that the basic effect of the perturbation applied appeared to be an increased growth rate of the shear layer. He also obtained $St_{\theta_n} \cong 0.012$, an indication that the instability characteristics of the reattaching shear layer (represented by the backward-facing step) are similar to those of free shear layer. Zaman and Hussain [48] showed that excitation could result in suppression of the broadband turbulence in jet flow. They found that the suppression effect occurred when the shear layer was excited at frequencies above the natural roll-up frequency; the most pronounced being at $St_\theta \approx 0.017$. They argued that this is because the fluctuation intensities encountered in the natural shear layer owing to the passage of strong vortices are suppressed by the inhibition of the formation of these energetic vortices when the flow is excited. Based on these findings, it is expected that the wakes in the present experiment will experience turbulence suppression. It was stated in section 4.3 that that the peak value

of the normalized normalized shear stress $-\overline{uv}/w_o^2$ for plate 1 is 0.12 whereas Wygnanski et al. [15] obtained a value of 0.05 for airfoil wake. Using equations 2.3 and 2.10 together with the values of W_o and θ in Table 4.3 it is discovered that the peak value of $-\overline{uv}$ in the present experiment is about 44% of the value obtained by Wygnanski et al. [15]. This suppression effect is consistent with the results obtained for jet flow [48].

The origin of the perturbation in the present experiment is not known precisely but there are a number of possible sources in the experimental facility (i.e. the wind tunnel). These sources are the fan blades, insufficient length of the contraction section and the short length of the diffuser section [50]. Mechanical vibration of the fan is also a possible source [51].

Since the perturbations experienced by the wakes of the four plates are similar, they cannot account for the differences observed between the growth rates of plate 4 and the other plates. In order to gain insight into the flow conditions in the wakes, the spanwise developments of the self-preservation state of the wakes were examined.

4.5 Spanwise Development of the Self-Preservation State

The cross-wire was rotated through 90° (from its initial position) in order to obtain the shear stress on the x-z plane. The strength of the $\overline{uw}$ in relation to $\overline{uv}$ is an indication of the extent of three-dimensionality in the flow. Measurements of the U-W profile were taken at 2 or 3 x locations for plates 1, 2 and 4. Plots of the shear stresses $\overline{uv}$ and $\overline{uw}$ for the three plates are shown in figures 4.49-4.51. The x locations where the measurements were taken are indicated in the figures. For plates 1 and 2, the peak of the $\overline{uv}$ is higher than that of the $\overline{uw}$ in both the near and far wake. The situation with plate 4 is, however, different. Figure 4.51 shows that $\overline{uw}$ is stronger than $\overline{uv}$ in the near wake. This shows that it exhibits much stronger three-dimensionality than the other two plates. The higher peak of the $\overline{uw}$ profile in plate 4 is expected due to its trailing edge geometry, which has a sharp inflection point at the mid-span position. This ensures a higher spreading rate in the x-z plane, hence the smaller growth rate for plate 4.

Measurements were taken for plates 1, 2 and 4 at $z/d = \pm 20$, where d is the plate thickness, in order to examine the spanwise variation of the self-preservation state. The variations of w_o and L_o with distance from the trailing edge are shown for the three spanwise positions in figures 4.52-4.54. The figures show that the flows exhibit self-preservation at the three spanwise positions considered. In the case of plate 1, the self-preservation states (represented by the slopes of the straight lines in

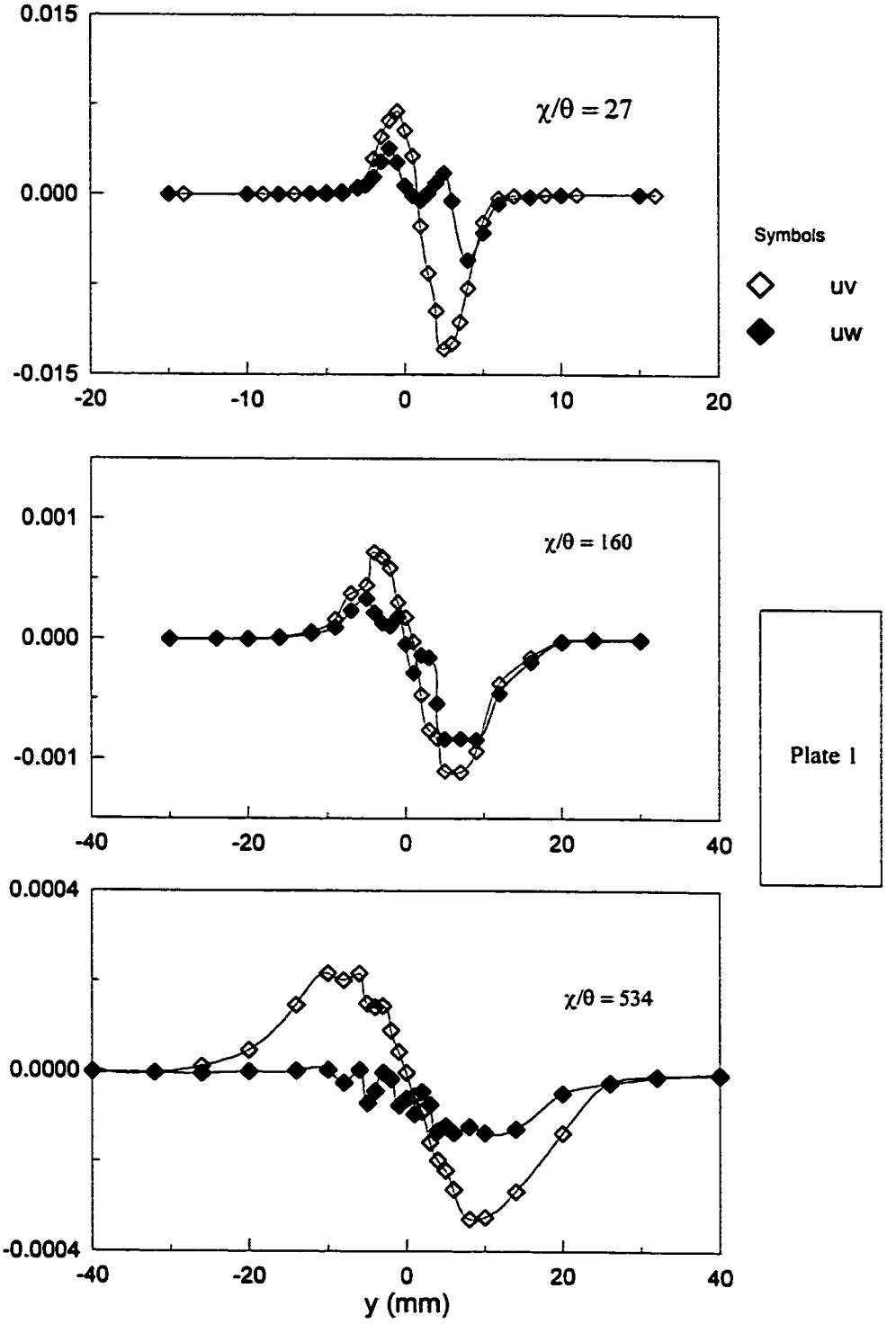

Figure 4.49. Plots of the Reynolds shear stresses at $z = 0$ normalized by the freestream velocity; Plate 1; $U_\infty = 10 m/s$.

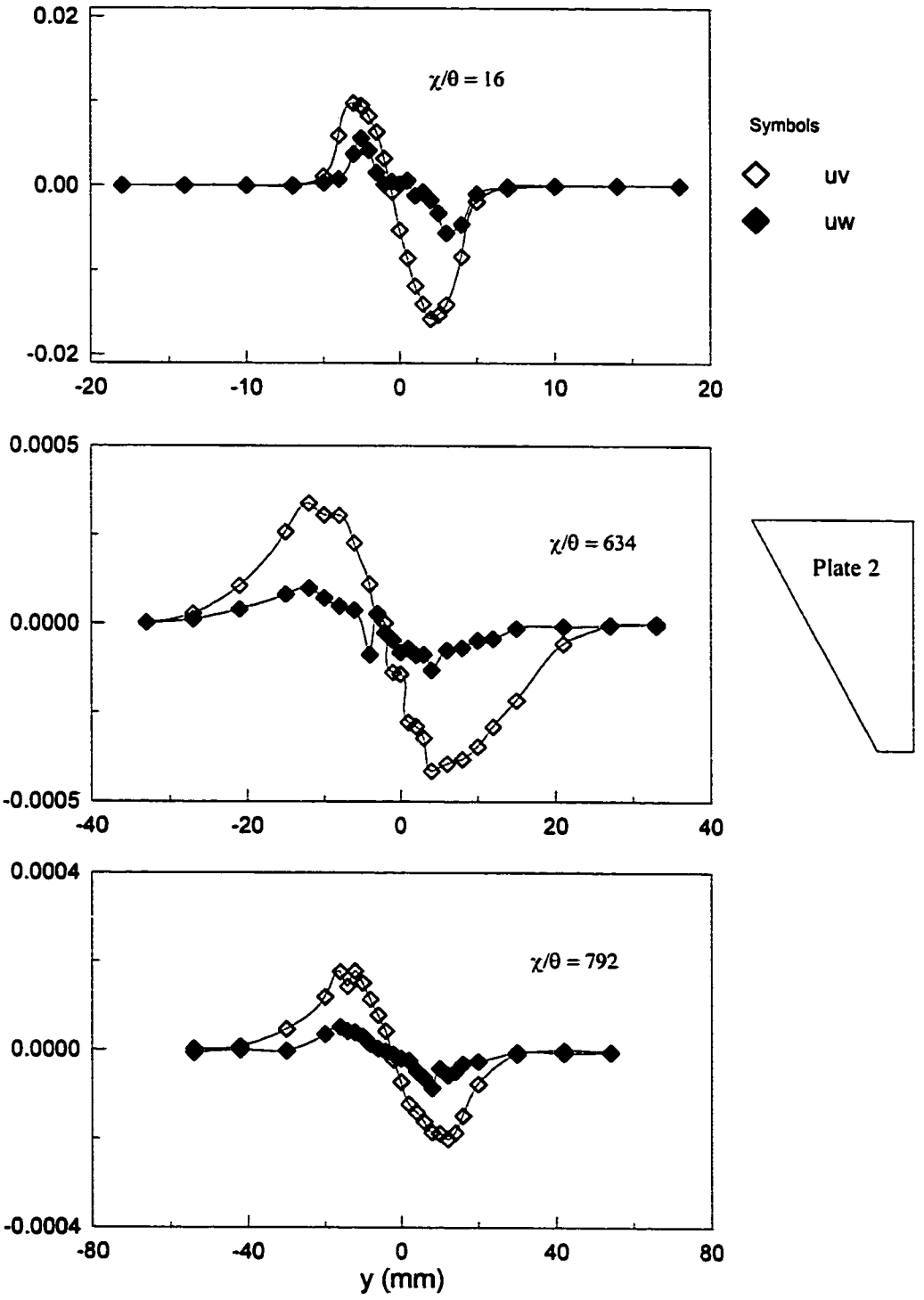

Figure 4.50. Plots of the Reynolds shear stresses at z = 0 normalized by the freestream velocity; Plate 2; $U_\infty = 10 m/s$.

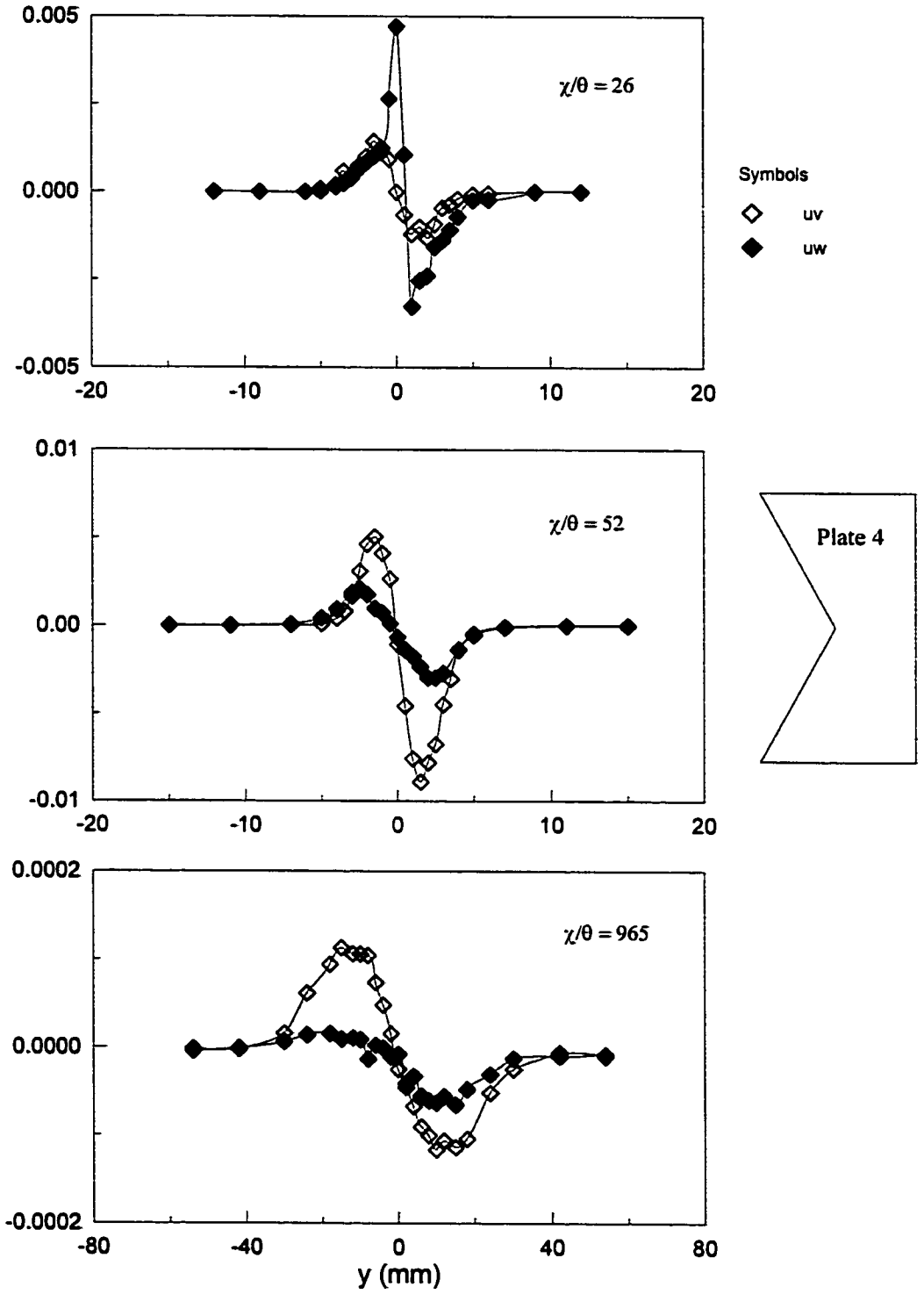

Figure 4.51. Plots of the Reynolds shear stresses at z = 0 normalized by the freestream velocity; Plate 4; $U_\infty = 10\,m/s$.

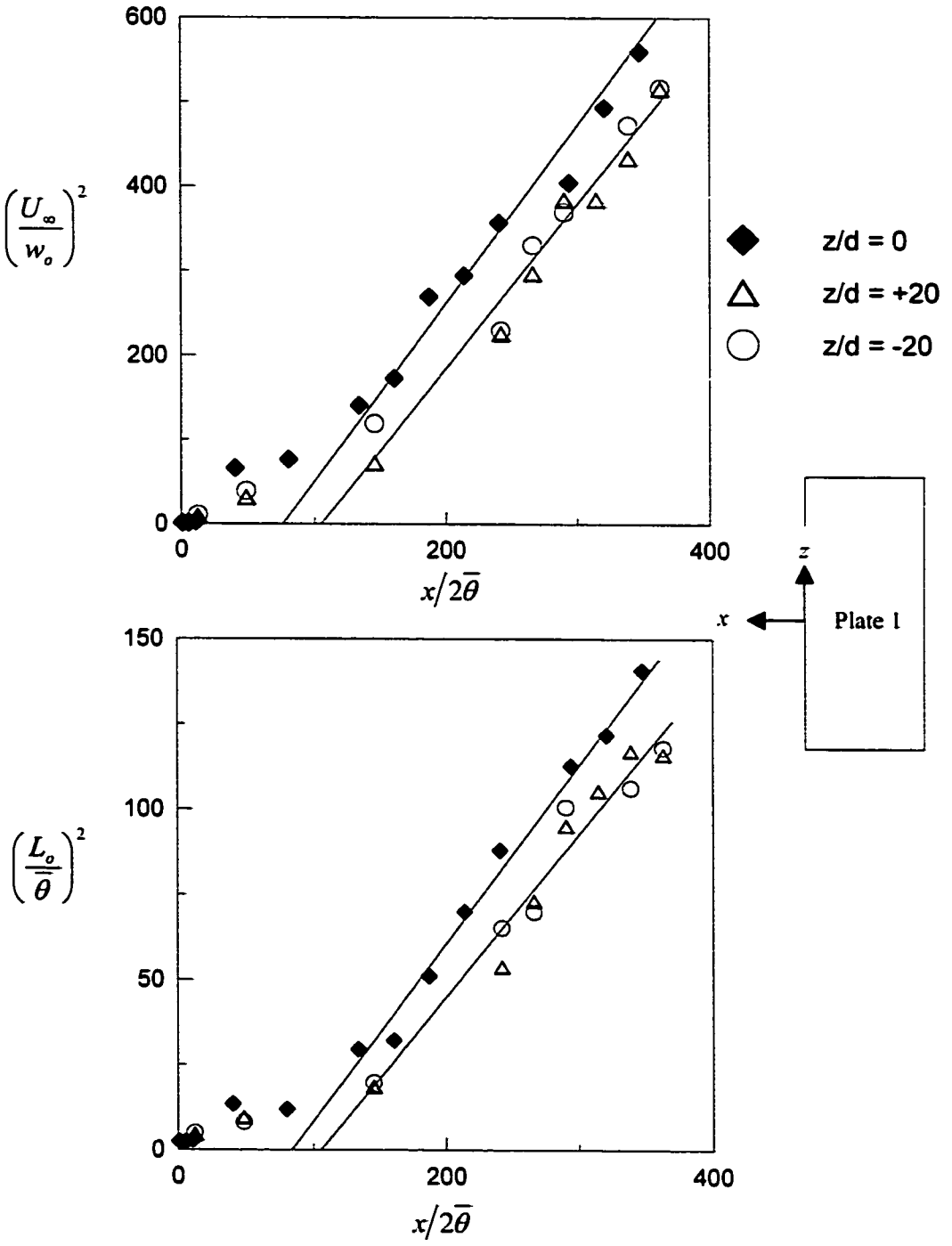

Figure 4.52 Variation of the center-line velocity defect and the half-wake width on and off the mid-span position for plate 1; $U_\infty = 10 m/s$.

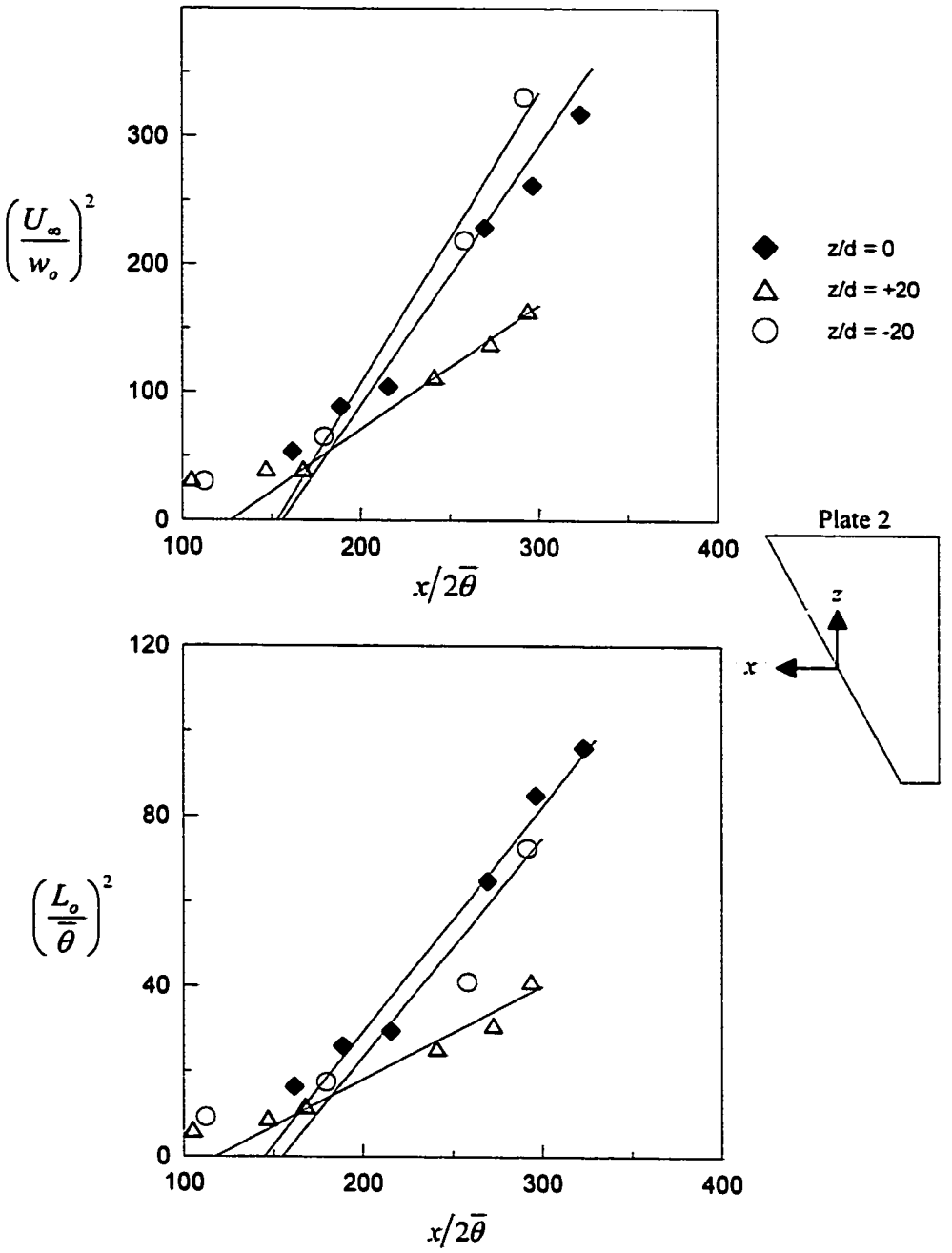

Figure 4.53 Variation of the center-line velocity defect and the half-wake width on and off the mid-span position for plate 2; $U_\infty = 10\,m/s$.
Note: x is the distance measured from the trailing edge at the specific z/d location.

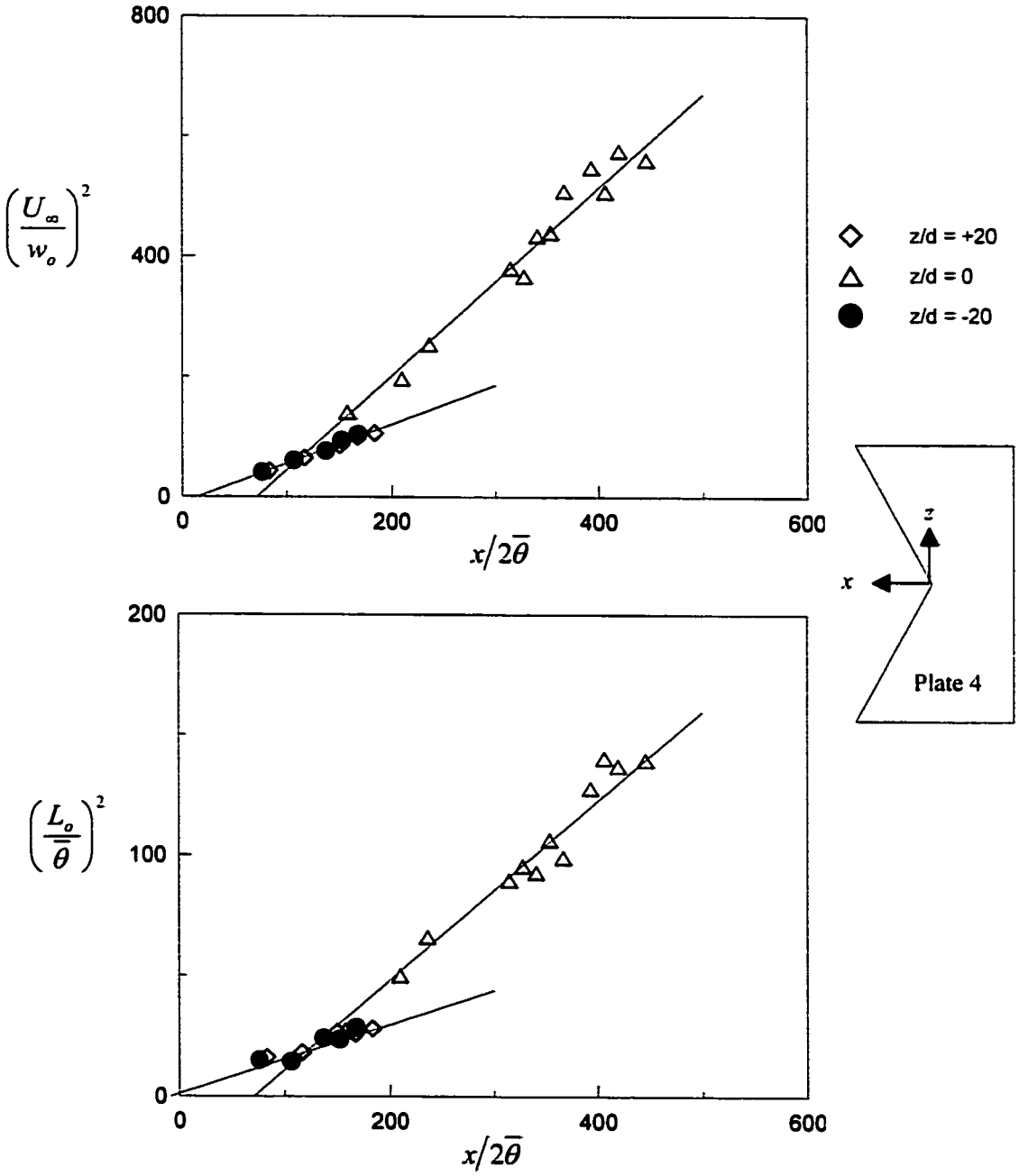

Figure 4.54 Variation of the center-line velocity defect and the half-wake width on and off the mid-span position for plate 4; $U_\infty = 10\,m/s$.
Note: x is the distance measured from the trailing edge at the specific z/d location.

figure 4.52) are identical at the three positions. However, there is a downstream shift in the location of the virtual origin as we move from the mid-span position to $z/d = \pm 20$. Plates 2 and 4 clearly display three-dimensionality as figures 4.53 and 4.54 show that the asymptotic state obtained depends on where the measurement is taken. Comparison of the wake parameters on and off the mid-span positions are made in Table 4.4. In all cases, the momentum thickness is higher at off the mid-span positions. This may be a result of being closer to the wall at these positions. Symmetry of flow about $z = 0$ is demonstrated by plates 1 and 4 (in terms of $x/2\theta$, A and B). It is important to note the patterns established by the constants A and B for plates 2 and 4. It is on the basis of these patterns that an explanation will now be offered to justify the self-preservation states obtained at the mid-span position, as presented in Table 4.2.

For plates 2 and 4, the flow separates from the plates at different x locations in the spanwise direction. On the longer side ($z/d = +20$ for plate 2 and $z/d = \pm 20$ for plate 4) the growth rate (value of A) is lower as a result of the flow staying longer on the plate. On the shorter side ($z/d = -20$ for plate 2) the growth rate is higher as a result of early separation from the plate. At the mid-span position for plate 2, the effects of the two sides ($z > 0$ and $z < 0$) tend to counteract each other. This explains why the results for plates 1 and 2 at $z = 0$ are very close. For plate 4, the wake grows faster at the mid-span position than elsewhere as a result of its early separation from the plate. It is interesting to note that the growth rates obtained at $z/d = \pm 20$ of plate

Table 4.4: Wake Parameters On and Off the Mid-span Position

		θ	$x_o/2\theta$	A	B	W_o	Δ_o	$W_o\Delta_o$
Plate 1	z/d = +20	1.24	114	2.007	0.495	0.998	0.497	0.497
	z/d = 0	1.12	70	2.017	0.502	0.996	0.501	0.499
	z/d = -20	1.24	100	2.001	0.478	1.000	0.489	0.489
Plate 2	z/d = +20	1.430	122	0.971	0.218	1.435	0.330	0.474
	z/d = 0	1.150	148	2.110	0.490	0.974	0.495	0.482
	z/d = -20	1.337	154	2.277	0.519	0.937	0.509	0.477
Plate 4	z/d = +20	1.801	10	0.641	0.130	1.767	0.255	0.450
	z/d = 0	1.15	89	1.656	0.420	1.099	0.458	0.504
	z/d = -20	1.972	4	0.682	0.156	1.712	0.279	0.479

4 are very close to the values obtained by Wygnanski et al. [15] for their flat plate without forcing.

4.6 Flow Visualization

Flow visualization studies of the four plates were carried out for both side and plan views in order to have some qualitative analysis of the flow field. The flow photographs on the side views of the four plates are presented in figures 4.55 – 4.58. The pictures in the figures reveal, in each case, that the flow started as a continuous stream with small disturbances. It later rolled up into discrete vortices to give a vortex street pattern of alternate signed vortices growing in the transverse direction as they convect downstream. Some of the pictures suggest the presence of swirling motion, but this is merely due to the inability of the camera to capture the minute details of the flow structures. In the actual experiment, clear vortex street pattern was observed.

The side views appear to suggest that the vortex street development follows the same pattern in the wakes of the four plates. This may lead one to conclude that the wakes quickly lost memory of their origins. However, the plan views suggest otherwise. Figures 4.59-4.62 show the photographs of the flow structure in the plan view when the wire was placed horizontally and the camera positioned on the roof of.

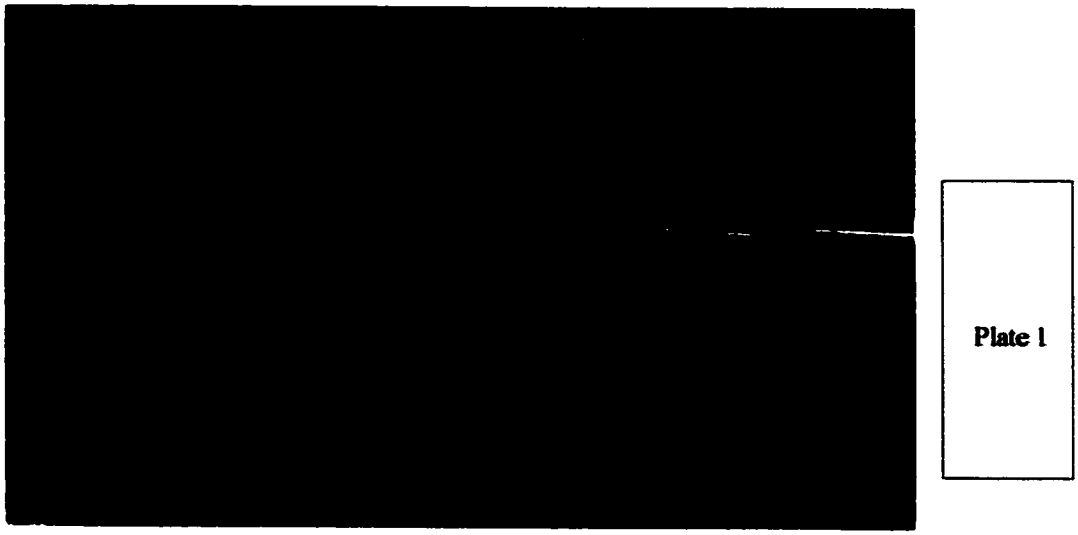

Figure 4.55 Instantaneous side view smoke visualization photograph at $U_\infty \approx 2m/s$ for plate 1. The flow is from right to left.

Figure 4.56 Instantaneous side view smoke visualization photograph at $U_\infty \approx 2m/s$ for plate 2. The flow is from right to left.

Figure 4.57 Instantaneous side view smoke visualization photograph at $U_\infty \approx 2m/s$ for plate 3. The flow is from right to left.

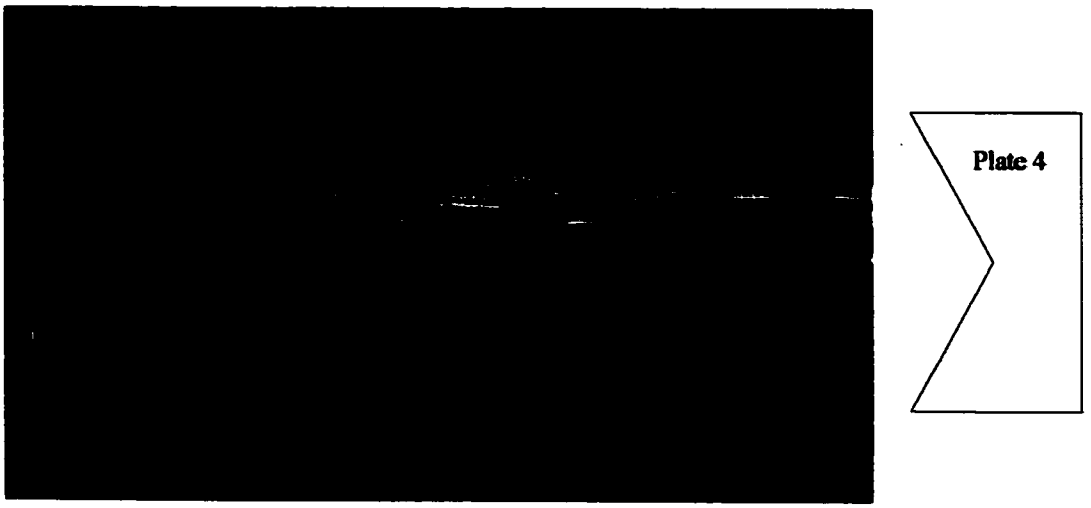

Figure 4.58 Instantaneous side view smoke visualization photograph at $U_\infty \approx 2m/s$ for plate 4. The flow is from right to left.

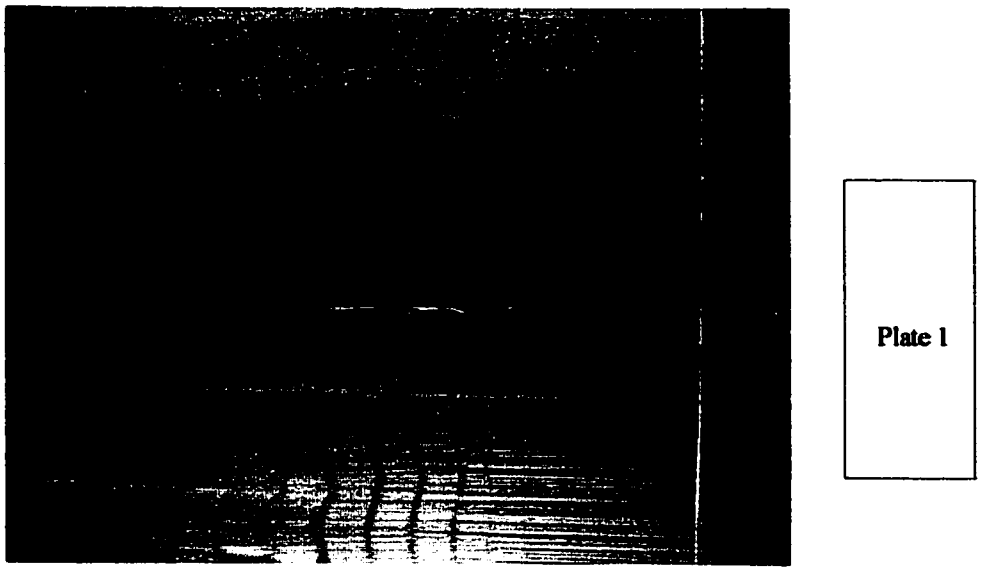

Figure 4.59 Instantaneous plan view smoke visualization photograph at $U_\infty \approx 2m/s$ for plate 1. The flow is from right to left.

Figure 4.60 Instantaneous plan view smoke visualization photograph at $U_\infty \approx 2m/s$ for plate 2. The flow is from right to left.

Figure 4.61 Instantaneous plan view smoke visualization photograph at $U_\infty \approx 2m/s$ for plate 3. The flow is from right to left.

Figure 4.62 Instantaneous plan view smoke visualization photograph at $U_\infty \approx 2m/s$ for plate 4. The flow is from right to left.

the tunnel. As the flow separates from the plate (figure 4.59), the streakline shows a continuous stream of fluid, which later breaks up. However, the break-up is not initiated at the same downstream location in the z-direction, thus resulting in undulation in the spanwise direction. This arrangement continues into the far wake. The extreme left position in figure 4.59 corresponds to $x = 870\,mm$ from the trailing edge. The hot-wire measurements showed that this position is in the far wake where self-preservation is well established. It is obvious that the vortex street pattern observed in the side view is not spanwise. The three-dimensional structure observed through the plan view does not show any tendency to change. We can therefore conclude that the flow did not lose memory of its origin. A similar observation was made by Breidenthal [52] in his flow visualization studies of shear layers and wakes subjected to three-dimensional disturbances. The plan views for plates 2 - 4 (figures 4.60 – 4.62) reveal the influence of the trailing edge on the flow structure. The same undulation of the structure observed in the case of plate 1 is present in all of them. However, the structures tend to align themselves parallel to the trailing edge. The arrangements do not change even in the far wake. While the structures for plates 1 – 3 tend to be generally straight (safe for the undulation), that of plate 4 is V-shaped. This probably creates strains, which result in strong three-dimensionality and consequent slowing down of the flow. The hot-wire measurements have already shown that plate 4 has the least wake growth rate.

One cannot generally claim that the results of the flow visualization experiment at $U_\infty = 2\,m/s$ apply to flows at 7.5 *m/s* and 10 *m/s* (where measurements were made). The choice of $U_\infty = 2\,m/s$ is a consequence of the limitation imposed by the flow visualization method used. The smoke-wire technique is limited to a Reynolds number based on wire diameter of $\mathrm{Re}_{dia} \leq 40$ [41]. At a higher Reynolds number, the vortices shed by the wire will contaminate the results.

CHAPTER 5

NUMERICAL COMPUTATION

5.1 Introduction

The experimental results presented in Chapter 4 revealed that there are significant differences between the growth rates of the wakes of plate 4 and those of plates 1,2 and 3, apparently because of the differences in the trailing edge configurations of the plates. The aim of the present numerical computation is to computationally examine the effect of trailing edge configuration on the wake growth rates. To carry out the investigation, the computation has to be three-dimensional. Preliminary investigations showed that only $1/8th$ of the spatial domain of the experiments could be successfully handled due to the demands of grid resolution and the maximum image size (storage capacity) allowed by FORTRAN. As a first step, the width of the computational domain was made to be half of the width of the tunnel. Taking advantage of the symmetry of flow in the transverse and spanwise directions further reduces the domain by a factor of 4. For plate 2, however, there is no symmetry in the z-direction. Therefore, no computation was performed for plate 2.

5.2 Computational Domain

The computational domain is a rectangular cylinder representing the test section of the wind tunnel. The schematic of the x-y and x-z planes of the domain is shown in figure 5.1, together with the positioning of plate 4. Since there are no adequate experimental data with which to start the computation in the wake, the inlet of the computational domain has to be upstream of the plate where the velocity components and turbulent intensity can be prescribed. The flow has a uniform velocity at the inlet section as shown. Boundary conditions on the other faces of the domain are also shown in the figure. The implementation of these boundary conditions will be discussed in section 5.5.

5.3 Governing Equations

The computations were performed by solving the Navier-Stokes equations for incompressible, turbulent flow in Cartesian coordinates. The governing equations are as follows:

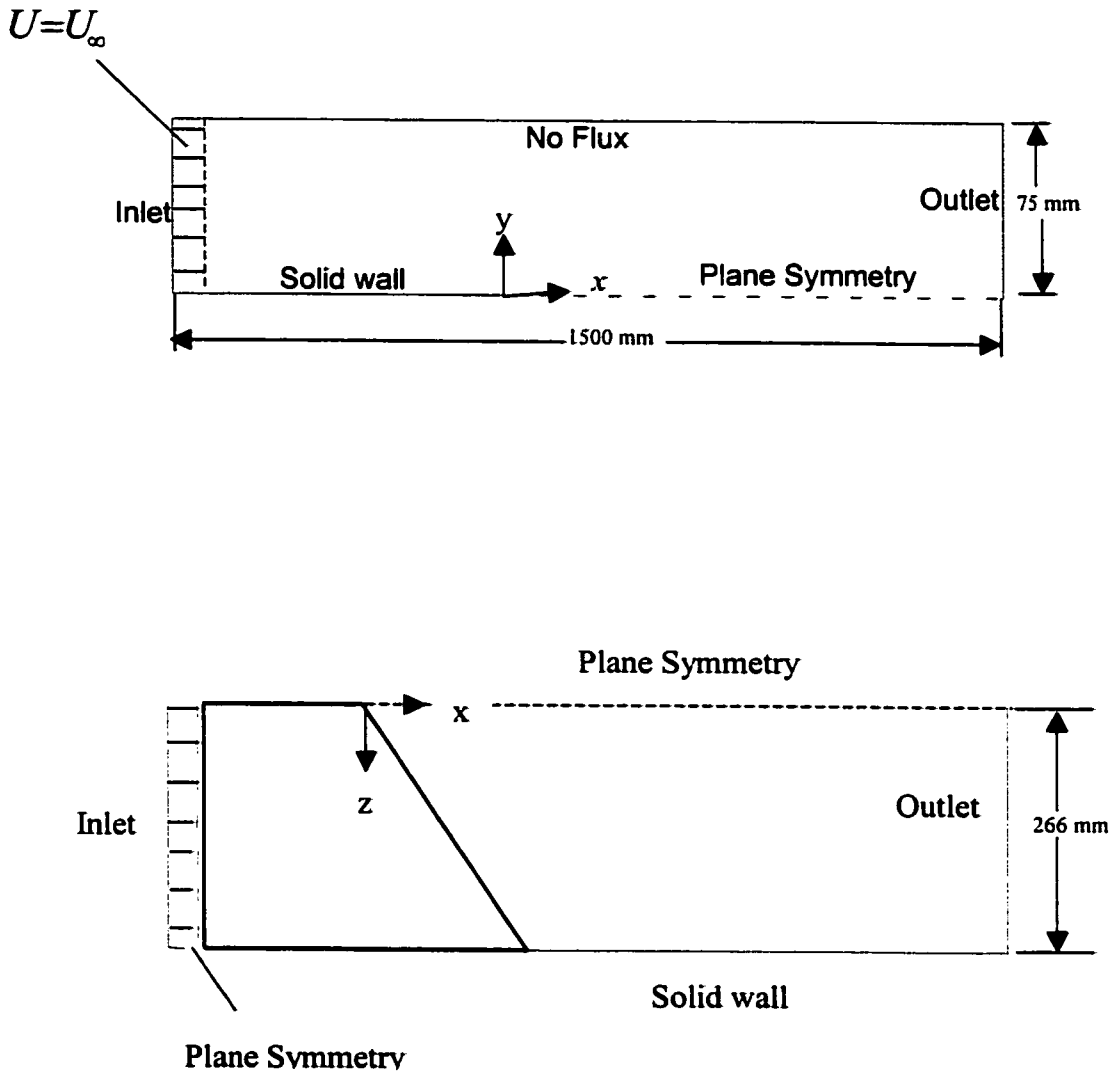

Figure 5.1 Schematic of the computational domain.

Continuity equation

$$\frac{\partial U}{\partial x}+\frac{\partial V}{\partial y}+\frac{\partial W}{\partial z}=0 \tag{5.1}$$

Momentum equations

$$\rho U\frac{\partial U}{\partial x}+\rho V\frac{\partial U}{\partial y}+\rho W\frac{\partial U}{\partial z}= \downarrow$$
$$-\frac{\partial}{\partial x}\left(\overline{p}+\frac{2}{3}\rho k\right)+\frac{\partial}{\partial x}\left(\mu_{eff}\frac{\partial U}{\partial x}\right)+\frac{\partial}{\partial y}\left(\mu_{eff}\frac{\partial U}{\partial y}\right)+\frac{\partial}{\partial z}\left(\mu_{eff}\frac{\partial U}{\partial z}\right) \tag{5.2}$$

$$\rho U\frac{\partial V}{\partial x}+\rho V\frac{\partial V}{\partial y}+\rho W\frac{\partial V}{\partial z}= \downarrow$$
$$-\frac{\partial}{\partial y}\left(\overline{p}+\frac{2}{3}\rho k\right)+\frac{\partial}{\partial x}\left(\mu_{eff}\frac{\partial V}{\partial x}\right)+\frac{\partial}{\partial y}\left(\mu_{eff}\frac{\partial V}{\partial y}\right)+\frac{\partial}{\partial z}\left(\mu_{eff}\frac{\partial V}{\partial z}\right) \tag{5.3}$$

$$\rho U\frac{\partial W}{\partial x}+\rho V\frac{\partial W}{\partial y}+\rho W\frac{\partial W}{\partial z}= \downarrow$$
$$-\frac{\partial}{\partial y}\left(\overline{p}+\frac{2}{3}\rho k\right)+\frac{\partial}{\partial x}\left(\mu_{eff}\frac{\partial W}{\partial x}\right)+\frac{\partial}{\partial y}\left(\mu_{eff}\frac{\partial W}{\partial y}\right)+\frac{\partial}{\partial z}\left(\mu_{eff}\frac{\partial W}{\partial z}\right) \tag{5.4}$$

where, $\mu_{eff}=\mu+\mu_t$. Here, ρ is the fluid density, *U, V, W* are the mean velocity components in the *x, y and z* directions respectively, $\overline{p}$ is the pressure, *k* is the turbulent kinetic energy, μ is the molecular viscosity and μ_t is the eddy viscosity that will be modeled by an appropriate turbulence model.

Some researchers (e.g. [30]) neglected the diffusion term in the longitudinal direction (marked with arrows in equations 5.2 – 5.4) in the calculation of two-dimensional wake, thus making the equations to become parabolic. The conditions under which this could be done are spelt out by Patankar and Spalding [53], one of which is that the diffusion of momentum is negligible in a predominant direction of flow. In the present case, however, the presence of the leading and trailing edges of the plate in the computational domain means that all the terms must be retained because the condition for parabolic flow, stated above, does not hold at the edges. Schlichting [16] emphasized this in the discussion of simplification of the Navier-Stokes equations to Boundary layer equation.

5.4 Turbulence Model

In order to account for the eddy viscosity term, μ_t, in the momentum equations, an appropriate turbulence model must be used. The $k-\varepsilon$ model of turbulence is employed for the computation. The standard $k-\varepsilon$ model equations are as follows [54]:

$$\rho U\frac{\partial k}{\partial x}+\rho V\frac{\partial k}{\partial y}+\rho W\frac{\partial k}{\partial z}=\frac{\partial}{\partial x}\left\{\left(\mu+\frac{\mu_t}{\sigma_k}\right)\frac{\partial k}{\partial x}\right\}+ \frac{\partial}{\partial y}\left\{\left(\mu+\frac{\mu_t}{\sigma_k}\right)\frac{\partial k}{\partial y}\right\}+\frac{\partial}{\partial z}\left\{\left(\mu+\frac{\mu_t}{\sigma_k}\right)\frac{\partial k}{\partial z}\right\}+G-\rho\varepsilon \qquad (5.5)$$

$$\rho U\frac{\partial \varepsilon}{\partial x}+\rho V\frac{\partial \varepsilon}{\partial y}+\rho W\frac{\partial \varepsilon}{\partial z}=\frac{\partial}{\partial x}\left\{\left(\mu+\frac{\mu_t}{\sigma_\varepsilon}\right)\frac{\partial \varepsilon}{\partial x}\right\}+$$
$$\frac{\partial}{\partial y}\left\{\left(\mu+\frac{\mu_t}{\sigma_\varepsilon}\right)\frac{\partial \varepsilon}{\partial y}\right\}+\frac{\partial}{\partial z}\left\{\left(\mu+\frac{\mu_t}{\sigma_\varepsilon}\right)\frac{\partial \varepsilon}{\partial z}\right\}+C_{\varepsilon 1}G\frac{\varepsilon}{k}-C_{\varepsilon 2}\rho\frac{\varepsilon^2}{k} \qquad (5.6)$$

where the term representing the production of turbulent kinetic energy, G, is given in tensor notation by

$$G=\mu_t\frac{\partial U_i}{\partial x_j}\left[\frac{\partial U_i}{\partial x_j}+\frac{\partial U_j}{\partial x_i}\right] \qquad (5.7)$$

and the eddy viscosity is given by

$$\mu_t=\rho C_\mu k^2/\varepsilon \qquad (5.8)$$

The Reynolds normal and shear stresses can be computed from the formula

$$-\overline{u_i u_j}=\frac{\mu_t}{\rho}\left[\frac{\partial U_i}{\partial x_j}+\frac{\partial U_j}{\partial x_i}\right]-\frac{2}{3}\delta_{ij}k \qquad (5.9)$$

where δ_{ij} is the Kronecker delta given by $\delta_{ij}=1$ if $i=j$ and $\delta_{ij}=0$ if $i\neq j$. The values of the model constants, which appear in equations 5.5, 5.6 and 5.8, are $C_\mu=0.09$, $C_{\varepsilon 1}=1.44$, $C_{\varepsilon 2}=1.92$, $\sigma_k=1.0$ and $\sigma_\varepsilon=1.3$.

In order to improve the robustness of the algorithm, Illinca and Pelletier [55] suggested a change of variable in the source terms of the k and ε equations using the eddy viscosity definition (equation *5.8*). Thus, ε in the terms indicated with arrows in equations 5.5 and 5.6 are eliminated with the use of equation 5.8.

The standard $k-\varepsilon$ model is primarily valid for high Reynolds number flows far from the wall. One of the methods often employed to extend the solution to the wall is the use of the wall functions [56, 57]. These are a collection of semi-empirical formulas and functions that bridge the solution variables at the near-wall cells and the corresponding quantities on the wall. However, the wall function approach is not reliable for three-dimensional flows [57] and was therefore not used for the present investigation.

Various authors [58-63] have tried to extend the standard $k-\varepsilon$ model to accommodate low Reynolds number extension for flows close to solid walls. These extensions are in the form of extra terms and coefficients, which take into account the influence of low Reynolds number and of wall proximity. A number of these modifications were tried for the computation of two-dimensional wake in order to determine their suitability to the problem. They were found to be slow in converging and they sometimes indicated a tendency for breakdown. They were therefore not used for the computation.

The low-Reynolds number model used is that of the two-layer model. In the two-layer model, the flow domain is divided into a viscosity-affected region I and a fully-turbulent region II [64]. The demarcation of the two regions is determined by a wall-distance based, turbulent Reynolds number, Re_y, defined as

$$\mathrm{Re}_y = \frac{\rho\sqrt{k}y}{\mu} \tag{5.10}$$

where y is the distance to the nearest wall. All cells whose centers are within $\mathrm{Re}_y \leq 200$ fall into region I; the rest are in region II. In region II, the standard $k-\varepsilon$ model is employed. For the viscosity-affected near-wall region (i.e. region I), the one-equation model of Wolfstein [65] is employed. In the one-equation model, the k equation of the standard $k-\varepsilon$ model is retained. However, the ε field and the turbulent viscosity are computed as follows:

$$\varepsilon = \frac{k^{3/2}}{l_\varepsilon} \tag{5.11}$$

$$\mu_t = \rho C_\mu \sqrt{k} l_\mu \tag{5.12}$$

The length scales that appear in equations *(5.11)* and *(5.12)* are computed from

$$l_\mu = C_l y\left[1-\exp\left(-\frac{\mathrm{Re}_y}{A_\mu}\right)\right] \tag{5.13}$$

$$l_\varepsilon = C_l y\left[1-\exp\left(-\frac{\mathrm{Re}_y}{A_\varepsilon}\right)\right] \qquad (5.14)$$

The constants in equations *(5.13)* and *(5.14)* are given by Chen and Patel [64] as $C_l = 0.418 C_\mu^{-3/4}$, $A_\mu = 70$, $A_\varepsilon = 2C_l$. The coefficient 0.418 in the formula for C_l is the von Karman constant in the logarithmic law of the wall for turbulent flow.

5.5 Boundary Conditions

The boundary condition information is included in the schematic of the computational domain in figure 5.1. Five types of boundary conditions – inlet, wall, plane symmetry, no-flux, and outlet – were used. The inlet plane was located 50 *mm* upstream of the tunnel test section. Here, a uniform velocity $U = U_\infty$ was imposed while other velocity components and k and ε were set to zero. On the wall, the no-slip boundary condition (*i.e.* $U = V = W = 0$) was applied. Also k and ε were set to zero on the wall.

The computational domain is bounded by symmetry planes at $y = 0$, $z = 0$ and $z = width$. The third symmetry plane coincides with the center of the tunnel. It should be noted that some portions of the symmetry planes coincide with walls. For such portions, the wall condition was used. Imposition of the symmetry boundary

condition was done by setting the normal component of velocity and the gradient of all other quantities to zero. At the top boundary of the computational domain is an impermeable boundary at which a no-flux condition was imposed. The implementation of the no-flux condition is identical to that of the symmetry boundary condition. The use of this condition allowed a substantial reduction of the height of the domain, which otherwise would have extended to the roof of the tunnel. This type of boundary condition was applied by Keimasi and Taeibi-Rahni [66] in a three-dimensional computation of turbulent flow of square jets injected perpendicularly into a cross flow. The height of the computational domain (75 *mm*) was arrived at through guidance from the experimental data such that the height is at least twice the wake width at the last measurement station.

The outlet plane was located at least 1200 *mm* downstream of the trailing edge (measured from the mid-span position of the plate). This is because the experiment has shown that the flow is well within the self-preserving region at that downstream location. The total length of the computational domain was therefore different for each plate. The location, which was arrived at after careful analysis of experimental data, was such that allowed the reduction of the governing equations from elliptic to parabolic. For all quantities, but U, the outlet boundary condition was applied at the boundary nodes by cutting off the link with the downstream node [67]. This is however inappropriate for the U equation since there is still another unknown- the

downstream pressure. To ensure that overall continuity was satisfied, the nodal equation for U at the outlet boundary, $U_{NI,J,K}$, was set as follows:

$$U_{NI,J,K} = U_{NI-1,J,K}\left(\dot{M}_{in}/\dot{M}_{out}\right) \qquad (5.15)$$

where $\dot{M}_{in}$ is the total mass flux through the entire inlet boundary and $\dot{M}_{out}$ is the total mass flux through the plane containing the nodes $U_{NI-1,J,K}$ [31, 66].

5.6 Computational Methodology

A computer code was developed to solve the system of equations *(5.1) – (5.8)* over the computational domain. Discretization of the equations is based on finite volume formulation. The formulation complies with the four basic rules given by Patankar [67], which ensure the stable convergence of a finite-volume-based algorithm towards a physically realistic numerical solution. The flow property values at volume faces were obtained by linear interpolation, when necessary. For the computation of the convective fluxes, the power-law differencing scheme of Patankar [67] was used. The code uses a non-uniform staggered grid arrangement in which the velocity components are located on the control volume surfaces and the scalar quantities are located inside the control volumes. Even though only plate 1 has a rectangular shape, the geometry of the other plates are simple enough to accommodate a Cartesian coordinate system with no need for coordinate transformation. For those plates, the

step size in the x-direction was made to be very small around the trailing edge in order to adequately represent the true shape of the trailing edge. Three different grids, $NI \times NJ \times NK$ = 190 x 45 x 50, 220 x 50 x 55 and 240 x 60 x 55 were used for plate1 in order to obtain grid-independent solution. The parameters W_o and Δ_o (defined in equations 2.10 and 2.11) were used to compare the results obtained using different grids. It was discovered that the difference in the results obtained with the three grids were within 2% of each other. The results to be presented (in Chapter 6) are for the first grid. For plates 3 and 4, only one grid, 200 x 45 x 50 was used. The criterion for grid-independent solution is explained in the presentation of results (Chapter 6). The system of equations was solved by using the Semi-Implicit Method for Pressure-Linked Equations (SIMPLE) algorithm. This is an algorithm in which the principle of mass-flux continuity is imposed indirectly via the solution of pressure-correction equations. The descretized algebraic equations were solved by applying a line-by-line method on the tri-diagonal matrix algorithm (TDMA). The line-by-line traverse was done in the three directions to ensure that boundary condition information from the ends was quickly brought to the interior. Under-relaxation factors of 0.3 and 0.2 were applied on the momentum and pressure correction equations respectively. For the k and ε equations, the under-relaxation factor was varied gradually during the iteration from 0.1 until it reached a value of 0.3. To start the computation, an initial uniform field of $U = \frac{1}{2}U_\infty$, $V = 0$, $W = 0$, $\overline{P} = 0$, $k = 0$, $\varepsilon = 0$ was prescribed for all the

nodes except for boundary nodes with Dirichlet boundary conditions[+]. The computed solution was assumed to have converged to its steady state when the magnitudes of the residual of mass source (in the pressure-correction equation) normalized by the inlet mass flux is less than 10^{-4}.

[+] Specified value of variable at the boundary.

CHAPTER 6

COMPUTATIONAL RESULTS

The computer program presented in Appendix E was applied to plates 1, 3 and 4. These three plates have symmetry in the spanwise direction and therefore required less computer memory and execution time. An inlet speed of $U_\infty = 10 m/s$ was applied. The results were analyzed in the similarity coordinates for self-preserving wake as presented in chapter 2.

The streamwise development of the displacement thickness (δ), momentum thickness (θ) and the shape factor (H) for the three plates is shown in figure 6.1. Both δ and θ have been doubled in order to represent the values across the wake as expressed in equation 2.9. It is observed from the figure that the value of the displacement thickness reduces gradually along the wake to approach the value of the momentum thickness. The shape factor therefore approaches a value of unity in the far wake. The value of the momentum thickness too reduces along the wake but the reduction is so small (compared to that of δ) that it can be regarded as essentially constant. The variation of θ within the region regarded as far wake is less than 1%. Its value at the exit plane of the computational domain was used to normalize all length

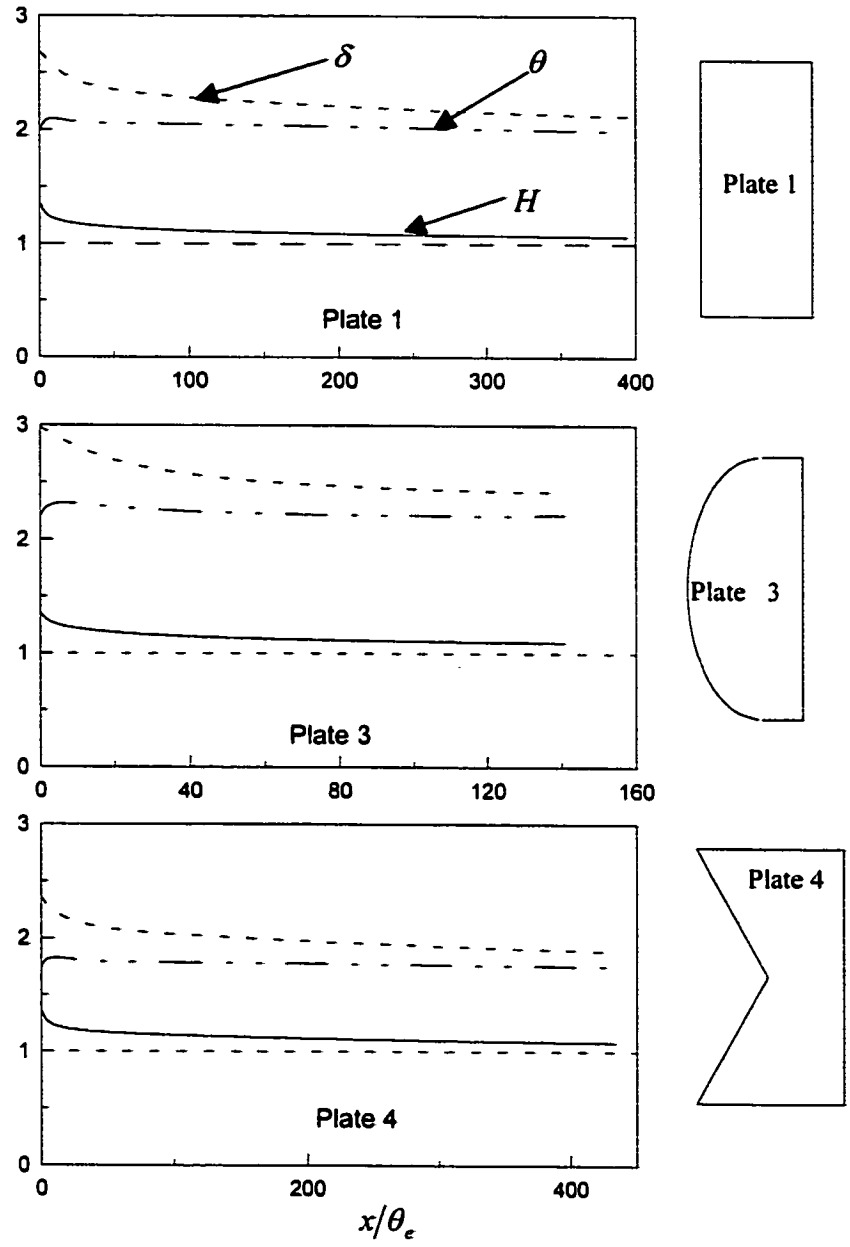

Figure 6.1 The streamwise development of the displacement thickness, momentum thickness and shape factor (obtained by numerical computation). δ and θ are in mm. θ_e is the momentum thickness at the at the exit plane of the computational domain.

scales and distances. The developments of δ, θ and H obtained from the computation bear qualitative resemblance to those of the experiments.

The profiles of the far wake mean velocity defect (at four specified locations for each plate) are shown in figure 6.2. The broken line represents the theoretical asymptotic profile of equation 2.6. In the inner wake ($\eta \leq 1$), there is a good collapse of the data onto the asymptotic profile. However, there is disagreement with the asymptotic profile in the outer wake. In their calculation of two-dimensional far wake, Patel and Scheuerer [30] made a similar observation about the poor agreement of the computed results with the asymptotic profile in the far wake. The disagreement with the asymptotic profile has been attributed to the presence of intermittency in the outer wake, which the $k-\varepsilon$ model is unable to account for [34]. Using their proposed $k-\varepsilon-\gamma$ model, Cho and Chung [34] obtained results that were in better agreement with the asymptotic theory. The Cho and Chung model applies to fully turbulent flow only. This makes it inappropriate for the present problem whose domain includes laminar, transitional and turbulent regions. The $k-\varepsilon-\gamma$ model was therefore not considered for the problem.

Figure 6.3 shows the computed profiles of the normal stress. The plot for plate 1 shows a good collapse of the data on a single curve. Those for plates 3 and 4 do not show neat collapse. The computed normal stress has double peaks when both sides of the plate are considered. The profiles for the normalized shear stress are shown in

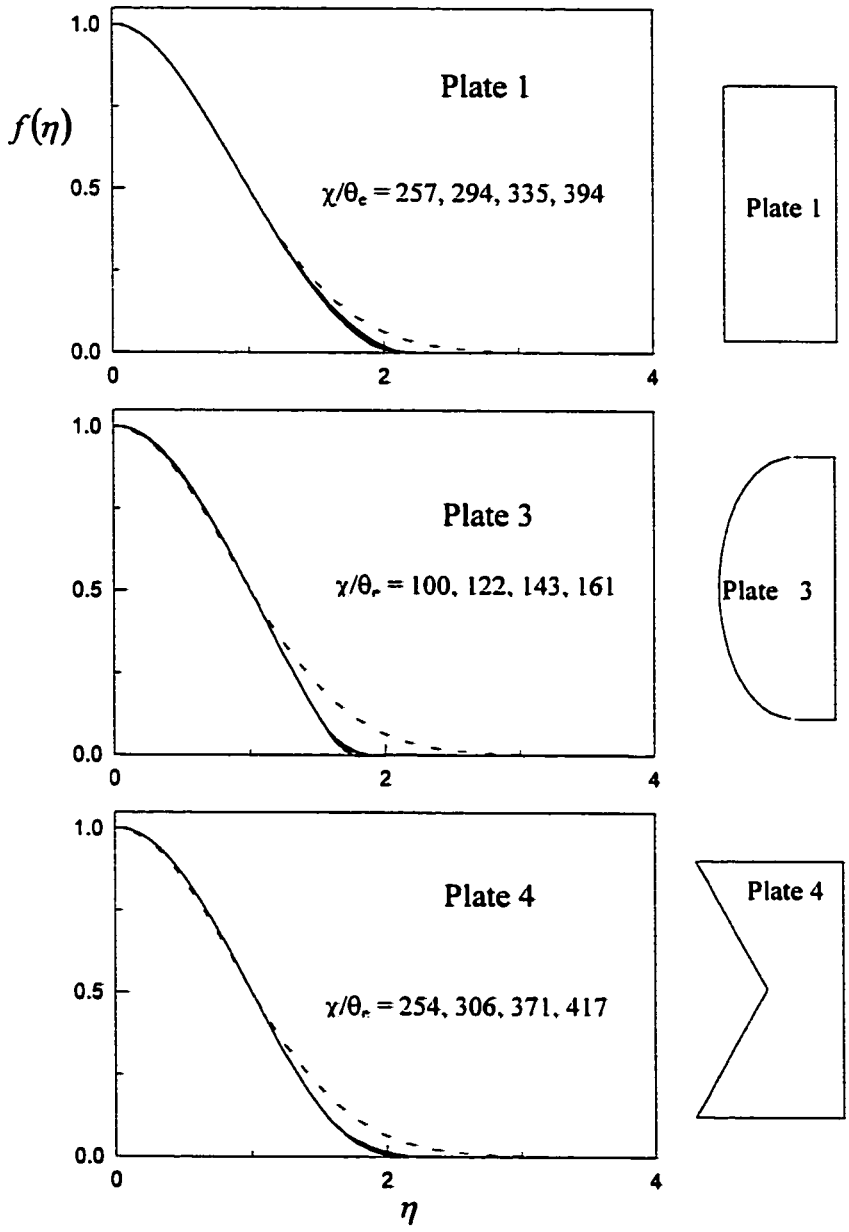

Figure 6.2 The computed mean velocity defect in the far wake (at z = 0) expressed in similarity coordinates. The x locations of the velocity defects are shown on the plots. The broken line is the theoretical asymptotic profile.

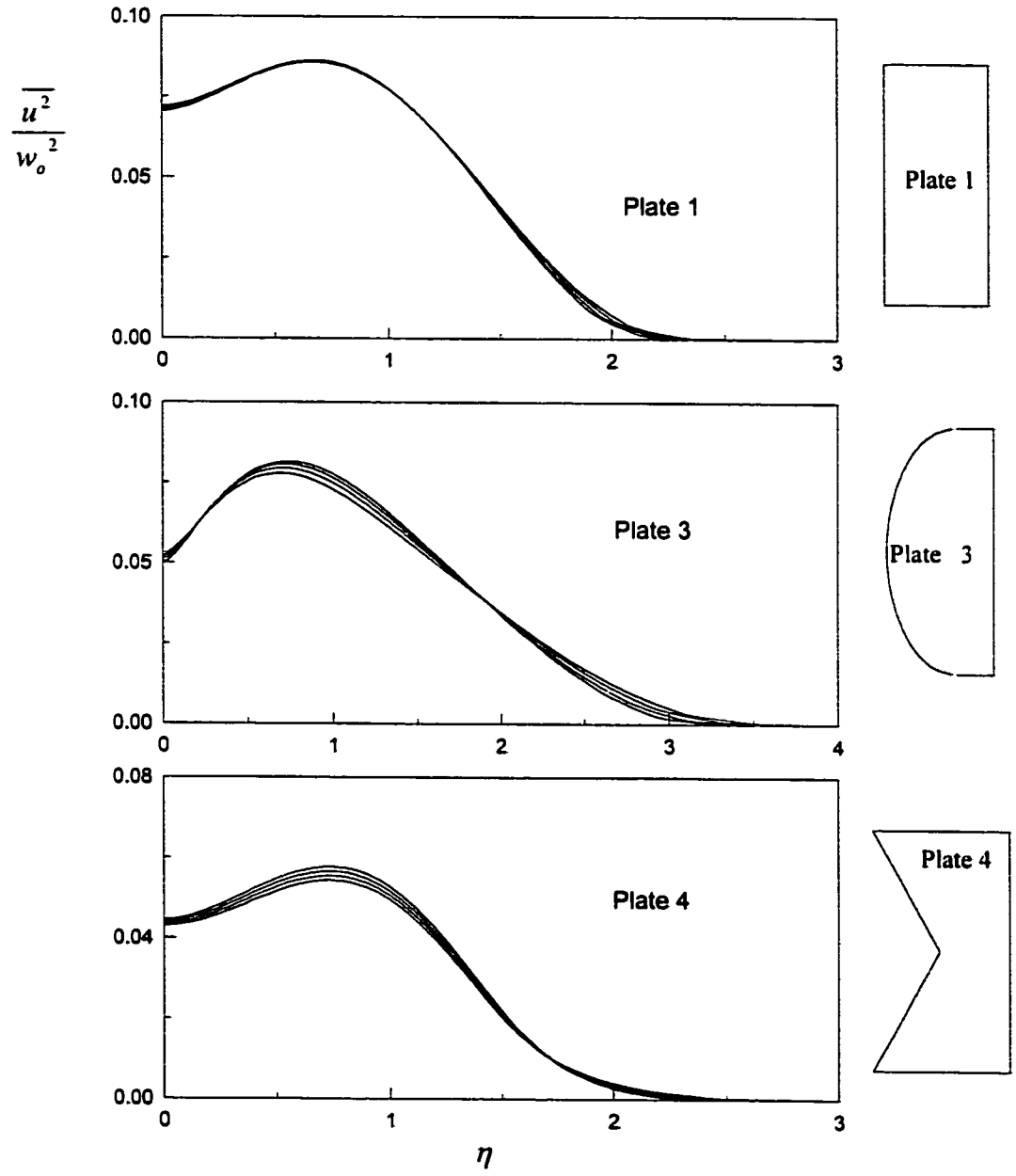

Figure 6.3 The computed normal stress (at z = 0) in the far wake expressed in similarity coordinates. The x locations are the same as those of figure 6.2.

figure 6.4. All the profiles show good collapse on a single curve. It is noticed that the peak value of the normalized shear stress for plate 4 is less than those of plates 1 and 3. The trend is in agreement with the experimental results.

The streamwise developments of the velocity and length scales are shown in figure 6.5. It is evident that the self-preservation state was reached for each plate since the curves later became straight lines. The figure shows that the growth rate of the wake of plate 4 is significantly lower than those of plates 1 and 3. This is the exact trend obtained from the experiments. The wake parameters calculated from the straight portions of the plots of figure 6.5 are shown in table 6.1. The results obtained for plates 1 and 3 are very close to the growth rates obtained by Wygnanski et al. [15] for the case of wake not subjected to external forcing (Table 4.3).

All the results obtained through numerical computation show qualitative agreements with the experimental results. The numerical computation supports the finding that the growth rate of the wake of plate 4 is significantly different from those of the other plates. This confirms that the development of wake is dependent on the nature of the wake generator. However, there is no quantitative agreement between the results of the experiment and the numerical computation. It has been argued in chapter IV that the wake generated during the course of the experiment was under the influence of external forcing. The work of Wygnanski et al. [15] has shown clearly that wake development is susceptible to external disturbances. It is not possible to incorporate external forcing into the numerical computation. This is why Moser et al. [37]

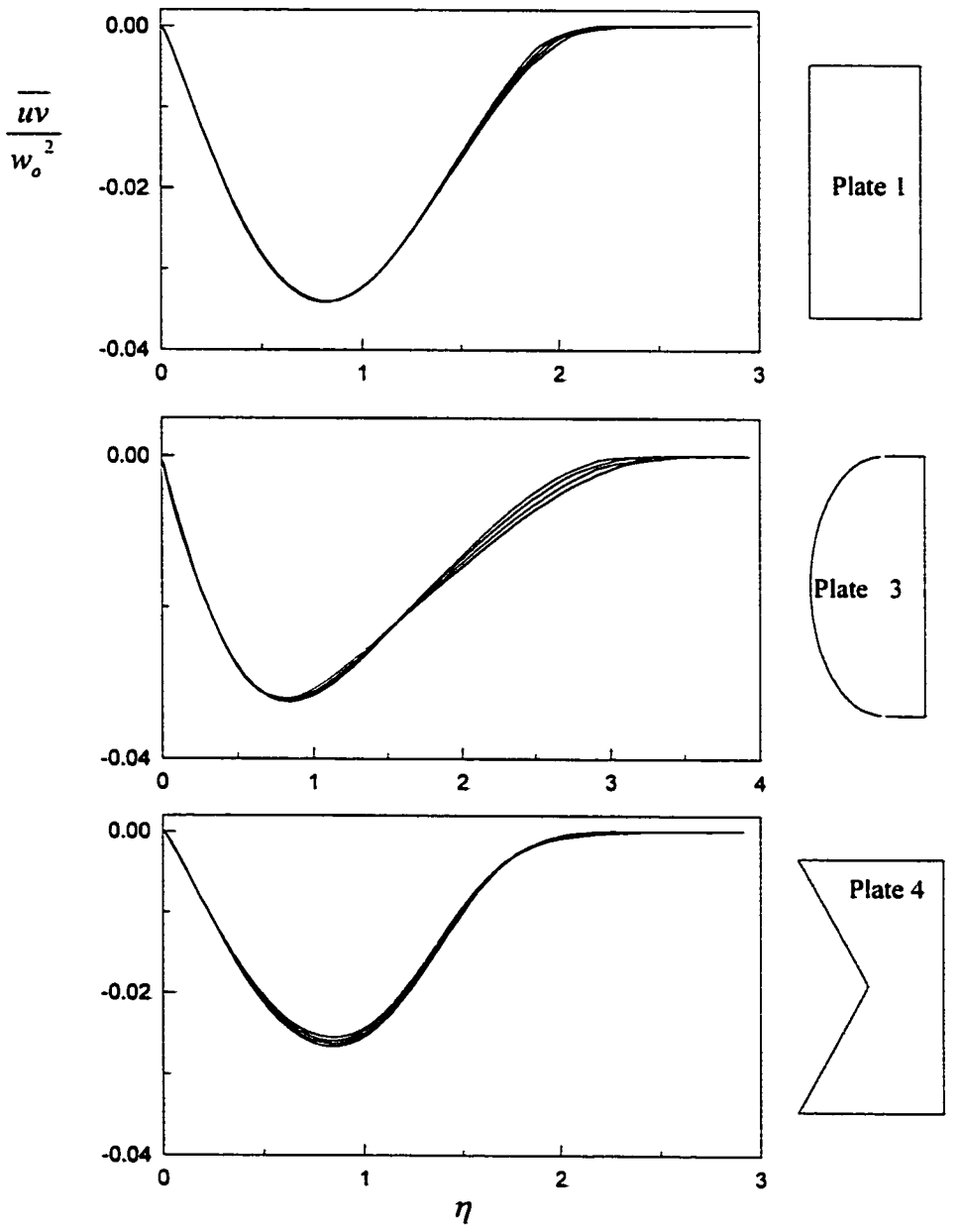

Figure 6.4 The computed shear stress (at z = 0) in the far wake expressed in similarity coordinates. The x locations are the same as those of figure 6.2.

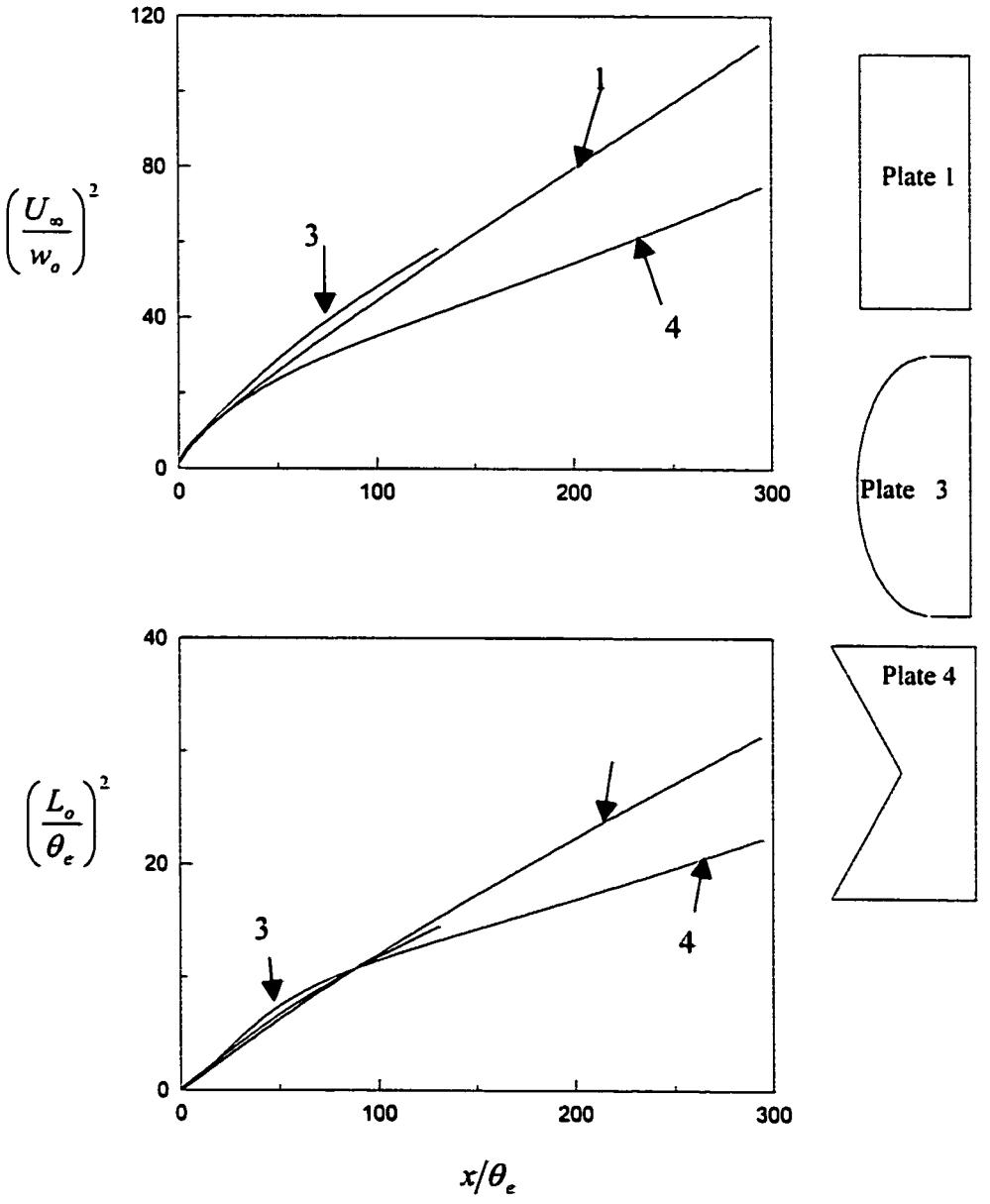

Figure 6.5 The streamwise developments of the velocity and length scales from the trailing edge to the exit plane of the computational domain.

Table 6.1: Prediction of the Wakes Properties in the Self-Similar Region

	U_∞ (m/s)	θ (mm)	$\frac{x_o}{2\theta}$	A	B	W_o	Δ_o	$W_o\Delta_o$
Plate 1	10	1.99	-18	0.698	0.186	1.693	0.301	0.516
Plate 3	10	2.21	-20	0.670	0.177	1.728	0.297	0.514
Plate 4	10	1.75	-22	0.468	0.123	2.068	0.248	0.513

concluded that no standard turbulence model would be capable of predicting the wake flow since they are insensitive to the features of the initial or inlet conditions that control the state of the wake.

CHAPTER 7

CONCLUSIONS AND RECOMMENDATIONS

7.1 Conclusions

The field properties in wake flow formed behind four different flat plates have been studied experimentally and computationally. Measurements were performed with the hot-wire anemometry system, mainly at the mid-span position of the plates. Measurements were also taken off the mid-span position at some x locations in order to investigate the variation of the self-preservation state in the spanwise direction. In order to gain some qualitative insights into the flow fields, flow visualization studies were performed using the smoke-wire technique. Numerical computation was performed to predict the wake growth rate at the plates' mid-span positions. The computation was performed by numerically solving the three-dimensional time-averaged Navier-Stokes equations together with the κ-ε model equations of turbulence. A FORTRAN program was developed for the computation. The following conclusions can be drawn from the study:

1. The wake formed behind a solid body evolves, after a sufficiently far distance from the generator, into a self-preserving state for which the flow can be described by a single velocity scale and a single length scale. This is evident by the collapse of the mean velocity defect profiles at several streamwise locations onto a single curve. The Reynolds stresses also collapse on their respective curves.
2. The self-preserving state of a wake depends on the nature of the generator. This is supported by the results obtained in this study, which shows that the growth rate of the wake of plate 4 at the mid-span position is significantly different from those of the other plates. Uncertainty analysis of the results shows that the differences cannot be attributed to experimental error. The reduced growth rate observed for plate 4 is a result of its trailing edge geometry, which has a sharp inflection point at the mid-span position, leading to a higher spreading rate on the x-z plane.
3. The effect of spanwise variation of separation points is to have spanwise variation of the wake's self-preservation state. This is demonstrated by the results observed at z/d = -20, 0 and +20 for plates 2 and 4, which have varying trailing edge positions in the z direction. Plate 2 has a decreasing wake growth rate (increasing W_o and decreasing Δ_o) from z/d = -20 to 0 and then to +20. Plate 4, on the other hand, has reduced wake growth rate on either side of the mid-span position. The variations of the growth rates appear to follow the configuration of the trailing edge positions.

4. The wake does not lose memory of its origin. This was confirmed by the fact that the reduced far wake growth rate recorded for plate 4 is traceable to the higher shear stress on the x-z plane in the region close to the trailing edge.
5. The self-preserving state of a wake is susceptible to external disturbances. In this study, it was shown through spectrum analysis that the wake generated was under the influence of external forcing. The work of Wygnanski et al supported the view that external forcing could alter the state of a wake.
6. The performance of the $k-\varepsilon$ model of turbulence is inadequate, to some degree, for the solution of wake flow problems. This is evident in its inability to predict the mean velocity defect with accuracy. Its major deficiency in this case is the inability to account for intermittency in the outer wake.

7.2 Recommendations

In view of the limitations experienced during the study, the following recommendations are made:

1. Flat plates of other shapes should be investigated in order to be able to establish a valid relationship between wake and its generator. This could be of immense industrial use in the control of wakes.

2. The source of external forcing in our wind tunnel should be investigated. Elimination of such source will enhance the quality of work done with the facility.
3. Facilities in our wind tunnel, many of which are in bad shape now, should be upgraded. Since measurements with hot-wire are highly influenced by temperature variation, it is desirable to have an effective cooling facility for the wind tunnel. That was the most difficult problem faced during the experiments.

APPENDIX A

THE SELF-PRESERVATION QUANTITIES FOR PLANE FAR WAKES

A.1 Introduction

The quantities which define the self-preservation state of a plane wake are the velocity and length scales as presented in equations *(7)* and *(8)* of chapter II. In this appendix, these quantities and the equation for mean velocity defect (equation *(6)*) are derived from the momentum equation, for flow with no pressure gradient.

A.2 Momentum Equation

By estimating the orders of magnitude of the terms of the momentum equations, Tennekes and Lumley [22] showed that the momentum equation in the longitudinal direction reduces to

$$U\frac{\partial U}{\partial x}+\frac{\partial(\overline{uv})}{\partial y}=0 \qquad \text{A.1}$$

For far wakes, $U \approx U_\infty$. Therefore, equation A.1 can be simplified further as

$$U_\infty \frac{\partial U}{\partial x} + \frac{\partial(\overline{uv})}{\partial y} = 0 \qquad \text{A.2}$$

A.3 Momentum Thickness

Since U_∞ is constant, equation A.1 can be written as

$$U \frac{\partial(U - U_\infty)}{\partial x} + \frac{\partial(\overline{uv})}{\partial y} = 0 \qquad \text{A.3}$$

Integrating the above equation over the entire flow and noting that $\overline{uv}$ vanishes at sufficiently large values of y, we obtain

$$\frac{d}{dx}\int_{-\infty}^{\infty} U(U - U_\infty)dy = 0 \qquad \text{A.4}$$

Therefore,

$$\rho \int_{-\infty}^{\infty} U(U - U_\infty)dy = M \qquad \text{A.5}$$

where M is a constant.

Equation A.5 can be written as

$$-\rho U_\infty^{\,2}\theta = M \qquad \text{A.6}$$

where θ is the momentum thickness defined by

$$\theta = \int_{-\infty}^{\infty} \frac{U}{U_\infty}\left(1 - \frac{U}{U_\infty}\right)dy \qquad \text{A.7}$$

A.4 The Velocity and Length Scales

According to the self-preservation theory the mean velocity defect and the Reynolds stress, when expressed in terms of the local length and velocity scales, become independent of x. They are expressed as follows:

$$(U_\infty - U)/w_o = f(\eta) \tag{A.8}$$

$$-\overline{uv} = w_o^{\,2} g(\eta) \tag{A.9}$$

where $\eta = y/L_o$.

Substituting equations A.8 and A.9 into equation A.2, and noting that

$$\frac{\partial U}{\partial x} = -\frac{dw_o}{dx} f(\eta) + \frac{w_o}{L_0}\frac{dL_o}{dx}\eta f'(\eta) \tag{A.10}$$

we have

$$-\frac{U_\infty L_o}{w_o^{\,2}}\frac{dw_o}{dx} f + \frac{U_\infty}{w_0}\frac{dL_o}{dx}\eta f' = g' \tag{A.11}$$

For f and g to be universal functions the coefficients of f and $\eta f'$ in equation A.11 must be constant. Therefore

$$\left.\begin{aligned} \frac{L_o}{w_o^{\,2}}\frac{dw_o}{dx} &= cons\tan t \\ \frac{1}{w_o}\frac{dL_o}{dx} &= cons\tan t \end{aligned}\right\} \tag{A.12}$$

The general solution to the pair (A.12) is

$$\left.\begin{aligned} L_o &\sim x^n \\ w_o &\sim x^{n-1} \end{aligned}\right\} \quad \text{A.13}$$

The value of n can be determined by using the momentum integral constraint. Substituting equation A.8 into equation A.5, we have

$$U_\infty w_o L_o \int_{-\infty}^{\infty} f(\eta)d\eta - w_o^2 L_o \int_{-\infty}^{\infty} f^2(\eta)d\eta = -M/\rho \qquad \text{A.14}$$

Noting that the second term is of order w_o/U_∞ to the first term and that w_o/U_∞ is very small, the second term can be neglected. Substituting equation A.6 into equation A.14, we have

$$w_o L_o \int_{-\infty}^{\infty} f(\eta)d\eta = U_\infty \theta \qquad \text{A.15}$$

The product $w_o L_o$ in equation A.15 must be independent of x. Using the pair (A.13) we have

$$w_o L_o = x^{2n-1} \qquad \text{A.16}$$

Therefore, $n = 1/2$. Thus, the velocity and length scales are given by

$$\left.\begin{aligned} w_o &= Ax^{-1/2} \\ L_o &= Bx^{1/2} \end{aligned}\right\} \quad \text{A.17}$$

A.5 The Mean Velocity Profile

Substituting equation A.17 into equation A11, we obtain

$$\frac{1}{2}(U_\infty B/A)[\eta f' + f] = g' \qquad \text{A.18}$$

We define an eddy viscosity, υ_τ, by $-\overline{uv} = \upsilon_\tau \partial U/\partial y$. Using equation A.8 we have

$$\upsilon_\tau = -w_o L_o \, g/f' \qquad \text{A.19}$$

Assuming υ_τ is constant, we can differentiate equation A.19 to obtain

$$g' = -\frac{1}{R_T} f'' \qquad \text{A.20}$$

where $R_T = w_o L_o/\upsilon_\tau$.

Substituting equation A.20 into equation A.18, we have

$$\alpha(\eta f' + f) + f'' = 0 \qquad \text{A.21}$$

where $\alpha = \frac{1}{2} R_T U_\infty B/A$.

Equation A.21 can be expressed as

$$\alpha \frac{d(\eta f)}{d\eta} + f'' = 0 \qquad \text{A.22}$$

Upon integration, we have

$$\frac{f'}{f} = -\alpha\eta + \frac{C_1}{\eta f} \qquad \text{A.23}$$

For equation A.23 to remain bounded at $\eta = 0$ (where $f = 1$), $C_1 = 0$. Therefore,

$$\frac{f'}{f} = -\alpha\eta \qquad \text{A.24}$$

Integration of equation A.24 yields

$$\ln f = -\frac{1}{2}\alpha\eta^2 + C_2 \qquad \text{A.25}$$

Since $f(0) = 1$, $C_2 = 0$. Therefore, equation A.25 simplifies to

$$f = \exp\left(-\frac{1}{2}\alpha\eta^2\right) \qquad \text{A.26}$$

If we define the length scale L_o as the half wake-width, i.e. the value of y for which the velocity defect is half of the center line defect, then $f(1) = 0.5$. Therefore we obtain the value of α in equation A.26 to be $2\ln 2$.

Therefore equation A.26 becomes

$$f = \exp(-\eta^2 \ln 2) \qquad \text{A.27}$$

APPENDIX B

HOT-WIRE CALIBRATION AND DATA ANALYSIS PROCEDURES

B1. Effective Velocity

The directional sensitivity of inclined sensors is given by Jorgensen's equation of effective cooling velocity as

$$Q^2 = V_N{}^2 + k^2 V_T{}^2 + h^2 V_{BN}{}^2 \qquad \text{B1}$$

where, Q is the effective velocity, V_N, V_T are the velocity components normal and tangential to sensor axis, V_{BN} is the velocity component normal to the plane of the sensors and k and h are constants.

For a cross-wire, the assumption is made that the velocity is in the plane of the sensors. For cross-wires, therefore, equation A1 reduces to

$$Q^2 = V_N{}^2 + k^2 V_T{}^2 \qquad \text{B2}$$

This equation translates to

$$Q_1^2 = |V^2|[\sin^2(\alpha+\theta)+k^2\cos^2(\alpha+\theta)] \quad \text{B3}$$

for sensor 1, and

$$Q_2^2 = |V^2|[\sin^2(\alpha-\theta)+k^2\cos^2(\alpha-\theta)] \quad \text{B4}$$

for sensor 2. V is the velocity magnitude, θ is the flow angle and α is the inclination of the sensors to the probe axis.

For a single-wire, the flow is normal to the sensor axis. Therefore, for a single-wire equation B1 reduces to

$$Q = V_N \quad \text{B5}$$

B2. Calibration

For both calibration and actual measurements the cross-wire axis is aligned with the longitudinal direction as shown in figures B1 and B2. During calibration the probe is located in the freestream, where the flow angle is zero. Equations B3 and B4, therefore, reduce to

$$Q_1^2, Q_2^2 = |V^2|[\sin^2\alpha+k^2\cos^2\alpha] \quad \text{B6}$$

The basic calibration is a curve fit of the effective velocity, Q, as a function of the bridge voltage, E, using a third-order polynomial fit,

$$Q = a_0 + a_1 E + a_2 E^2 + a_3 E^3 \qquad \text{B7}$$

Q is obtained from the known velocity, V, through equation B6.

B3. Data Analysis Procedure

During measurements, the sensors are inclined to the flow direction as shown in figure B2. The analysis procedure involves the calculation of the velocity magnitude and the flow angle θ, from which *V1* and *V2* are calculated.

First, the effective velocities Q_1 and Q_2 for sensors 1 and 2 are determined from the bridge voltages with the use of equation B7.

From equations B3 and B4:

$$A = \frac{Q_1}{Q_2} = \frac{\sin^2(\alpha+\theta) + k^2 \cos^2(\alpha+\theta)}{\sin^2(\alpha-\theta) + k^2 \cos^2(\alpha-\theta)} \qquad \text{B8}$$

Equation B8 is independent of the velocity magnitude; it depends solely on the angle θ. Substituting $\alpha = 45°$ into equation B8, the equation is manipulated into a quadratic equation

$$\left[1+k^2-A-Ak^2\right]\tan^2\theta+\left[2-2k^2+2A-2ak^2\right]\tan\theta+\left[1+k^2-A-Ak^2\right]=0 \qquad \text{B9}$$

Equation B9 yields two solutions θ_1 and θ_2. The minimum value is the flow angle, i.e. $\theta = \min(\theta_1,\theta_2)$.

Using equation B3, the velocity magnitude is determined as

$$|V| = \frac{Q_1}{\left[\sin^2(\alpha+\theta)+k^2\cos^2(\alpha+\theta)\right]^{1/2}} \qquad \text{B10}$$

The velocity components are obtained as follows:

$$u = |V|\cos\theta \qquad \text{B11}$$

$$v = |V|\sin\theta \qquad \text{B12}$$

APPENDIX C

PROGRAM FOR THE COMPUTATION OF MEAN VELOCITY AND REYNOLDS STRESSES FROM THE HOT-WIRE DATA

```
      REAL A1(200730),B1(200730),U(200730),V(200730),UM(40),VM(40),
     &     UF(40),VF(40),UVF(40),T(40),FACTOR(40),Y(40),UMN(40),
     &     UD(40),ETA(40),F(40),G1(40),G2(40),G3(40),L1,L2,L,MOM
! ---------- Section 1: Open input and output files ----------
      OPEN(UNIT=1,FILE='WK2140L.P01',STATUS='OLD')
      OPEN(UNIT=2,FILE='WK2140L.P02',STATUS='OLD')
      OPEN(UNIT=3,FILE='WK2140L.P03',STATUS='OLD')
      OPEN(UNIT=4,FILE='WK2140L.P04',STATUS='OLD')
      OPEN(UNIT=5,FILE='WK2140L.P05',STATUS='OLD')
      OPEN(UNIT=6,FILE='WK2140L.P06',STATUS='OLD')
      OPEN(UNIT=7,FILE='WK2140L.P07',STATUS='OLD')
      OPEN(UNIT=8,FILE='WK2140L.P08',STATUS='OLD')
      OPEN(UNIT=9,FILE='WK2140L.P09',STATUS='OLD')
      OPEN(UNIT=10,FILE='WK2140L.P10',STATUS='OLD')
      OPEN(UNIT=11,FILE='WK2140L.P11',STATUS='OLD')
      OPEN(UNIT=12,FILE='WK2140L.P12',STATUS='OLD')
      OPEN(UNIT=13,FILE='WK2140L.P13',STATUS='OLD')
      OPEN(UNIT=14,FILE='WK2140L.P14',STATUS='OLD')
      OPEN(UNIT=15,FILE='WK2140L.P15',STATUS='OLD')
      OPEN(UNIT=16,FILE='WK2140L.P16',STATUS='OLD')
      OPEN(UNIT=17,FILE='WK2140L.P17',STATUS='OLD')
      OPEN(UNIT=18,FILE='WK2140L.P18',STATUS='OLD')
      OPEN(UNIT=19,FILE='WK2140L.P19',STATUS='OLD')
      OPEN(UNIT=20,FILE='WK2140L.P20',STATUS='OLD')
      OPEN(UNIT=21,FILE='WK2140L.P21',STATUS='OLD')
      OPEN(UNIT=22,FILE='WK2140L.P22',STATUS='OLD')
      OPEN(UNIT=23,FILE='WK2140L.P23',STATUS='OLD')
```

```
      OPEN(UNIT=24,FILE='WK2140L.P24',STATUS='OLD')
      OPEN(UNIT=25,FILE='WK2140L.P25',STATUS='OLD')
      OPEN(UNIT=50,FILE='PROFILE.IN',STATUS='OLD')
      OPEN(UNIT=60,FILE='PROFILE.OUT',STATUS='UNKNOWN')
! ---------- End of Section 1 ----------
! ---- Section 2: Compute temp. compensation factor for each point & read y-coordinate of each point -------
      TS=300                                  ! Sensor temperature (deg F)
      TC= 77.5                                ! Calibration temperature (deg F)
      M=25                                    ! Number of points
      T(1)=78.0                               ! Temperature at 1st measurement point (deg F)
      T(M)=80.5                               ! Temperature at last measurement point (deg F)
      TC=(TC-32)*5/9
      T(1)=(T(1)-32)*5/9
      T(M)=(T(M)-32)*5/9
      DO  I=1,M
         T(I)=T(1)+(FLOAT(I-1)/(M-1))*(T(M)-T(1))
         FACTOR(I)=SQRT((TS-TC)/(TS-T(I)))
      ENDDO
      READ(50,*)(Y(I),I=1,M)
! ---------- End of Section 2 ----------
! ---------- Section 3: Compute mean velocity components & Reynolds stresses ----------
      GAIN=3                          ! The magnification factor of output voltage
      K=0
      DO WHILE (K<M)
         K=K+1
         N=0
         I=0
         J=0
 1       IF (.NOT. EOF (K)) THEN
           N=N+1
           READ(K,*)P,Q
           IF(MOD(N,2).EQ.1)THEN
              I=I+1
              A1(I)=(Q/GAIN)*FACTOR(K)
```

```
 ENDIF
 IF(MOD(N,2).EQ.0)THEN
    J=J+1
    B1(J)=(Q/GAIN)*FACTOR(K)
 ENDIF
 GOTO 1
ENDIF
SUM1=0
SUM2=0
JJ=0
DO II=1,I
   CALL VEL(A1(II),B1(II),U(II),V(II),FLAG)
   IF(FLAG.EQ.2)JJ=JJ+1
   SUM1=SUM1+U(II)
   SUM2=SUM2+V(II)
ENDDO
UM(K)=SUM1/(I-JJ)                    ! Longitudinal mean velocity
VM(K)=SUM2/(I-JJ)                    ! Transverse mean velocity
SUM1=0
SUM2=0
SUM3=0
DO II=1,I
   SUM1=SUM1+(U(II)-UM(K))**2
   SUM2=SUM2+(V(II)-VM(K))**2
   SUM3=SUM3+(U(II)-UM(K))*(V(II)-VM(K))
 ENDDO
 SUM1=SUM1-JJ*UM(K)**2
 SUM2=SUM2-JJ*VM(K)**2
 SUM3=SUM3-JJ*UM(K)*VM(K)
 UF(K)=SUM1/(I-JJ)                   ! longitudinal Reynolds stress component
 VF(K)=SUM2/(I-JJ)                   ! transverse Reynolds stress component
 UVF(K)=SUM3/(I-JJ)                  ! Reynolds shear stress
 WRITE(*,3)Y(K),UM(K),VM(K),UF(K),VF(K),UVF(K)
 WRITE(60,3)Y(K),UM(K),VM(K),UF(K),VF(K),UVF(K)
```

```
3         FORMAT(F7.2,5X,2(F7.3,3X),3(E12.4,2X))
      ENDDO
! ---------- End of Section 3 ----------
! --------- Section 4: Compute dis. & mom. thicknesses, shape factor and search for max. velocity defect ----
      UO=0
      DISP=0.0
      MOM=0.0
      II=0
      UMAX=MIN(UM(1),UM(K))
      DO I=1,K
         IF(UM(I).GT.UMAX)UM(I)=UMAX
         UMN(I)=UM(I)/UMAX
         UD(I)=1-UMN(I)
         IF(I.GT.1)THEN
            DISP=DISP+0.5*(UD(I-1)+UD(I))*(Y(I-1)-Y(I))
            MOM=MOM+0.5*(UMN(I-1)*UD(I-1)+UMN(I)*UD(I))*(Y(I-1)-Y(I))
         ENDIF
         IF(UD(I).GE.UO)THEN
           UO=UD(I)
           II=I
         ENDIF
      ENDDO
      SHAPE=DISP/MOM
      WRITE(60,110)DISP,MOM,SHAPE
110   FORMAT(/'DISP = ',5X,F6.3/'MOM  = ',5X,F6.3/'SHAPE = ',4X,F6.3)
! ---------- End of Section 4 ----------
! ---------- Section 5: Adjust the y coordinate and compute the length scale ----------
      REF=Y(II)                                  ! Position of the max. velocity defect
      DO I=1,K
         Y(I)=Y(I)-REF
      ENDDO
      DO J=II,2,-1
         IF(UD(J).GE.UO/2.AND.UD(J-1).LE.UO/2)THEN
           L1=ABS(Y(J)+(Y(J-1)-Y(J))*(UO/2-UD(J))/(UD(J-1)-UD(J)))
```

```
            GOTO 125
          ENDIF
        ENDDO
125     DO J=II,K-1
          IF(UD(J).GE.UO/2.AND.UD(J+1).LE.UO/2)THEN
            L2=ABS(Y(J)+(Y(J+1)-Y(J))*(UO/2-UD(J))/(UD(J+1)-UD(J)))
            GOTO 135
          ENDIF
        ENDDO
135     L=0.5*(L1+L2)
! ---------- End of Section 5 ----------
! ---------- Section 6: Compute mean vel. Defects & stresses in similarity coordinates ----------
        DO J=1,K
          ETA(J)=Y(J)/L
          F(J)=UD(J)/UO
          G1(J)=UF(J)/(UO*UMAX)**2
          G2(J)=VF(J)/(UO*UMAX)**2
          G3(J)=UVF(J)/(UO*UMAX)**2
          WRITE(60,145)ETA(J),F(J),G1(J),G2(J),G3(J)
145       FORMAT(F7.3,2X,E10.3,E10.3,4X,2(E10.3,5X))
        ENDDO
        WRITE(60,150)UO,L1,L2,L
150     FORMAT(//3X,'UO = ',F8.5/3X,'L1 = ',F8.4,/3X,'L2 = ',F8.4/
     &     3X,'L  = ',F8.4)
! ---------- End of Section 6 ----------
        END

! ---------- Subroutine to compute velocity components (see Appendix B) ----------
        SUBROUTINE VEL(E1,E2,U,V,FLAG)
        REAL A1(5),A2(5),K
        K=0.2
        PI=4*ATAN(1.0)
        A1(1) = -621828.9328          ! A1(1) – A1(5) are polynomial coeffs. for calibration of 1st sensor.
        A1(2) = 1907008.981
```

```
A1(3) = -2192719.338
A1(4) = 1120324.956
A1(5) = -214605.6662

A2(1) = 94995.5452          ! A2(1) – A2(5) are polynomial coeffs. for calibration of 2nd sensor.
A2(2) = -285578.6008
A2(3) = 321889.8972
A2(4) = -161236.3579
A2(5) = 30287.53727

Q1=A1(1)+A1(2)*E1+A1(3)*(E1**2)+A1(4)*(E1**3)+A1(5)*(E1**4)
Q2=A2(1)+A2(2)*E2+A2(3)*(E2**2)+A2(4)*(E2**3)+A2(5)*(E2**4)

A=(Q1/Q2)**2
P=-(1-K**2)*(1+A)
X=4*(1-A*K**2)*(A-K**2)
FLAG=1
IF(X.LT.0)THEN
   FLAG=2
   U=0
   V=0
   GOTO 5
ENDIF
R=SQRT(X)
 S=(1+K**2)*(1-A)
ANGLE1=ATAN((P+R)/S)
ANGLE2=ATAN((P-R)/S)
IF(ABS(ANGLE1).LT.ABS(ANGLE2))THEN
ANGLE=ANGLE1
ELSE
  ANGLE=ANGLE2
ENDIF
VELO=Q1/SQRT(SIN(PI/4+ANGLE)**2+(K*COS(PI/4+ANGLE))**2)
U=VELO*COS(ANGLE)
```

```
      V=VELO*SIN(ANGLE)
5     RETURN
      END
```

APPENDIX D

UNCERTAINTY ANALYSIS

D1. Introduction

An estimate of the error in a measured variable is known as uncertainty of the variable. Uncertainty is expressed in terms of two limits: the bias limit, *Be* and the precision limit, *Pe* The bias limit is an estimate of the bias errors, which are caused by calibration errors, scale-reading errors, data-acquisition errors, installation errors and systematic errors. The precision limit is an estimate of the precision errors, which are caused by random fluctuations inherent in a measurement system [40].

In many cases, the value of the experimental result is not measured directly, but obtained by combining some measured variables in a data reduction equation. The uncertainties in the measured variables propagate into the experimental results. The overall uncertainty is obtained by using the rules for combining uncertainties [68]. In the present experiment, the experimental results are the parameters W_0 and Δ_0 defined in equations 2.10 and 2.11. The uncertainties in the variables combined in these equations are first estimated before the overall uncertainties in W_0 and Δ_0 are determined.

D2. Uncertainties in the Coefficients of the Calibration Equation

D2.1 Bias limits of the polynomial coefficients

Hot-wire calibration was done by fitting a 3rd order polynomial equation to the velocity/voltage calibration data. The polynomial equation is

$$U = a_0 + a_1 E + a_2 E^2 + a_3 E^3 \qquad \text{D.1}$$

where E is the anemometer output voltage, U is the velocity and the $a_i's$ are the polynomial coefficients.

The velocity (U) data was obtained from the piezometric head (Δh) data, from the manometer, with the equation

$$U = 20.54\sqrt{\Delta h} \qquad \text{D.2}$$

The bias in the velocity data is due to the bias in the manometer reading and is given by

$$Be_U = \left[\left(\frac{dU}{dh} Be_{\Delta h}\right)^2\right]^{1/2} \qquad \text{D.3}$$

where $Be_{\Delta h}$ is the bias limit for the piezometric head data and is equal to 0.005 inches of water for each data point. The bias limit for the anemometer output voltage is very small compared to the bias in U and is therefore neglected.

The polynomial coefficients $a_i's$ were obtained by the method of least squares [43]. The equations for the coefficients, expressed in matrix form, are as follows:

$$\begin{bmatrix} 1/Be_{U,j}^2 & \sum E_j/Be_{U,j}^2 & \sum E_j^2/Be_{U,j}^2 & \sum E_j^3/Be_{U,j}^2 \\ \sum E_j/Be_{U,j}^2 & \sum E_j^2/Be_{U,j}^2 & \sum E_j^3/Be_{U,j}^2 & \sum E_j^4/Be_{U,j}^2 \\ \sum E_j^2/Be_{U,j}^2 & \sum E_j^3/Be_{U,j}^2 & \sum E_j^4/Be_{U,j}^2 & \sum E_j^5/Be_{U,j}^2 \\ \sum E_j^3/Be_{U,j}^2 & \sum E_j^4/Be_{U,j}^2 & \sum E_j^5/Be_{U,j}^2 & \sum E_j^6/Be_{U,j}^2 \end{bmatrix} \begin{bmatrix} a_0 \\ a_1 \\ a_2 \\ a_3 \end{bmatrix} = \begin{bmatrix} \sum U_j/Be_{U,j}^2 \\ \sum E_j U_j/Be_{U,j}^2 \\ \sum E_j^2 U_j/Be_{U,j}^2 \\ \sum E_j^3 U_j/Be_{U,j}^2 \end{bmatrix} \quad \text{D.4}$$

The uncertainty in the estimation of the coefficients is given by the variance of each coefficient as follows [43]:

$$Be_{a_i} = \left[\sum_j \left\{ Be_{Uj}^2 \left(\frac{\partial a_i}{\partial U_j} \right)^2 \right\} \right]^{1/2} \quad \text{D.5}$$

A sample calibration data set is shown in Table D1. The polynomial coefficients and the associated uncertainties obtained with the data of Table D1 are presented in Table D2.

D2.2 Precision limits of the polynomial coefficients

There is no precision error since the uncertainty in the polynomial coefficients is entirely due to bias in the manometer reading.

Table D1 A Sample Hot-Wire Calibration Data and the Uncertainties in Velocity

E (Volts)	Δh (in. of water)	U (m/s)	Be_U (m/s)
4.1449	0.28	10.8687	0.00970
4.0887	0.229	9.8292	0.01073
4.0403	0.19	8.9532	0.01178
3.9987	0.16	8.2160	0.01284
3.9454	0.13	7.4058	0.01424
3.8841	0.1	6.4953	0.01624
3.8281	0.08	5.8096	0.01815
3.7618	0.06	5.0313	0.02096
3.6781	0.04	4.1080	0.02568
3.6122	0.03	3.5576	0.02965
3.549	0.02	2.9048	0.03631
3.4496	0.011	2.1543	0.04896
3.3615	0.005	1.4524	0.07262
2.7777	0	0	0

Table D2 Polynomial Coefficients and the Uncertainties for a Sample Hot-Wire Calibration Data

i	Coefficient a_i	Uncertainty
0	-14.5035	0.0000025
1	24.0177	0.00234
2	-11.7413	0.00116
3	1.7904	0.000143

D3. Uncertainty in Velocity Measurements

D3.1 Bias limit in U

During actual measurements, the fluid temperature may be different from the calibration temperature. The process of obtaining the fluid temperature for each measurement has been explained in Section 3.3. The anemometer output voltage used in equation D.1 is obtained by applying a temperature correction on the measured voltage as follows:

$$E = E_m \sqrt{\frac{T_s - T}{T_s - T_c}} \qquad \text{D.6}$$

where E_m is the measured output voltage, T_s is the sensor temperature, T_c is the fluid temperature during calibration and T is the fluid temperature during measurement.

The bias in E_m consists of the bias from the anemometer (IFA 100), Be_{Em1}, and due to analog-to-digital conversion in IFA 200, Be_{Em2} (see section 3.3).

From the IFA 100 Instruction manual [69], $Be_{Em1} = 0.001V$. From the IFA 200 Instruction manual [70], $Be_{Em2} = 1/4096\ V$.

The bias in the output voltage is obtained by using the root-sum square (RSS) method [68, 71], i.e.

$$Be_{Em} = \left[Be_{Em1}^{\ 2} + Be_{Em2}^{\ 2} \right]^{1/2} \qquad \text{D.7}$$

The estimated bias limits in the temperatures are $Be_{T_s} = 1°C$; $Be_{T_c} = 0.25°C$; $Be_T = 0.25°C$.

By substituting equation D.6 into equation D.1, the bias limit in the velocity measurement, Be_U, is obtained as follows:

$$Be_U = \left[\sum_{i=0}^{3} \left(\frac{\partial U}{\partial a_i} Be_{a_i} \right)^2 + \left(\frac{\partial U}{\partial E_m} Be_{E_m} \right)^2 + \left(\frac{\partial U}{\partial T_s} Be_{T_s} \right)^2 + \left(\frac{\partial U}{\partial T_c} Be_{T_c} \right)^2 + \left(\frac{\partial U}{\partial T} Be_T \right)^2 + 2 * \frac{\partial U}{\partial T_c} \frac{\partial U}{\partial T} Be_{T_c} Be_T \right]^{1/2} \quad \text{D.8}$$

The last term in equation D.8 is the correlated bias for T_c and T since they were both measured with the same thermometer [71].

The bias limit in the velocity measurement was computed for many points in the wake. The highest value of $Be_U = 0.024 m/s$ was recorded at $U_\infty = 10 m/s$ and $Be_U = 0.022 m/s$ was recorded at $U_\infty = 7.5 m/s$. For simplicity, these values will be used as the bias limits in the velocity.

D3.2 Precision limit in U

The precision limit was determined with measurements in the free-stream. The precision limit for a sample population of N velocity readings is given as follows [68]:

$$Pe_U = tS_U \quad \text{D.9}$$

where t is obtained from the statistical t-distribution and S_U is the precision index given by

$$S_U = \left[\frac{1}{N-1}\sum_{i=1}^{N}\left(U_i - \overline{U}\right)^2\right]^{1/2} \qquad \text{D.10}$$

Data sampling was at 20KHz. Each record at this frequency has 1024 samples. At least 40 records were taken for each velocity measurement. Therefore, the sample size is, at least, $N = (1024)(40) = 40960$. It was reported in section 3.1 that the free-stream turbulence intensity in the test section of the wind tunnel was about 0.5%. This means

$$T.I. = \frac{1}{U_\infty}\left[\sum_{i=1}^{N}\left(U_i - \overline{U}\right)^2\right]^{1/2} = 0.005 \qquad \text{D.11}$$

For a 95% confidence interval and $N > 121$, the t-distribution table [68] gives $t = 1.96$. Using this value together with equations D.9 –11 gives $Pe_U = 0.000048U_\infty$. This value of the precision limit is negligible compared with the bias limit and is, therefore, neglected.

D4. Uncertainty in the Far Wake Momentum Thickness

D4.1 Bias error in θ

The momentum thickness in the wake is given as

$$\theta = \int_{-\infty}^{\infty} \frac{U}{U_\infty}\left(1 - \frac{U}{U_\infty}\right)dy \qquad \text{D.12}$$

The bias in θ consists of the bias that results through the biases in U and y, $Be_{\theta 1}$, and the bias due to estimation of the integral by a numerical approximation method, $Be_{\theta 2}$.

i) Bias that propagates through U and y

Let
$$\theta_1 = \frac{U}{U_\infty}\left(1-\frac{U}{U_\infty}\right)\Delta y. \qquad \text{D.13}$$

Therefore,

$$Be_{\theta 1}^{\ 2} = \left(\frac{\partial \theta_1}{\partial U} Be_U\right)^2 + \left(\frac{\partial \theta_1}{\partial U_\infty} Be_{U_\infty}\right)^2 + \left(\frac{\partial \theta_1}{\partial \Delta y} Be_{\Delta y}\right)^2 + 2\frac{\partial \theta_1}{\partial U}\frac{\partial \theta_1}{\partial U_\infty} Be_U Be_{U_\infty} \qquad \text{D.14}$$

$Be_{\theta 1}$ was computed at various locations in the wakes of the plates and the highest value found was $Be_{\theta 1} = 0.0005\,mm$ at $U_\infty = 10\,m/s$ and $Be_{\theta 1} = 0.0008\,mm$ at $U_\infty = 7.5\,m/s$.

ii) Bias due to numerical integration

The momentum thickness was obtained by integration of equation D.12 using the trapezoidal rule [72]. If equation 2.1 is used to eliminate U in equation D.12, the equation for momentum thickness becomes

$$\theta = \int_{\eta_1}^{\eta_2} L_0\left[\frac{w_0}{U_\infty} f(\eta) - \left(\frac{w_0}{U_\infty} f(\eta)\right)^2\right] d\eta \qquad \text{D.15}$$

where $f(\eta)$ is as given in equation 2.6. Here, the limits of integration have been

reduced to the points where the function $f(\eta)$ is sufficiently close to zero. Typically, $\eta_2 = -\eta_1 = 4$.

According to Cheney and Kincaid [72], the error bound for integration by trapezoidal rule is given by

$$Be_{\theta 2} = \frac{1}{12}(\eta_2 - \eta_1)(\Delta\eta)^2 L_0 \frac{d^2}{d\eta^2}\left\{\frac{w_0}{U_\infty} f(\eta) - \left(\frac{w_0}{U_\infty} f(\eta)\right)^2\right\} \qquad \text{D.16}$$

The maximum value of the bracketed term in equation D.16 occurs at $\eta = 0$, for which $f = 1$. Equation D.16, therefore, reduces to

$$Be_{\theta 2} = \frac{\ln 2}{6}(\eta_2 - \eta_1)(\Delta\eta)^2 L_0 \left(\frac{w_0}{U_\infty}\right)\left[2\frac{w_0}{U_\infty} - 1\right] \qquad \text{D.17}$$

Computation of $Be_{\theta 2}$ was performed at various x locations in the far wakes of all the plates. The highest value found was $Be_{\theta 2} = 0.056mm$ at $U_\infty = 10m/s$ and $Be_{\theta 2} = 0.076mm$ at $U_\infty = 7.5m/s$. These values are used as the biases in the momentum thickness since the values of $Be_{\theta 1}$ are negligible compared to those of $Be_{\theta 2}$.

D4.2 Precision error in θ

The value of θ used for the computation of W_0 and Δ_0 is the average of the values of θ recorded at all the x locations where measurements were taken in the far wake. The precision error for a sample population of N calculated values of θ is

$$Pe_\theta = t\left[\frac{1}{N-1}\sum_{i=1}^{N}\left(\theta_i - \bar{\theta}\right)^2\right]^{1/2} \qquad \text{D.18}$$

where t is obtained from the statistical t-distribution [2].

The overall uncertainty was obtained from the bias and precision errors using the root-sum square as explained in Section D3. The detailed calculation of the errors in the calculated values of θ, obtained using the above procedure, are presented in Table D3. The values of the uncertainty in θ are also shown in Tables 4.1, 4.2 and 4.3.

D5. Uncertainties in the Velocity Scale, w_o and the Length Scale, L_o

The velocity scale is the difference between the free-stream velocity and the minimum velocity (i.e. the center-line velocity) in the wake profile and is expressed as follows:

$$w_o = U_\infty - U_{\min} \qquad \text{D.19}$$

The bias error in w_o is expressed as follows:

$$Be_{w_o} = \left[\left(\frac{\partial w_o}{\partial U_\infty} Be_{U_\infty}\right)^2 + \left(\frac{\partial w_o}{\partial U_{\min}} Be_{U_{\min}}\right)^2\right]^{1/2} + \frac{\partial w_o}{\partial U_\infty}\frac{\partial w_o}{\partial U_{\min}} Be_{U_\infty} Be_{U_{\min}} \qquad \text{D.20}$$

The bias in w_o was computed at each x location in the far wake and found to be very small ($<10^{-5}$). It is therefore neglected in subsequent calculations.

Table D3 Error Estimate for Far Wake Average Momentum Thickness

Plate 1				Plate 2				Plate 3		Plate 4			
U_∞ = 7.5 m/s		U_∞ = 10 m/s		U_∞ = 7.5 m/s		U_∞ = 10 m/s		U_∞ = 10 m/s		U_∞ = 7.5 m/s		U_∞ = 10 m/s	
j	θ (mm)	j	θ (mm)	j	θ (mm)	j	θ (mm)	j	θ (mm)	j	θ (mm)	j	θ (mm)
1	1.4082	1	1.084	1	1.288	1	1.316	1	1.4058	1	1.393	1	1.085
2	1.4671	2	1.093	2	1.511	2	1.152	2	1.5710	2	1.769	2	1.202
3	1.1430	3	1.179	3	1.25	3	1.22	3	1.6040	3	1.539	3	1.204
4	1.4060	4	1.072	4	1.313	4	1.173	4	1.5130	4	1.452	4	1.052
5	1.3580	5	1.222	5	1.356	5	1.085	5	1.4710	5	1.557	5	1.209
6	1.5098	6	1.096	6	1.314	6	1.147	6	1.4583			6	1.025
7	1.4040	7	1.136			7	1.235	7	1.5328			7	1.199
8	1.4040	8	1.108			8	1.056	8	1.6250			8	1.095
9	1.4190	9	1.041			9	1.131	9	1.4830			9	1.148
		10	1.064			10	1.102	10	1.5570			10	1.144
		11	1.120			11	1.118	11	1.5040			11	1.169
		12	1.188			12	1.145					12	1.162
		13	1.130			13	1.063					13	1.169
												14	1.242
θ_{avg} =	1.3910	θ_{avg} =	1.118	θ_{avg} =	1.339	θ_{avg} =	1.149	θ_{avg} =	1.5204	θ_{avg} =	1.542	θ_{avg} =	1.150
σ =	0.1026	σ =	0.053	σ =	0.091	σ =	0.073	σ =	0.0657	σ =	0.143	σ =	0.064
t =	2.306	t =	2.179	t =	2.571	t =	2.179	t =	2.228	t =	2.776	t =	2.160
Pe_θ =	0.2365	Pe_θ =	0.115	Pe_θ =	0.235	Pe_θ =	0.160	Pe_θ =	0.1463	Pe_θ =	0.398	Pe_θ =	0.138
Be_θ =	0.076	Be_θ =	0.056	Be_θ =	0.076	Be_θ =	0.056	Be_θ =	0.056	Be_θ =	0.076	Be_θ =	0.056
UC_θ =	0.2484	UC_θ =	0.128	UC_θ =	0.247	UC_θ =	0.169	UC_θ =	0.1567	UC_θ =	0.405	UC_θ =	0.149

For each wake profile, the length scale, L_o, (or half-wake width) was determined by linear interpolation between points in which one has velocity defect greater than and the other less than half the center line velocity defect. The equation for the linear interpolation is as follows:

$$L_o = y_1 + (y_2 - y_1)\left\{\frac{\frac{1}{2}[1+U_o]-U_1}{U_2-U_1}\right\} \qquad \text{D.21}$$

All the terms used in equation D.21 are shown in figure D1.

The bias error in the calculated value of L_o is calculated with the following equation:

$$Be_{L_o}^{\ 2} = \left(\frac{\partial L_o}{\partial y_1} Be_{y_1}\right)^2 + \left(\frac{\partial L_o}{\partial y_2} Be_{y_2}\right)^2 + \left(\frac{\partial L_o}{\partial u_o} Be_{u_o}\right)^2 + \left(\frac{\partial L_o}{\partial u_1} Be_{u_1}\right)^2 + \left(\frac{\partial L_o}{\partial u_2} Be_{u_2}\right)^2 + \qquad \text{D.22}$$

$$2\frac{\partial L_o}{\partial y_1}\frac{\partial L_o}{\partial y_2} Be_{y_1} Be_{y_2} + 2\frac{\partial L_o}{\partial u_o}\frac{\partial L_o}{\partial u_1} Be_{u_o} Be_{u_1} + 2\frac{\partial L_o}{\partial u_o}\frac{\partial L_o}{\partial u_2} Be_{u_o} Be_{u_2} + 2\frac{\partial L_o}{\partial u_1}\frac{\partial L_o}{\partial u_2} Be_{u_1} Be_{u_2}$$

The bias error in L_o was found to be equal to the bias in y (= 0.0127 *mm*) in every case because some terms in equation D.22 cancel out.

There is no precision error in either w_o or L_o.

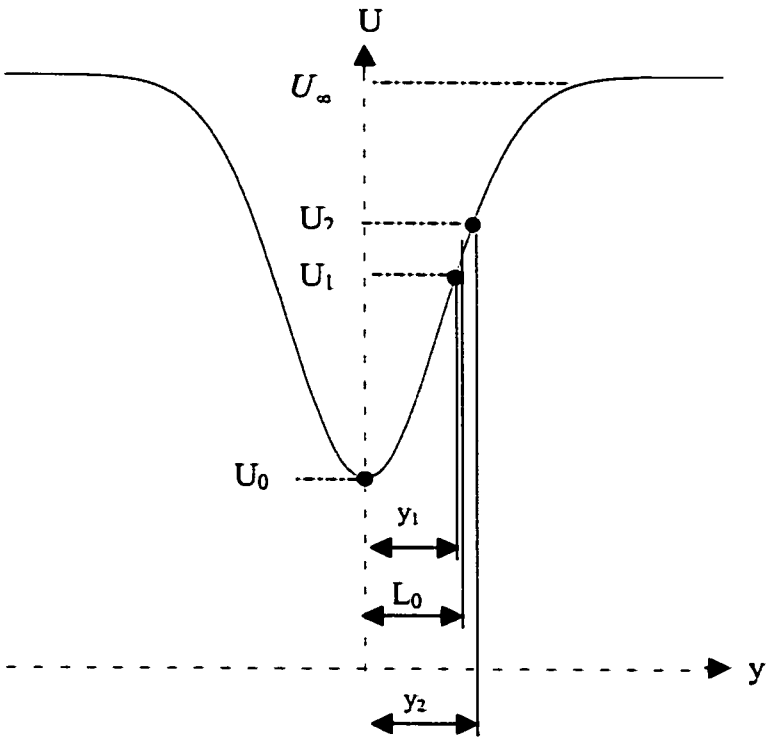

Figure D1 Determination of the half-wake width from the measured mean velocity profile by linear interpolation.
Note: $(U_\infty - U_2) \le 0.5(U_\infty - U_o) \le (U_\infty - U_1)$. The terms in parenthesis are the velocity defects at the points shown with dots in the figure.

D6. Uncertainty in the Calculation of the Parameter W_o

W_o is obtained from the slope of the $(U_\infty / w_o)^2$ versus $x/2\theta$ curve as

$$W_o = \sqrt{2/A} \qquad \text{D.23}$$

where A is the slope of the curve. In the far wake, the curve is a straight line. In order to ascribe all the uncertainties to the dependent variable, the plot of $2\theta(U_\infty / w_o)^2$ *vs* x is used instead. This does not change the value of the slope. The slope is obtained by the least squares method using equation similar to equation D.4. The error in the slope is obtained by using equation similar to equation D.5. The error in W_o is obtained from the error in the calculated value of A as follows:

$$Be_{W_o} = \left[\left(\frac{\partial W_o}{\partial A} Be_A \right)^2 \right]^{1/2} \qquad \text{D.24}$$

$$Pe_{W_o} = \left[\left(\frac{\partial W_o}{\partial A} Pe_A \right)^2 \right]^{1/2} \qquad \text{D.25}$$

The detailed calculation of the error in W_o is presented in Table D4.

Table D4 Error Estimate for Parameter W_o

Plate 1				Plate 2				Plate 3		Plate 4			
U_∞ =	7.5 m/s	U_∞ =	10 m/s	U_∞ =	7.5 m/s	U_∞ =	10 m/s	U_∞ =	10 m/s	U_∞ =	7.5 m/s	U_∞ =	10 m/s
x	uo/Uf	x	uo/Uf	x	uo/Uf	x	uo/Uf	x	uo/Uf	x	uo/Uf	x	uo/Uf
360	0.165	180	0.114	540	0.082	360	0.137	480	0.069	360	0.12	300	0.099
420	0.110	300	0.084	780	0.057	420	0.106	600	0.059	480	0.09	360	0.084
540	0.074	360	0.076	960	0.049	480	0.098	660	0.057	540	0.08	420	0.078
660	0.062	420	0.061	1020	0.046	540	0.085	720	0.055	600	0.07	480	0.071
720	0.061	480	0.058	1080	0.043	600	0.066	750	0.052	690	0.06	540	0.063
780	0.053	540	0.053			660	0.062	780	0.050	720	0.06	660	0.053
840	0.050	600	0.047			720	0.056	840	0.045	900	0.05	720	0.051
900	0.045	660	0.050			840	0.047	900	0.043	990	0.05	750	0.052
		720	0.045			900	0.045	960	0.044	1050	0.05	780	0.048
		780	0.042			960	0.042	1080	0.042	1140	0.05	810	0.048
		840	0.041			1020	0.041	1140	0.039			840	0.044
		900	0.037			1080	0.038					900	0.043
		960	0.036			1110	0.037					960	0.042
						1140	0.037						
A =	2.1811	A =	2.0092	A =	2.0816	A =	2.1100	A =	2.0304	A =	1.6553	A =	1.6562
Wo =	0.9576	Wo =	0.9977	Wo =	0.9802	Wo =	0.9736	Wo =	0.9925	Wo =	1.0992	Wo =	1.0989
Be_A =	0.0031	Be_A =	0.0015	Be_A =	0.0095	Be_A =	0.0012	Be_A =	0.0047	Be_A =	0.0021	Be_A =	0.0017
Be_{wo} =	0.0007	Be_{wo} =	0.0004	Be_{wo} =	0.0022	Be_{wo} =	0.0003	Be_{wo} =	0.0012	Be_{wo} =	0.0007	Be_{wo} =	0.0006
Pe_A =	0.0297	Pe_A =	0.0063	Pe_A =	0.0899	Pe_A =	0.0094	Pe_A =	0.0317	Pe_A =	0.0567	Pe_A =	0.0102
Pe_{wo} =	0.0065	Pe_{wo} =	0.0016	Pe_{wo} =	0.0212	Pe_{wo} =	0.0022	Pe_{wo} =	0.0078	Pe_{wo} =	0.0188	Pe_{wo} =	0.0034
UC_{Wo} =	0.0066	UC_{Wo} =	0.0016	UC_{Wo} =	0.0213	UC_{Wo} =	0.0022	UC_{Wo} =	0.0078	UC_{Wo} =	0.0188	UC_{Wo} =	0.0034

D7. Uncertainty in the Calculation of the Parameter Δ_o

Δ_o is obtained from the slope of the $(L_o/\theta)^2$ versus $x/2\theta$ curve as

$$\Delta_o = \sqrt{B/2} \qquad \text{D.26}$$

where B is the slope of the curve. In the far wake, the curve is a straight line. As in the case of W_o, the plot of $2L_o^2/\theta$ *vs* x is used in order to ascribe all the uncertainties to the dependent variable. . The slope is obtained by the least squares method. The error in the slope is obtained by using equation similar to equation D.5. The error in Δ_o is obtained from the error in the calculated value of B as follows:

$$Be_{\Delta_o} = \left[\left(\frac{\partial \Delta_o}{\partial B} Be_B\right)^2\right]^{1/2} \qquad \text{D.24}$$

$$Pe_{\Delta_o} = \left[\left(\frac{\partial \Delta_o}{\partial B} Pe_B\right)^2\right]^{1/2} \qquad \text{D.25}$$

The detailed calculation of the error in Δ_o is presented in Table D5.

Table D5 Error Estimate for Parameter Δ_o

Plate 1				Plate 2				Plate 3		Plate 4			
U_∞ =	7.5 m/s	U_∞ =	10 m/s	U_∞ =	7.5 m/s	U_∞ =	10 m/s	U_∞ =	10 m/s	U_∞ =	7.5 m/s	U_∞ =	10 m/s
x	Lo	x	Lo	x	Lo	x	Lo	x	Lo	x	Lo	x	Lo
360	3.420	180	3.872	540	6.618	360	4.496	480	11.101	360	5.453	300	5.154
420	4.258	300	6.111	780	10.793	420	5.660	600	12.372	480	6.805	360	5.988
540	7.246	360	6.370	960	13.427	480	6.041	660	12.743	540	7.614	420	7.070
660	10.844	420	8.023	1020	13.670	540	7.690	720	14.703	600	9.289	480	8.091
720	11.496	480	9.393	1080	14.780	600	8.961	750	15.374	690	11.103	540	9.293
780	12.384	540	10.532			660	10.256	780	14.693	720	10.411	660	9.867
840	12.357	600	11.418			720	10.908	840	15.878	900	13.843	720	10.831
900	14.280	660	11.921			840	11.657	900	15.943	990	15.410	750	11.180
		720	12.389			900	13.054	960	16.616	1050	15.384	780	11.024
		780	13.321			960	14.339	1080	18.457	1140	16.026	810	11.803
		840	14.041			1020	13.894	1140	19.196			840	11.385
		900	13.782			1080	14.686					900	12.939
		960	15.226			1110	14.608					960	13.398
						1140	15.120						
B =	0.5063	B =	0.5020	B =	0.5007	B =	0.4903	B =	0.4863	B =	0.4031	B =	0.4199
Δo =	0.5031	Δo =	0.5010	Δo =	0.5003	Δo =	0.4951	Δo =	0.4931	Δo =	0.4489	Δo =	0.4582
Be_B =	0.0001	Be_B =	0.0001	Be_B =	0.0004	Be_B =	0.0001	Be_B =	0.0003	Be_B =	0.0001	Be_B =	0.0001
$Be_{\Delta o}$ =	0.0001	$Be_{\Delta o}$ =	0.0000	$Be_{\Delta o}$ =	0.0002	$Be_{\Delta o}$ =	0.0000	$Be_{\Delta o}$ =	0.0001	$Be_{\Delta o}$ =	0.0000	$Be_{\Delta o}$ =	0.0000
Pe_B =	0.0012	Pe_B =	0.0003	Pe_B =	0.0039	Pe_B =	0.0006	Pe_B =	0.0019	Pe_B =	0.0023	Pe_B =	0.0005
$Pe_{\Delta o}$ =	0.0023	$Pe_{\Delta o}$ =	0.0006	$Pe_{\Delta o}$ =	0.0077	$Pe_{\Delta o}$ =	0.0013	$Pe_{\Delta o}$ =	0.0040	$Pe_{\Delta o}$ =	0.0064	$Pe_{\Delta o}$ =	0.0013
$UC_{\Delta o}$ =	0.0023	$UC_{\Delta o}$ =	0.0006	$UC_{\Delta o}$ =	0.0077	$UC_{\Delta o}$ =	0.0013	$UC_{\Delta o}$ =	0.0040	$UC_{\Delta o}$ =	0.0064	$UC_{\Delta o}$ =	0.0013

APPENDIX E

PROGRAM FOR NUMERICAL COMPUTATION OF THE WAKE FLOW BEHIND A FLAT PLATE

```
! THE PROCEDURE FOR THIS PROGRAM IS EXPLAINED IN CHAPTER 5 OF THE
DISSERTATION. THE PROGRAM USES THE ALGORITHM OUTLINED IN REFERENCE
[67] OF THIS DISSERTATION.

! THIS PROGRAM APPLIES TO PLATE # 4.

! ------------------------------------ Declaration of variables ----------------------------------------
      IMPLICIT DOUBLE PRECISION (A-H,O-Z)
      INTEGER TRAIL1,TRAIL2,II,JJ,KK
      PARAMETER (II=210, JJ=50, KK=55)
      DOUBLE PRECISION MASS,MU,KT(0:II,0:JJ,0:KK),KTin,LEP,LU,MOM,L,
     &                 KE,KW,KN,KS
     DIMENSION U(0:II,0:JJ,0:KK),V(0:II,0:JJ,0:KK),W(0:II,0:JJ,0:KK),
     & EP(0:II,0:JJ,0:KK),P(II,JJ,KK),PP(0:II,0:JJ,0:KK),DX(II),DY(0:JJ),
     & DZ(0:KK),VISC(II,JJ,KK),G(II,JJ,KK),AE(II,JJ,KK),AW(II,JJ,KK),
     & AN(II,JJ,KK),AS(II,JJ,KK),AT(II,JJ,KK),AB(II,JJ,KK),SC(II,JJ,KK),
     & SP(II,JJ,KK),A(II),B(II),C(II),D(II),PHI(II),DU(II,JJ,KK),
     & DV(II,JJ,KK),DW(II,JJ,KK),X(II),Y(JJ),Z(KK),ST11(II,JJ),
     & ST22(II,JJ),ST33(II,JJ),ST12(II,JJ),ST13(II,JJ),L(II),
     & UO(II),ETA(II)

! ---------------------- Statement Function to determine if a node is on top of the plate -----------
      ZP(XP,SIDE1,SIDE2,WIDTH)=(SIDE1-XP)*WIDTH/(SIDE1-SIDE2)
! ------------------------------------------------------------------------------------------------------

      OPEN(UNIT=2,FILE='PL4A.OUT',STATUS='UNKNOWN')
      OPEN(UNIT=3,FILE='PL4B.OUT',STATUS='UNKNOWN')
      OPEN(UNIT=4,FILE='PL4C.OUT',STATUS='UNKNOWN')
      OPEN(UNIT=5,FILE='PL4D.OUT',STATUS='UNKNOWN')
      OPEN(UNIT=6,FILE='PL4E.OUT',STATUS='UNKNOWN')
!
! DIVIDE THE DOMAIN INTO GRIDS BY DIFINING DX, DY AND DZ.
      LDX=200          ! Number of grids in the x direction
      LDY=45           ! Number of grids in the y direction
      LDZ=50           ! Number of grids in the z direction
```

```
      INLET=10          ! Number of grids upstream of the tunnel wall
      LEAD=20           ! Number of grids upstream of the plate's leading edge
      TRAIL1=140        ! Number of grids upstream of the trailing edge (longer side)
      TRAIL2=70         ! Number of grids upstream of the trailing edge (shorter side)
      SIDE1=0.560       ! SIDE1 & SIDE2 define the lengths (m) of the sides of the plates
      SIDE2=0.406

! ---------- Define the grid sizes in the x direction ----------
      DX(1)=0.005
       DO I=2,LDX
          IF(I.LE.INLET+1)THEN
            DX(I)=0.85*DX(I-1)
          ELSEIF(I.GT.INLET+1.AND.I.LE.LEAD+1)THEN
            DX(I)=0.99*DX(I-1)
          ELSEIF(I.GT.LEAD+1.AND.I.LE.TRAIL2-17)THEN
            DX(I)=1.1142*DX(I-1)
          ELSEIF(I.GT.TRAIL2-17.AND.I.LE.TRAIL2)THEN
            DX(I)=0.836*DX(I-1)
          ELSEIF(I.GT.TRAIL2.AND.I.LE.TRAIL1)THEN
            DX(I)=1.0133*DX(I-1)
          ELSE
            DX(I)=1.045*DX(I-1)
          ENDIF
      ENDDO
! ---------------------------------------------------------------------------------------------
! ---------- Define the grid sizes in the y direction ----------
      DY(0)=0.00006
      DY(1)=DY(0)
       DO J=2,LDY
          IF(J.LE.LDY-10)THEN
            DY(J)=1.122*DY(J-1)
          ELSE
            DY(J)=1.1*DY(J-1)
          ENDIF
       ENDDO
! ---------------------------------------------------------------------------------------------
! ---------- Define the grid sizes in the z direction ----------
      DZ(0)=0.0001
       DZ(1)=DZ(0)
       DO K=2,LDZ
          IF(K.LE.LDZ-20)THEN
            DZ(K)=1.156*DZ(K-1)
          ELSE
            DZ(K)=MIN(1.044*DZ(K-1),DBLE(0.020))
          ENDIF
       ENDDO
       DZ(LDZ+1)=DZ(LDZ)
! ---------------------------------------------------------------------------------------------
! ------- Compute distances of nodal points from walls & longitudinal distances from inlet -------
```

```
          X(1)=0
          DO I=2,LDX+1
          X(I)=X(I-1)+DX(I-1)
          IF(I.GT.LEAD.AND.X(I).LE.X(LEAD)+SIDE2)IT=I    ! The begining of wake
          ENDDO
          XA=X(INLET)
          XB=X(LEAD)-XA
          XC=X(TRAIL1)-X(LEAD)
          XD=X(TRAIL2)-X(LEAD)

          Y(1)=-0.5*DY(0)
          DO J=2,LDY+1
             Y(J)=Y(J-1)+0.5*(DY(J-2)+DY(J-1))
          ENDDO

          Z(1)=-0.5*DZ(0)
          DO K=2,LDZ+2
             Z(K)=Z(K-1)+0.5*(DZ(K-2)+DZ(K-1))
          ENDDO
          WIDTH=Z(LDZ+2)-0.5*DZ(LDZ+1)
! ------------------------------------------------------------------------------------------------

! ---------------------------------- Set input parameters ----------------------------------------
          UINF=DBLE(10.0)              ! Inlet velocity
          RHO=DBLE(1.1774)             ! Density
          MU=DBLE(1.846E-5)            ! Viscosity
          ALPHA=0.3                    ! Relaxation factor for momentum equations
          ALPHA2=0.2                   ! Relaxation factor for pressure correction equation
          ALPHA3=0.3                   ! Relaxation factor for the k-□ equations
          CMU=0.09                     ! CMU to AEP are k-□ model constants
          ZK=1.0
          CEP1=1.44
          CEP2=1.92
          ZEP=1.3
          CL=0.418*(CMU**(-0.75))
          AEP=2*CL
          Vin=0                        ! Inlet velocity in the y direction
          Win=0                        ! Inlet velocity in the z direction
          KTin=0
          EPin=0
          NUMBER=2
          MM1=200                      ! # of iterations to be paerformed as laminar flow
          MM2=1500                     ! total # of iterations to be performed
          PI=4*ATAN(1.0)

! *** STEP1: GUESS THE PRESSURE FIELD P* AND INITIALIZE OTHER VARIABLES ***
          DO I=1,LDX+1
             DO J=1,LDY+1
                DO K=1,LDZ+2
                   P(I,J,K)=0.0_8
                   VISC(I,J,K)=0.0_8
                   DU(I,J,K)=DBLE(1.0)
```

```
                DV(I,J,K)=DBLE(1.0)
                DW(I,J,K)=DBLE(1.0)
              ENDDO
            ENDDO
          ENDDO
          DO I=0,LDX+1
            DO J=0,LDY+1
              DO K=0,LDZ+2
                IF(I.EQ.0.OR.J.EQ.0.OR.K.EQ.0)THEN
                  U(I,J,K)=0
                  V(I,J,K)=0
                   W(I,J,K)=0
                  KT(I,J,K)=0
                  EP(I,J,K)=0
                ELSE
                  U(I,J,K)=0.5*UINF
                  V(I,J,K)=0.0_8
                  W(I,J,K)=0.0_8
                  KT(I,J,K)=0.01
                  EP(I,J,K)=0.01
                ENDIF
              ENDDO
            ENDDO
          ENDDO

          DO J=1,LDY+1
            DO K=1,LDZ+2
              U(1,J,K)=UINF
            ENDDO
          ENDDO

! ---------- compute inlet mass flow rate ----------
          FLOWin=0
          DO J=2,LDY+1
            DO K=2,LDZ+1
              FLOWin=FLOWin+RHO*U(1,J,K)*DY(J-1)*DZ(K-1)
            ENDDO
          ENDDO
          FLOWout=FLOWin      ! To initialize FLOWout
          CMASS=FLOWin        ! To initialize CMASS
! ------------------------------------------------------------------------------------------
          M=0
   33     M=M+1
          IF(MOD(M,10).EQ.0)THEN
           WRITE(*,1)M,RESu,RESv,RESw,CMASS/FLOWin,RESk,RESe
    1     FORMAT(1X,I4,6(1X,E10.4))
          ENDIF

          IF(M.EQ.MM2+1)THEN
            WRITE(*,*)'How many more iterations?'
            READ(*,*)MORE
            MM2=MM2+MORE
          ENDIF
```

```
          IF(M.EQ.MM2+1)GOTO 72
          IF(M.GT.MM1+1.AND.CMASS/FLOWin.LE.1.0E-4)GOTO 72

! ---------- compute outlet mass flow rate ----------
        IF(M.GT.20)THEN
          FLOWout=0
          DO J=2,LDY+1
            DO K=2,LDZ+1
              FLOWout=FLOWout+RHO*U(LDX,J,K)*DY(J-1)*DZ(K-1)
            ENDDO
          ENDDO
        ENDIF
        RATIO=FLOWin/FLOWout
! ------------------------------------------------------------------------------------------

! *******STEP 2: SOLVE THE MOMENTUM EQUATION TO OBTAIN U*, V* AND W* ****

! ---------- Solve the U* equation ----------
        RESu=0
        DO I=1,LDX+1
          DO J=1,LDY+1
            DO K=1,LDZ+2
              IF(I.EQ.1)THEN
                AE(I,J,K)=0
                AW(I,J,K)=0
                AN(I,J,K)=0
                AS(I,J,K)=0
                AT(I,J,K)=0
                AB(I,J,K)=0
                SC(I,J,K)=U(1,J,K)*1.0E30
                SP(I,J,K)=-1.0E30
              ELSEIF(J.EQ.1)THEN
                AE(I,J,K)=0
                AW(I,J,K)=0
                AN(I,J,K)=1.0
                AS(I,J,K)=0
                AT(I,J,K)=0
                AB(I,J,K)=0
                SC(I,J,K)=0
                SP(I,J,K)=0
              ELSEIF(K.EQ.1)THEN
                AE(I,J,K)=0
                AW(I,J,K)=0
                AN(I,J,K)=0
                AS(I,J,K)=0
                AT(I,J,K)=1.0
                AB(I,J,K)=0
                SC(I,J,K)=0
                SP(I,J,K)=0
              ELSEIF(I.EQ.LDX+1)THEN
                AE(I,J,K)=0
                AW(I,J,K)=RATIO
```

```
                AN(I,J,K)=0
                AS(I,J,K)=0
                AT(I,J,K)=0
                AB(I,J,K)=0
                SC(I,J,K)=0
                SP(I,J,K)=RATIO-1
              ELSEIF(K.EQ.LDZ+2)THEN
                AE(I,J,K)=0
                AW(I,J,K)=0
                AN(I,J,K)=0
                AS(I,J,K)=0
                AT(I,J,K)=0
                AB(I,J,K)=1.0
                SC(I,J,K)=0
                SP(I,J,K)=0
              ELSE
                CALL XEQUA(RHO,U(I-1,J,K),U(I,J,K),
     &          U(I+1,J,K),V(I-1,J-1,K),V(I,J-1,K),
     &          V(I-1,J,K),V(I,J,K),W(I-1,J,K-1),W(I,J,K-1),
     &          W(I-1,J,K),W(I,J,K),P(I-1,J,K),P(I,J,K),
     &          KT(I-1,J,K),KT(I,J,K),MU+VISC(I-1,J-1,K),
     &          MU+VISC(I-1,J,K-1),MU+VISC(I-1,J,K),
     &          MU+VISC(I-1,J,K+1),MU+VISC(I-1,J+1,K),
     &          MU+VISC(I,J-1,K),MU+VISC(I,J,K-1),MU+VISC(I,J,K),
     &          MU+VISC(I,J,K+1),MU+VISC(I,J+1,K),DX(I-1),DX(I),
     &          DY(J-2),DY(J-1),DY(J),DZ(K-2),DZ(K-1),DZ(K),
     &          AE(I,J,K),AW(I,J,K),AN(I,J,K),AS(I,J,K),
     &          AT(I,J,K),AB(I,J,K),SC(I,J,K),SP(I,J,K))
                IF(J.EQ.LDY+1)THEN
                  AN(I,J,K)=0
                 ENDIF
                IF(J.EQ.2)THEN
                  XP=X(I)
                    IF(XP.LT.X(LEAD))THEN
                      IFLAG=1
                    ELSEIF(XP.GT.X(LEAD)+SIDE1)THEN
                      IFLAG=1
                    ELSE
                    IF(XP.GT.X(LEAD)+SIDE2.AND.
     &              ZP(XP-X(LEAD),SIDE1,SIDE2,WIDTH).LT.Z(K))THEN
                       IFLAG=1
                     ELSE
                       IFLAG=2
                     ENDIF
                  ENDIF

                   IF(IFLAG.EQ.2)THEN
                    AS(I,J,K)=0
                    SP(I,J,K)=SP(I,J,K)-(MU/Y(2))* 0.5*(DX(I-1)+DX(I))*DZ(K-1)
                   ENDIF
                ENDIF
                 IF(K.EQ.2.AND.I.GT.INLET)THEN
                   AB(I,J,K)=0
```

```
                    SP(I,J,K)=SP(I,J,K)-(MU/Z(2))*0.5*(DX(I-1)+DX(I))*DY(J-1)
                  ENDIF
                ENDIF
              DU(I,J,K)=AE(I,J,K)+AW(I,J,K)+AN(I,J,K)+AS(I,J,K)+AT(I,J,K)+
     &        AB(I,J,K)-SP(I,J,K)
            ENDDO
          ENDDO
        ENDDO

!       DO NN=1,NUMBER
! X SWEEP
          DO I=1,LDX+1
            DO K=1,LDZ+2
              DO J=1,LDY+1
                A(J)=AE(I,J,K)+AW(I,J,K)+AN(I,J,K)+AS(I,J,K)+AT(I,J,K)+
     &            AB(I,J,K)-SP(I,J,K)
                B(J)=AN(I,J,K)
                C(J)=AS(I,J,K)
                D(J)=AE(I,J,K)*U(I+1,J,K)+AW(I,J,K)*U(I-1,J,K)+
     &            AT(I,J,K)*U(I,J,K+1)+AB(I,J,K)*U(I,J,K-1)+SC(I,J,K)
                A(J)=A(J)/ALPHA
                D(J)=D(J)+(1-ALPHA)*A(J)*U(I,J,K)
              ENDDO
              CALL TDMA(A,B,C,D,LDY+1,PHI)
              DO J=1,LDY+1
                U(I,J,K)=PHI(J)
              ENDDO
            ENDDO
          ENDDO
! Y SWEEP
          DO J=1,LDY+1
            DO K=1,LDZ+2
              DO I=1,LDX+1
                A(I)=AE(I,J,K)+AW(I,J,K)+AN(I,J,K)+AS(I,J,K)+AT(I,J,K)+
     &            AB(I,J,K)-SP(I,J,K)

                B(I)=AE(I,J,K)
                C(I)=AW(I,J,K)
                D(I)=AN(I,J,K)*U(I,J+1,K)+AS(I,J,K)*U(I,J-1,K)+
     &            AT(I,J,K)*U(I,J,K+1)+AB(I,J,K)*U(I,J,K-1)+SC(I,J,K)
                A(I)=A(I)/ALPHA
                D(I)=D(I)+(1-ALPHA)*A(I)*U(I,J,K)
              ENDDO
              CALL TDMA(A,B,C,D,LDX+1,PHI)
              DO I=1,LDX+1
                U(I,J,K)=PHI(I)
              ENDDO
            ENDDO
          ENDDO

! Z SWEEP
          DO I=1,LDX+1
            DO J=1,LDY+1
```

```
                DO K=1,LDZ+2
                    A(K)=AE(I,J,K)+AW(I,J,K)+AN(I,J,K)+AS(I,J,K)+AT(I,J,K)+
     &                  AB(I,J,K)-SP(I,J,K)
                     B(K)=AT(I,J,K)
                     C(K)=AB(I,J,K)
                     D(K)=AE(I,J,K)*U(I+1,J,K)+AW(I,J,K)*U(I-1,J,K)+
     &               AN(I,J,K)*U(I,J+1,K)+AS(I,J,K)*U(I,J-1,K)+SC(I,J,K)
                    A(K)=A(K)/ALPHA
                    D(K)=D(K)+(1-ALPHA)*A(K)*U(I,J,K)
                 ENDDO
                CALL TDMA(A,B,C,D,LDZ+2,PHI)
                 DO K=1,LDZ+2
                    U(I,J,K)=PHI(K)
                 ENDDO
                 IF(NN.EQ.NUMBER)THEN
                    DO K=1,LDZ+1
                        R=A(K)*U(I,J,K)-B(K)*U(I,J,K+1)-C(K)*U(I,J,K-1)-D(K)
                       IF(ABS(R).GT.ABS(RESu))RESu=R
                     ENDDO
                 ENDIF
              ENDDO
           ENDDO
        ENDDO
! ------------------------------------------ Solve the V* equation ------------------------------------
         RESv=0
         DO I=1,LDX
            DO J=1,LDY+1
               DO K=1,LDZ+2
                  IF(J.EQ.1)THEN
                     AE(I,J,K)=0
                     AW(I,J,K)=0
                     AN(I,J,K)=0
                     AS(I,J,K)=0
                     AT(I,J,K)=0
                     AB(I,J,K)=0
                     SC(I,J,K)=0
                     SP(I,J,K)=-1.0E30
                  ELSEIF(K.EQ.1)THEN
                     AE(I,J,K)=0
                     AW(I,J,K)=0
                     AN(I,J,K)=1.0
                     AS(I,J,K)=0
                     AT(I,J,K)=1.0
                     AB(I,J,K)=0
                     SC(I,J,K)=0
                     SP(I,J,K)=0
                  ELSEIF(J.EQ.LDY+1)THEN
                     AE(I,J,K)=0
                     AW(I,J,K)=0
                     AN(I,J,K)=0
                     AS(I,J,K)=0
                     AT(I,J,K)=0
```

```
            AB(I,J,K)=0
            SC(I,J,K)=0
            SP(I,J,K)=-1.0E30
          ELSEIF(K.EQ.LDZ+2)THEN
            AE(I,J,K)=0
            AW(I,J,K)=0
            AN(I,J,K)=0
            AS(I,J,K)=0
            AT(I,J,K)=0
            AB(I,J,K)=1.0
            SC(I,J,K)=0
            SP(I,J,K)=0
          ELSE
            IF(I.LT.LDX)THEN
             IFLAG=1
            ELSE
             IFLAG=2
            ENDIF
           CALL YEQUA(RHO,U(I,J,K),U(I,J+1,K),U(I+1,J,K),
     &                          U(I+1,J+1,K),V(I,J-1,K),V(I,J,K),V(I,J+1,K),
     &              W(I,J,K-1),W(I,J+1,K-1),W(I,J,K),W(I,J+1,K),
     &              P(I,J,K),P(I,J+1,K),KT(I,J,K),KT(I,J+1,K),
     &             MU+VISC(I-1,J,K),MU+VISC(I-1,J+1,K),
     &             MU+VISC(I,J,K-1),MU+VISC(I,J,K),
     &             MU+VISC(I,J,K+1),MU+VISC(I,J+1,K-1),
     &             MU+VISC(I,J+1,K),MU+VISC(I,J+1,K+1),
     &             MU+VISC(I+1,J,K),MU+VISC(I+1,J+1,K),DX(I-1),
     &             DX(I),DX(I+1),DY(J-1),DY(J),DZ(K-2),DZ(K-1),
     &             DZ(K),IFLAG,AE(I,J,K),AW(I,J,K),AN(I,J,K),
     &             AS(I,J,K),AT(I,J,K),AB(I,J,K),SC(I,J,K),
     &             SP(I,J,K))
            IF(I.EQ.1)THEN
              h=DY(J)/(DY(J-1)+DY(J))
              Uw=h*U(I,J,K)+(1-h)*U(I,J+1,K)
              DXW=0.5*DX(I)
              DYC=0.5*(DY(J-1)+DY(J))
              DZC=DZ(K-1)
              AW(I,J,K)=0
              SP(I,J,K)=SP(I,J,K)-MU*DYC*DZC/DXW-RHO*Uw*DYC*DZC
              SC(I,J,K)=SC(I,J,K)+(RHO*Uw+MU/DXW)*Vin*DYC*DZC
             ENDIF
             IF(K.EQ.2.AND.I.GT.INLET)THEN
              AB(I,J,K)=0
              SP(I,J,K)=SP(I,J,K)-(MU/Z(2))*DX(I)*(0.5*(DY(J-1)+DY(J)))
             ENDIF
           ENDIF
          DV(I,J,K)=AE(I,J,K)+AW(I,J,K)+AN(I,J,K)+AS(I,J,K)+AT(I,J,K)+
     &              AB(I,J,K)-SP(I,J,K)
       ENDDO
     ENDDO
  ENDDO

 DO NN=1,NUMBER
```

```
! X SWEEP
            DO I=1,LDX
               DO K=1,LDZ+2
                  DO J=1,LDY+1
                    A(J)=AE(I,J,K)+AW(I,J,K)+AN(I,J,K)+AS(I,J,K)+AT(I,J,K)+
          &              AB(I,J,K)-SP(I,J,K)
                    B(J)=AN(I,J,K)
                    C(J)=AS(I,J,K)
                    D(J)=AE(I,J,K)*V(I+1,J,K)+AW(I,J,K)*V(I-1,J,K)+
          &              AT(I,J,K)*V(I,J,K+1)+AB(I,J,K)*V(I,J,K-1)+SC(I,J,K)
                   A(J)=A(J)/ALPHA
                   D(J)=D(J)+(1-ALPHA)*A(J)*V(I,J,K)
                  ENDDO
                 CALL TDMA(A,B,C,D,LDY+1,PHI)
                 DO J=1,LDY+1
                    V(I,J,K)=PHI(J)
                  ENDDO
               ENDDO
            ENDDO
! Y SWEEP
            DO J=1,LDY+1
               DO K=1,LDZ+2
                  DO I=1,LDX
                     A(I)=AE(I,J,K)+AW(I,J,K)+AN(I,J,K)+AS(I,J,K)+AT(I,J,K)+
          &               AB(I,J,K)-SP(I,J,K)

                     B(I)=AE(I,J,K)
                     C(I)=AW(I,J,K)
                     D(I)=AN(I,J,K)*V(I,J+1,K)+AS(I,J,K)*V(I,J-1,K)+
          &             AT(I,J,K)*V(I,J,K+1)+AB(I,J,K)*V(I,J,K-1)+SC(I,J,K)
                    A(I)=A(I)/ALPHA
                    D(I)=D(I)+(1-ALPHA)*A(I)*V(I,J,K)
                  ENDDO
                 CALL TDMA(A,B,C,D,LDX,PHI)
                 DO I=1,LDX
                    V(I,J,K)=PHI(I)
                  ENDDO
               ENDDO
            ENDDO

! Z SWEEP
            DO I=1,LDX
               DO J=1,LDY+1
                  DO K=1,LDZ+2
                     A(K)=AE(I,J,K)+AW(I,J,K)+AN(I,J,K)+AS(I,J,K)+AT(I,J,K)+
          &               AB(I,J,K)-SP(I,J,K)
                      B(K)=AT(I,J,K)
                      C(K)=AB(I,J,K)
                      D(K)=AE(I,J,K)*V(I+1,J,K)+AW(I,J,K)*V(I-1,J,K)+
          &             AN(I,J,K)*V(I,J+1,K)+AS(I,J,K)*V(I,J-1,K)+SC(I,J,K)
                     A(K)=A(K)/ALPHA
                     D(K)=D(K)+(1-ALPHA)*A(K)*V(I,J,K)
                  ENDDO
```

```
                    CALL TDMA(A,B,C,D,LDZ+2,PHI)
                    DO K=1,LDZ+2
                        V(I,J,K)=PHI(K)
                    ENDDO
                    IF(NN.EQ.NUMBER)THEN
                        DO K=1,LDZ+1
                            R=A(K)*V(I,J,K)-B(K)*V(I,J,K+1)-C(K)*V(I,J,K-1)-D(K)
                            IF(ABS(R).GT.ABS(RESv))RESv=R
                        ENDDO
                    ENDIF
                ENDDO
            ENDDO
        ENDDO
! ------------------------------------ Solve the W* equation ----------------------------------
        RESw=0
        DO I=1,LDX
            DO J=1,LDY+1
                DO K=1,LDZ+1
                    IF(J.EQ.1)THEN
                        AE(I,J,K)=0
                        AW(I,J,K)=0
                        AN(I,J,K)=1.0
                        AS(I,J,K)=0
                        AT(I,J,K)=0
                        AB(I,J,K)=0
                        SC(I,J,K)=0
                        SP(I,J,K)=0
                    ELSEIF(K.EQ.1)THEN
                        AE(I,J,K)=0
                        AW(I,J,K)=0
                        AN(I,J,K)=0
                        AS(I,J,K)=0
                        AT(I,J,K)=0
                        AB(I,J,K)=0
                        SC(I,J,K)=0
                        SP(I,J,K)=-1.0E30
                    ELSEIF(K.EQ.LDZ+1)THEN
                        AE(I,J,K)=0
                        AW(I,J,K)=0
                        AN(I,J,K)=0
                        AS(I,J,K)=0
                        AT(I,J,K)=0
                        AB(I,J,K)=0
                        SC(I,J,K)=0
                        SP(I,J,K)=-1.0
                    ELSE
                        IF(I.LT.LDX)THEN
                            IFLAG=1
                        ELSE
                            IFLAG=2
                        ENDIF
                        CALL ZEQUA(RHO,U(I,J,K),U(I,J,K+1),U(I+1,J,K),
```

```
     &                U(I+1,J,K+1),V(I,J-1,K),V(I,J-1,K+1),V(I,J,K),
     &          V(I,J,K+1),W(I,J,K-1),W(I,J,K),W(I,J,K+1),
     &          P(I,J,K),P(I,J,K+1),
     &          KT(I,J,K),KT(I,J,K+1),MU+VISC(I-1,J,K),
     &          MU+VISC(I-1,J,K+1),MU+VISC(I,J-1,K),
     &          MU+VISC(I,J-1,K+1),MU+VISC(I,J,K),
     &          MU+VISC(I,J,K+1),MU+VISC(I,J+1,K),
     &          MU+VISC(I,J+1,K+1),MU+VISC(I+1,J,K),
     &          MU+VISC(I+1,J,K+1),DX(I-1),DX(I),DX(I+1),
     &          DY(J-2),DY(J-1),DY(J),DZ(K-1),DZ(K),IFLAG,
     &          AE(I,J,K),AW(I,J,K),AN(I,J,K),AS(I,J,K),
     &          AT(I,J,K),AB(I,J,K),SC(I,J,K),SP(I,J,K))
        IF(J.EQ.LDY+1)THEN
          AN(I,J,K)=0
         ENDIF
        IF(I.EQ.1)THEN
          h=DZ(K)/(DZ(K-1)+DZ(K))
          Uw=h*U(I,J,K)+(1-h)*U(I,J,K+1)
          DXW=0.5*DX(I)
          DYC=DY(J-1)
          DZC=0.5*(DZ(K-1)+DZ(K))
          AW(I,J,K)=0
          SP(I,J,K)=SP(I,J,K)-MU*DYC*DZC/DXW-RHO*Uw*DYC*DZC
          SC(I,J,K)=SC(I,J,K)+(RHO*Uw+MU/DXW)*Win*DYC*DZC
        ENDIF
        IF(J.EQ.2)THEN
          XP=X(I)+0.5*DX(I)
          IF(XP.LT.X(LEAD))THEN
            IFLAG=1
          ELSEIF(XP.GT.X(LEAD)+SIDE1)THEN
            IFLAG=1
          ELSE
            IF(XP.GT.X(LEAD)+SIDE2.AND.ZP(XP-X(LEAD),SIDE1,SIDE2,
     &              WIDTH).LT.Z(K)+0.5*DZ(K-1))THEN
              IFLAG=1
            ELSE
              IFLAG=2
            ENDIF
          ENDIF
          IF(IFLAG.EQ.2)THEN
            AS(I,J,K)=0
            SP(I,J,K)=SP(I,J,K)-(MU/Y(2))*DX(I)*(0.5*(DZ(K-1)+DZ(K)))
          ENDIF
        ENDIF
       ENDIF
      DW(I,J,K)=AE(I,J,K)+AW(I,J,K)+AN(I,J,K)+AS(I,J,K)+AT(I,J,K)+
     &          AB(I,J,K)-SP(I,J,K)
    ENDDO
   ENDDO
  ENDDO

  DO NN=1,NUMBER
! X SWEEP
```

```
            DO I=1,LDX
               DO K=1,LDZ+1
                  DO J=1,LDY+1
                    A(J)=AE(I,J,K)+AW(I,J,K)+AN(I,J,K)+AS(I,J,K)+AT(I,J,K)+
     &                   AB(I,J,K)-SP(I,J,K)
                    B(J)=AN(I,J,K)
                    C(J)=AS(I,J,K)
                    D(J)=AE(I,J,K)*V(I+1,J,K)+AW(I,J,K)*W(I-1,J,K)+
     &                     AT(I,J,K)*W(I,J,K+1)+AB(I,J,K)*W(I,J,K-1)+SC(I,J,K)
                   A(J)=A(J)/ALPHA
                   D(J)=D(J)+(1-ALPHA)*A(J)*W(I,J,K)
                  ENDDO
                 CALL TDMA(A,B,C,D,LDY+1,PHI)
                 DO J=1,LDY+1
                    W(I,J,K)=PHI(J)
                  ENDDO
               ENDDO
             ENDDO
! Y SWEEP
             DO J=1,LDY+1
                DO K=1,LDZ+1
                   DO I=1,LDX
                      A(I)=AE(I,J,K)+AW(I,J,K)+AN(I,J,K)+AS(I,J,K)+AT(I,J,K)+
     &                     AB(I,J,K)-SP(I,J,K)

                      B(I)=AE(I,J,K)
                      C(I)=AW(I,J,K)
                      D(I)=AN(I,J,K)*W(I,J+1,K)+AS(I,J,K)*W(I,J-1,K)+
     &                    AT(I,J,K)*W(I,J,K+1)+AB(I,J,K)*W(I,J,K-1)+SC(I,J,K)
                     A(I)=A(I)/ALPHA
                     D(I)=D(I)+(1-ALPHA)*A(I)*W(I,J,K)
                   ENDDO
                  CALL TDMA(A,B,C,D,LDX,PHI)
                  DO I=1,LDX
                     W(I,J,K)=PHI(I)
                   ENDDO
                ENDDO
              ENDDO

! Z SWEEP
              DO I=1,LDX
                 DO J=1,LDY+1
                    DO K=1,LDZ+1
                       A(K)=AE(I,J,K)+AW(I,J,K)+AN(I,J,K)+AS(I,J,K)+AT(I,J,K)+
     &                      AB(I,J,K)-SP(I,J,K)
                       B(K)=AT(I,J,K)
                       C(K)=AB(I,J,K)
                       D(K)=AE(I,J,K)*W(I+1,J,K)+AW(I,J,K)*W(I-1,J,K)+
     &                     AN(I,J,K)*W(I,J+1,K)+AS(I,J,K)*W(I,J-1,K)+SC(I,J,K)
                      A(K)=A(K)/ALPHA
                      D(K)=D(K)+(1-ALPHA)*A(K)*W(I,J,K)
                    ENDDO
                  CALL TDMA(A,B,C,D,LDZ+1,PHI)
```

```
                    DO K=1,LDZ+1
                        W(I,J,K)=PHI(K)
                     ENDDO
                    IF(NN.EQ.NUMBER)THEN
                       DO K=1,LDZ+1
                            R=A(K)*W(I,J,K)-B(K)*W(I,J,K+1)-C(K)*W(I,J,K-1)-D(K)
                          IF(ABS(R).GT.ABS(RESw))RESw=R
                        ENDDO
                    ENDIF
                  ENDDO
               ENDDO
            ENDDO
!
C ****************STEP 3: SOLVE THE P' EQUATION ****************************
C
         MASS=0
         DO I=0,LDX
            DO J=0,LDY+1
               DO K=0,LDZ+2
                  PP(I,J,K)=0.0_8
               ENDDO
            ENDDO
         ENDDO

         DO 49 LP=1,3
        CMASS=0
         DO I=1,LDX
              DO J=1,LDY+1
                 DO K=1,LDZ+2
                   IF(I.EQ.1.AND.J.EQ.1.AND.K.EQ.1)THEN
                      AE(I,J,K)=0
                      AW(I,J,K)=0
                      AN(I,J,K)=0
                      AS(I,J,K)=0
                      AT(I,J,K)=0
                      AB(I,J,K)=0
                      SC(I,J,K)=0
                      SP(I,J,K)=-1.0E30
                   ELSEIF(J.EQ.1)THEN
                      AE(I,J,K)=0
                      AW(I,J,K)=0
                      AN(I,J,K)=1.0
                      AS(I,J,K)=0
                      AT(I,J,K)=0
                      AB(I,J,K)=0
                      SC(I,J,K)=0
                      SP(I,J,K)=0
                  ELSEIF(K.EQ.1)THEN
                      AE(I,J,K)=0
                      AW(I,J,K)=0
                      AN(I,J,K)=0
                      AS(I,J,K)=0
                      AT(I,J,K)=1.0
```

```
                AB(I,J,K)=0
                SC(I,J,K)=0
                SP(I,J,K)=0
              ELSEIF(K.EQ.LDZ+2)THEN
                AE(I,J,K)=0
                AW(I,J,K)=0
                AN(I,J,K)=0
                AS(I,J,K)=0
                AT(I,J,K)=0
                AB(I,J,K)=1.0
                SC(I,J,K)=0
                SP(I,J,K)=0
            ELSE
              IFLAG1=1
              IFLAG2=1
              IFLAG3=1
              IFLAG4=1
              IFLAG5=1
              IFLAG6=1
              IF(I.EQ.1)IFLAG1=2
              IF(I.EQ.LDX)IFLAG2=2
              IF(J.EQ.2)IFLAG3=2
              IF(J.EQ.LDY+1)IFLAG4=2
             IF(K.EQ.2)IFLAG5=2
              IF(K.EQ.LDZ+1)IFLAG6=2
             CALL PRESS(RHO,U(I,J,K),U(I+1,J,K),V(I,J-1,K),V(I,J,K),
     &                  W(I,J,K-1),W(I,J,K),DU(I,J,K),DU(I+1,J,K),
     &           DV(I,J-1,K),DV(I,J,K),DW(I,J,K-1),DW(I,J,K),
     &           DX(I),DY(J-1),DZ(K-1),IFLAG1,
     &          IFLAG2,IFLAG3,IFLAG4,IFLAG5,IFLAG6,AE(I,J,K),
     &          AW(I,J,K),AN(I,J,K),AS(I,J,K),AT(I,J,K),
     &          AB(I,J,K),SC(I,J,K))
              SP(I,J,K)=0
              IF(ABS(SC(I,J,K)).GT.ABS(MASS))MASS=SC(I,J,K)
              CMASS=CMASS+ABS(SC(I,J,K))
            ENDIF
          ENDDO
        ENDDO
      ENDDO

        DO NN=1,NUMBER
! X SWEEP
          DO I=1,LDX
            DO K=1,LDZ+2
              DO J=1,LDY+1
                A(J)=AE(I,J,K)+AW(I,J,K)+AN(I,J,K)+AS(I,J,K)+AT(I,J,K)+
     &               AB(I,J,K)-SP(I,J,K)
                B(J)=AN(I,J,K)
                C(J)=AS(I,J,K)
                D(J)=AE(I,J,K)*PP(I+1,J,K)+AW(I,J,K)*PP(I-1,J,K)+
     &                AT(I,J,K)*PP(I,J,K+1)+AB(I,J,K)*PP(I,J,K-1)+SC(I,J,K)
               A(J)=A(J)/ALPHA
               D(J)=D(J)+(1-ALPHA)*A(J)*PP(I,J,K)
```

```
                ENDDO
                CALL TDMA(A,B,C,D,LDY+1,PHI)
                DO J=1,LDY+1
                   PP(I,J,K)=PHI(J)
                ENDDO
             ENDDO
          ENDDO
! Z SWEEP
           DO I=1,LDX
              DO J=1,LDY+1
                 DO K=1,LDZ+2
                    A(K)=AE(I,J,K)+AW(I,J,K)+AN(I,J,K)+AS(I,J,K)+AT(I,J,K)+
     &                   AB(I,J,K)-SP(I,J,K)
                    B(K)=AT(I,J,K)
                    C(K)=AB(I,J,K)
                    D(K)=AE(I,J,K)*PP(I+1,J,K)+AW(I,J,K)*PP(I-1,J,K)+
     &                   AN(I,J,K)*PP(I,J+1,K)+AS(I,J,K)*PP(I,J-1,K)+SC(I,J,K)
                    A(K)=A(K)/ALPHA
                    D(K)=D(K)+(1-ALPHA)*A(K)*PP(I,J,K)
                 ENDDO
                 CALL TDMA(A,B,C,D,LDZ+2,PHI)
                 DO K=1,LDZ+2
                    PP(I,J,K)=PHI(K)
                 ENDDO
              ENDDO
           ENDDO

! Y SWEEP
           DO J=1,LDY+1
              DO K=1,LDZ+2
                 DO I=1,LDX
                    A(I)=AE(I,J,K)+AW(I,J,K)+AN(I,J,K)+AS(I,J,K)+AT(I,J,K)+
     &                   AB(I,J,K)-SP(I,J,K)

                    B(I)=AE(I,J,K)
                    C(I)=AW(I,J,K)
                    D(I)=AN(I,J,K)*PP(I,J+1,K)+AS(I,J,K)*PP(I,J-1,K)+
     &                   AT(I,J,K)*PP(I,J,K+1)+AB(I,J,K)*PP(I,J,K-1)+SC(I,J,K)
                    A(I)=A(I)/ALPHA
                    D(I)=D(I)+(1-ALPHA)*A(I)*PP(I,J,K)
                 ENDDO
                 CALL TDMA(A,B,C,D,LDX,PHI)
                 DO I=1,LDX
                    PP(I,J,K)=PHI(I)
                 ENDDO
              ENDDO
           ENDDO
        ENDDO
     49 CONTINUE
!
! ********** STEP 4: CALCULATE P BY ADDING P' TO P* **********
           DO K=1,LDZ+2
              DO J=1,LDY+1
```

```
                DO I=1,LDX
                   P(I,J,K)=P(I,J,K)+ALPHA2*PP(I,J,K)
                 ENDDO
               ENDDO
             ENDDO
!
! ********** STEP 5: CALCULATE U,V,W FROM U*,V*,W* **********
!
           DO K=1,LDZ+2
              DO J=1,LDY+1
                DO I=2,LDX
                   U(I,J,K)=U(I,J,K)+(DY(J-1)*DZ(K-1)/DU(I,J,K))*(PP(I-1,J,K)-PP(I,J,K))
                   IF(I.EQ.LDX)U(I+1,J,K)=RATIO*U(I,J,K)
                ENDDO
              ENDDO
            ENDDO
            DO K=1,LDZ+2
              DO J=2,LDY
                 DO I=1,LDX
                   V(I,J,K)=V(I,J,K)+(DX(I)*DZ(K-1)/DV(I,J,K))*(PP(I,J,K)-PP(I,J+1,K))
                 ENDDO
              ENDDO
            ENDDO
           DO K=2,LDZ
              DO J=1,LDY+1
                DO I=1,LDX
                   W(I,J,K)=W(I,J,K)+(DX(I)*DY(J-1)/DW(I,J,K))*(PP(I,J,K)-PP(I,J,K+1))
                 ENDDO
              ENDDO
            ENDDO
           IF(M.LE.MM1)GOTO 33

! ---------- Compute the eddy viscosity for each node ----------
            DO I=1,LDX
               XP=X(I)+0.5*DX(I)
               DO K=2,LDZ+1
                  IF(XP.LT.X(LEAD))THEN
                     IFLAG=1
                  ELSEIF(XP.GT.X(LEAD)+SIDE1)THEN
                     IFLAG=1
                  ELSE
                     IF(XP.GT.X(LEAD)+SIDE2.AND.
     &                    ZP(XP-X(LEAD),SIDE1,SIDE2,WIDTH).LT.Z(K))THEN
                       IFLAG=1
                      ELSE
                        IFLAG=2
                      ENDIF
                  ENDIF
                  DO J=2,LDY+1
                   IF(EP(I,J,K).EQ.0)THEN
                      GAMMA=0
                   ELSE
                      IF(IFLAG.EQ.2.AND.ABS(Y(J)).LE.ABS(Z(K)))THEN
```

```
                        RY=SQRT(KT(I,J,K))*Y(J)/(MU/RHO)
                        IF(RY.LT.200)THEN
                           LU=CL*Y(J)*(1-EXP(-RY/70))
                          GAMMA=RHO*CMU*SQRT(KT(I,J,K))*LU
                        ELSE
                            GAMMA=RHO*CMU*(KT(I,J,K)**2)/EP(I,J,K)
                        ENDIF
                       ELSEIF(I.GT.INLET)THEN
                        RZ=SQRT(KT(I,J,K))*Z(K)/(MU/RHO)
                        IF(RZ.LT.200)THEN
                           LU=CL*Z(K)*(1-EXP(-RZ/70))
                          GAMMA=RHO*CMU*SQRT(KT(I,J,K))*LU
                        ELSE
                            GAMMA=RHO*CMU*(KT(I,J,K)**2)/EP(I,J,K)
                        ENDIF
                      ELSE
                          GAMMA=RHO*CMU*(KT(I,J,K)**2)/EP(I,J,K)
                       ENDIF
                    ENDIF
                     VISC(I,J,K)=(1-ALPHA3)*VISC(I,J,K)+ALPHA3*GAMMA
                    IF(J.EQ.2)VISC(I,J-1,K)=VISC(I,J,K)
                    IF(K.EQ.2)VISC(I,J,K-1)=VISC(I,J,K)
                    IF(K.EQ.LDZ+1)VISC(I,J,K+1)=VISC(I,J,K)
                  ENDDO
                ENDDO
              ENDDO
!
! ********************STEP 6: SOLVE FOR K AND EPSILON ************************

! ---------- Compute the value of G (production term) for each node ----------
            DO I=2,LDX
               XP=X(I)+0.5*DX(I)
               DO K=2,LDZ+1
                  IF(XP.LT.X(LEAD))THEN
                     IFLAG=1
                  ELSEIF(XP.GT.X(LEAD)+SIDE1)THEN
                     IFLAG=1
                  ELSE
                     IF(XP.GT.X(LEAD)+SIDE2.AND.
     &                   ZP(XP-X(LEAD),SIDE1,SIDE2,WIDTH).LT.Z(K))THEN
                        IFLAG=1
                     ELSE
                        IFLAG=2
                     ENDIF
                  ENDIF
                  DO J=2,LDY+1
                     DUX=(U(I+1,J,K)-U(I,J,K))/DX(I)
                      U1=0.5*(U(I,J-1,K)+U(I+1,J-1,K))
                     U2=0.5*(U(I,J,K)+U(I+1,J,K))
                     U3=0.5*(U(I,J+1,K)+U(I+1,J+1,K))
                     IF(J.EQ.2)THEN
                        IF(IFLAG.EQ.2)THEN
                          Us=0
```

```
   ELSE
     Us=((2*DY(1)+DY(2))*U2-DY(1)*U3)/(DY(1)+DY(2))
  ENDIF
 ELSE
    Us=U1+(DY(J-2)/(DY(J-2)+DY(J-1)))*(U2-U1)
 ENDIF
IF(J.LT.LDY+1)THEN
     Un=U2+(DY(J-1)/(DY(J-1)+DY(J)))*(U3-U2)
ELSE
    Un=U2
 ENDIF
DUY=(Un-Us)/DY(J-1)
 U1=0.5*(U(I,J,K-1)+U(I+1,J,K-1))
U2=0.5*(U(I,J,K)+U(I+1,J,K))
U3=0.5*(U(I,J,K+1)+U(I+1,J,K+1))
 IF(K.EQ.2)THEN
    IF(I.GT.INLET)THEN
      Ub=0
   ELSE
      Ub=((2*DZ(1)+DZ(2))*U2-DZ(1)*U3)/(DZ(1)+DZ(2))
    ENDIF
 ELSE
    Ub=U1+(DZ(K-2)/(DZ(K-2)+DZ(K-1)))*(U2-U1)
ENDIF
 IF(K.EQ.LDZ+1)THEN
   Ut=U1+(U2-U1)*(DZ(LDZ-2)+2*DZ(LDZ-1))/(DZ(LDZ-2)+DZ(LDZ-1))
 ELSE
   Ut=U2+(DZ(K-1)/(DZ(K-1)+DZ(K)))*(U3-U2)
ENDIF
DUZ=(Ut-Ub)/DZ(K-1)
 V1=0.5*(V(I-1,J-1,K)+V(I-1,J,K))
V2=0.5*(V(I,J-1,K)+V(I,J,K))
IF(I.LT.LDX)THEN
   V3=0.5*(V(I+1,J-1,K)+V(I+1,J,K))
    Vw=V1+(DX(I-1)/(DX(I-1)+DX(I)))*(V2-V1)
    Ve=V2+(DX(I)/(DX(I)+DX(I+1)))*(V3-V2)
   DVX=(Ve-Vw)/DX(I)
 ELSE
    DVX=(V2-V1)/(0.5*(DX(I-1)+DX(I)))
 ENDIF
 DVY=(V(I,J,K)-V(I,J-1,K))/DY(J-1)
 V1=0.5*(V(I,J-1,K-1)+V(I,J,K-1))
V2=0.5*(V(I,J-1,K)+V(I,J,K))
V3=0.5*(V(I,J-1,K+1)+V(I,J,K+1))
IF(K.EQ.2)THEN
    IF(I.GT.INLET)THEN
       Vb=0
    ELSE
       Vb=((2*DZ(1)+DZ(2))*V2-DZ(1)*V3)/(DZ(1)+DZ(2))
    ENDIF
 ELSE
    Vb=V1+(DZ(K-2)/(DZ(K-2)+DZ(K-1)))*(V2-V1)
ENDIF
```

```
                IF(K.EQ.LDZ+1)THEN
                  Vt=V1+(V2-V1)*(DZ(LDZ-2)+2*DZ(LDZ-1))/(DZ(LDZ-2)+DZ(LDZ-1))
                ELSE
                  Vt=V2+(DZ(K-1)/(DZ(K-1)+DZ(K)))*(V3-V2)
                ENDIF
                DVZ=(Vt-Vb)/DZ(K-1)
                W1=0.5*(W(I-1,J,K-1)+W(I-1,J,K))
                W2=0.5*(W(I,J,K-1)+W(I,J,K))
                IF(I.LT.LDX)THEN
                  W3=0.5*(W(I+1,J,K-1)+W(I+1,J,K))
                  Ww=W1+(DX(I-1)/(DX(I-1)+DX(I)))*(W2-W1)
                  We=W2+(DX(I)/(DX(I)+DX(I+1)))*(W3-W2)
                  DWX=(We-Ww)/DX(I)
                ELSE
                  DWX=(W2-W1)/(0.5*(DX(I-1)+DX(I)))
                ENDIF
                W1=0.5*(W(I,J-1,K-1)+W(I,J-1,K))
                W2=0.5*(W(I,J,K-1)+W(I,J,K))
                W3=0.5*(W(I,J+1,K-1)+W(I,J+1,K))
                IF(J.EQ.2)THEN
                  IF(IFLAG.EQ.2)THEN
                    Ws=0
                  ELSE
                    Ws=((2*DY(1)+DY(2))*W2-DY(1)*W3)/(DY(1)+DY(2))
                  ENDIF
                ELSE
                  Ws=W1+(DY(J-2)/(DY(J-2)+DY(J-1)))*(W2-W1)
                ENDIF
                IF(J.LT.LDY+1)THEN
                  Wn=W2+(DY(J-1)/(DY(J-1)+DY(J)))*(W3-W2)
                ELSE
                  Wn=W2
                ENDIF
                DWY=(Wn-Ws)/DY(J-1)
                DWZ=(W(I,J,K)-W(I,J,K-1))/DZ(K-1)
                GNEW=VISC(I,J,K)*(2*(DUX**2)+2*(DVY**2)+2*(DWZ**2)+
     &                          (DVX+DUY)**2+(DUZ+DWX)**2+(DVZ+DWY)**2)
                G(I,J,K)=(1-ALPHA3)*G(I,J,K)+ALPHA3*GNEW
              ENDDO
            ENDDO
          ENDDO
!
! ---------- Solve for kinetic energy ----------
        RESk=0
        DO I=1,LDX
          XP=X(I)+0.5*DX(I)
          DO J=1,LDY+1
            DO K=1,LDZ+2
              IF(I.EQ.1)THEN
                AE(I,J,K)=0
                AW(I,J,K)=0
                AN(I,J,K)=0
                AS(I,J,K)=0
```

```
                AT(I,J,K)=0
                AB(I,J,K)=0
                SC(I,J,K)=KTin*1.0E30
                SP(I,J,K)=-1.0E30
              ELSEIF(J.EQ.1)THEN
                AE(I,J,K)=0
                AW(I,J,K)=0
                AN(I,J,K)=1.0
                AS(I,J,K)=0
                AT(I,J,K)=0
                AB(I,J,K)=0
                SC(I,J,K)=0
                SP(I,J,K)=0
            ELSEIF(K.EQ.LD1)THEN
                AE(I,J,K)=0
                AW(I,J,K)=0
                AN(I,J,K)=0
                AS(I,J,K)=0
                AT(I,J,K)=1.0
                AB(I,J,K)=0
                SC(I,J,K)=0
                SP(I,J,K)=0

            ELSEIF(K.EQ.LDZ+2)THEN
                AE(I,J,K)=0
                AW(I,J,K)=0
                AN(I,J,K)=0
                AS(I,J,K)=0
                AT(I,J,K)=0
                AB(I,J,K)=1.0
                SC(I,J,K)=0
                SP(I,J,K)=0
              ELSE
                IF(I.LT.LDX)THEN
                  IFLAG=1
                ELSE
                  IFLAG=2
                ENDIF
                CALL KEQUA(MU,RHO,U(I,J,K),U(I+1,J,K),V(I,J-1,K),
&                    V(I,J,K),W(I,J,K-1),W(I,J,K),
&                   KT(I,J,K),MU+VISC(I-1,J,K)/ZK,
&                   MU+VISC(I,J,K)/ZK,MU+VISC(I+1,J,K)/ZK,
&                   MU+VISC(I,J-1,K)/ZK,MU+VISC(I,J+1,K)/ZK,
&                   MU+VISC(I,J,K-1)/ZK,MU+VISC(I,J,K+1)/ZK,
&                   ZK,G(I,J,K),EP(I,J,K),CMU,DX(I-1),DX(I),DX(I+1),
&                   DY(J-2),DY(J-1),DY(J),DZ(K-2),DZ(K-1),DZ(K),
&                   IFLAG,AE(I,J,K),AW(I,J,K),AN(I,J,K),
&                   AS(I,J,K),AT(I,J,K),AB(I,J,K),SC(I,J,K),
&                   SP(I,J,K))
               IF(J.EQ.LDY+1)THEN
                  AN(I,J,K)=0
                ENDIF
               IF(J.EQ.2)THEN
```

```
                    IF(XP.LT.X(LEAD))THEN
                      IFLAG=1
                    ELSEIF(XP.GT.X(LEAD)+SIDE1)THEN
                      IFLAG=1
                    ELSE
                      IF(XP.GT.X(LEAD)+SIDE2.AND.
     &                    ZP(XP-X(LEAD),SIDE1,SIDE2,WIDTH).LT.Z(K))THEN
                        IFLAG=1
                      ELSE
                        IFLAG=2
                      ENDIF
                    ENDIF
                      IF(IFLAG.EQ.2)THEN
                        AS(I,J,K)=0
                        SP(I,J,K)=SP(I,J,K)-(MU/Y(2))*DX(I)*DZ(K-1)
                      ENDIF
                    ENDIF
                     IF(K.EQ.2.AND.I.GT.INLET)THEN
                       AB(I,J,K)=0
                     SP(I,J,K)=SP(I,J,K)-(MU/Z(2))*DX(I)*DY(J-1)
                    ENDIF
                  ENDIF
                ENDDO
              ENDDO
            ENDDO

          DO NN=1,NUMBER
! X SWEEP
            DO I=1,LDX
              DO K=1,LDZ+2
                DO J=1,LDY+1
                  A(J)=AE(I,J,K)+AW(I,J,K)+AN(I,J,K)+AS(I,J,K)+AT(I,J,K)+
     &                 AB(I,J,K)-SP(I,J,K)
                  B(J)=AN(I,J,K)
                  C(J)=AS(I,J,K)
                  D(J)=AE(I,J,K)*KT(I+1,J,K)+AW(I,J,K)*KT(I-1,J,K)+
     &                   AT(I,J,K)*KT(I,J,K+1)+AB(I,J,K)*KT(I,J,K-1)+SC(I,J,K)
                 A(J)=A(J)/ALPHA3
                 D(J)=D(J)+(1-ALPHA3)*A(J)*KT(I,J,K)
                ENDDO
               CALL TDMA(A,B,C,D,LDY+1,PHI)
               DO J=1,LDY+1
                  KT(I,J,K)=PHI(J)
                ENDDO
              ENDDO
            ENDDO
! Y SWEEP
            DO J=1,LDY+1
              DO K=1,LDZ+2
                DO I=1,LDX
                  A(I)=AE(I,J,K)+AW(I,J,K)+AN(I,J,K)+AS(I,J,K)+AT(I,J,K)+
     &                 AB(I,J,K)-SP(I,J,K)
```

```
                    B(I)=AE(I,J,K)
                    C(I)=AW(I,J,K)
                    D(I)=AN(I,J,K)*KT(I,J+1,K)+AS(I,J,K)*KT(I,J-1,K)+
     &              AT(I,J,K)*KT(I,J,K+1)+AB(I,J,K)*KT(I,J,K-1)+SC(I,J,K)
                    A(I)=A(I)/ALPHA3
                    D(I)=D(I)+(1-ALPHA3)*A(I)*KT(I,J,K)
                  ENDDO
                  CALL TDMA(A,B,C,D,LDX,PHI)
                  DO I=1,LDX
                    KT(I,J,K)=PHI(I)
                  ENDDO
                ENDDO
              ENDDO
! Z SWEEP
              DO I=1,LDX
                DO J=1,LDY+1
                  DO K=1,LDZ+2
                    A(K)=AE(I,J,K)+AW(I,J,K)+AN(I,J,K)+AS(I,J,K)+AT(I,J,K)+
     &                AB(I,J,K)-SP(I,J,K)
                    B(K)=AT(I,J,K)
                    C(K)=AB(I,J,K)
                    D(K)=AE(I,J,K)*KT(I+1,J,K)+AW(I,J,K)*KT(I-1,J,K)+
     &              AN(I,J,K)*KT(I,J+1,K)+AS(I,J,K)*KT(I,J-1,K)+SC(I,J,K)
                    A(K)=A(K)/ALPHA3
                    D(K)=D(K)+(1-ALPHA3)*A(K)*KT(I,J,K)
                  ENDDO
                  CALL TDMA(A,B,C,D,LDZ+2,PHI)
                  DO K=1,LDZ+2
                    KT(I,J,K)=PHI(K)
                  ENDDO
                  IF(NN.EQ.NUMBER)THEN
                    DO K=1,LDZ+1
                      R=A(K)*KT(I,J,K)-B(K)*KT(I,J,K+1)-C(K)*KT(I,J,K-1)-D(K)
                      IF(ABS(R).GT.ABS(RESk))RESk=R
                    ENDDO
                  ENDIF
                ENDDO
              ENDDO
            ENDDO
!
! ------------------------- Solve for energy dissipation ε ----------------------------------
            RESe=0
            DO I=1,LDX
              XP=X(I)+0.5*DX(I)
              DO K=1,LDZ+2
                IF(XP.LT.X(LEAD))THEN
                  IFLAG=1
                ELSEIF(XP.GT.X(LEAD)+SIDE1)THEN
                  IFLAG=1
                ELSE
                  IF(XP.GT.X(LEAD)+SIDE2.AND.
     &              ZP(XP-X(LEAD),SIDE1,SIDE2,WIDTH).LT.Z(K))THEN
                    IFLAG=1
```

```
          ELSE
            IFLAG=2
          ENDIF
        ENDIF
      DO J=1,LDY+1
          IF(IFLAG.EQ.2.AND.ABS(Y(J)).LE.ABS(Z(K)))THEN
            RY=SQRT(KT(I,J,K))*Y(J)/(MU/RHO)
          ELSEIF(I.GT.INLET)THEN
            RZ=SQRT(KT(I,J,K))*Z(K)/(MU/RHO)
          ENDIF
          IF(I.EQ.1)THEN
            AE(I,J,K)=0
            AW(I,J,K)=0
            AN(I,J,K)=0
            AS(I,J,K)=0
            AT(I,J,K)=0
            AB(I,J,K)=0
            SC(I,J,K)=EPin*1.0E30
            SP(I,J,K)=-1.0E30
          ELSEIF(J.EQ.1)THEN
            AE(I,J,K)=0
            AW(I,J,K)=0
            AN(I,J,K)=1.0
            AS(I,J,K)=0
            AT(I,J,K)=0
            AB(I,J,K)=0
            SC(I,J,K)=0
            SP(I,J,K)=0
          ELSEIF(K.EQ.1)THEN
            AE(I,J,K)=0
            AW(I,J,K)=0
            AN(I,J,K)=0
            AS(I,J,K)=0
            AT(I,J,K)=1.0
            AB(I,J,K)=0
            SC(I,J,K)=0
            SP(I,J,K)=0
          ELSEIF(K.EQ.LDZ+2)THEN
            AE(I,J,K)=0
            AW(I,J,K)=0
            AN(I,J,K)=0
            AS(I,J,K)=0
            AT(I,J,K)=0
            AB(I,J,K)=1.0
            SC(I,J,K)=0
            SP(I,J,K)=0
          ELSEIF(IFLAG.EQ.2.AND.ABS(Y(J)).LE.ABS(Z(K)).
     &                                    AND.RY.LT.200)THEN
            LEP=CL*Y(J)*(1-EXP(-RY/AEP))
            AE(I,J,K)=0
            AW(I,J,K)=0
            AN(I,J,K)=0
            AS(I,J,K)=0
```

```
 AT(I,J,K)=0
 AB(I,J,K)=0
 IF(LEP.GT.0)THEN
    SC(I,J,K)=(KT(I,J,K)**1.5)/LEP
 ELSE
    SC(I,J,K)=0
 ENDIF
 SP(I,J,K)=-1.0
ELSEIF(I.GT.INLET.AND.RZ.LT.200)THEN
 LEP=CL*Z(K)*(1-EXP(-RZ/AEP))
 AE(I,J,K)=0
 AW(I,J,K)=0
 AN(I,J,K)=0
 AS(I,J,K)=0
 AT(I,J,K)=0
 AB(I,J,K)=0
 IF(LEP.GT.0)THEN
    SC(I,J,K)=(KT(I,J,K)**1.5)/LEP
 ELSE
    SC(I,J,K)=0
 ENDIF
 SP(I,J,K)=-1.0
ELSEIF(IFLAG.EQ.2.AND.ABS(Y(J)).LE.ABS(Z(K)))THEN
 LEP=CL*Y(J)*(1-EXP(-RY/AEP))
 AE(I,J,K)=0
 AW(I,J,K)=0
 AN(I,J,K)=0
 AS(I,J,K)=0
 AT(I,J,K)=0
 AB(I,J,K)=0
 IF(LEP.GT.0)THEN
    SC(I,J,K)=(KT(I,J,K)**1.5)/LEP
 ELSE
    SC(I,J,K)=0
 ENDIF
 SP(I,J,K)=-1.0
ELSEIF(I.GT.INLET)THEN
  LEP=CL*Z(K)*(1-EXP(-RZ/AEP))
  AE(I,J,K)=0
  AW(I,J,K)=0
  AN(I,J,K)=0
  AS(I,J,K)=0
  AT(I,J,K)=0
  AB(I,J,K)=0
  IF(LEP.GT.0)THEN
     SC(I,J,K)=(KT(I,J,K)**1.5)/LEP
  ELSE
     SC(I,J,K)=0
  ENDIF
     SP(I,J,K)=-1.0
  ELSE
     IF(I.LT.LDX)THEN
      IFLAG2=1
```

```
                    ELSE
                      IFLAG2=2
                    ENDIF
                   CALL EPEQUA(MU,RHO,U(I,J,K),U(I+1,J,K),V(I,J-1,K),
     &                  V(I,J,K),W(I,J,K-1),W(I,J,K),EP(I,J,K),
     &                  KT(I,J,K),MU+VISC(I-1,J,K)/ZEP,
     &                  MU+VISC(I,J,K)/ZEP,MU+VISC(I+1,J,K)/ZEP,
     &                  MU+VISC(I,J-1,K)/ZEP,MU+VISC(I,J+1,K)/ZEP,
     &                  MU+VISC(I,J,K-1)/ZEP,MU+VISC(I,J,K+1)/ZEP,
     &                  G(I,J,K),ZEP,CEP1,CEP2,CMU,
     &                  DX(I-1),DX(I),DX(I+1),DY(J-2),DY(J-1),DY(J),
     &                  DZ(K-2),DZ(K-1),DZ(K),IFLAG2,AE(I,J,K),
     &                  AW(I,J,K),AN(I,J,K),AS(I,J,K),AT(I,J,K),
     &                  AB(I,J,K),SC(I,J,K),SP(I,J,K))
                  IF(J.EQ.LDY+1)THEN
                    AN(I,J,K)=0
                   ENDIF
                  IF(J.EQ.2.AND.IFLAG.EQ.2)THEN
                    AS(I,J,K)=0
                    SP(I,J,K)=SP(I,J,K)-(MU/Y(2))*DX(I)*DZ(K-1)
                  ENDIF
                   IF(K.EQ.2.AND.I.GT.INLET)THEN
                    AB(I,J,K)=0
                    SP(I,J,K)=SP(I,J,K)-(MU/Z(2))*DX(I)*DY(J-1)
                  ENDIF
                ENDIF
              ENDDO
            ENDDO
          ENDDO

        DO NN=1,NUMBER
! X SWEEP
          DO I=1,LDX
            DO K=1,LDZ+2
              DO J=1,LDY+1
                A(J)=AE(I,J,K)+AW(I,J,K)+AN(I,J,K)+AS(I,J,K)+AT(I,J,K)+
     &              AB(I,J,K)-SP(I,J,K)
                B(J)=AN(I,J,K)
                C(J)=AS(I,J,K)
                D(J)=AE(I,J,K)*EP(I+1,J,K)+AW(I,J,K)*EP(I-1,J,K)+
     &              AT(I,J,K)*EP(I,J,K+1)+AB(I,J,K)*EP(I,J,K-1)+SC(I,J,K)
               A(J)=A(J)/ALPHA3
               D(J)=D(J)+(1-ALPHA3)*A(J)*EP(I,J,K)
              ENDDO
             CALL TDMA(A,B,C,D,LDY+1,PHI)
             DO J=1,LDY+1
               EP(I,J,K)=PHI(J)
              ENDDO
            ENDDO
          ENDDO
! Y SWEEP
          DO J=1,LDY+1
            DO K=1,LDZ+2
```

```
                DO I=1,LDX
                    A(I)=AE(I,J,K)+AW(I,J,K)+AN(I,J,K)+AS(I,J,K)+AT(I,J,K)+
     &                  AB(I,J,K)-SP(I,J,K)

                    B(I)=AE(I,J,K)
                    C(I)=AW(I,J,K)
                    D(I)=AN(I,J,K)*EP(I,J+1,K)+AS(I,J,K)*EP(I,J-1,K)+
     &              AT(I,J,K)*EP(I,J,K+1)+AB(I,J,K)*EP(I,J,K-1)+SC(I,J,K)
                   A(I)=A(I)/ALPHA3
                   D(I)=D(I)+(1-ALPHA3)*A(I)*EP(I,J,K)
                 ENDDO
                CALL TDMA(A,B,C,D,LDX,PHI)
                DO I=1,LDX
                   EP(I,J,K)=PHI(I)
                 ENDDO
              ENDDO
            ENDDO
! Z SWEEP
            DO I=1,LDX
               DO J=1,LDY+1
                  DO K=1,LDZ+2
                     A(K)=AE(I,J,K)+AW(I,J,K)+AN(I,J,K)+AS(I,J,K)+AT(I,J,K)+
     &                  AB(I,J,K)-SP(I,J,K)
                      B(K)=AT(I,J,K)
                      C(K)=AB(I,J,K)
                      D(K)=AE(I,J,K)*EP(I+1,J,K)+AW(I,J,K)*EP(I-1,J,K)+
     &                  AN(I,J,K)*EP(I,J+1,K)+AS(I,J,K)*EP(I,J-1,K)+SC(I,J,K)
                     A(K)=A(K)/ALPHA3
                     D(K)=D(K)+(1-ALPHA3)*A(K)*EP(I,J,K)
                   ENDDO
                  CALL TDMA(A,B,C,D,LDZ+2,PHI)
                   DO K=1,LDZ+2
                      EP(I,J,K)=PHI(K)
                   ENDDO
                   IF(NN.EQ.NUMBER)THEN
                      DO K=1,LDZ+1
                         R=A(K)*EP(I,J,K)-B(K)*EP(I,J,K+1)-C(K)*EP(I,J,K-1)-D(K)
                        IF(ABS(R).GT.ABS(RESe))RESe=R
                      ENDDO
                   ENDIF
                ENDDO
             ENDDO
          ENDDO
          GOTO 33
! ------------------------------------------------------------------------------
      72  K=LDZ+1              ! This corresponds to the symmetry plane
! ---------------------- Compute Reynolds stresses ------------------------------
          DO J=2,LDY
             DO I=IT+1,LDX
               U1=0.5*(U(I,J-1,K)+U(I+1,J-1,K))
               U2=0.5*(U(I,J,K)+U(I+1,J,K))
               U3=0.5*(U(I,J+1,K)+U(I+1,J+1,K))
               IF(J.EQ.2)THEN
```

```
                Us=((2*DY(1)+DY(2))*U2-DY(1)*U3)/(DY(1)+DY(2))
              ELSE
                Us=U1+(DY(J-2)/(DY(J-2)+DY(J-1)))*(U2-U1)
              ENDIF
                Un=U2+(DY(J-1)/(DY(J-1)+DY(J)))*(U3-U2)
                DUY=(Un-Us)/DY(J-1)
                 DVX=(V(I,J,K)+V(I,J-1,K)-V(I-1,J,K)-V(I-1,J-1,K))/
&                     (DX(I-1)+DX(I))
               DWX=(W(I,J,K)+W(I,J,K-1)-W(I-1,J,K)-W(I-1,J,K-1))/
&                    (DX(I-1)+DX(I))

                ST11(I,J)=-(VISC(I,J,K)/RHO)*2*(U(I+1,J,K)-U(I,J,K))/DX(I)+
&                     (2.0/3)*KT(I,J,K)
                ST22(I,J)=-(VISC(I,J,K)/RHO)*2*(V(I,J,K)-V(I,J-1,K))/DY(J-1)+
&                     (2.0/3)*KT(I,J,K)
              ST33(I,J)=-(VISC(I,J,K)/RHO)*2*(W(I,J,K)-W(I,J,K-1))/DZ(K-1)+
&                     (2.0/3)*KT(I,J,K)
              ST12(I,J)=-(VISC(I,J,K)/RHO)*(DUY+DVX)
              ST13(I,J)=-(VISC(I,J,K)/RHO)*DWX      ! Note: DUZ=0 at the center.
            ENDDO
          ENDDO
! ------------ Compute displ. thickness, mom. Thickness, shape factor & velocity defects --------
          R=Y(2)/Y(3)
          Y(1)=0
          DO I=IT+1,LDX
              U(I,1,K)=(R*U(I,3,K)-U(I,2,K))/(R-1)
              ST11(I,1)=(R*ST11(I,3)-ST11(I,2))/(R-1)
              ST22(I,1)=(R*ST22(I,3)-ST22(I,2))/(R-1)
              ST33(I,1)=(R*ST33(I,3)-ST33(I,2))/(R-1)
              ST12(I,1)=(R*ST12(I,3)-ST12(I,2))/(R-1)
              ST13(I,1)=(R*ST13(I,3)-ST13(I,2))/(R-1)
          ENDDO                    ! To find centerline velocity$ Reynolds stresses
          DO I=IT+1,LDX
          DISP=0
          MOM=0
          DO J=2,LDY+1
             IF(J.GT.1)THEN
                UN1=U(I,J-1,K)/U(I,LDY+1,K)
                UN2=U(I,J,K)/U(I,LDY+1,K)
                UD1=1-UN1
                UD2=1-UN2
               DISP=DISP+0.5*(UD1+UD2)*(Y(J)-Y(J-1))
               MOM=MOM+0.5*(UN1*UD1+UN2*UD2)*(Y(J)-Y(J-1))
             ENDIF
          ENDDO
          SHAPE=DISP/MOM
          UO(I)=U(I,LDY+1,K)-U(I,1,K)

! ---------------------- Compute the length scale ----------------------------------
          UH=U(I,LDY+1,K)-0.5*UO(I)          ! Velocity at half-wake width
          DO J=1,LDY
              IF(U(I,J,K).LE.UH.AND.U(I,J+1,K).GE.UH)THEN
                 L(I)=Y(J)+(Y(J+1)-Y(J))*(UH-U(I,J,K))/(U(I,J+1,K)-U(I,J,K))
```

```
            ENDIF
          ENDDO

! ------ Print results for displ. & mom. thicknesses, shape factor, velocity & length scales -----
          WRITE(2,110)X(I)*1000,DISP*1000,MOM*1000,SHAPE,
     &          UO(I)/U(I,LDY+1,K),L(I)*1000
  110   FORMAT(2X,F10.3,3(2X,F6.3),2X,F8.5,2X,F10.5)
! ------------------------------------------------------------------------------------------------------------
          ENDDO
          WRITE(5,*)
          DO I=IT+1,LDX
              PHI(I)=U(I,LDY+1,K)  ! To store the velocity at the edge of the boundary layer.
          ENDDO
          DO J=LDY+1,1,-1
              DO I=IT+1,LDX
                  U(I,J,K)=(PHI(I)-U(I,J,K))/UO(I)          ! Velocity defect
                  ETA(I)=Y(J)/L(I)
                 ST11(I,J)=ST11(I,J)/UO(I)**2
                 ST22(I,J)=ST22(I,J)/UO(I)**2
                 ST33(I,J)=ST33(I,J)/UO(I)**2
                 ST12(I,J)=ST12(I,J)/UO(I)**2
                 ST13(I,J)=ST13(I,J)/UO(I)**2
              ENDDO
! ---------- Print results for mean velocity defect and stresses ----------
              WRITE(2,102)(ETA(I),U(I,J,K),ST11(I,J),ST22(I,J),ST33(I,J),
     &                    ST12(I,J),ST13(I,J),I=LDX-28,LDX,2)
  102       FORMAT(15(7(2X,F9.4),4X))
! ------------------------------------------------------------------------------------------------------------
          ENDDO
          END

! ---------------------------------------------------------------------------
! SUBROUTINE TO SOLVE A SYSTEM OF EQUATIONS USING TRI-DIAGONAL MATRIX
ALGORITHM
          SUBROUTINE TDMA(a,b,c,d,N,T)
          IMPLICIT DOUBLE PRECISION (A-H,O-Z)
           DOUBLE PRECISION a(N),b(N),c(N),d(N),P(N),Q(N),T(N)
          P(1)=b(1)/a(1)
          Q(1)=d(1)/a(1)
          DO I=2,N
              DEN=(a(I)-c(I)*P(I-1))
              IF(DEN.EQ.0)DEN=DBLE(1.0E-100)
             P(I)=b(I)/DEN
            Q(I)=(d(I)+c(I)*Q(I-1))/DEN
          ENDDO
          T(N)=Q(N)
          DO I=N-1,1,-1
             T(I)=P(I)*T(I+1)+Q(I)
          ENDDO
          RETURN
          END
! ---------------------------------------------------------------------------
!
```

```
! SUBROUTINE TO DETERMINE THE COEFFICIENTS OF X-DIRECTION MOMENTUM
EQUATION
      SUBROUTINE XEQUA(RHO,UW,UC,UE,VWC,VCC,VWN,VCN,
     &                 WWC,WCC,WWT,WCT,P1,P2,K1,K2,VISWSC,VISWCB,
     &                 VISWCC,VISWCT,VISWNC,VISCSC,VISCCB,VISCCC,
     &                 VISCCT,VISCNC,DXW,DXC,DYS,DYC,DYN,DZB,DZC,DZT,
     &                 AE,AW,AN,AS,AT,AB,SC,SP)
      IMPLICIT DOUBLE PRECISION (A-H,K,O-Z)
      F(X1,X2)=X2/(X1+X2)
      GAMMA(FF,GAMMA1,GAMMA2)=FF*GAMMA1+(1-FF)*GAMMA2
      A(P)=AMAX1(0.0,(1-0.1*ABS(P))**5)
      h1=F(DXW,DXC)
      h2=F(DYC,DYN)
      h3=F(DYS,DYC)
      h4=F(DZC,DZT)
      h5=F(DZB,DZC)
       GAMMA1=GAMMA(h1,VISWNC,VISCNC)
      GAMMA2=GAMMA(h1,VISWCC,VISCCC)
      GAMMA3=GAMMA(h1,VISWSC,VISCSC)
       GAMMA4=GAMMA(h1,VISWCT,VISCCT)
      GAMMA5=GAMMA(h1,VISWCC,VISCCC)
      GAMMA6=GAMMA(h1,VISWCB,VISCCB)
      VISCn=GAMMA(h2,GAMMA2,GAMMA1)
      VISCs=GAMMA(h3,GAMMA3,GAMMA2)
      VISCt=GAMMA(h4,GAMMA5,GAMMA4)
      VISCb=GAMMA(h5,GAMMA6,GAMMA5)
      Fe=0.5*RHO*(UC+UE)*DYC*DZC
      De=VISCCC*DYC*DZC/DXC
      Pe=Fe/De
      Fw=0.5*RHO*(UW+UC)*DYC*DZC
      Dw=VISWCC*DYC*DZC/DXW
      Pw=Fw/Dw
       Fn=RHO*(h1*VWN+(1-h1)*VCN)*DZC*(DXW+DXC)/2
      Dn=VISCn*DZC*(DXW+DXC)/(DYC+DYN)
      Pn=Fn/Dn
      Fs=RHO*(h1*VWC+(1-h1)*VCC)*DZC*(DXW+DXC)/2
      Ds=VISCs*DZC*(DXW+DXC)/(DYS+DYC)
      Ps=Fs/Ds
       Ft=RHO*(h1*WWT+(1-h1)*WCT)*DYC*(DXW+DXC)/2
      Dt=VISCt*DYC*(DXW+DXC)/(DZC+DZT)
      Pt=Ft/Dt
       Fb=RHO*(h1*WWC+(1-h1)*WCC)*DYC*(DXW+DXC)/2
      Db=VISCb*DYC*(DXW+DXC)/(DZB+DZC)
      Pb=Fb/Db
       AE=De*A(Pe)+DMAX1(-Fe,0.0_8)
      AW=Dw*A(Pw)+DMAX1(Fw,0.0_8)
      AN=Dn*A(Pn)+DMAX1(-Fn,0.0_8)
      AS=Ds*A(Ps)+DMAX1(Fs,0.0_8)
      AT=Dt*A(Pt)+DMAX1(-Ft,0.0_8)
      AB=Db*A(Pb)+DMAX1(Fb,0.0_8)
      SC=((P1+(2./3)*RHO*K1)-(P2+(2./3)*RHO*K2))*DYC*DZC
       SP=0
      RETURN
```

```
      END
! ------------------------------------------------------------------------------
!
! SUBROUTINE TO DETERMINE THE COEFFICIENTS OF Y-DIRECTION MOMENTUM
EQUATION
      SUBROUTINE YEQUA(RHO,UCS,UCC,UES,UEC,VS,VC,VN,WSC,
     &                 WCC,WST,WCT,P1,P2,K1,K2,VISWSC,VISWCC,VISCSB,
     &                 VISCSC,VISCST,VISCCB,VISCCC,VISCCT,VISESC,
     &                 VISECC,DXW,DXC,DXE,DYS,DYC,DZB,DZC,DZT,
     &                 IFLAG,AE,AW,AN,AS,AT,AB,SC,SP)
       IMPLICIT DOUBLE PRECISION (A-H,K,O-Z)
      F(X1,X2)=X2/(X1+X2)
      GAMMA(FF,GAMMA1,GAMMA2)=FF*GAMMA1+(1-FF)*GAMMA2
      A(P)=DMAX1(0.0_8,(1-0.1*ABS(P))**5)
      h1=F(DYS,DYC)
      h2=F(DXC,DXE)
      h3=F(DXW,DXC)
      h4=F(DZC,DZT)
      h5=F(DZB,DZC)
      IF(IFLAG.EQ.1)GAMMA1=GAMMA(h1,VISESC,VISECC)
      GAMMA2=GAMMA(h1,VISCSC,VISCCC)
      GAMMA3=GAMMA(h1,VISWSC,VISWCC)
      GAMMA4=GAMMA(h1,VISCST,VISCCT)
      GAMMA5=GAMMA(h1,VISCSC,VISCCC)
      GAMMA6=GAMMA(h1,VISCSB,VISCCB)
      IF(IFLAG.EQ.1)VISCe=GAMMA(h2,GAMMA2,GAMMA1)
      VISCw=GAMMA(h3,GAMMA3,GAMMA2)
      VISCt=GAMMA(h4,GAMMA5,GAMMA4)
      VISCb=GAMMA(h5,GAMMA6,GAMMA5)
      IF(IFLAG.EQ.1)THEN
        Fe=RHO*(h1*UES+(1-h1)*UEC)*DZC*(DYS+DYC)/2
        De=VISCe*DZC*(DYS+DYC)/(DXC+DXE)
        Pe=Fe/De
      ENDIF
       Fw=RHO*(h1*UCS+(1-h1)*UCC)*DZC*(DYS+DYC)/2
      Dw=VISCw*DZC*(DYS+DYC)/(DXW+DXC)
      Pw=Fw/Dw
      Fn=0.5*RHO*(VC+VN)*DZC*DXC
      Dn=VISCCC*DZC*DXC/DYC
      Pn=Fn/Dn
      Fs=0.5*RHO*(VS+VC)*DZC*DXC
      Ds=VISCSC*DZC*DXC/DYS
      Ps=Fs/Ds
       Ft=RHO*(h1*WST+(1-h1)*WCT)*DXC*(DYS+DYC)/2
      Dt=VISCt*DXC*(DYS+DYC)/(DZC+DZT)
      Pt=Ft/Dt
       Fb=RHO*(h1*WSC+(1-h1)*WCC)*DXC*(DYS+DYC)/2
      Db=VISCb*DXC*(DYS+DYC)/(DZB+DZC)
      Pb=Fb/Db
      IF(IFLAG.EQ.1)THEN
        AE=De*A(Pe)+DMAX1(-Fe,0.0_8)
      ELSE
        AE=0
```

```
      ENDIF
      AW=Dw*A(Pw)+DMAX1(Fw,0.0_8)
      AN=Dn*A(Pn)+DMAX1(-Fn,0.0_8)
      AS=Ds*A(Ps)+DMAX1(Fs,0.0_8)
      AT=Dt*A(Pt)+DMAX1(-Ft,0.0_8)
      AB=Db*A(Pb)+DMAX1(Fb,0.0_8)
       SC=((P1+(2./3)*RHO*K1)-(P2+(2./3)*RHO*K2))*DXC*DZC
      SP=0
      RETURN
      END
! ------------------------------------------------------------------------------
!
! SUBROUTINE TO DETERMINE THE COEFFICIENTS OF Z-DIRECTION MOMENTUM
EQUATION
        SUBROUTINE ZEQUA(RHO,UCB,UCC,UEB,UEC,VCB,VCC,VNB,VNC,WB,
     &                   WC,WT,P1,P2,K1,K2,VISWCB,VISWCC,
     &                   VISCSB,VISCSC,VISCCB,VISCCC,VISCNB,VISCNC,
     &                   VISECB,VISECC,DXW,DXC,DXE,DYS,DYC,DYN,DZB,DZC,
     &                   IFLAG,AE,AW,AN,AS,AT,AB,SC,SP)
         IMPLICIT DOUBLE PRECISION (A-H,K,O-Z)
        F(X1,X2)=X2/(X1+X2)
        GAMMA(FF,GAMMA1,GAMMA2)=FF*GAMMA1+(1-FF)*GAMMA2
        A(P)=DMAX1(0.0_8,(1-0.1*ABS(P))**5)
        h1=F(DZB,DZC)
        h2=F(DXC,DXE)
        h3=F(DXW,DXC)
        h4=F(DYC,DYN)
        h5=F(DYS,DYC)
        IF(IFLAG.EQ.1)GAMMA1=GAMMA(h1,VISECB,VISECC)
        GAMMA2=GAMMA(h1,VISCCB,VISCCC)
        GAMMA3=GAMMA(h1,VISWCB,VISWCC)
        GAMMA4=GAMMA(h1,VISCNB,VISCNC)
        GAMMA5=GAMMA(h1,VISCCB,VISCCC)
        GAMMA6=GAMMA(h1,VISCSB,VISCSC)
        IF(IFLAG.EQ.1)VISCe=GAMMA(h2,GAMMA2,GAMMA1)
        VISCw=GAMMA(h3,GAMMA3,GAMMA2)
        VISCn=GAMMA(h4,GAMMA5,GAMMA4)
        VISCs=GAMMA(h5,GAMMA6,GAMMA5)
        IF(IFLAG.EQ.1)THEN
            Fe=RHO*(h1*UEB+(1-h1)*UEC)*DYC*(DZB+DZC)/2
           De=VISCe*DYC*(DZB+DZC)/(DXC+DXE)
           Pe=Fe/De
        ENDIF
         Fw=RHO*(h1*UCB+(1-h1)*UCC)*DYC*(DZB+DZC)/2
        Dw=VISCw*DYC*(DZB+DZC)/(DXW+DXC)
        Pw=Fw/Dw
         Fn=RHO*(h1*VNB+(1-h1)*VNC)*DXC*(DZB+DZC)/2
        Dn=VISCn*DXC*(DZB+DZC)/(DYC+DYN)
        Pn=Fn/Dn
        Fs=RHO*(h1*VCB+(1-h1)*VCC)*DXC*(DZB+DZC)/2
        Ds=VISCs*DXC*(DZB+DZC)/(DYS+DYC)
        Ps=Fs/Ds
        Ft=0.5*RHO*(WC+WT)*DXC*DYC
```

```
      Dt=VISCCC*DXC*DYC/DZC
      Pt=Ft/Dt
      Fb=0.5*RHO*(WB+WC)*DXC*DYC
      Db=VISCCB*DXC*DYC/DZB
      Pb=Fb/Db
      IF(IFLAG.EQ.1)THEN
        AE=De*A(Pe)+DMAX1(-Fe,0.0_8)
      ELSE
        AE=0
      ENDIF
      AW=Dw*A(Pw)+DMAX1(Fw,0.0_8)
      AN=Dn*A(Pn)+DMAX1(-Fn,0.0_8)
      AS=Ds*A(Ps)+DMAX1(Fs,0.0_8)
      AT=Dt*A(Pt)+DMAX1(-Ft,0.0_8)
      AB=Db*A(Pb)+DMAX1(Fb,0.0_8)
       SC=((P1+(2./3)*RHO*K1)-(P2+(2./3)*RHO*K2))*DXC*DYC
      SP=0
      RETURN
      END
! ------------------------------------------------------------------------------
! SUBROUTINE TO DETERMINE THE PRESSURE CORRECTION EQUATION
      SUBROUTINE PRESS(RHO,UC,UE,VC,VN,WC,WT,DUC,
     &                 DUE,DVC,DVN,DWC,DWT,
     &                 DXC,DYC,DZC,IFLAG1,IFLAG2,IFLAG3,IFLAG4,IFLAG5,
     &                 IFLAG6,AE,AW,AN,AS,AT,AB,SC)
       IMPLICIT DOUBLE PRECISION (A-H,M,O-Z)
      IF(IFLAG2.EQ.1)THEN
        AE=RHO*(DYC*DZC/DUE)*DYC*DZC
      ELSE
        AE=0
       ENDIF
       IF(IFLAG1.EQ.1)THEN
        AW=RHO*(DYC*DZC/DUC)*DYC*DZC
      ELSE
        AW=0
       ENDIF
      IF(IFLAG4.EQ.1)THEN
       AN=RHO*(DXC*DZC/DVN)*DXC*DZC
      ELSE
        AN=0
       ENDIF
       IF(IFLAG3.EQ.1)THEN
        AS=RHO*(DXC*DZC/DVC)*DXC*DZC
       ELSE
        AS=0
       ENDIF
       IF(IFLAG6.EQ.1)THEN
        AT=RHO*(DXC*DYC/DWT)*DXC*DYC
       ELSE
        AT=0
       ENDIF
       IF(IFLAG5.EQ.1)THEN
        AB=RHO*(DXC*DYC/DWC)*DXC*DYC
```

```
            ELSE
               AB=0
             ENDIF
             SC=RHO*((UC-UE)*DYC*DZC+(VC-VN)*DXC*DZC+(WC-WT)*DXC*DYC)
             RETURN
             END
! ------------------------------------------------------------------------------
! SUBROUTINE TO DETERMINE THE COEFFICIENTS OF K EQUATION
            SUBROUTINE KEQUA(MU,RHO,UC,UE,VC,VN,WC,WT,KC,VISCW,
          &                  VISCC,VISCE,VISCS,VISCN,VISCB,VISCT,ZK,G,
          &                 EP,CMU,DXW,DXC,DXE,DYS,DYC,DYN,DZB,DZC,
          &                 DZT,IFLAG,IFLAG2,AE,AW,AN,AS,AT,AB,SC,SP)
             IMPLICIT DOUBLE PRECISION (A-H,K,O-Z)
             DOUBLE PRECISION MU,MUt
            F(X1,X2)=X2/(X1+X2)
            GAMMA(FF,GAMMA1,GAMMA2)=FF*GAMMA1+(1-FF)*GAMMA2
            A(P)=DMAX1(0.0_8,(1-0.1*ABS(P))**5)
            IF(IFLAG.EQ.1)h1=F(DXC,DXE)
            h2=F(DXW,DXC)
            h3=F(DYC,DYN)
            h4=F(DYS,DYC)
            h5=F(DZC,DZT)
            h6=F(DZB,DZC)
            IF(IFLAG.EQ.1)GAMMAe=GAMMA(h1,VISCC,VISCE)
            GAMMAw=GAMMA(h2,VISCW,VISCC)
            GAMMAn=GAMMA(h3,VISCC,VISCN)
            GAMMAs=GAMMA(h4,VISCS,VISCC)
            GAMMAt=GAMMA(h5,VISCC,VISCT)
            GAMMAb=GAMMA(h6,VISCB,VISCC)
            IF(IFLAG.EQ.1)THEN
               Fe=RHO*UE*DYC*DZC
              De=GAMMAe*DYC*DZC/(0.5*(DXC+DXE))
              Pe=Fe/De
             ENDIF
            Fw=RHO*UC*DYC*DZC
            Dw=GAMMAw*DYC*DZC/(0.5*(DXW+DXC))
            Pw=Fw/Dw
            Fn=RHO*VN*DXC*DZC
            Dn=GAMMAn*DXC*DZC/(0.5*(DYC+DYN))
            Pn=Fn/Dn
            Fs=RHO*VC*DXC*DZC
            Ds=GAMMAs*DXC*DZC/(0.5*(DYS+DYC))
            Ps=Fs/Ds
            Ft=RHO*WT*DXC*DYC
            Dt=GAMMAt*DXC*DYC/(0.5*(DZC+DZT))
            Pt=Ft/Dt
            Fb=RHO*WC*DXC*DYC
            Db=GAMMAb*DXC*DYC/(0.5*(DZB+DZC))
            Pb=Fb/Db
             IF(IFLAG.EQ.1)THEN
               AE=De*A(Pe)+DMAX1(-Fe,0.0_8)
            ELSE
               AE=0
```

```
      ENDIF
      AW=Dw*A(Pw)+DMAX1(Fw,0.0_8)
      AN=Dn*A(Pn)+DMAX1(-Fn,0.0_8)
      AS=Ds*A(Ps)+DMAX1(Fs,0.0_8)
      AT=Dt*A(Pt)+DMAX1(-Ft,0.0_8)
      AB=Db*A(Pb)+DMAX1(Fb,0.0_8)
      SC=G*DXC*DYC*DZC
      MUt=ZK*(VISCC-MU)
      IF(MUt.EQ.0.OR.IFLAG2.EQ.1)THEN
        SP=(-RHO*EP/KC)*DXC*DYC*DZC
      ELSE
        SP=-(RHO**2)*(CMU*KC/MUt)*DXC*DYC*DZC
      ENDIF
      RETURN
      END

! ------------------------------------------------------------------------------
! SUBROUTINE TO DETERMINE THE COEFFICIENTS OF EPSILON EQUATION
      SUBROUTINE EPEQUA(MU,RHO,UC,UE,VC,VN,WC,WT,EPC,KT,VISCW,VISCC,
     &     VISCE,VISCS,VISCN,VISCB,VISCT,G,ZEP,CEP1,CEP2,
     &     CMU,DXW,DXC,DXE,DYS,DYC,DYN,DZB,DZC,DZT,IFLAG,
     &     AE,AW,AN,AS,AT,AB,SC,SP)
      IMPLICIT DOUBLE PRECISION (A-H,K,O-Z)
      DOUBLE PRECISION MU,MUt
      F(X1,X2)=X2/(X1+X2)
      GAMMA(FF,GAMMA1,GAMMA2)=FF*GAMMA1+(1-FF)*GAMMA2
      A(P)=DMAX1(0.0_8,(1-0.1*ABS(P))**5)
      IF(IFLAG.EQ.1)h1=F(DXC,DXE)
      h2=F(DXW,DXC)
      h3=F(DYC,DYN)
      h4=F(DYS,DYC)
      h5=F(DZC,DZT)
      h6=F(DZB,DZC)
      IF(IFLAG.EQ.1)GAMMAe=GAMMA(h1,VISCC,VISCE)
      GAMMAw=GAMMA(h2,VISCW,VISCC)
      GAMMAn=GAMMA(h3,VISCC,VISCN)
      GAMMAs=GAMMA(h4,VISCS,VISCC)
      GAMMAt=GAMMA(h5,VISCC,VISCT)
      GAMMAb=GAMMA(h6,VISCB,VISCC)
      IF(IFLAG.EQ.1)THEN
        Fe=RHO*UE*DYC*DZC
        De=GAMMAe*DYC*DZC/(0.5*(DXC+DXE))
        Pe=Fe/De
      ENDIF
      Fw=RHO*UC*DYC*DZC
      Dw=GAMMAw*DYC*DZC/(0.5*(DXW+DXC))
      Pw=Fw/Dw
      Fn=RHO*VN*DXC*DZC
      Dn=GAMMAn*DXC*DZC/(0.5*(DYC+DYN))
      Pn=Fn/Dn
      Fs=RHO*VC*DXC*DZC
      Ds=GAMMAs*DXC*DZC/(0.5*(DYS+DYC))
      Ps=Fs/Ds
```

```
      Ft=RHO*WT*DXC*DYC
      Dt=GAMMAt*DXC*DYC/(0.5*(DZC+DZT))
      Pt=Ft/Dt
      Fb=RHO*WC*DXC*DYC
      Db=GAMMAb*DXC*DYC/(0.5*(DZB+DZC))
      Pb=Fb/Db
       IF(IFLAG.EQ.1)THEN
         AE=De*A(Pe)+DMAX1(-Fe,0.0_8)
      ELSE
          AE=0
       ENDIF
       AW=Dw*A(Pw)+DMAX1(Fw,0.0_8)
      AN=Dn*A(Pn)+DMAX1(-Fn,0.0_8)
      AS=Ds*A(Ps)+DMAX1(Fs,0.0_8)
      AT=Dt*A(Pt)+DMAX1(-Ft,0.0_8)
      AB=Db*A(Pb)+DMAX1(Fb,0.0_8)
       MUt=ZEP*(VISCC-MU)
       IF(MUt.EQ.0)THEN
          SC=(CEP1*G*EPC/KT)*DXC*DYC*DZC
       ELSE
          SC=(RHO*CMU*CEP1*KT*G/MUt)*DXC*DYC*DZC
      ENDIF
      SP=-(EPC/KT)*CEP2*RHO*DXC*DYC*DZC
      RETURN
      END
! ------------------------------------------------------------------------------------------
```

NOMENCLATURE

A	slope of the $(U_\infty / w_o)^2$ versus $\bar{x}$ line
B	slope of the $(L_o/\theta)^2$ versus $\bar{x}$ line
Be	bias error
f	normalized velocity defect
fr	frequency
H	shape factor $(=\delta/\theta)$
k	turbulent kinetic energy
l_ε, l_μ	length scales for viscous damping effects in the two-layer approach of the k-ε turbulence model
L_o	half-wake width
$\overline{P}$	pressure
Pe	precision error
Re_y	Reynolds number based on distance from the wall in the computational domain $(=\rho\sqrt{k}y/\mu)$

Re_{dia} Reynolds number based on wire diameter for smoke-wire flow visualization technique ($= \rho U_\infty .dia/\mu$)

Re_θ Reynolds number based on momentum thickness on the plate's trailing edge ($= \rho U_\infty \theta/\mu$)

St_θ Strouhal number based on momentum thickness ($= fr\,\theta/U_\infty$)

t value of the statistical t-distribution

u longitudinal fluctuating velocity component

$\overline{u^2}$ longitudinal Reynolds stress component

U longitudinal time-averaged velocity

UC uncertainty

U_∞ freestream velocity

$\overline{uv}$ Reynolds shear stress on the x-y plane

$\overline{uw}$ Reynolds shear stress on the x-z plane

v transverse fluctuating velocity component

$\overline{v^2}$ transverse Reynolds stress component

V transverse time-averaged velocity

w_o center-line mean velocity defect

W time-averaged velocity in the spanwise direction

W_o normalized velocity scale

x streamwise coordinate

x_o location of the virtual origin of the self-preservation state

$\bar{x}$ normalized distance from the location of the virtual origin, $(=(x-x_0)/2\theta)$

y transverse coordinate

z spanwise coordinate

Greek Symbols

C_μ, $C_{\varepsilon 1}$, $C_{\varepsilon 2}$ constants for k-ε turbulence model

δ displacement thickness $\left(= \int_{-\infty}^{\infty} \left(1-\frac{U}{U_\infty}\right)dy$ for wake, $\int_0^{\infty} \left(1-\frac{U}{U_\infty}\right)dy$ for boundary layer$\right)$

Δ_o normalized length scale

ε kinetic energy dissipation

η transverse coordinate normalized by half-wake width $(= y/L_o)$

μ molecular viscosity

μ_{eff} effective viscosity $(= \mu + \mu_t)$

μ_t eddy viscosity

θ momentum thickness $\left(= \int_{-\infty}^{\infty} \frac{U}{U_\infty}\left(1 - \frac{U}{U_\infty}\right)dy \right.$ for wake, $\left. \int_{0}^{\infty} \frac{U}{U_\infty}\left(1 - \frac{U}{U_\infty}\right)dy \right.$ for boundary layer$\left.\right)$

ρ fluid density

$\left.\begin{matrix}\sigma_k \\ \sigma_\varepsilon\end{matrix}\right\}$ turbulent Prandtl numbers for k and ε

REFERENCES

[1] Townsend, A.A., *The Structure of Turbulent Shear Flow*, 2nd Ed., Cambridge Univ. Press, 1976.

[2] Dehnhardt, G., Mauck, B. and Bleckmann, H., "Seal whiskers detect water movements," *Nature*, Vol. 394, July 16, 1998, pp. 235-236.

[3] Dehnhardt, G., Mauck, B., Hanke, W. and Bleckmann, H., "Hydrodynamic Trail-Following in Harbor Seals (Phoca vitulina)," *Science*, Vol. 293, July 6, 2001, pp.102-104.

[4] Sideridis, G.A., Kastrinakis, E.G. and Nychas, S.G., "Turbulence Production and Transport in Quasi-Two-Dimensional Wake/Boundary-Layer Interaction," *AIAA Journal*, Vol. 38, No. 2, Feb. 2000, pp. 259-265.

[5] Hasan, M.A.Z., "The near wake structure of a square cylinder," *Int. Journal of Heat and Fluid Flow*, Vol. 10, No. 4, Dec. 1989, pp. 339-348.

[6] Holzapfel, F., Gerz, T., Frech, M. and Dornbrack, A. "Wake Vortices in Convective Boundary Layer and Their Influence on Following Aircraft," *Journal of Aircraft*, Vol. 37, No. 6, Nov. 2000, pp. 1001-7.

[7] Darracq, D., Corjon, A., Ducros, F., Keane, M., Buckton, D. and Redfern, M., "Simulation of Wake Vortex Detection with Airborne Doppler Lidar," *Journal of Aircraft*, Vol. 37, No.6, Nov-Dec 2000, pp. 984-993.

[8] Rokhsaz, K., Foster, S.R., and Miller, L.S. "*Exploratory Study of Aircraft Wake Vortex Filaments in a Water Tunnel,*" *Journal of Aircraft*, Vol. 37, No. 6, Nov. 2000, pp.1001-7.

[9] Proctor, P., "Tests Planned for Airport Wake Turbulence Safety Net," *Aviation Week & Space Technology*, Vol. 153, No. 3, July 17, 2000, pp. 56-57.

[10] Fulghum, D.A., "Counterstealth Tackles U.S. Aerial Dominance," Aviation Week & Space Technology, Feb. 5, 2001, pp. 55-57.

[11] Narasimha, R. and Prabhu, A., "Equilibrium and Relaxation in Turbulent Wakes," *Journal of Fluid Mechanics, Vol. 54, 1972, pp. 1-17.*

[12] Ramaprian, B.R., Patel, V.C., and Sastry, M.S., "The Symmetric Turbulent Wake of a Flat Plate," *AIAA Journal*, vol.20, No. 9 Sept. 1982, pp. 1228-1235.

[13] Sreenivasan, K.R., "Approach to Self-Preservation in Plane Turbulent Wakes," *AIAA Journal*, vol. 19, 1981, pp. 1365-1367.

[14] Sreenivasan, K.R. and Narasimha, R., "Equilibrium Parameters for Two-Dimensional Turbulent Wakes," *Journal of Fluids Engineering*, vol. 104, June 1982, pp. 167-170.

[15] Wygnanski, I., Champagne, F. and Marasli, B., "On the large-scale structures in two-dimensional small-deficit, turbulent wakes," *Journal of Fluid Mechanics*, vol. 168, 1986, pp 31-71.

[16] Schlichting, H. *Boundary-Layer Theory*, 7th ed., McGraw-Hill, New York, 1979.

[17] Sato, H and Kuriki, K., "The mechanism of transition in the wake of a thin flat plate placed parallel to a uniform flow," *Journal of Fluid Mechanics,* Vol. 11, 1961, pp. 321-352.

[18] Michalke, A., "On the inviscid instability of the hyperbolic-tangent velocity profile," *Journal of Fluid Mechanics,* Vol. 19, 1964, pp. 543-556.

[19] Michalke, A., "Vortex formation in a free boundary layer according to stability theory," *Journal of Fluid Mechanics,* Vol. 22, part 2, 1965, pp. 371-383.

[20] Michalke, A., "On spatially growing disturbances in an inviscid shear layer," *Journal of Fluid Mechanics,* Vol. 23, part 3, 1965, pp. 521-544.

[21] Mattingly, G.E. and Criminale, W.O., "The stability of an incompressible two-dimensional wake," *Journal of Fluid Mechanics,* Vol. 51, part 2, 1972, pp. 233-272.

[22] Goldstein, S., "Concerning dome solutions of the boundary layer equations in hydrodynamics," *Proceedings of the Cambridge Philosophical Society,* Vol. 26, Part 1, 1930, pp. 1-30.

[23] Messiter, A.F., "Boundary-Layer Flow Near the Trailing Edge of a Flat Plate," *SIAM Journal of Applied Mathematics,* Vol. 18, No.1, Jan. 1970, pp. 241-257.

[24] Alber, I.E., "Turbulent Wake of a Thin Flat Plate," *AIAA Journal,* Vol. 18, No. 9, Sept. 1980, pp. 1044-1051.

[25] Chevray, R. and Kovasznay, L.S.G., "Turbulence Measurements in the Wake of a Thin Flat Plate," *AIAA Journal,* Vol. 7, No. 8, August 1969, pp. 1641-1643.

[26] Tennekes, H. and Lumley, J.L., *A First Course in Turbulence,* The MIT Press, Cambridge, Massachusetts, 1994.

[27] Townsend, A.A., *The Structure of Turbulent Shear Flow,*2^{nd} Ed., Cambridge Univ. Press, 1956.

[28] Prasad, A. and Williamson, C.H.K., "Three-dimensional effects in turbulent bluff-body wakes," *Journal of Fluid Mechanics,* Vol. 343, 1997, pp. 235-265.

[29] Hayakawa, M., and Hussain, F., "Three-dimensionality of organized structures in a plane turbulent wake," *Journal of Fluid Mechanics*, vol. 206,1989, pp. 375-404.

[30] Patel, V.C. and Scheuerer, G., "Calculation of Two-Dimensinal Near and Far Wakes," *AIAA Journal,* Vol. 20, No. 7, July 1982, pp. 900-907.

[31] Versteeg, H.K. and Malalasekera, W., *An Introduction to Computational Fluid Dynamics: The Finite Volume Method,* Longman Scientific & Technical, Essex, England, 1995.

[32] Robinson, D.F., Harris, J.E. and Hassan, H.A., "Unified Turbulence Closure Model for Axisymmetric and Planar Free Shear Flows," *AIAA Journal,* Vol. 33, No. 12, Dec. 1995, pp. 2325-2331.

[33] Robinson, D.F., and Hassan, H.A., "Two-Equation Turbulence Closure Model for Wall Bounded and Free Shear Flows," *AIAA Journal*, Vol. 36, No. 1, Jan. 1998, pp. 109-111.

[34] Cho, J.R. and Chung, M.K., "A $k-\varepsilon-\gamma$ equation turbulence model," *Journal of Fluid Mechanics,* Vol. 237, 1992, pp. 301-322.

[35] Dewan, A. and Arakeri, J.H., "Use of $k-\varepsilon-\gamma$ Model to Predict Intermittency in Turbulent Boundary-Layers," *Journal of Fluids Engineering,* Vol. 122, Sept. 2000, pp. 542-546.

[36] Wang, Y.Q. and Derksen, R.W., "Prediction of Developing Turbulent Pipe Flow by a Modified $k-\varepsilon-\gamma$ Model," *AIAA Journal,* Vol. 37, No. 2, Feb. 1999, pp. 268-270.

[37] Moser, R.D., Rogers, M.M. and Ewing, D.W., "Self-Similarity of Time-evolving Plane Wakes," *Journal of Fluid Mechanics,* Vol. 367, 1998, pp. 255-289.

[38] Bradshaw, P., *An Introduction to Turbulence and its Measurement,* Pergamon Press, Oxford, 1971.

[39] John, J. and Schobeiri, T., "A Simple and Accurate Method of Calibrating X-Probes," *Journal of Fluids Engineering,* Vol. 115, 1993, pp 148-152.

[40] Price, A.B., Smith, T.F. and Suby, A.A., "Uncertainty Analysis," Heating/Piping/Air Conditioning Engineering, Vol. 72, Oct. 2000, pp. 39-43.

[41] Merzkirch, W. *Flow Visualization*, 2nd ed., Academic Press, Florida, 1987.

[42] Mueller, T.J., "Gases: Smokes" in *Handbook of Flow Visualization*, Yang, W.
(editor), Hemisphere Publishing, New York, 1989.

[43] Bevington, P.R. and Robinson, D.K., *Data Reduction and Error Analysis for the Physical Sciences*, 2nd Edition, McGraw-Hill, New York, 1992.

[44] Symes, C.R. and Fink, L.E., In *Structures and Mechanisms of Turbulence I*, proceedings. 1977, p. 86, Berlin.

[45] Oppenheim, A.V. and Schafer, R.W., *Digital Signal Processing*, Prentice-Hall, Inc., 1975.

[46] Husain, Z.D. and Hussain, A.K.M.F., "Natural Instability of Free Shear Layers," *AIAA Journal*, Vol. 21, 1983, pp. 1512-1517.

[47] Hasan, M.A.Z., "The flow over a backward-facing step under controlled perturbation: laminar separation," *Journal of Fluid Mechanics*, Vol. 238, 1992, pp. 73-96.

[48] Zaman, K.B.M.Q. and Hussain, A.K.M.F., "Turbulence Suppression in Free Shear Flows by Controlled Excitation," *Journal of Fluid Mechanics*, Vol. 103, 1981, pp. 133-159.

[49] Hussain, A.K.M.F. and Hasan, M.A.Z., Turbulence Suppression in Free Turbulent Shear Flows under Controlled Excitation. Part 2. Jet-Noise Reduction," *Journal of Fluid Mechanics*, Vol. 150, 1985, pp. 159-168.

[50] Hasan, M.A.Z., Private communication.

[51] Rae, W. H. and Pope, A., Low-Speed Wind Tunnel Testing, 2nd Ed., John Wiley & Sons, New York, 1984.

[52] Breidenthal, R., "Response of plane shear layers and wakes to strong three-dimensional disturbances," Physics of Fluids, Vol. 23, October 1980, pp. 1929-1934.

[53] Patankar, S.V. and Spalding, D.B., "A Calculation Procedure for Heat, Mass and Momentum Transfer in Three-Dimensional Parabolic Flows," *International Journal of Heat and Mass Transfer*, Vol. 15, 1972, pp. 1787-1805.

[54] Nagano, Y. and Hishida, M., "Improved Form of the $k-\varepsilon$ Model for Wall Turbulent Shear Flows," *Journal of Fluids Engineering*, Vol. 109, 1987, pp. 156-160.

[55] Ilinca, F. and Pelletier, D., "Positivity Preservation and Adaptive Solution for the $k-\varepsilon$ Model of Turbulence," *AIAA Journal*, Vol. 36, No. 1, Jan.1998, pp. 44-50.

[56] Kays, W.M. and Crawford, M.E., *Convective Heat and Mass Transfer*, 3rd edition, McGraw-Hill, Inc., New York, 1993.

[57] FLUENT Users' Manual Version 4.52 (1996), Fluent Inc., USA

[58] Jones, W.P. and Launder, B.E., "The Prediction of Laminarization with a Two-Equation Model of Turbulence," *International Journal of Heat and Mass Transfer*, Vol. 15, 1972, pp. 301-314.

[59] Chien, K-Y., "Predictions of Channel and Boundary-Layer Flows with a Low-Reynolds-Number Turbulence Model," *AIAA Journal*, vol. 20, Jan. 1982, pp. 33-38.

[60] Patel, V.C., Rodi, W. and Scheuerer, G., "Turbulence Models for Near-Wall and Low Reynolds Number Flows: A Review," *AIAA Journal*, Vol. 23, Sept. 1985, pp. 1308-1319.

[61] Michelassi, V., Rodi, W. and Zhu, J., "Testing a Low Reynolds Number $k-\varepsilon$ Turbulence Model Based on Direct Simulation Data," AIAA Journal, Vol. 31, Sept. 1993, pp. 1720-1723.

[62] Hwang, C.B. and Lin, C.A., "Improved Low-Reynolds-Number $k-\tilde{\varepsilon}$ Model Based on Direct Numerical Simulation Data," *AIAA Journal*, Vol. 36, Jan. 1998, pp. 38-43.

[63] Baek, S.G., Chung, M.K. and Lim, H.J., "$k-\varepsilon$ Model for Predicting Transitional Boundary-Layer Flows Under Zero-Pressure Gradient," AIAA Journal, Vol. 39, Sept. 2001, pp. 1699-1705.

[64] Chen, H.C. and Patel, V.C., "Near-Wall Turbulence Models for Complex Flows Including Separation," *AIAA Journal*, Vol. 26, June 1988, pp. 641-648.

[65] Wolfshtein, M., "The Velocity and Temperature Distribution in One-Dimensional Flow Turbulence Augmentation and Pressure Gradient," *International Journal of Heat and Mass Transfer*, Vol. 12, 1969, pp. 301-318.

[66] Keimasi, M.R. and Taeibi-Rahni, M., "Numerical Simulation of Jets in a Crossflow Using Different Turbulence Models," AIAA Journal, Vol. 39, Dec. 2001, pp. 2268-2277.

[67] Patankar, S.V., *Numerical Heat Transfer and Fluid Flow,* Hemisphere Publishing Corporation, New York, 1980.

[68] Coleman, H.W. and Steele, W.G., *Experimentation and Uncertainty Analysis for Engineers,* John Wiley, New York, 1989.

[69] IFA 100 System Instruction Manual, Revision F, 1993, TSI Inc., USA.

[70] Model DAP IFA Thermal Anemometry Software Package, Instruction Manual, Revision A, 1993, TSI Inc., USA.

[71] Coleman, H.W., Steele, W.G. and Robert, P.T., "Implications of Correlated Bias Uncertainties in Single and Comparative Tests," *Journal of Fluids Engineering*, Vol. 117, Dec. 1995, pp.552-556.

[72] Cheney, W. and Kincaid, D., Numerical Mathematics and Computing, 3rd Edition, Brooks/Cole Publishing, California, 1994.

VITA

TAOFEEK FOLUSO AYINDE

- Obtained B.Sc. degree in Mechanical Engineering from Obafemi Awolowo University, Ile-Ife, Nigeria in October 1990.
- Had a one-year national youth service at the Nigerian Industrial Development Bank Limited, Bauchi, Nigeria between October 1990 and September 1991.
- Worked as Graduate Assistant in Mechanical Engineering Department of Obafemi Awolowo University, Ile-Ife, Nigeria from June 1992 to September 1995.
- Earned the Msc. Degree in Mechanical Engineering from the University of Ibadan, Nigeria in October 1995.
- Worked as Assistant Lecturer in Mechanical Engineering Department of Obafemi Awolowo University, Ile-Ife, Nigeria from October 1995 to January 1997.
- Joined KFUPM as a PhD student in February 1997.